PRELIMINARY TURBOSHAFT ENGINE DESIGN METHODOLOGY FOR ROTORCRAFT APPLICATIONS

A Thesis
Presented to
The Academic Faculty

by

Stephen A. Suhr

In Partial Fulfillment
Of the Requirements for the Degree
Master of Science in Aerospace Engineering

Georgia Institute of Technology
December 2006

PRELIMINARY TURBOSHAFT ENGINE DESIGN METHODOLOGY FOR ROTORCRAFT APPLICATIONS

Approved by:

Dr. Daniel Schrage, Advisor
School of Aerospace Engineering
Georgia Institute of Technology

Dr. Dimitri Mavris
School of Aerospace Engineering
Georgia Institute of Technology

Dr. Mark Costello
School of Aerospace Engineering
Georgia Institute of Technology

Date Approved: November 10, 2006

For my loving wife, Laurisa, and my two beautiful children, Alivia and Joseph, whose endless support and understanding truly define what is important in life.

ACKNOWLEDGEMENTS

I would like to formally recognize and express my gratitude to Dr. Daniel Schrage, my academic advisor, for his mentorship and guidance throughout my time as a graduate student at Georgia Tech. Thank you for encouraging me to pursue a thesis in turboshaft engine design – the experience has been both academically challenging and personally rewarding in many ways.

Thank you to the Committee members, Dr. Dimitri Mavris and Dr. Mark Costello, for your time and consideration concerning my work on this thesis. Your level of knowledge and expertise proved invaluable in guiding and assessing my academic research efforts.

I want to also thank Mr. Russell Denney for his support and counsel over the past year. Your suggestions, patience, and eagerness to help were essential in reinforcing my understanding of this complex subject.

Finally, many thanks go out to the members of the 2006 AHS Graduate Student Design Team. Your hard work and companionship in the study of rotorcraft system design truly enriched both my personal and professional experience at Georgia Tech.

TABLE OF CONTENTS

PART II: PROPULSION SYSTEM DESIGN AND ANALYSIS

LIST OF TABLES

LIST OF FIGURES

Page

LIST OF SYMBOLS AND ABBREVIATIONS

Symbols:

A	Area [in^2]
a	Speed of sound [ft/s]
AN^2	Blade stress factor [in^2 RPM^2]
b	Diffuser width [in]
c	Chord [in]
c_p	Specific heat at constant pressure [BTU/(lbm-^oR)]
c_v	Specific heat at constant volume [BTU/(lbm-^oR)]
D	Diffusion factor; diameter [in]
E	Energy [BTU]
f	Fuel-to-air ratio
h	Specific enthalpy [BTU/lbm]; blade height [in]
k	Duct pressure loss factor
K	Pressure loss coefficient
M	Mach number
N	Rotational velocity [RPM]
n_b	Number of blades
n_v	Number of vanes
P	Pressure [lbf/in^2]
Q	Heat [BTU]
R	Radius [in]
S	Entropy [BTU/^oR]
S	Specific entropy [BTU/(lbm-^oR)]; blade spacing [in]
T	Temperature [^oR]
U	Internal energy [BTU]
U	Axial velocity [ft/s]
U_2	Impeller tip speed [ft/s]
V	Tangential velocity [ft/s]
V'	Turbine reference velocity [ft/s]
W	Work [HP]
w	Radial velocity [ft/s]

W_d	Disk width [in]
W_{dr}	Rim web thickness [in]
W_{ds}	Width of disk at shaft [in]
W_r	Rim width [in]
Z	Zweifel coefficient

α	Velocity angle [deg]
β	Velocity angle [deg]
β_{2b}	Blade backsweep angle [deg]
E	Cooling effectiveness factor
ε	Slip factor
ϕ	Empty weight to gross weight ratio
$\phi_{rotor,\ stator}$	Rotor/stator loss coefficient
Φ	Stage flow coefficient
γ	Ratio of specific heats
η	Efficiency
Λ	Degree of reaction
π	Pressure ratio
ρ	Density [slugs/ft^3]
σ	Solidity
σ_c	Centrifugal stress [lb/in^2]
σ_d	Disk material strength [lb/in^2]
σ_r	Rim material strength [lb/in^2]
τ	Temperature ratio
υ	Specific volume [in^3/lbm]
ω	Angular velocity [rad/s]
ωr	Wheel speed [ft/s]
ψ	Stage loading coefficient
ζ	Hub-to-tip ratio

Subscripts:

0	Total, or stagnation condition
b	Burner
c	Compressor
d	Disk
e	Exhaust
h	Hub
m	Mean
p	Polytropic
R	Relative reference frame
r	Rim
t	Turbine; tip

Abbreviations:

AHS	American Helicopter Association
APU	Auxiliary power unit
BSAS	Barium-Strontium-Alumino-Silicate
CAD	Computer aided design
CAM	Computer aided manufacturing
CERT	Center for Rotorcraft Excellence
CMC	Ceramic matrix composite
COMPR	Compressor Preliminary Design Program
CTE	Coefficient of thermal expansion
DFA	Design for assembly
DFM	Design for manufacture
DSF	Disk shape factor
EAPS	Engine air particle separator
EBC	Environmental barrier coating
EBF	Engine barrier filter
ECU	Electronic control unit
EGR	Exhaust gas reingestion
FAA	Federal Aviation Administration
FADEC	Full-authority digital electronic control
FAR	Federal Aviation Regulation
FOD	Foreign object damage

GTGH	Georgia Tech Generic Helicopter
HMA	Hydro-mechanical unit
HPA	High pressure air
HPG	High pressure gas
HPT	High pressure turbine
HUMS	Health and usage monitoring system
IBF	Inlet barrier filter
IPPD	Integrated Product and Process Development
IPS	Integrated particle separator
IR	Infrared radiation
KE	Kinetic energy
LPA	Low pressure air
LPG	Low pressure gas
LPT	Low pressure turbine
MCP	Maximum continuous power
MFP	Mass flow parameter
MGT	Measured gas temperature
NEPP	NASA Engine Performance Program
OEI	One engine inoperative
PART	Parametric Representation of Turbines
PE	Potential energy
PF	Pattern factor
PT	Power turbine
RCS	Radar cross-section
RFP	Request for proposal
SF	Safety factor
SFC	Specific fuel consumption
SLS	Sea-level standard
TOP	Takeoff power
TRL	Technology readiness level
TSFC	Thrust specific fuel consumption
TURBN	Turbine Preliminary Design Program
VTOL	Vertical takeoff and landing
WATE	Weight Estimation for Turbine Engines

SUMMARY

In the development of modern rotorcraft vehicles, many unique challenges emerge due to the highly coupled nature of individual rotorcraft design disciplines – therefore, the use of an integrated product and process development (IPPD) methodology is necessary to drive the design solution. Through the use of parallel design and analysis, this approach achieves the design synthesis of numerous product and process requirements that is essential in ultimately satisfying the customer's demands. Over the past twenty years, Georgia Tech's Center for Excellence in Rotorcraft Technology (CERT) has continuously focused on refining this IPPD approach within its rotorcraft design course by using the annual American Helicopter Society (AHS) Student Design Competition as the design requirement catalyst. Despite this extensive experience, however, the documentation of this preliminary rotorcraft design approach has become out of date or insufficient in addressing a modern IPPD methodology.

In no design discipline is this need for updated documentation more prevalent than in propulsion system design, specifically in the area of gas turbine technology. From an academic perspective, the vast majority of current propulsion system design resources are focused on fixed-wing applications with very limited reference to the use of turboshaft engines. Additionally, most rotorcraft design resources are centered on aerodynamic considerations and largely overlook propulsion system integration. This research effort is aimed at bridging this information gap by developing a preliminary turboshaft engine design methodology that is applicable to a wide range of potential rotorcraft propulsion system design problems. The preliminary engine design process

begins by defining the design space through analysis of the initial performance and mission requirements dictated in a given request for proposal (RFP). Engine cycle selection is then completed using tools such as GasTurb and the NASA Engine Performance Program (NEPP) to conduct thorough parametric and engine performance analysis. Basic engine component design considerations are highlighted to facilitate configuration trade studies and to generate more detailed engine performance and geometric data. Throughout this approach, a comprehensive engine design case study is incorporated based on a two-place, turbine training helicopter known as the Georgia Tech Generic Helicopter (GTGH). This example serves as a consistent propulsion system design reference – highlighting the level of integration and detail required for each step of the preliminary turboshaft engine design methodology.

CHAPTER 1

INTRODUCTION

The overarching goal of this research effort is aimed at providing a preliminary turboshaft engine design methodology that is compatible with modern rotorcraft development procedures. Figure 1.1 depicts the integrated product and process development (IPPD) approach used at Georgia Tech for the preliminary design of rotorcraft vehicles – emphasizing the complexity of the interdisciplinary relationships required to achieve a synthesized design solution. This thesis describes a propulsion system design process that is fully-integrated with this approach; specifically addressing the critical role of engine development in preliminary vehicle sizing and performance analysis.

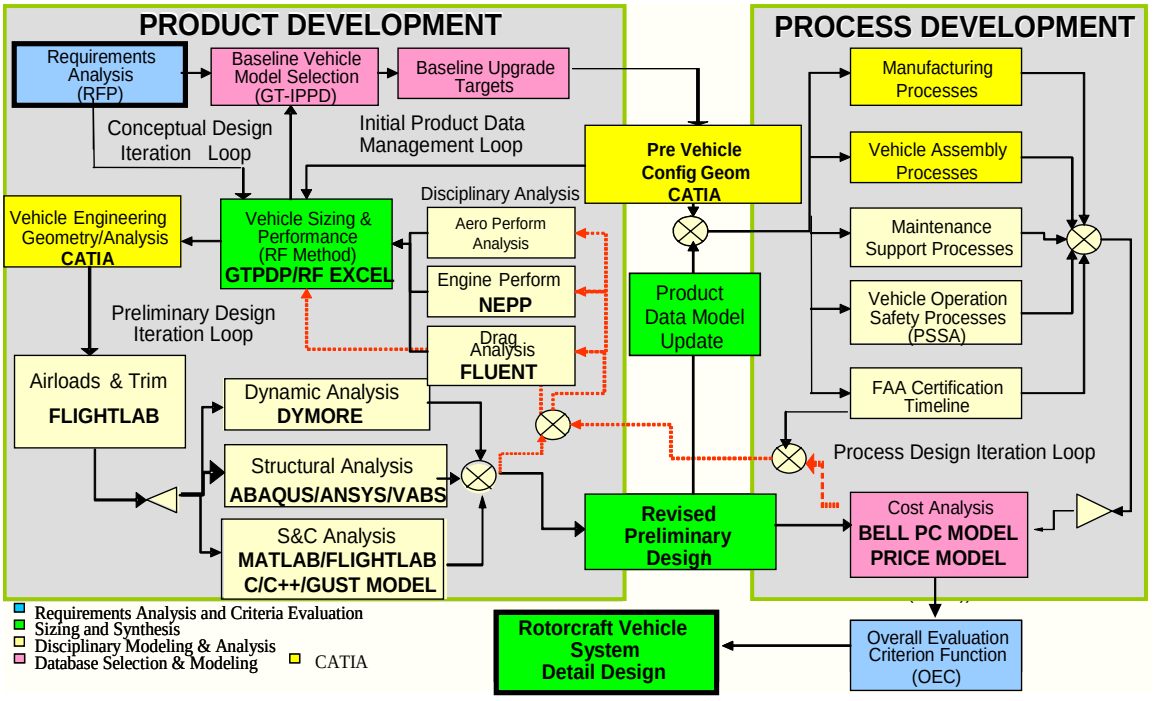

Figure 1.1: Georgia Tech Rotorcraft Preliminary Design Product and Process Development[1]

The challenge is to develop and document a preliminary design approach for helicopter propulsion system applications in the format of a design handbook – providing effective guidelines for the selection of simplifying assumptions and engine parameters that are consistent with modern technological capabilities. The *Helicopter Engineering Handbook: Part One – Preliminary Design* serves as a starting point for this effort; however, significant changes and additions are included to update its content with respect to turboshaft engine performance and analysis. Finally, a case study turboshaft engine model, developed during the 2006 American Helicopter Society (AHS) Student Design Competition, is incorporated to provide a consistent reference that highlights the detailed progression and integration of propulsion system design within the total vehicle development process.

---

[1] Daniel P. Schrage, *AE6333 Rotorcraft Design I: Individual and Team Projects* (Atlanta, GA: Georgia Institute of Technology, 2005).

CHAPTER 2

MOTIVATION

As mentioned in the introduction, there is a definite need for a propulsion system design approach that focuses on rotorcraft specific requirements. Traditional rotorcraft design resources such as *Principles of Helicopter Aerodynamics* by Gordon Leishman, *Helicopter Theory* by Wayne Johnson, and *Helicopter Performance, Stability, and Control* by Raymond Prouty describe numerous important individual design disciplines, but not within the context of an integrated developmental approach. In the case of propulsion system integration, specifically, these resources insufficiently address the tightly-coupled relationship between preliminary vehicle sizing and performance and engine design. From a propulsion system design perspective, there are many excellent resources that describe gas turbine engine development and analysis techniques; however, their overwhelming focus considers only fixed-wing vehicle applications as the framework for their design process and working examples. Typically, the turboshaft engine is simply referred to as a close derivative of the turboprop configuration with little to no further explanation regarding the unique considerations of rotary-wing versus fixed-wing applications.

From the initial requirements analysis to the selection of the engine design and performance parameters, rotorcraft propulsion system design presents several unique challenges that are incongruous with a fixed-wing design approach. A rotorcraft specific engine design handbook is required to capture these unique considerations and to guide the design solution based on modern turboshaft engine capabilities. Only through an

integrated approach to rotorcraft propulsion system development can an optimized total vehicle design solution be achieved. Therefore, this effort is aimed at developing an engine design methodology that effectively addresses rotorcraft specific challenges and ultimately advances the state-of-the-art for rotorcraft system design.

CHAPTER 3

RESEARCH SCOPE

The scope of this thesis is based on providing a propulsion system design handbook that effectively outlines a development strategy for turboshaft engines – offering insight on the key trade studies and analysis required to effectively drive the design to an optimized solution that best meets the requirements of a given RFP. Therefore, the subjects to be included in this thesis are listed below:

- Thermodynamics fundamentals
- Introduction to gas turbine engines
- Propulsion system analysis
- Preliminary turbomachinery component design
- Engine-Airframe integration
- Regulatory requirements
- Emerging concepts
- Case study based on 2006 AHS Student Design Competition

This handbook will be limited to turboshaft engine applications at the preliminary design level; therefore, the following areas are considered beyond the scope of this thesis and will not be formally addressed:

- Reaction drive system applications
- Lubrication system design
- Auxiliary power units (APU)
- Fuel system design

PART I

FUNDAMENTAL PROPULSION SYSTEM CONCEPTS

CHAPTER 4

THERMODYNAMICS FUNDAMENTALS

Before exploring the specific design and analysis techniques used for turboshaft engines, it is important to first review some of the basic concepts of thermodynamics to ensure a fundamental understanding of the laws of nature which govern such work. The following information is intended to serve as a cursory review of the thermodynamic principles that apply to the study of gas turbine engines. By understanding the application of these fundamental principles, the analytical tools used later to perform engine cycle design will seem more transparent and less like a "black box" approach. However, for a more thorough explanation and derivation of the information included in this chapter, the thermodynamics textbooks listed in the references section are recommended.

Basic Definitions and Assumptions

The following concepts encompass the foundation of knowledge and introductory assumptions required for propulsion system analysis. In defining a thermodynamics related problem, the first step is to determine the appropriate analytical approach to be used. This decision is often based on the fundamental difference between a system and a control volume. A system, or control mass, is defined as a quantity of matter of fixed mass and identity within a prescribed boundary.[1] This boundary can either be rigid or movable, separating the system from its surroundings. A control volume is any prescribed volume in space bounded by a control surface through which matter may flow and across which interactions with the surroundings may occur.[2] Although most

thermodynamics problems can be solved using either approach, there is usually a better choice in terms of problem simplification. Therefore, for fluid flow problems, the control volume approach is typically used.

Another set of basic concepts at the root of every thermodynamics problem is the precise understanding of the terms heat and work. Heat (Q) is defined as the form of energy that is transferred across the boundary of a system at a given temperature to another system at a lower temperature by virtue of the temperature difference between the two systems.[1] The unique characteristic of heat is that it exists only in the interaction of two systems and cannot be measured as a system property until a transition across a system boundary occurs. Work (W) is similar to heat in that it only exists as an interactive quantity and can be defined such that work is done by a system if the sole effect on the surroundings (everything external to the system) could be the raising of a weight.[1] Convention dictates that the work done *by* a system is positive, while work done *on* a system is negative.

More key terms in the study of thermodynamics include energy, enthalpy, and entropy. Energy (E) is simply defined as the measure of a system's potential to perform work. The forms of energy most applicable to thermodynamics problems are kinetic energy (due to motion), potential energy (due to position), and internal energy (sum of kinetic and potential energy at the molecular level). The term enthalpy (h) is an extensive property used to describe the sum of the internal energy of a system and the energy of the work done by the system on its surroundings. The following equation best describes this relationship:

$$h = u + p\upsilon \qquad [4.1]$$

Where h is specific enthalpy, u is the internal energy, p is the pressure, and υ is the specific volume. Entropy (S) is another extensive property of matter that measures the degree of randomization or disorder at the microscopic level.[2] While the absolute level of entropy is not typically considered, the change in entropy is used to determine the efficiency of a process in terms of its proximity to the limits of what is "ideally" possible.

Along with these definitions, there are several fundamental assumptions that help to describe and simplify thermodynamic processes. An adiabatic process is one in which there is no transfer of heat. An isentropic process is an adiabatic process where there is no change in entropy. In terms of fluid mechanics, the flow properties are assumed to be steady and one-dimensional. Steady flow means that the fluid properties such as velocity and density at any point in a space do not vary with time. In control volume scenarios, this assumption greatly simplifies the problem by eliminating the need to consider the behavior of the control volume contents – only the inputs and outputs affect the thermodynamic analysis.[3] One-dimensional flow, also known as uniform flow, means that the fluid conditions are assumed to vary only in the direction of the streamline.[3] Although this assumption fails to address the multi-dimensional flow properties that exist near a wall, historical precedence has shown that it still provides a meaningful approximation in the study of fluid thermodynamics.

With these basic terms and assumptions previously described, it is now necessary to consider a conceptual foundation for thermodynamics rooted in the laws of nature. The following sections describe the application of several key concepts that will serve as the building blocks for every thermodynamic analysis tool used to design and predict the performance of modern gas turbine propulsion systems.

1st Law of Thermodynamics

The concept of conservation of energy is defined by the 1st Law of Thermodynamics and can be tailored to describe the specific characteristics of a system or control volume. Using the latter as the best suited form for fluid flow analysis, the 1st Law of Thermodynamics for a control volume can be written as follows:

$$\frac{dQ}{dt} - \frac{dW}{dt} = \frac{dE}{dt} \qquad [4.2]$$

Where Q is heat, W is work, and E is the total energy of the system. The total energy of the system can be further described as the sum of its internal energy (U), potential energy (PE), and kinetic energy (KE), as follows:

$$E = U + PE + KE \qquad [4.3]$$

For fluid flow problems, it is often best to consider the energy formula as a rate equation as follows:

$$\dot{Q} - \dot{W}_x = \dot{m}\left(h + \frac{V^2}{2g_c} + \frac{gz}{g_c}\right)_{out} - \dot{m}\left(h + \frac{V^2}{2g_c} + \frac{gz}{g_c}\right)_{in} + \frac{dE_\sigma}{dt} \qquad [4.4]$$

Where $\dot{Q}$ is the rate of heat transfer, $\dot{W}_x$ is the power, $\dot{m}$ is the mass flow rate, h is the specific enthalpy, V is the velocity, g_c is the gravitational constant, $\frac{gz}{g_c}$ is the potential energy, and $\frac{dE_\sigma}{dt}$ is the energy production rate within the control volume (this term equals zero using the steady flow assumption).[2]

2nd Law of Thermodynamics

The 2nd Law of Thermodynamics states that it is impossible to construct a heat engine that operates in a cycle, receives a given amount of heat from a high-temperature body, and does an equal amount of work.[3] This law establishes a framework for the definition of entropy as an entity that can only be created, and never destroyed. Recognizing entropy as a quantitative measure of the amount of thermal energy not available to do work, its rate of change can be described using the following relationship:

$$dS \geq \frac{\delta Q}{T} \qquad [4.5]$$

Where S is entropy, Q is heat, and T is temperature. In order to apply this formula to control volume applications, the following equation results:

$$\frac{dS_{\sigma}}{dt} + \dot{S}_{out} - \dot{S}_{in} \geq \frac{1}{T}\frac{dQ}{dt} \qquad [4.6]$$

Where $\frac{dS_{\sigma}}{dt}$ is the entropy production rate within the control volume, $\dot{S}$ is the entropy flux through the control surface, $\frac{dQ}{dt}$ is the heat flux, and T is the temperature of the fluid adjacent to the control surface.[2] The equality in this formula relates to the concept of reversibility in which an ideal process cycle has no effect on the system or its surroundings (i.e. no losses). In a real process, however, the relationship is irreversible due to factors such as friction, heat transfer, mixing of substances, and unrestrained expansion. Therefore, entropy is used to define the efficiency of a process by comparing the ratio of real, or actual, performance to the ideal case.

Conservation of Mass

The concept of conservation of mass can be applied to a control volume using the following relationship:

$$\frac{dm_\sigma}{dt} + \dot{m}_{out} - \dot{m}_{in} = 0 \qquad [4.7]$$

Where $\frac{dm_\sigma}{dt}$ is the rate of accumulation of mass within the control volume and $\dot{m}$ is the mass flow rate into and out of the control volume through the control surface. Using the steady flow assumption, the conservation of mass equation reduces to the following:

$$\dot{m}_{out} = \dot{m}_{in} \qquad [4.8]$$

If the flow is also considered to be one-dimensional, then the mass flow rate can be expressed as follows:

$$\dot{m} = \rho A V_n \qquad [4.9]$$

Where ρ is the density, A is the area, and V_n is the velocity component normal to the area.[2]

Momentum Equation

From Newton's 2nd Law of Motion, the instantaneous rate of change of the momentum in the x-direction of a system of fixed mass is equal to the sum of the forces in the x-direction acting on the mass at that instant.[2] The following expression shows this relationship:

$$\sum F_x = \frac{1}{g_c}\frac{dM_x}{dt} \qquad [4.10]$$

Where F_x is the force in the x-direction, g_c is Newton's constant, and M_x is the momentum in the x-direction. Using a control volume approach, Equation 4.10 becomes:

$$\sum F_\sigma = \frac{1}{g_c}\left(\frac{dM_\sigma}{dt} + \dot{M}_{out} - \dot{M}_{in}\right) \qquad [4.11]$$

Where the net force acting on the control volume equals the time rate of increase of momentum within the control volume and the net flux of momentum from the control volume.[2] Once again, with the steady flow assumption, the first term on the right hand side of Equation 4.11 goes to zero – leaving only the inputs and outputs, not the actual contents, of the control volume to be considered.

Ideal Gas Properties

With the fundamental laws of nature that apply to study of gas turbine engines previously described, it is now important to consider the characteristics of a perfect gas. This topic begins with the equation of state for a perfect gas as follows:

$$p\upsilon = RT \qquad [4.12]$$

Where p is the static pressure, υ is the specific volume, R is the gas constant, and T is the static temperature. This equation of state establishes the definition of a pure substance as one that has only two independent static properties. Substituting Equation 4.12 into Equation 4.1 indicates that enthalpy is only a function of temperature.

$$h = h(T) \qquad [4.13]$$

This relationship between internal energy, enthalpy, and temperature introduces the definition of two terms known as specific heat at constant pressure (c_p) and specific heat at constant volume (c_υ):

$$c_p = \frac{dh}{dT} \qquad c_\upsilon = \frac{du}{dT} \tag{4.14}$$

The relationship between specific heats for a perfect gas is described by the following equation:

$$c_p = c_\upsilon + R \tag{4.15}$$

The ratio of specific heats (γ) is defined as:

$$\gamma \equiv \frac{c_p}{c_\upsilon} \tag{4.16}$$

The Gibbs equation relates the specific entropy (s) to the other thermodynamic properties of a substance and for a perfect gas, it can be written as follows:[3]

$$ds = c_p \frac{dT}{T} - R \frac{dp}{p} \tag{4.17}$$

For a calorically perfect gas (exhibits constant specific heats) undergoing an isentropic process, the following three equations describe the thermodynamic property changes between states 1 and 2:

$$\frac{T_2}{T_1} = \left(\frac{p_2}{p_1} \right)^{\frac{(\gamma-1)}{\gamma}} \tag{4.18}$$

$$\frac{T_2}{T_1} = \left(\frac{\rho_2}{\rho_1} \right)^{(\gamma-1)} \tag{4.19}$$

$$\frac{p_2}{p_1} = \left(\frac{\rho_2}{\rho_1} \right)^{\gamma} \tag{4.20}$$

Compressible Flow Considerations

Compressibility is defined as the fractional change in volume of the fluid element per unit change in pressure.[4] For slow moving fluids, these changes due to compression are relatively small and are typically ignored. However, for certain flows moving at speeds above approximately Mach 0.3, the compressibility effects become significant enough that they should be considered.[4] In the previous section, it was shown that the equation of state for a simple compressible pure substance is determined by defining two independent intensive properties. For a gas in motion, though, a third property of velocity is required to fully define the state of the gas at a specific point in the flow field. Consideration of the gas velocity introduces some new terminology: static, total, and ram properties. Static properties refer to the properties of the moving flow in its local velocity flow field (i.e. static temperature (T) and static pressure (p)). Total, or stagnation, properties are defined as the state that would be reached by a fluid if it was isentropically slowed until it had zero velocity and are denoted with a zero subscript (i.e. total temperature (T_0) and total pressure (p_0)). Ram properties are the properties that result directly from the fluid's motion. The following temperature equation shows the relationship between these three property types:

$$T_{total} = T_{static} + T_{ram} \qquad [4.21]$$

Figure 4.1 further demonstrates this relationship by depicting an increase in ram properties at increasing fluid velocities. It also shows that the total and static properties are equal when the fluid velocity is zero.

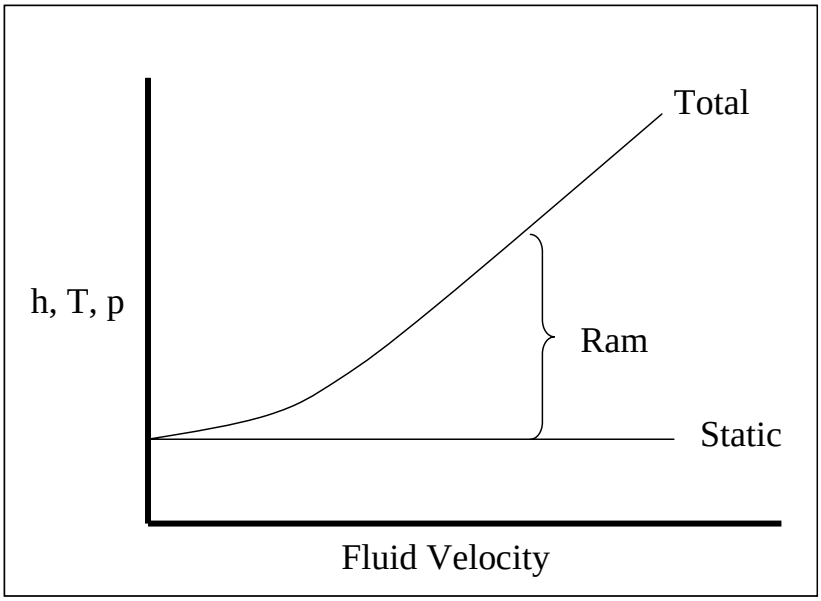

Figure 4.1: Generic Fluid Property Comparison Graph[5]

The specific definitions of total enthalpy and total temperature are best described using a simplified version of Equation 4.4. By dividing by $\dot{m}$ and assuming steady flow and no gravity effects, the energy equation becomes:

$$q - w_x = \left(h + \frac{V^2}{2g_c} \right)_{out} - \left(h + \frac{V^2}{2g_c} \right)_{in} \qquad [4.22]$$

Where q is the specific heat, w_x is the specific work, and the term total enthalpy (h_0) is now defined as:

$$h_0 \equiv h + \frac{V^2}{2g_c} \qquad [4.23]$$

Where h is the static enthalpy. By assuming a calorically perfect gas, Equation 4.22 becomes:

$$q - w_x = c_p \left(T + \frac{V^2}{2g_c c_p} \right)_{out} - c_p \left(T + \frac{V^2}{2g_c c_p} \right)_{in} \qquad [4.24]$$

Where T is the static temperature and the term total temperature (T_0) is now defined as:

$$T_0 \equiv T + \frac{V^2}{2g_c c_p} \quad [4.25]$$

Based on these definitions for a calorically perfect gas, the following two equations result:[2]

$$\Delta h_0 = c_p \Delta T_0 \quad [4.26]$$

$$q - w_x = c_p \left(T_{0out} - T_{0in} \right) \quad [4.27]$$

Finally, the total pressure is defined using Equation 4.18 as follows:

$$p_0 \equiv p \left(\frac{T_0}{T} \right)^{\frac{\gamma}{(\gamma-1)}} \quad [4.28]$$

In Figure 4.2, the graph demonstrates the relationship between total enthalpy or temperature and total pressure. In an adiabatic flow in which no work occurs (i.e. $q\text{-}w_x = 0$), the total enthalpy and total pressure are constant regardless of the reversibility of the process. However, the total pressure is reduced by the increasing irreversibility of the process (indicated by increasing entropy). Figure 4.2 shows that the total pressure at state 2 (p_{02}) is less than the total pressure at state 1 (p_{01}) while the total enthalpy or total temperature remain constant – in the absence of work, this is a direct measure of the irreversibility of the process.[3]

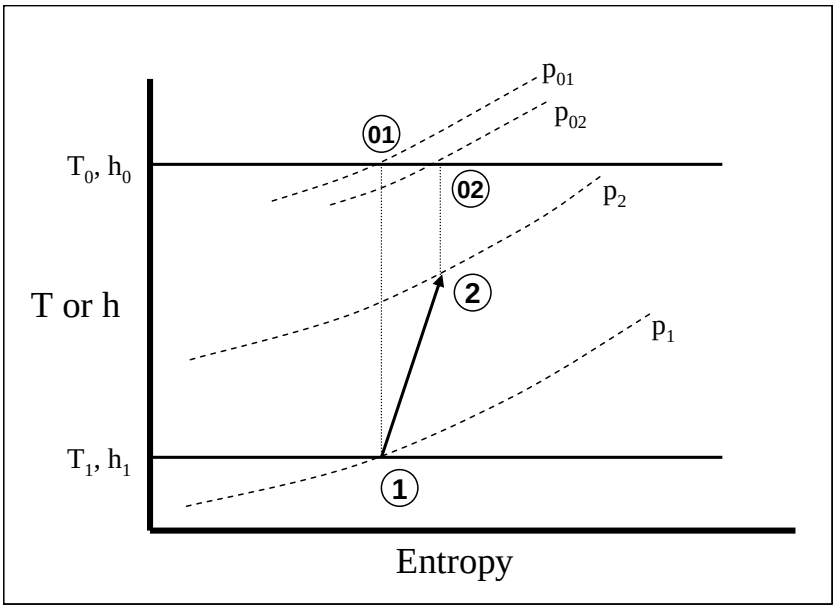

Figure 4.2: Stagnation State Diagram for a Typical Gas

Another key parameter to consider in evaluating compressible flow is the Mach number (M) defined as follows:

$$M \equiv \frac{V}{a} \qquad [4.29]$$

Where V is the flow velocity and *a* is the local speed of sound in the fluid. For a perfect gas, the speed of sound is defined as:

$$a = \sqrt{\gamma g_c RT} \qquad [4.30]$$

The Mach number is useful because it allows for three important gas flow property ratios to be expressed in terms of only one variable:

$$\frac{h_0}{h} = \left(1 + \frac{\gamma - 1}{2} M^2\right) \qquad [4.31]$$

$$\frac{T_0}{T} = \left(1 + \frac{\gamma - 1}{2} M^2\right) \qquad [4.32]$$

$$\frac{p_0}{p} = \left(1 + \frac{\gamma - 1}{2} M^2\right)^{\frac{\gamma}{\gamma - 1}} \qquad [4.33]$$

Mattingly also defines a new property, the mass flow parameter (MFP), as a function of only M, R, and γ for a calorically perfect gas:[6]

$$MFP(M) = \frac{\dot{m}\sqrt{T_t}}{p_t A} = \frac{M\sqrt{\gamma g_c / R}}{\left\{1 + \left[(\gamma - 1)/2\right] M^2\right\}^{(\gamma+1)/[2(\gamma-1)]}} \qquad [4.34]$$

This relationship proves useful in the limiting the design variables involved in component flowpath analysis discussed in Chapter 10.

See APPENDIX A for a reference list of standard terminology used in the study and analysis of thermodynamic relationships.

---

[1] Richard E. Sonntag and Gordon J. Van Wylen, *Introduction to Thermodynamics: Classical and Statistical* (New York, NY: John Wiley and Sons, 1991).

[2] Jack D. Mattingly, *Elements of Gas Turbine Propulsion* (Reston, VA: AIAA, 2005).

[3] Phillip G. Hill and Carl R. Peterson, *Mechanics and Thermodynamics of Propulsion* (Reading, MA: Addison-Wesley Publishing, 1992).

[4] John D. Anderson, Jr., *Fundamentals of Aerodynamics* (Boston, MA: McGraw-Hill, 2001).

[5] Joseph F. Alcock and J. Walter Smith, *Introduction to Gas Turbine Performance Analysis* (West Palm Beach, FL: Pratt and Whitney Aircraft Group, 1979).

[6] Jack D. Mattingly, William H. Heiser, and David T. Pratt, *Aircraft Engine Design*, 2nd ed. (Reston, VA: AIAA, 2002).

CHAPTER 5

INTRODUCTION TO GAS TURBINE ENGINES

The creation of the modern gas turbine engine – credited equally, yet separately, to the work of Sir Frank Whittle of Great Britain and Hans von Ohain of Germany in the 1930s, revolutionized the aerospace industry by providing drastic improvements in the power-to-weight ratio of propulsion systems. The development of the gas turbine engine made it possible for aircraft to fly faster and higher than ever before – an advantage realized within fixed-wing and rotary-wing applications alike. Over the years, gas turbine engines have evolved into four main categories that classify their use in modern aircraft: the turbojet, turbofan, turboprop, and turboshaft engine. For rotorcraft, specifically, the turboshaft version of the gas turbine engine is used and serves as the basis for this research effort. Similar to the turboprop, this configuration is designed to extract the maximum shaft work from a given airflow with little to no propulsive thrust gained through the exhaust. And while this method of work extraction makes the turboshaft engine unique, all gas turbine engines share a common feature in that they all operate on the same fundamental principle at their core – the Brayton cycle.

Brayton Cycle

The Brayton cycle is the thermodynamic model used to describe an ideal gas turbine power cycle. The four key processes of the ideal Brayton cycle are described below:

- Isentropic compression (2 – 3)

- Constant-pressure heat addition (3 – 4)
- Isentropic expansion (4 – 5)
- Constant-pressure heat rejection (5 – 1)

Figure 5.1 shows a graphic depiction of the temperature-entropy (T-s) diagram and the pressure-volume (p-υ) diagram for an open-cycle of a gas turbine. Jet engines operate with an open-cycle, which means that fresh gas is drawn into the compressor and the products are exhausted from the turbine and not reused.[1]

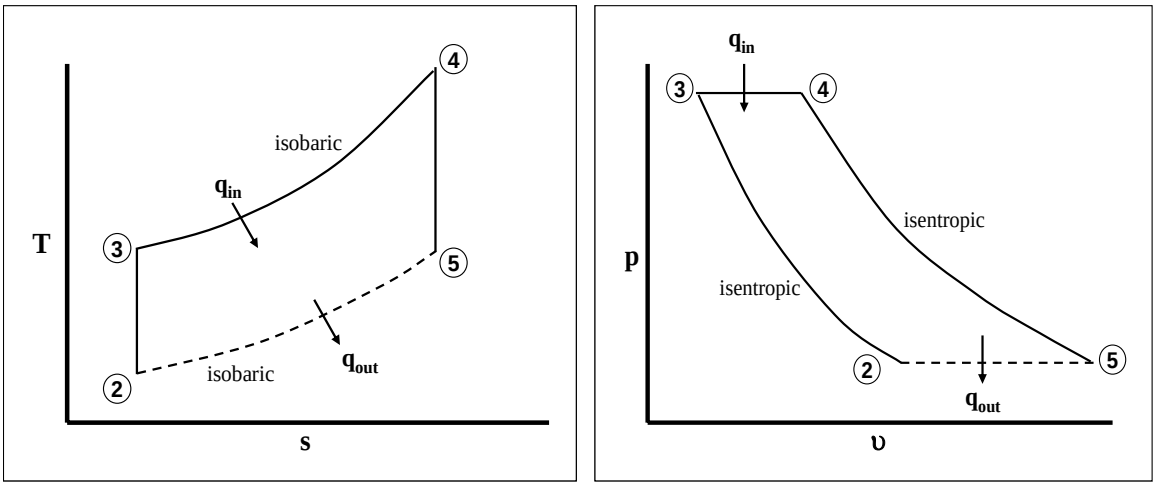

Figure 5.1: Ideal Brayton Cycle Diagrams (Open-Cycle)

Figure 5.2 shows the generic geometry of an open Brayton cycle - highlighting the relationship between engine components and their specific processes. The "core" of a typical gas turbine engine is comprised of the compressor, combustor, and turbine sections. The ideal compressor stage, from 2 to 3, is where mechanical work is performed on the fluid causing an isentropic rise in both enthalpy (or temperature) and pressure. During the ideal combustion stage, from 3 to 4, heat is added to the fluid by burning a mixture of fuel and air at a constant pressure – greatly increasing its enthalpy.

In the ideal turbine stage, from 4 to 5, work is mechanically extracted from the fluid through isentropic expansion. The common shaft connection between the turbine and the compressor sections is what allows the work extracted by the turbine to be translated into the driving force for the compressor.

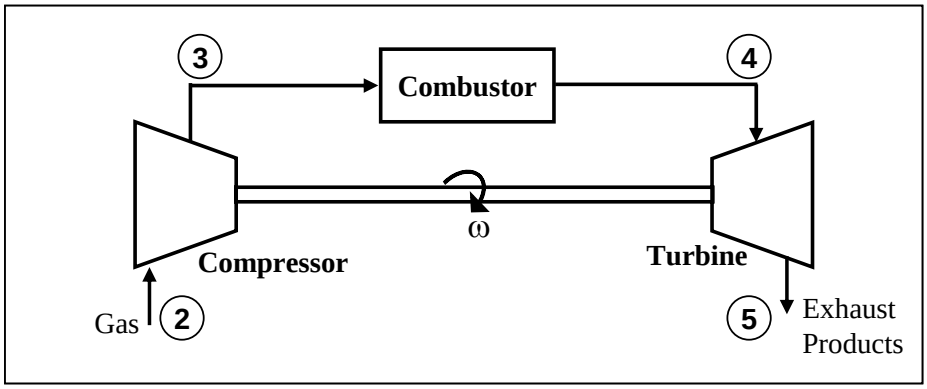

Figure 5.2: Open Brayton Cycle Architecture[1]

In the closed Brayton cycle shown in Figure 5.3, the combustion stage is replaced with a heat exchanger and the hot gas from the turbine is cooled with a heat exchanger and returned directly to the compressor from stage 5 to 2. The problem with the closed-cycle geometry is the size requirement associated with the heat exchanger. The added weight and volume requirements make it an impractical choice for aviation applications. Similar limitations exist in most of the Brayton cycle variations that are designed to increase the overall thermodynamic efficiency of the power generation process. Derivative geometries such as regeneration and reheat have a proven track record in improving process efficiency, however, their volume requirements typically limit their applicability to only ground power generation.

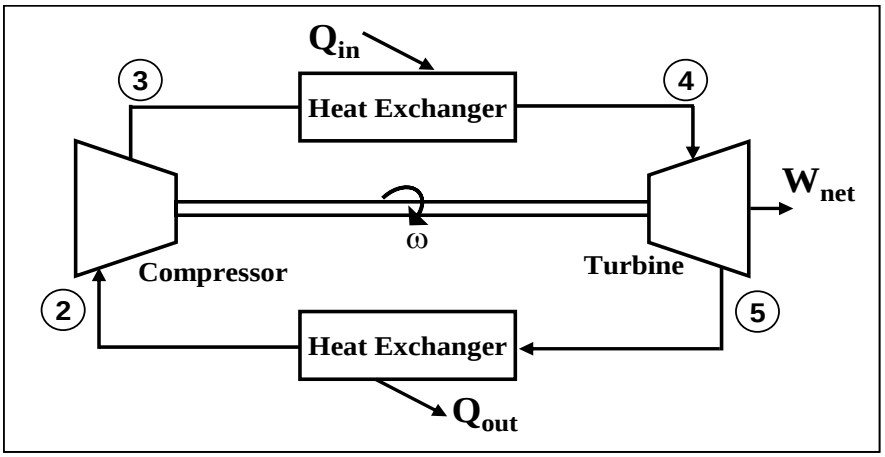

Figure 5.3: Closed Brayton Cycle Architecture[1]

Thermal Efficiency and Work Output

The thermal efficiency term is used to define the ratio of gas turbine work output to the energy input from burning fuel, as follows:[2]

$$\eta_{th} = \frac{\text{net}\,\dot{W}_{out}}{\dot{Q}_{in}} = \frac{\text{net}\,\dot{W}_{out}}{\dot{m}_f\,\Delta H} \qquad [5.1]$$

Where $\dot{m}_f$ is the mass flow rate of fuel and ΔH is the lower heating value of the fuel, which is the chemical energy converted to thermal energy on complete combustion in air if the water in the products remains as a vapor.[2] For turboshaft engines, specifically, thermal efficiency is indirectly measured by the specific fuel consumption (SFC) for a given engine cycle in terms of fuel burn rate per horsepower.

For the ideal Brayton cycle, the thermal efficiency can be simplified to the following:

$$\eta_{th} = 1 - \left(\frac{1}{PR}\right)^{\frac{(\gamma-1)}{\gamma}} = \frac{\left(\frac{T_3}{T_2}\right) - 1}{\left(\frac{T_3}{T_2}\right)} \qquad [5.2]$$

Where PR is the pressure ratio (p_3/p_2). This relationship shows that thermal efficiency approaches 100% with an indefinitely increasing pressure ratio. The maximum work output, however, occurs when the area of the T-s diagram is maximized and is, therefore, directly influenced by the heater exit temperature (T_4). By assuming a fixed ambient temperature (T_2) and a maximum heater exit temperature (T_4), the following expression identifies the optimum pressure ratio, or temperature ratio, that corresponds to the maximum work output per unit mass:[3]

$$\left(\frac{p_3}{p_2}\right)_{\text{max work}}^{\frac{(\gamma-1)}{\gamma}} = \left(\frac{T_3}{T_2}\right)_{\text{max work}} = \sqrt{\frac{T_4}{T_2}} \qquad [5.3]$$

Figure 5.4 shows that the pressure ratio for maximum work output is much less than the pressure ratio for maximum thermal efficiency. While the graph represents an ideal Brayton cycle, this trend of competing demands for power and efficiency is indicative of non-ideal engines, as well. Typically, the pressure ratios for maximum power and maximum efficiency are on the order of 12 and 30, respectively.[4] The reason this occurs is that at low pressure ratios the efficiency increases so rapidly that more of the heat is converted to work. However, with a maximum turbine inlet temperature, the relative allowable heat input is also limited and at higher pressure ratios, the heat input decreases more rapidly with pressure than the corresponding increase in efficiency.[2]

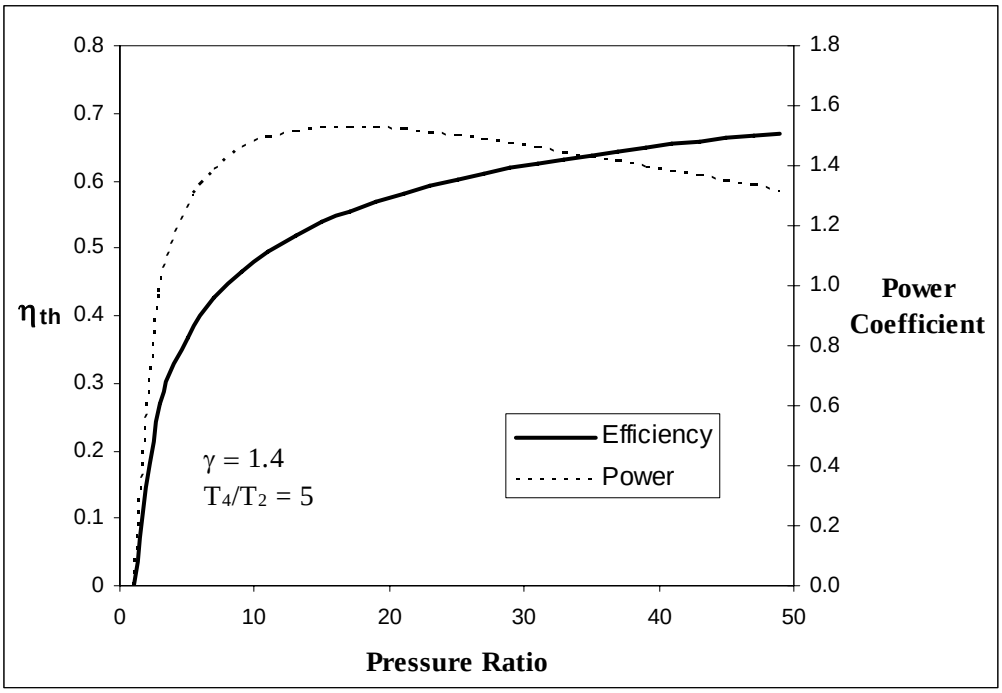

Figure 5.4: Thermal Efficiency of Ideal Brayton Cycle

Ideal Versus Real Cycle Comparison

Up to this point, only the ideal Brayton cycle has been considered. In reality, deviations from the ideal cycle result from real gas effects, heat added through combustion, and losses that occur in each engine component. While component losses will be covered in the next section, the effects of real gases and heat added through combustion can be examined using the following three scenarios for comparison:

- Ideal Brayton cycle, ideal gases, heat added externally
- Ideal Brayton cycle, real gases, heat added externally
- Ideal Brayton cycle, real gases, heat added by combustion

Real gas effects mean that the specific heat at constant pressure (c_p) and the ratio of specific heats (γ) are no longer constant. In comparing the first two scenarios, the ideal Brayton cycle evaluated with real gas effects will exhibit a higher net specific work

output and a lower thermal efficiency because the value of c_p for real air is greater than that of ideal air. This translates to the addition of more heat in the real case, producing more work at a lower efficiency. By comparing these results with the third scenario, the heat added through combustion produces an increase in specific work due to the added mass flow of the fuel and a decrease in thermal efficiency because the fuel is mixed with air at ambient temperatures.[5]

Component Descriptions and Configurations

In this section, the role of each engine component is briefly described and the characteristics of their unique design considerations are discussed. Only those components with turboshaft engine applicability are described. Figure 5.5 shows a schematic diagram of a typical turboshaft engine architecture – highlighting the major components of interest and their associated station numbers.

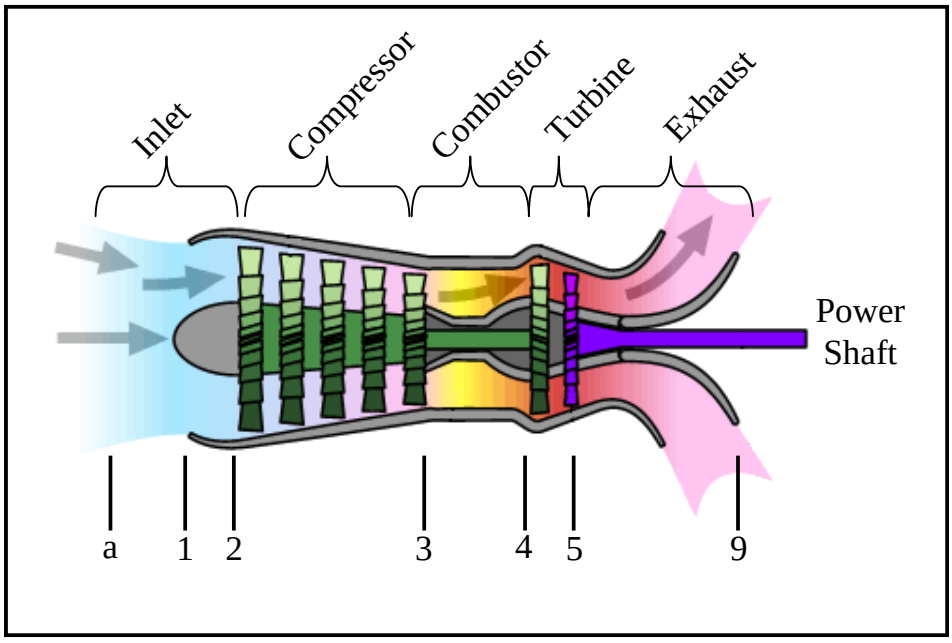

Figure 5.5: Typical Turboshaft Engine Schematic[6]

Inlet

The role of the inlet is to convert the kinetic energy associated with the freestream of airflow or forward velocity into stagnation temperature and pressure.[4] Based on the Bernoulli Theorem, this is done by diffusing the airflow (reducing its velocity and increasing its pressure) to achieve the conditions required at the entrance to the compressor with minimal pressure loss. For helicopters and other subsonic vertical take-off and landing (VTOL) vehicles, the design and performance of the inlet is relatively less complicated in comparison to that of supersonic vehicle applications.

Design Performance

For an ideal inlet, the temperature and pressure relationships are isentropic and can be described with the following two expressions:

$$\frac{T_{02}}{T_a} = \left(1 + \frac{\gamma - 1}{2} M_a^2\right) \qquad [5.4]$$

$$\frac{p_{02}}{p_a} = \left(\frac{T_{02}}{T_a}\right)^{\frac{(\gamma-1)}{\gamma}} \qquad [5.5]$$

Where the subscript *a* is the ambient or freestream condition. Therefore, the temperature and pressure at the exit of the diffuser can be determined based on the freestream Mach number and static properties. In describing the performance of a real inlet, the main difference to consider is the effect of pressure losses due to non-isentropic behavior. Using the assumption that diffusers operate adiabatically, Figure 5.6 shows a typical h-s diagram for a subsonic inlet – highlighting the difference between an ideal and a real case. Ideally, the pressure at the exit of the diffuser would equal p_{0a}; but due to the effects of an entropy rise from stage a to 2, the actual exit pressure is reduced to p_{02}. The

term total pressure recovery (π_d) is used to quantify such losses in the inlet stage as follows:[1]

$$\pi_d = \frac{p_{02}}{p_{0a}} \qquad [5.6]$$

For turboshaft engines, the inlet pressure losses typically range from 1-3% and can be assumed constant over varying flight and power requirements.[4]

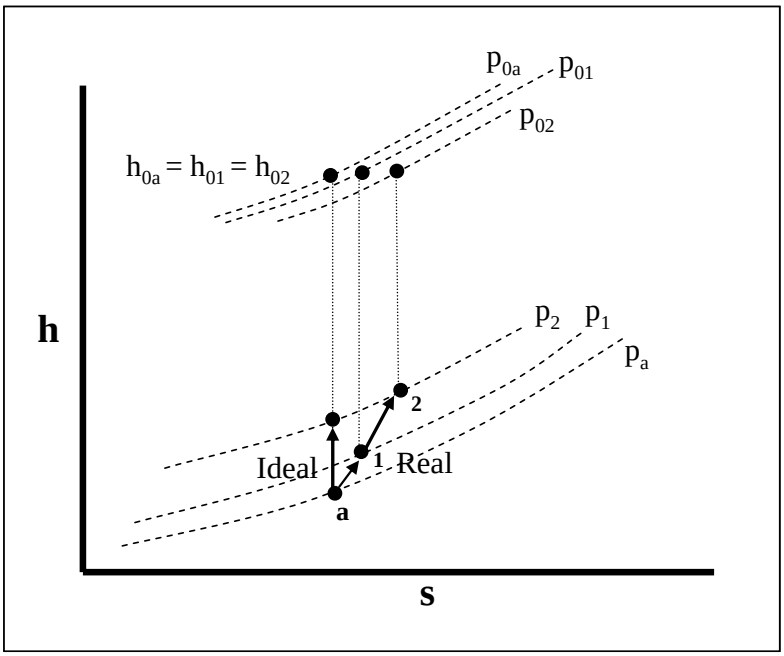

Figure 5.6: Ideal and Real Inlet h-s Diagram[1]

Compressor

The purpose of the compressor is to increase the pressure of the incoming air so that the processes that follow compression are more efficiently operated. From Figure 5.4, the thermal efficiency of the Brayton cycle increases with increasing pressure ratio. In order to achieve high pressure ratios, however, more compression stages are required

which drive up the weight, complexity, and cost of the final design. For an ideal compressor, the total pressure ratio (π_c) is defined as follows:

$$\pi_c = \frac{p_{03}}{p_{02}} = \left[\tau_c\right]^{\frac{\gamma}{(\gamma-1)}} \quad [5.7]$$

Where $\tau_c = \frac{T_{03}}{T_{02}}$ is the total temperature ratio of a compressor.

Design Performance

The h-s diagram in Figure 5.7 shows the relationship between ideal and real compressor performance. For the ideal case, the pressure increase from state 2 to 3' occurs isentropically, whereas the real scenario shows an increase in entropy from state 2 to 3. While both the ideal and real processes reach the same total pressure, the real case requires more power to achieve the same result. This relationship is defined as the compressor adiabatic efficiency (η_c) for a given pressure ratio as follows:

$$\eta_c \equiv \frac{\text{ideal power}}{\text{actual power}} = \frac{h_{03}^{'} - h_{02}}{h_{03} - h_{02}} \quad [5.8]$$

Typically, modern compressors operate with maximum adiabatic efficiencies from 85-93%.[1] Using this definition, the following expression defines the total pressure ratio for a real compression process in terms of efficiency and temperature ratio:

$$\pi_c = \left[1 + \eta_c(\tau_c - 1)\right]^{\frac{\gamma}{(\gamma-1)}} \quad [5.9]$$

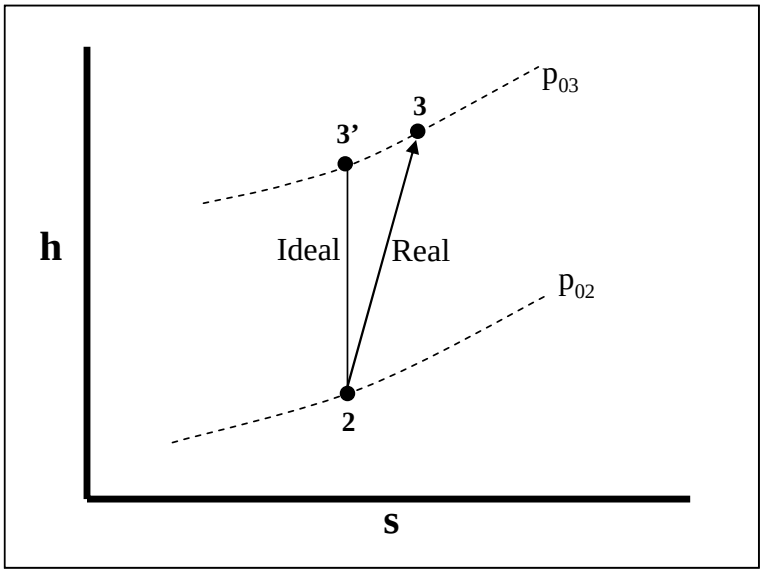

Figure 5.7: Ideal and Real Compressor h-s Diagram[1]

A second measure of compressor performance is known as polytropic efficiency (η_{pc}). Defined as the ratio of ideal to adiabatic work for an infinitesimal step in the compression process, this method is often equated to the level of technology for compressor design.[7] The advantage of this approach is that the polytropic efficiency is based on the design of a single stage at a certain level of technology – a value independent of the number of stages – providing a means of direct comparison between different size compressors. Modern engines all demonstrate nearly identical polytropic efficiencies at their peak design point, a figure currently between 90-92%.[1]

The following expression shows the relationship between adiabatic efficiency and polytropic efficiency for the compression stage:

$$\eta_c = \frac{\pi_c^{\frac{(\gamma-1)}{\gamma}} - 1}{\pi_c^{\frac{(\gamma-1)}{\eta_{pc}\gamma}} - 1} \qquad [5.10]$$

Figure 5.8 also shows a graphical representation of this relationship in which the compressor adiabatic efficiency decreases with increasing pressure ratio at a given polytropic efficiency.

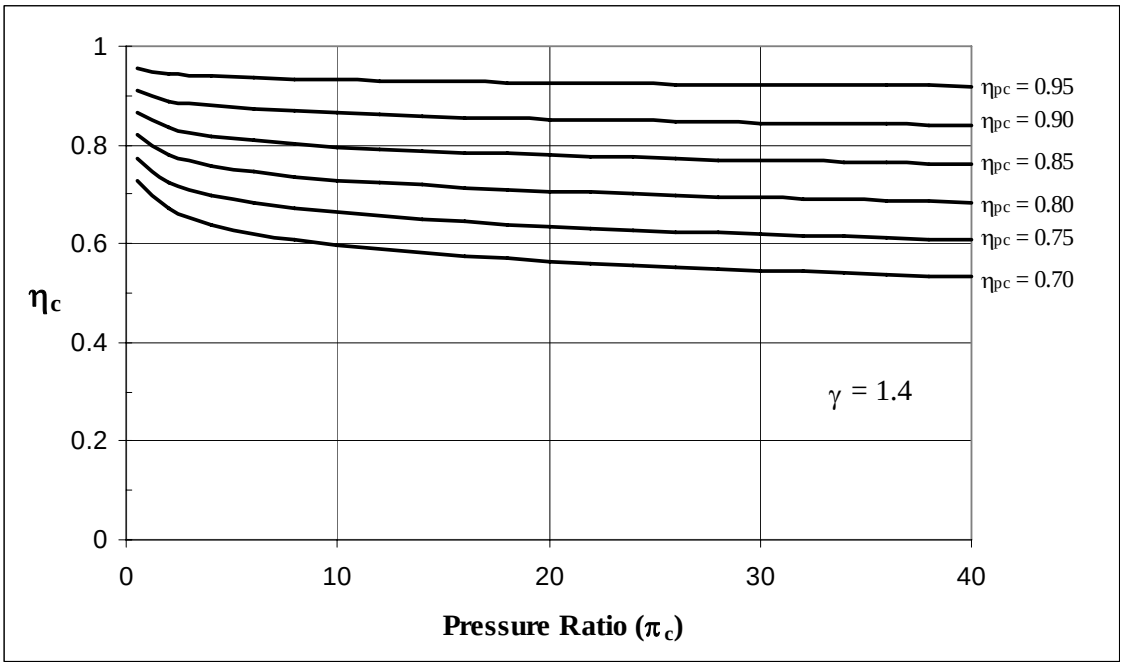

Figure 5.8: Adiabatic and Polytropic Compressor Efficiencies[7]

Design Configurations

Axial Compressor

The axial compressor consists of a series of rotating rotor blades and stationary stator vanes which perform work on the air – increasing the kinetic energy of the flow and converting it into an increase in pressure. Each combination of a single row of rotor blades and stator vanes represents a single stage of compression. Modern axial compressors typically achieve a stage pressure ratio between 1.15 and 1.28.[1] Therefore, in order to meet the total pressure ratio required for a typical engine cycle, multiple stages

of axial compression are used. Figure 5.9 shows a typical axial compressor design and Figure 5.10 shows a schematic of the axial airflow pattern.

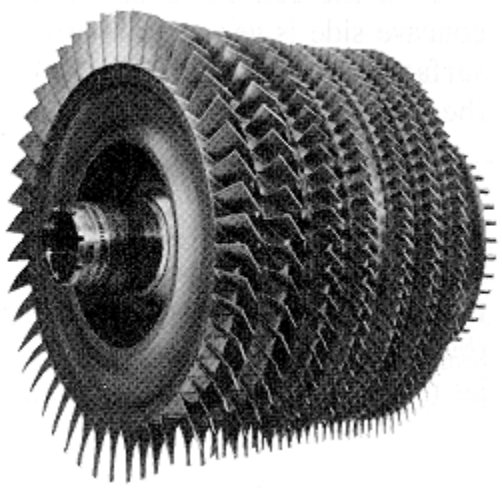

Figure 5.9: Typical Axial Compressor Design[8]

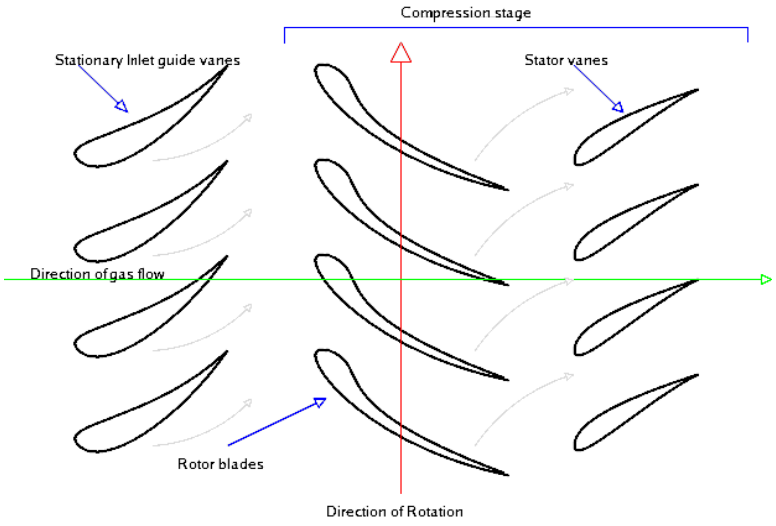

Figure 5.10: Axial Compressor Airflow Schematic[9]

The comparative design advantages of axial compressors are higher operating efficiency (except for very small mass flow applications), reduced frontal area, and an increased ability to handle high volume airflows. These characteristics make axial compressors the ideal choice for most large aircraft engines. The disadvantages,

however, are reduced pressure ratio per stage, increased problems related to distorted inflow conditions, and higher susceptibility to erosion and foreign object damage (FOD).

Centrifugal Compressor

Centrifugal compressors perform the same operation of converting the increased kinetic energy of a rotating fluid into an increase in total pressure. The means of achieving this result, however, is quite different. As depicted in Figure 5.11, centrifugal, or radial, compressors use a rotating impeller to accelerate and turn the flow 90^{o}, then a diffuser slows the flow and directs it to the discharge area just prior to combustion as a low-velocity, high-pressure gas. Modern centrifugal compressors can achieve a single stage pressure ratio greater than 5:1.

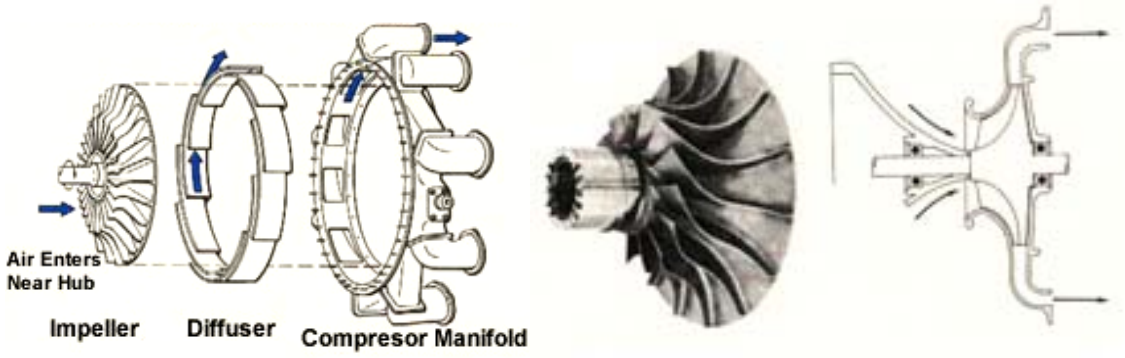

Figure 5.11: Centrifugal Compressor Diagram[10]

The main advantage of centrifugal compressors relates to their applicability to smaller engine designs typically used on helicopters. For large gas turbine engines on heavy fixed-wing aircraft, the axial compressor is used exclusively because it significantly reduces the cross-sectional area (reduced drag on the nacelle) and is more easily configured for multiple stages (higher overall pressure ratio). However, in rotorcraft engine applications – the optimum pressure ratio tends to be smaller and the

effect of increasing the engine diameter is not as critical to the overall vehicle design and performance. At mass flow rates less than 3 lbm/s, the centrifugal compressor is actually more efficient than an axial compressor because it is less sensitive to the effects of blade tip clearance.[11] Additionally, the centrifugal compressor is better suited to handle the distorted inflows more common to rotorcraft and is generally more durable due to its single piece design. The key disadvantages are the increased frontal area, lower operating efficiency at mass flow rates above 3 lbm/s, reduced ability to accommodate large inflows, and complex flow geometry for multi-stage designs. This complex ducting, as depicted in Figure 5.12, typically results in significant efficiency losses of approximately 5%.[1]

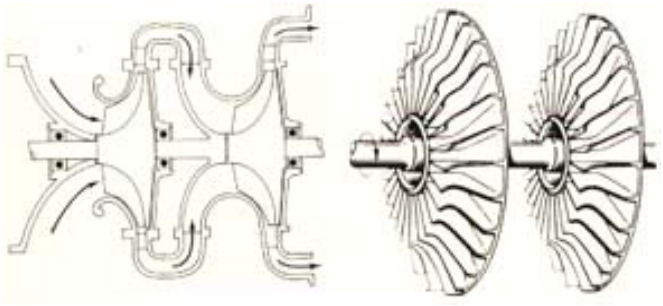

Figure 5.12: Two-Stage Centrifugal Compressor Diagram[10]

Axial-Centrifugal Compressor

A combination design of axial and centrifugal compressor stages is sometimes employed to capitalize on the advantages of each alternative. A series of axial stages is followed by a single radial stage in order to overcome the tip losses and manufacturing limitations associated with the smaller blades in the final stages of an axial compressor. Figure 5.13 shows the Allison Model 250 turboshaft engine compressor which uses six axial stages and one centrifugal stage to achieve a 7.1:1 pressure ratio.

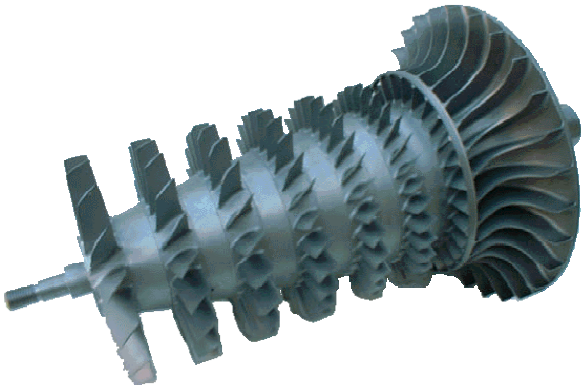

Figure 5.13: Allison Model 250 Compressor[12]

Combustor

Design Performance

The combustor, or burner, is designed to burn a mixture of fuel and air in order to add energy to the flow in the form of heat. For an ideal burner, the combustion process occurs completely at a constant pressure. In reality, however, the design of combustors is complicated by pressure losses and reduced efficiency from incomplete combustion. Figure 5.14 shows this difference between ideal and real combustor performance. An effective combustor design is characterized by the following properties:[3]

- High combustion efficiency
- Low total pressure loss
- Stability of combustion process
- Even temperature distribution at exit
- Short length and small cross section
- Elimination of the possibility of flameout
- In-flight relight capability
- Large operational envelope

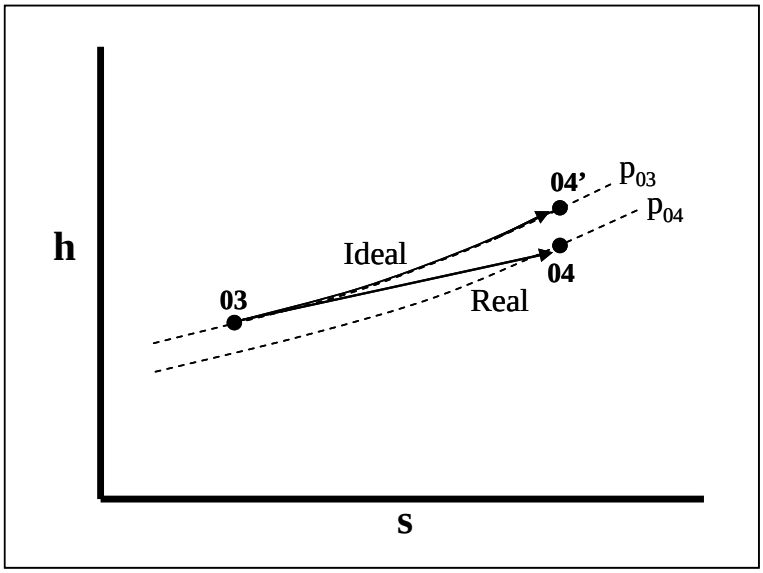

Figure 5.14: Ideal and Real Combustor h-s Diagram

Pressure losses result from the highly irreversible nature of combustion and increased viscous effects, friction, and turbulence in the fuel-air mixture.[1] Thus, the burner pressure ratio (π_b) is defined as:

$$\pi_b = \frac{p_{04}}{p_{03}} \qquad [5.11]$$

Typical, this parameter ranges between 92-98% for modern engines. Incomplete combustion occurs as a result of ineffective mixing of fuel and air, requirements to warm the cold fuel before combustion, heat transfer due to extremely high temperatures, and non-ideal fuel composition due to additives and impurities.[1] The combustion efficiency (η_b) is defined as:

$$\eta_b = \frac{(\dot{m} + \dot{m}_{fuel}) c_{pt} T_{04} - \dot{m} c_{pc} T_{03}}{\dot{m}_{fuel} \Delta H} \qquad [5.12]$$

Where c_{pt} is assumed to be the constant average value of specific heat for gases downstream of the burner and c_{pc} is the constant value upstream of the compressor.[3] Typical values for combustion efficiency are between 98-99%.

Design Configurations

The common configurations for combustors are known as can, annular, and can-annular. Figures 5.15 – 5.17 provide schematic diagrams that identify the major differences between each design. While the can design consists of one or more cylindrical burners in a burner case, the can-annular design is a derivative of this design with a series of cylindrical burners located in a common annulus. Turboshaft engines can also use a reverse-flow can-annular design which utilizes an S-shaped flowpath. This arrangement allows for reduced engine length, lower temperature distribution factors, lower emissions, higher stability, and better relight capability.[13] Finally, the annular combustor is a single burner with an annular arrangement – simplifying the design and improving combustion uniformity.[14]

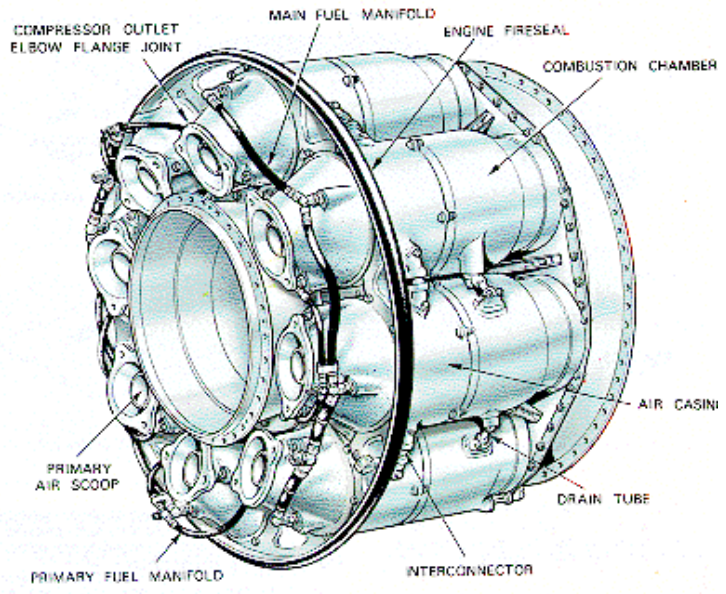

Figure 5.15: Can Combustor Diagram[8]

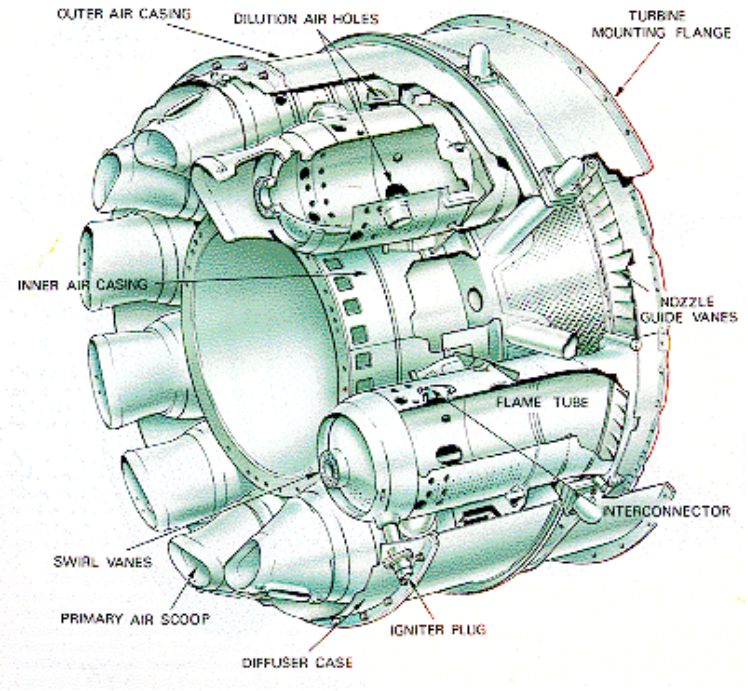

Figure 5.16: Can-annular Combustor Diagram[8]

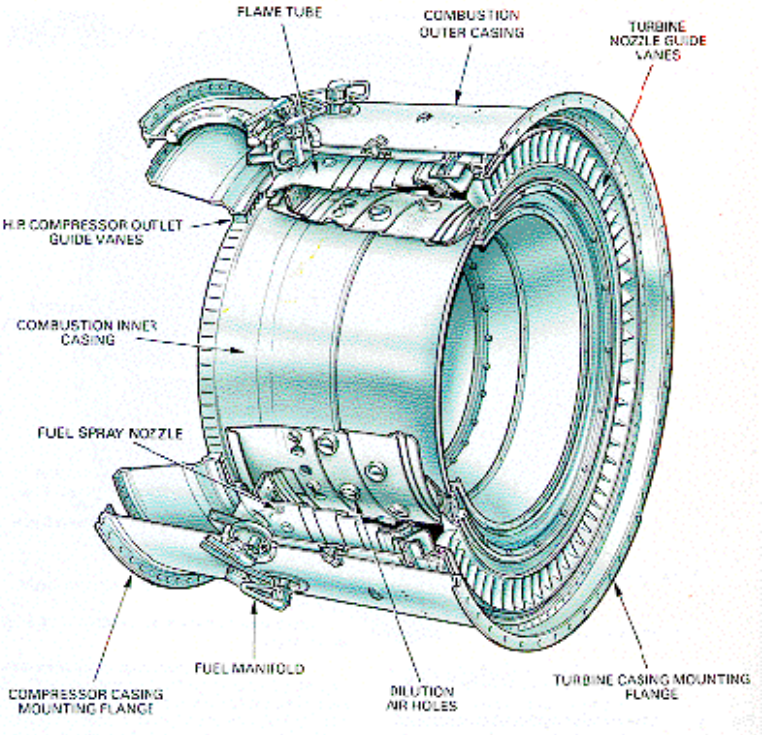

Figure 5.17: Annular Combustor Diagram[8]

Turbine

In most regards, the turbine acts similarly to the compressor, only with the opposite goal. Its purpose is to extract energy from the flow in the form of mechanical work used to drive the compressive and propulsive components. In a turboshaft engine, this energy is extracted completely in the form of shaft work with approximately 75% of the power being used for compression and the remainder for the vehicle propulsion system. During this stage, the pressure and temperature of the flow from the combustor decreases. This relationship results in a more favorable operating environment for the airfoils of a turbine – allowing them to achieve higher efficiency and higher aerodynamic loading than that of a compressor – resulting in fewer required stages.[1] The limiting factor for turbine design is typically related to structural integrity as opposed to aerodynamic performance. The extremely high inlet temperatures combined with high rotational speeds requires the use of high density and expensive materials for most turbine applications. For an ideal turbine, the following expression describes the total pressure ratio (π_t):

$$\pi_t = \frac{p_{05}}{p_{04}} = \left[\tau_t\right]^{\frac{\gamma}{(\gamma-1)}} \qquad [5.13]$$

Where $\tau_t = \frac{T_{05}}{T_{04}}$ is the total temperature ratio for the turbine.

Design Performance

Figure 5.18 shows an h-s diagram which describes the relationship between ideal and real turbine performance. The ideal turbine operates isentropically with a pressure reduction from state 4 to 5', whereas the real case experiences a reduced enthalpy drop

from state 4 to 5 due to the presence of increasing entropy and component losses. Similar to the compressor, the turbine adiabatic efficiency (η_t) for a given pressure ratio is defined as follows:

$$\eta_t \equiv \frac{\text{ideal power}}{\text{actual power}} = \frac{h_{04} - h_{05}}{h_{04} - h'_{05}} \qquad [5.14]$$

Typically, modern turbines can achieve maximum adiabatic efficiencies between 85-95%, slightly higher than compressors due to the aerodynamic benefits of decreasing pressure.[1] The following expression defines the total pressure ratio for a real turbine:

$$\pi_t = \left[1 - \frac{(1-\tau_t)}{\eta_t}\right]^{\frac{\gamma}{(\gamma-1)}} \qquad [5.15]$$

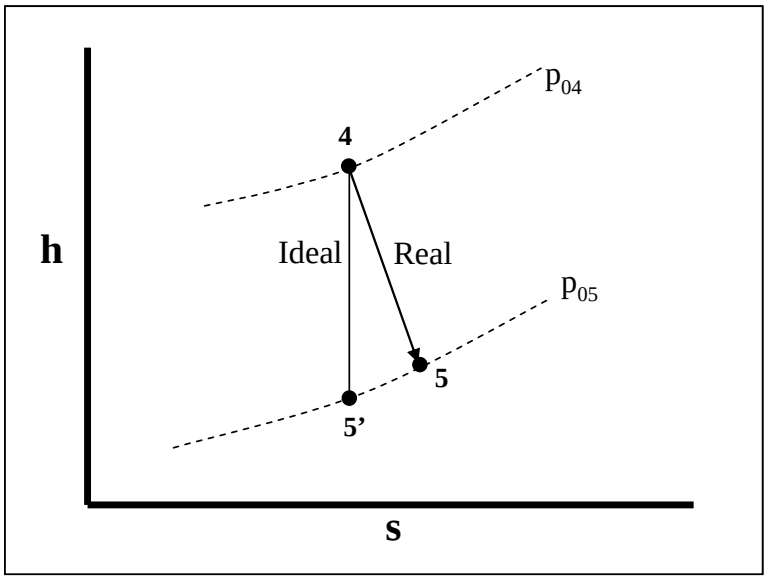

Figure 5.18: Ideal and Real Turbine h-s Diagram[1]

The turbine polytropic efficiency (η_{pt}) also applies as it did in the case of the compressor. The following equation describes the relationship between turbine adiabatic and polytropic efficiency:

$$\eta_t = \frac{1-\left[\pi_t\right]^{\eta_{pt}\frac{(\gamma-1)}{\gamma}}}{1-\left[\pi_t\right]^{\frac{(\gamma-1)}{\gamma}}} \qquad [5.16]$$

The major difference between compressor and turbine efficiency relationships can be shown as a function of increasing pressure ratio. Recall Figure 5.8 which showed that at a given polytropic efficiency, the adiabatic efficiency of a compressor decreases with increasing pressure ratio. Figure 5.19 shows that the opposite relationship is true for turbine adiabatic and polytropic efficiencies.

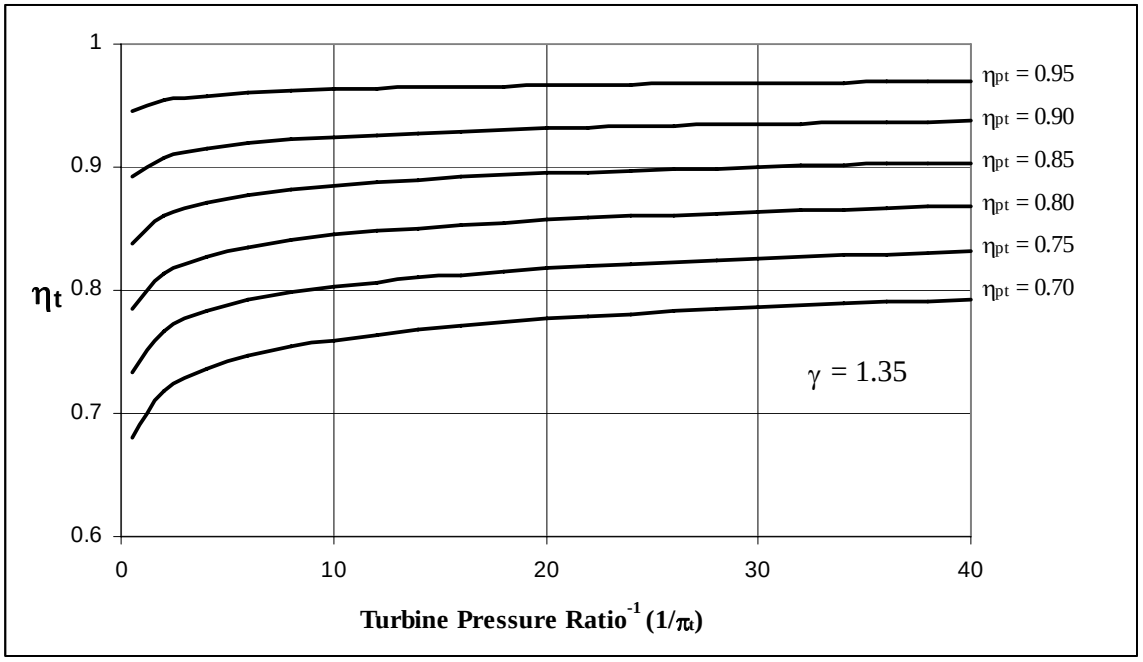

Figure 5.19: Adiabatic and Polytropic Turbine Efficiencies

Design Configurations

Axial Turbine

The architecture of an axial turbine is identical to that previously discussed for an axial compressor – a series of stationary stator vanes, or nozzles, followed by a series of

rotating rotor blades make up each stage. Figure 5.20 provides an axial turbine airflow diagram, showing that the airfoil shape of the blades in an axial turbine differ significantly from the airfoils of an axial compressor - mostly as a result of the added stress capability required for turbine blades to perform more work at higher temperatures. Figure 5.21 shows a typical axial turbine configuration from the Allison 250 turboshaft engine.

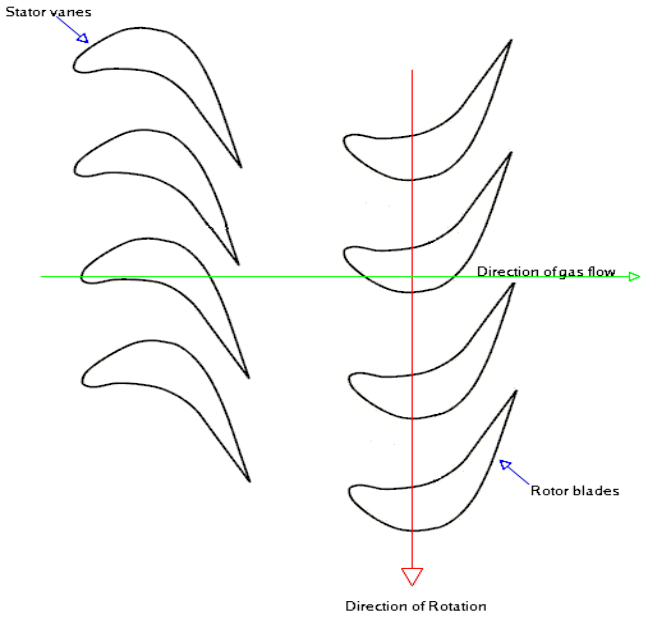

Figure 5.20: Axial Turbine Airflow Schematic

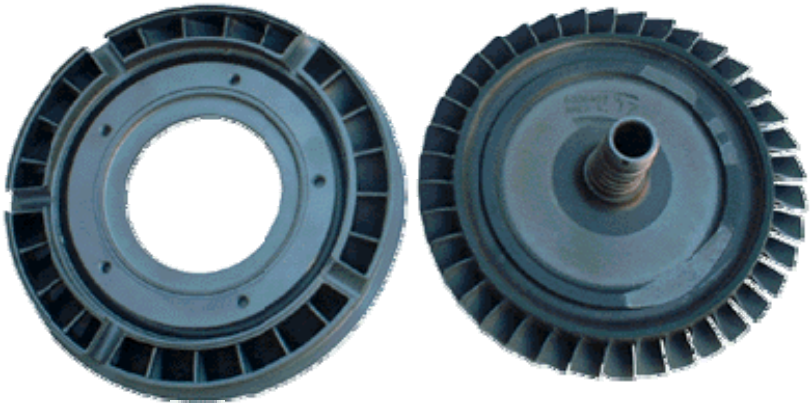

Figure 5.21: Allison Model 250 Axial Turbine[12]

The comparative design advantages of the axial turbine are a reduced frontal area, reduced inertia per stage, greater design speed flexibility for matching with the compressor, and easier manufacturing requirements when blade cooling is required.[14] The frontal area savings for axial versus radial turbines is greater than that of compressors due to the reduced gas density in the turbine section – a larger flow area is required to maintain subsonic flow velocities which would force the dimensions of a radial turbine to be much larger than desired in most cases. The main disadvantage of axial turbines lies in their inefficiency in handling small airflows due to increased blade tip losses.

Radial Turbine

The radial turbine, as depicted in Figure 5.22, closely resembles the design of the centrifugal compressor. Despite its main advantage of achieving a higher pressure ratio per stage, the radial turbine configuration has a limited scope of efficient design applicability because of the dimensional constraints previously mentioned for normal to high airflow engines. However, for lower airflow engines such as those often used in smaller rotorcraft, the radial turbine offers the potential for higher efficiency due to reduced blade tip clearance losses. Therefore, this configuration will be considered as a viable design alternative for modern turboshafts depending on the engine size requirements.

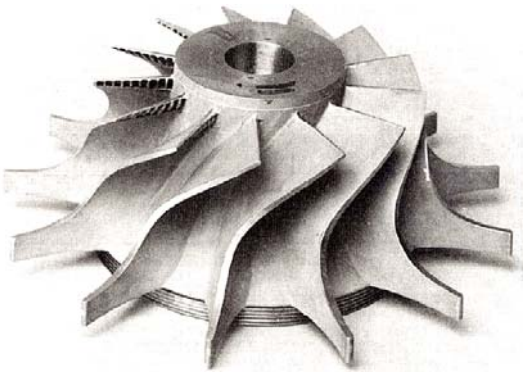

Figure 5.22: Typical Radial Turbine Design[14]

Exhaust

For most gas turbines used in aerospace applications, the exhaust system is designed as a nozzle – accelerating the exiting gas in order to produce some, or in many cases, all the vehicle's forward thrust. For most turboshaft engines, however, the role of the exhaust is reversed. Because the main rotor system of most helicopters provides all of the forward thrust capability, turboshaft engines are usually designed to maximize their shaft work output by converting as much of the kinetic energy in the turbine as possible. This design relationship dictates that the exhaust system is built for maximum diffusion in order to best support the production of shaft work.

Design Performance

The ideal exhaust system achieves an engine outlet pressure equal to ambient pressure. In reality, however, there are pressure losses that result between the turbine and the exit from friction and flow turbulence. This drop in pressure prevents the turbine from extracting the maximum work from the flow because the expansion must stop at a

pressure greater than atmospheric conditions. The following expression defines this exhaust pressure ratio (π_e):

$$\pi_e = \frac{p_{09}}{p_{05}} \qquad [5.17]$$

Where p_{09} is the total pressure at the exit – assumed to be equal to ambient pressure, p_a. Figure 5.23 provides an h-s diagram that depicts the loss in pressure between p_{05} and p_{09}. Also note that because the exit velocity of the flow is comparatively much lower than that of a nozzle, the static and total pressures are assumed to be equal at the exit. [1]

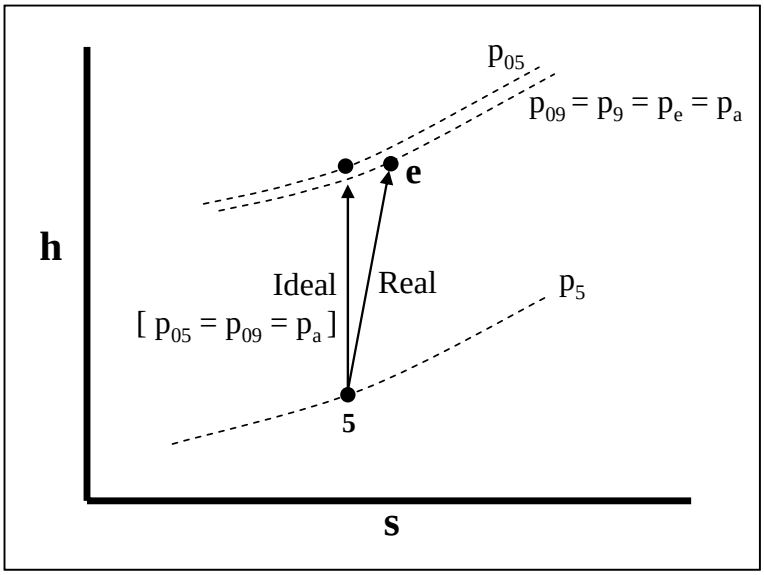

Figure 5.23: Ideal and Real Exhaust h-s Diagram

In order to reduce pressure losses in the exhaust duct, smooth walls and gradual curves should be incorporated into the design. A straight conical diffuser is the most efficient choice for engines with axial flow outlets, while elliptically-shaped ducts help to reduce losses for engines with radial flow outlets.[4] Typical exhaust pressure ratios for modern turboshaft engines range between 98-99%.

[1] Ronald D. Flack, *Fundamentals of Jet Propulsion with Applications* (New York, NY: Cambridge University Press, 2005).

[2] Nicholas Cumpsty, *Jet Propulsion* (New York, NY: Cambridge University Press, 2003).

[3] Jack D. Mattingly, *Elements of Gas Turbine Propulsion* (Reston, VA: AIAA, 2005).

[4] Headquarters, US Army Materiel Command, *AMC Pamphlet 706-201: Engineering Design Handbook: Helicopter Engineering, Part 1 – Preliminary Design* (Alexandria, VA: GPO, 1974).

[5] Joseph F. Alcock and J. Walter Smith, *Introduction to Gas Turbine Performance Analysis* (West Palm beach, FL: Pratt and Whitney Aircraft Group, 1979).

[6] Original image available from: http://commons.wikimedia.org/wiki/Image:Turboshaft_operation.png; Internet; accessed on 18 August 2006.

[7] Phillip G. Hill and Carl R. Peterson, *Mechanics and Thermodynamics of Propulsion* (Reading, MA: Addison-Wesley Publishing, 1992).

[8] Image available from: http://www.pilotfriend.com/training/flight_training/tech/jet_engine_components.htm, Internet; Accessed on 28 August 2006.

[9] Image available from: http://en.wikipedia.org/wiki/Image:Axial-flow-compressor.png, Internet; Accessed on 28 August 2006.

[10] Image available from: http://www.thaitechnics.com/engine/engine_type.html, Internet; accessed on 21 August 2006.

[11] Richard A. Leyes and William A. Fleming, *The History of North American Small Gas Turbine Aircraft Engine* (Reston, VA: AIAA, 1999).

[12] Image available from: http://members.cox.net/turbineyates/Allison250.htm, Internet; accessed on 23 August 2006.

[13] Jean Hourmouziadis and Horst B. Kreiner, "Advanced Component Development Design Basis for Next Generation Medium Power Helicopter Engines," *Helicopter Propulsion Systems: AGARD Conference Proceedings No. 302* (London, UK: Technical Editing and Reproduction, 1981).

[14] David J. H. Eames, "Turboshaft Engine Overview," *Rolls-Royce Presentation to University of Maryland Graduate Students*, 23 March 2006.

PART II

PROPULSION SYSTEM DESIGN AND ANALYSIS

CHAPTER 6

DESIGN PROCESS OVERVIEW

With the fundamental concepts of thermodynamics and gas turbine engines established, it is now time to focus on the design and analysis of the turboshaft engine as it relates to rotorcraft applications. The goal of this section is to outline a preliminary design methodology for the development of a propulsion system that is optimized for a specific set of operational constraints and performance requirements. Although every engine design problem is unique, the generic approach that follows is intended to be easily adaptable to a wide range of potential rotorcraft propulsion problems. Throughout this chapter, the engine design used on the Georgia Tech Generic Helicopter (GTGH) will be used as a working example to provide a consistent reference for the presented design methodology.

As depicted in Figure 6.1, the preliminary design loop begins with an analysis of the specific propulsion system requirements that were generated during the conceptual design phase for the overall vehicle. This set of requirements must be thoroughly evaluated in conjunction with mission and sensitivity analysis to develop an accurate framework for each subsequent step. Requirements analysis is an iterative process – continuously influenced by the overall vehicle sizing and performance estimate. As individual disciplines refine their analysis and update the baseline vehicle, propulsion system requirements must also adjust. Requirements analysis provides the input needed to conduct parametric and performance engine cycle analysis. During this process, the engine geometry and performance measures are defined and analyzed throughout the

entire flight envelope. Finally, a preliminary design of the engine's rotating components confirms if the solution is feasible. An engine design that meets all the requirements and feasibility checks can then be incorporated into the baseline vehicle. Iterations of this design loop continue until the propulsion system requirements converge and an optimized engine solution is determined.

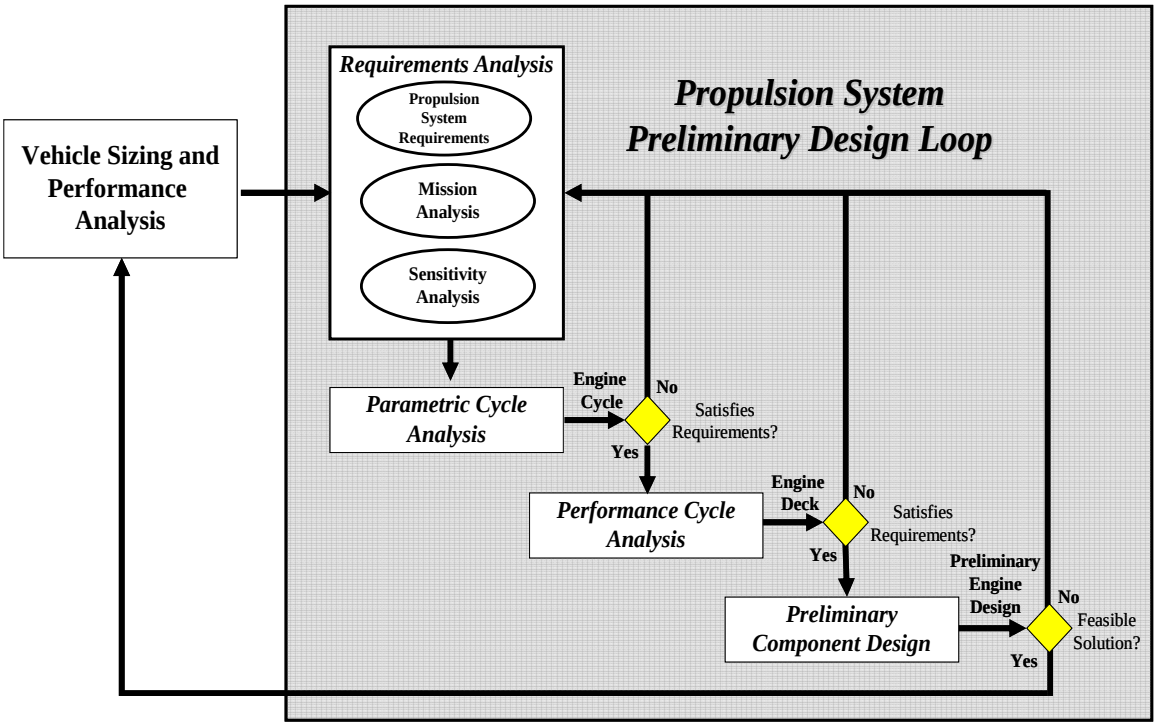

Figure 6.1: Integrated Propulsion System Design Methodology

CHAPTER 7

REQUIREMENTS ANALYSIS

In every case, the RFP serves as the driving force behind the design process – explicitly and, in most cases, implicitly identifying all of the requirements that must be met for a given proposal to be successful. Each explicit requirement outlined in the RFP must be clearly understood by the designer to ensure that the final solution will address each in sufficient detail. The most difficult challenge, however, is in identifying those requirements that are not specifically stated, but are nonetheless highly desired.

In his textbook *Engineering Design: A Materials and Processing Approach*, Dieter identifies four levels of customer requirements that should be met for a design to be successful: expecters, spokens, unspokens, and exciters. The first two categories are easily addressed – *expecters* are standard features that do not need to be specified and *spokens* are added features defined by the customer. The last two categories are much more elusive – *unspokens* are those attributes that the customer desires, but fails to define and *exciters* are those design features that make it unique and distinguish it from the competition.[1] Design competitions and design contracts are typically won and lost in these last two categories, with the "best" design achieving the optimum prioritization or balance of these implied requirements. Many design requests only provide a list of the minimum performance requirements or expectations. This promotes creativity – giving designers greater flexibility in determining their own optimum limits based on the competing demands of cost and performance within the context of their overall design.

Integrated Propulsion System Requirements

With a thorough understanding of the RFP, the preliminary sizing and performance analysis for the vehicle is completed utilizing a fuel balance, or R_f, approach – a process tightly coupled to the constraints of the propulsion system. As depicted in Figure 7.1, this method estimates the vehicle's installed power by simultaneously optimizing two design loops for a given vehicle sizing condition. The power loading loop produces a ratio of power available and power required while the gross weight loop produces a ratio of fuel available and fuel required. By iterating on both loops, an optimized solution for vehicle gross weight and power loading can be achieved when the fuel available equals the fuel required and the power available equals the power required.

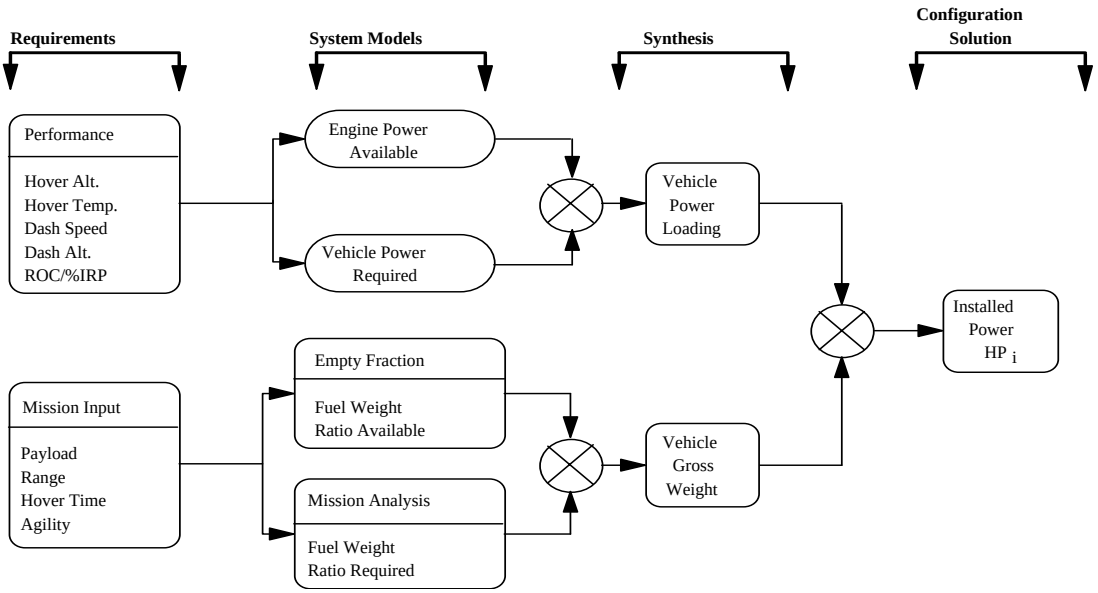

Figure 7.1: Preliminary Vehicle Sizing and Performance Estimation – R_f Method

Performance

While several propulsion system variables will ultimately determine the engine's final configuration, only two performance parameters prove to be critical during

preliminary vehicle sizing and performance analysis – power available and engine specific fuel consumption (SFC). From the propulsion perspective, these two variables indirectly account for the range, airspeed, payload, and hover capabilities of the overall vehicle.

The engine power available parameter estimates engine performance throughout a flight regime by incorporating the effects of temperature and altitude. Based on an initial assumption of power available at sea-level standard (SLS) for a given engine rating, the following expression is used:

$$HP_{Available} = HP_{Available\ (SLS)}\left(1 - 0.195h_1\right)\left(1 - 0.005\Delta T_S\right) \quad [7.1]$$

Where $h_1 = \frac{\text{Altitude}}{10000}$ and ΔT_S is the difference between "off" standard and standard temperature at the prescribed altitude (^oF).[2] Table 7.1 provides a list of the applicable engine ratings in accordance with current Federal Aviation Regulations (FAR). As a rule of thumb, the following equation estimates the "short duration" power available as a function of the operating time required ($\leq$ 30 minutes):

$$HP_{Short\,Duration} = HP_{MCP}\left(1 + 0.252e^{-0.0173t}\right) \quad [7.2]$$

Where t is the operating time required in minutes.[2] Based on the GTGH engine with an MCP rating of 154 HP at SLS, Figure 7.2 highlights the dramatic decrease in power available associated with high altitude and temperature conditions. Thus, as a design tool, Equations 7.1 and 7.2 are critically important in driving the conceptual engine design process because the engine must generate enough power to satisfy the power required for every flight condition stipulated in the RFP.

Table 7.1: Engine Power Ratings

Engine Rating		Time Limit
Maximum Continuous Power	MCP	Continuous
Takeoff Power	TOP	5 Min
One Engine Inoperative	OEI	Continuous
		30 Min
		2.5 Min
		2 Min
		30 Sec

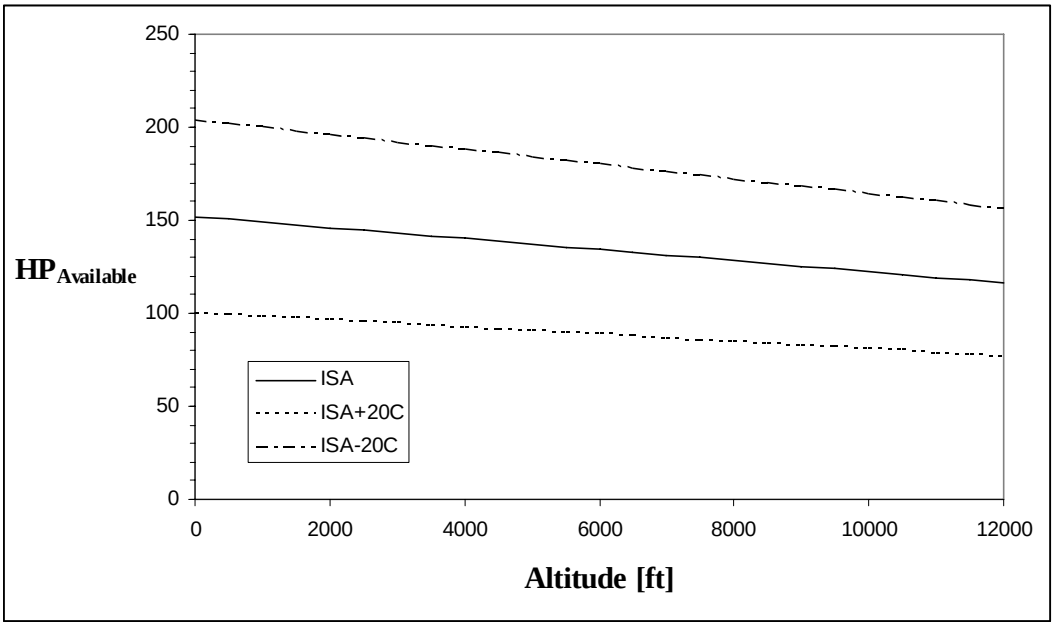

Figure 7.2: Power Available as a Function of Altitude and Temperature (GTGH)

The engine SFC, measured in lbs/hr/HP, has a significant influence on both the hover and range parameters used in the R_f method as it measures the overall efficiency of the propulsion system. Incorporating an accurate estimate of this parameter early in the conceptual design process greatly reduces the iterations required to reach an optimized solution and, thus, its importance cannot be overstated. The initial estimate for SFC depends on a number of factors: environmental conditions, engine power required, technology readiness levels, and partial power conditions. The altitude and temperature

can significantly effect an engine's operating efficiency as depicted in Figure 7.3, where SFC is shown to improve with increasing altitude and decreasing temperatures. In Figure 7.4, historical data shows that, on average, as the power output of an engine increases, so does its efficiency. Increased efficiency can also result from the use of advanced materials and improved manufacturing techniques – a direct function of the technology readiness level (TRL) and cost associated with a given design. Figure 7.5 shows historical improvements in SFC since the gas turbine was invented and while this plot depicts thrust specific fuel consumption (TSFC), it is still indicative of the trend in power SFC. Finally, the engine power condition associated with a given sizing criteria must be considered. If the engine is operating below its maximum power capability, the SFC will degrade primarily from the reduction in engine pressure ratio. Figure 7.6 depicts a typical relationship between engine power required and SFC at partial power settings.

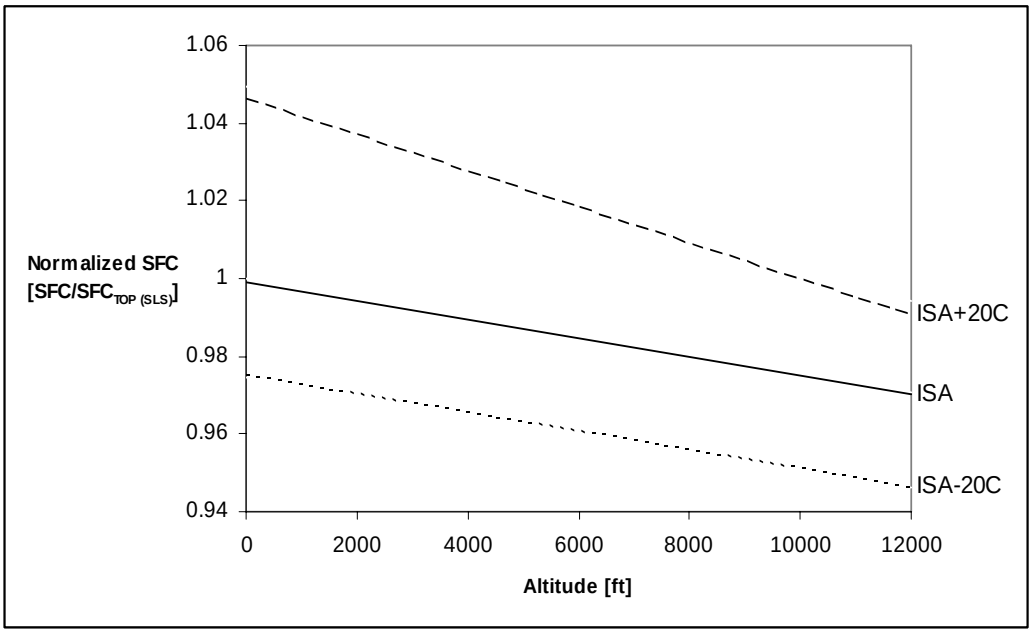

Figure 7.3: Engine SFC as a Function of Altitude and Temperature (Typical)

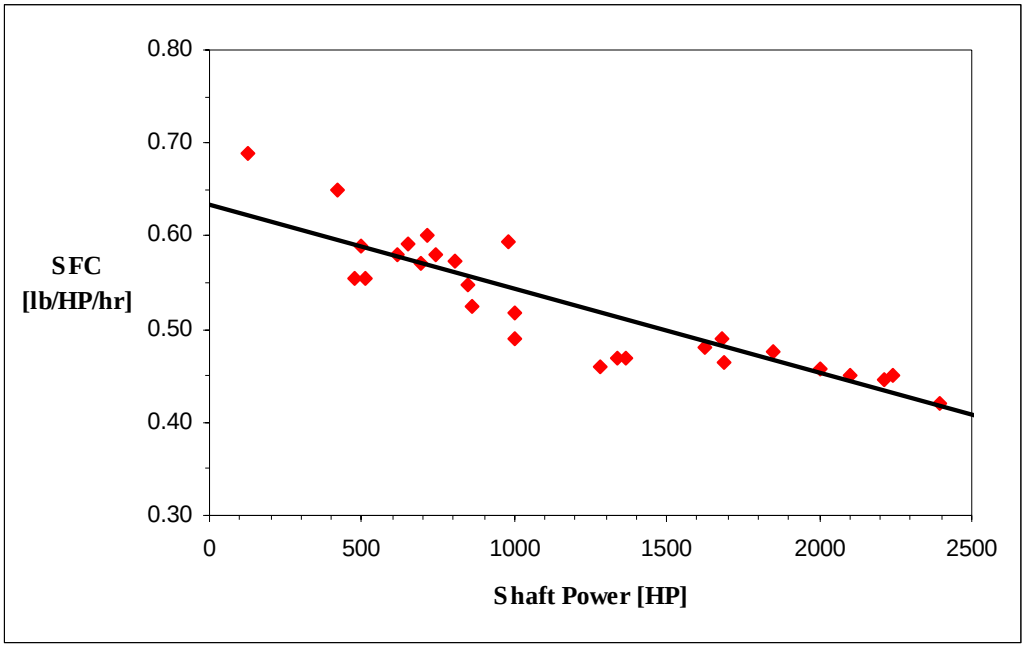

Figure 7.4: Engine SFC vs. Maximum Power Available[3]

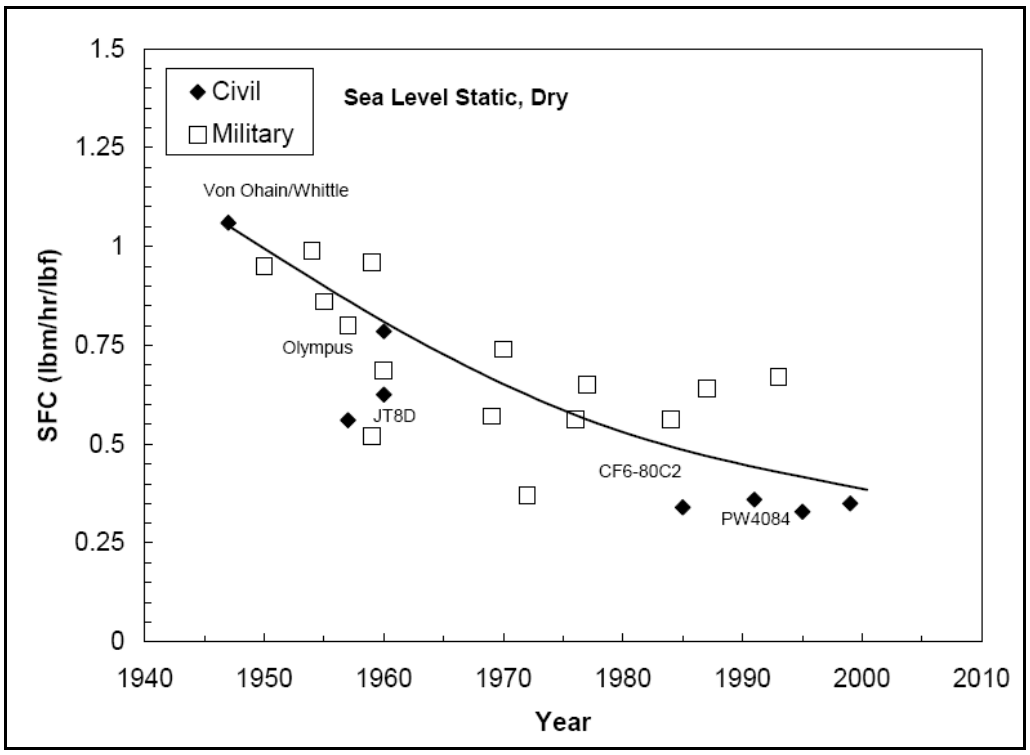

Figure 7.5: Historical SFC Improvements in Aircraft Engines[4]

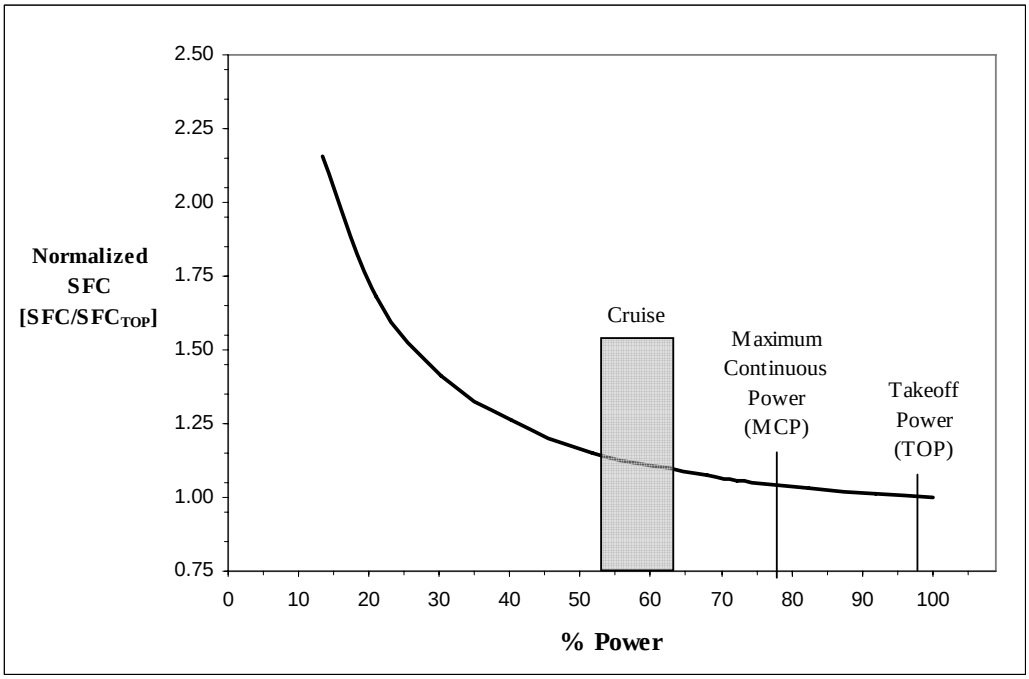

Figure 7.6: Engine SFC Degradation at Partial Power Conditions (Typical)

Geometric Constraints

In addition to the performance efficiency considerations, the RFP may also reference size limitations for the vehicle that will directly impact the propulsion system design. At this conceptual stage in the engine design process, geometric constraints for the length, width, and height of the engine cannot be addressed in any detail. However, by optimizing the engine weight as a function of power available, it becomes an integrated component in the R_f method and allows critical sizing requirements to be considered indirectly. The historical engine weight data presented in Figure 7.7 can be estimated using an exponential trendline as follows:

$$W_{engine} = 6.8916\left[HP_{installed}\right]^{0.5684} \qquad [7.3]$$

A correction factor can also be incorporated at the discretion of the design team based on the use of advanced technology design and lightweight materials that is not captured in the historical data analysis.

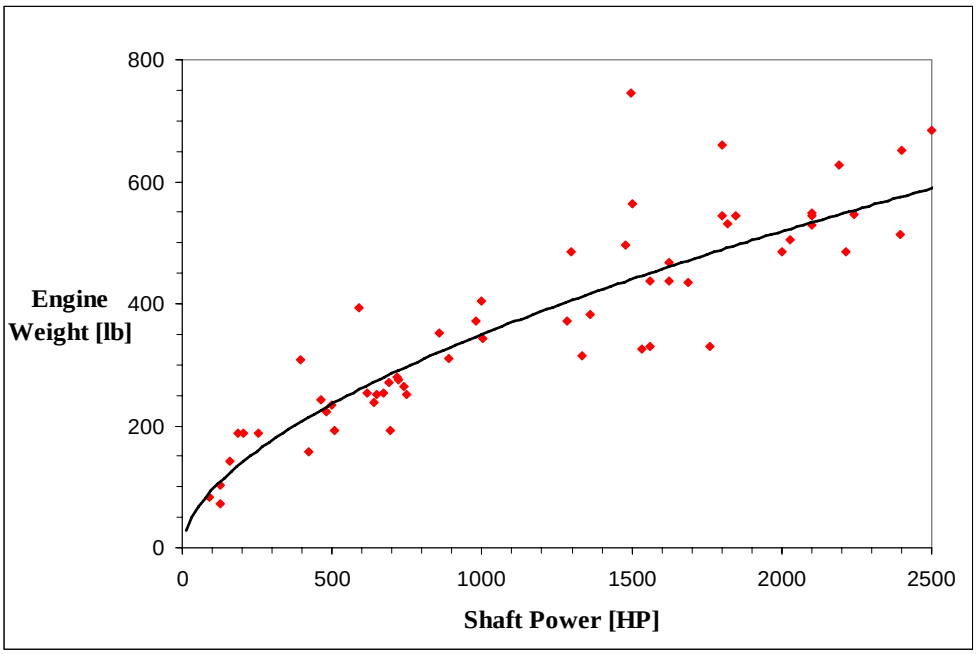

Figure 7.7: Engine Weight vs. Maximum Power Available[3]

Additional Factors

The RFP may stipulate additional design constraints which must be considered during the conceptual engine design phase such as cost limitations, emissions standards, noise signature, and technology readiness. For military applications, a low radar cross-section (RCS) and a low thermal signature may also be considered essential characteristics of the design. While most of these constraints are addressed in detail during the preliminary design stage, including them in the conceptual design phase is essential in avoiding the need for significant redesigns later in the process.

Mission Analysis

Mission analysis gives a realistic context for the engine performance and geometric requirements. For most design applications, requirements are usually presented in terms of minimal acceptable performance for each stand-alone metric. Mission analysis captures a broader view of the vehicle's performance by incorporating each of these individual metrics into an integrated mission scenario. These scenarios, or mission profiles, are an effective tool in defining the limits of a given design. They are essential in providing a realistic framework for mission accomplishment by creating a flight plan that exercises the maximum performance requirements of the vehicle – identifying the time period, altitude, temperature, and airspeed for each phase of a possible mission. In many cases, multiple mission profiles are required to adequately address all of the unique performance capabilities related to each specific mission application. For the GTGH, two training mission profiles were used – each identifying a different area of design emphasis. Figure 7.8 shows the mission profile for initial flight training – highlighting the need for hover efficiency and high altitude capability. Figure 7.9 shows the mission profile for advanced flight training – where range and forward speed capability are more prevalent.

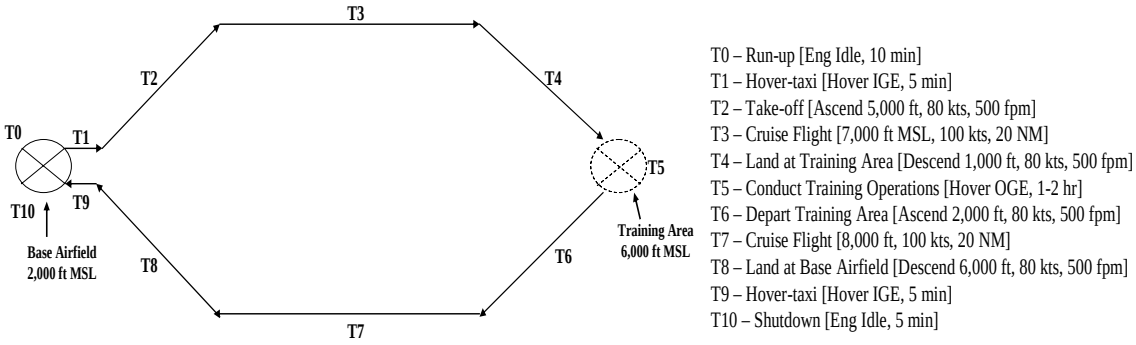

Figure 7.8: Initial Rotary-Wing Training Mission Profile

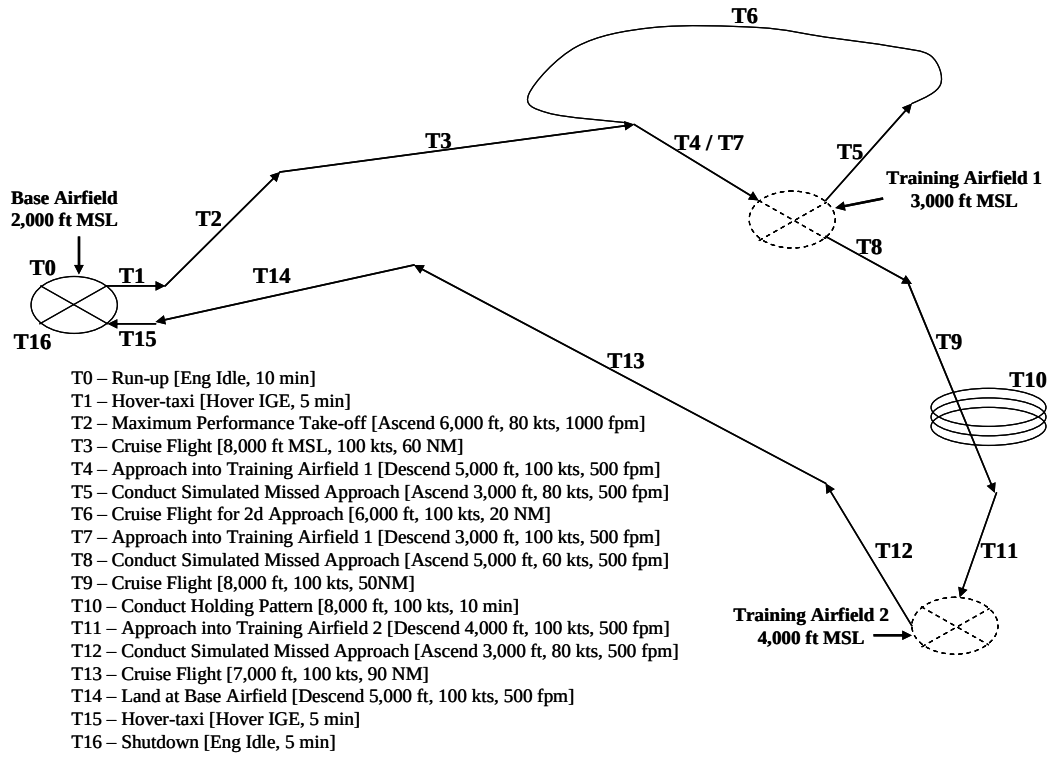

Figure 7.9: Advanced Rotary-Wing Training Mission Profile

With the mission profiles established, further mission analysis is possible by evaluating each scenario for fuel consumption as a function of the engine operating characteristics. This technique helps to refine the required fuel weight calculated during the preliminary sizing process by providing an instantaneous snapshot of typical fuel usage during a realistic mission timeline. Table 7.2 shows an example of the mission analysis results used for the GTGH initial rotary-wing training profile.

Table 7.2: Mission Analysis Results (GTGH)

	Mission Leg	Altitude [ft] Start	Altitude [ft] End	Airspeed [kt]	Rate of Climb/ Descent [FPM]	% Power Required [HP]	SFC [lb/hr/HP]	Time [min]	Dist [NM]	Fuel Burned [lb]	Fuel Remaining [lb]
T0	Run-up - Idle	2000	2000	0	0	25	0.79	5.0	0.0	3.0	137.0
	Run-up - 100% RPM	2000	2000	0	0	50	0.61	5.0	0.0	4.7	132.3
T1	Hover-taxi	2000	2000	5	0	75	0.52	5.0	0.4	6.0	126.3
T2	Climb-out	2000	7000	80	500	90	0.48	10.0	13.3	13.3	112.9
T3	Cruise	7000	7000	100	0	70	0.52	9.0	15.0	10.1	102.8
T4	Descent	7000	6000	80	-500	55	0.58	2.0	2.7	1.9	100.8
T5	Training Operations	6000	6000	0	0	80	0.50	46.0	0.0	56.6	44.2
T6	Climb-out	6000	8000	80	500	90	0.48	4.0	5.3	5.3	39.0
T7	Cruise	8000	8000	100	0	70	0.52	10.6	17.7	11.9	27.1
T8	Descend	8000	2000	80	-1000	50	0.60	6.0	8.0	5.5	21.6
T9	Hover-taxi	2000	2000	5	0	70	0.54	5.0	0.4	5.8	15.8
T10	Shutdown	2000	2000	0	0	25	0.79	5.0	0.0	3.0	12.8
							TOTAL	**112.6**	**62.8**	**127.2**	**12.8**
	Reserve Fuel Required	7000	7000	100	0	65	0.54	20.0	33.3	**21.5**	

Sensitivity Analysis

Sensitivity analysis provides useful information concerning the specific influence of each propulsion system design parameter. During the conceptual stage, these trade studies are essential in determining the design direction – providing justification for configuration selections and assumptions. The individual trade studies must be tailored to address the conflicting demands or design challenges for a given RFP. For example, Figure 7.10 depicts the effects of changing the engine SFC and the ratio of empty weight to gross weight (ϕ) in terms of range for the GTGH.

The goal of sensitivity analysis is to provide greater clarity in defining the requirements for a given project by testing the cause and effect relationships that exist between the key design parameters. Thorough consideration of the requirements and their interrelationships early in the design process will reduce the iterations needed to achieve an optimized solution. Sensitivity analysis is the final step in the requirements

analysis phase – delivering a clear definition of the minimum system performance goals that will successfully satisfy the RFP. For the propulsion system, specifically, a comprehensive understanding of the design goals for performance, size, and cost is essential in establishing a foundation for the thermodynamic cycle analysis to follow.

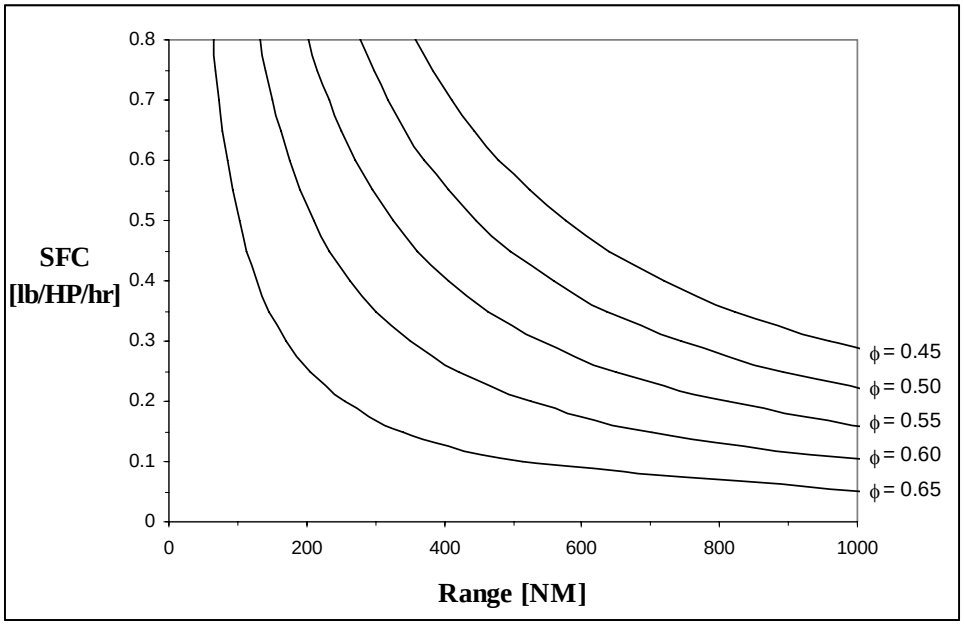

Figure 7.10: Range as a Function of Engine SFC and ϕ (GTGH)

---

[1] George E. Dieter, *Engineering Design: A Materials and Processing Approach* (Boston, MA: McGraw-Hill, 2000).

[2] Daniel P. Schrage, "Extension of R_f Method To VTOL Aircraft Conceptual and Preliminary Design," *AE6333 Rotorcraft Design I Course Notes* (Atlanta, GA: Georgia Institute of Technology, 2005).

[3] Data taken from: *Aviation Week and Space Technology* (January 17, 2005): 122-134.

[4] Dilip R. Ballal and Joseph Zelina, "Progress in Aero Engine Technology (1939-2003)," *AIAA Paper 2003-4412* (July 2003).

CHAPTER 8

PARAMETRIC CYCLE ANALYSIS

With the propulsion requirements sufficiently analyzed, the engine design process now considers the optimization of a thermodynamic cycle to achieve the desired results. This stage – known as parametric, or design point, engine cycle analysis – estimates the propulsion system performance parameters in terms of design limitations, flight conditions, and design choices. At this point in the engine's development, it is considered to be a "rubber" engine whose size and performance characteristics are scaleable to meet the particular mission requirements.[1] Before analyzing the thermodynamic characteristics of the engine, though, several key selections must be addressed in order to properly define the cycle analysis starting point.

Engine Configuration Selection

The basic turboshaft engine configuration must be selected in terms of the number of shafts to be used. The simplest version is the single-spool, or coupled, engine which employs a single shaft connection between the turbine and compressor sections. The shaft power in excess of that required to operate the compressor is available to power the helicopter. The second, and most common, version of the turboshaft engine is the dual-spool, or free turbine, engine which utilizes two shafts to separate the power extraction between the gas generator section and the power turbine section. The gas generator turbine extracts only enough power to drive the compressor while the power turbine

extracts the remaining power on a separate shaft to operate the vehicle. This physical separation between the gas generator and the power turbine prevents the transfer of any sudden detrimental loading conditions that could adversely effect engine operation. When higher compressor pressure ratios are required, a three-spool turboshaft may be appropriate. This configuration uses concentric shafts from two separate turbine sections to power two independent compressor sections, with a third shaft used to extract the excess power from the final turbine. Figure 8.1 provides a diagram highlighting the architectural differences between each engine design.

The key advantage of multi-shaft engine applications is an increase in operational flexibility over the single-spool engine design. This results from the ability to optimize the speed of the compressor section(s) independent of the required speed for the helicopter's rotor system – allowing for increased efficiency and more favorable pressure ratios and turbine inlet temperatures.[2] With each added shaft, the engine design flexibility further increases – providing the potential for greater performance optimization. However, the penalty for these benefits is an increase in engine complexity and weight. Thus, for applications in which the manufacturing cost and engine weight are exceptionally more important than performance, the single-spool engine may represent the best design alternative.

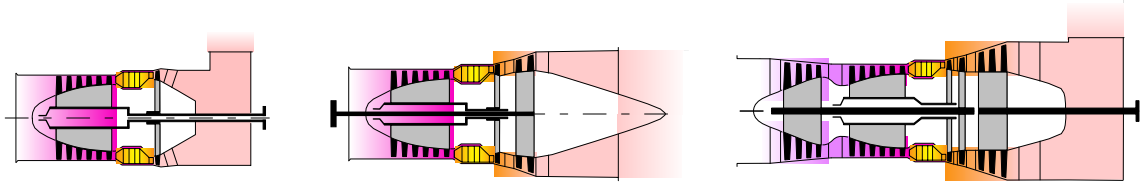

(a) Single-spool **(b) Dual-spool** **(c) Three-spool**

Figure 8.1: Engine Configuration Comparison[3]

Design Point Selection

The design point for a given engine typically represents the point in its required operational envelope that either is the most demanding, the most prevalent, or both – and, thus, is the most important point from an optimization perspective. Determining this point, however, is not a trivial exercise. It is often best to consider a few of the most demanding and/or most prevalent operating conditions in order to identify the trends that will ultimately drive the design to an optimized solution. Modern engine analysis computer codes allow for instantaneous assessments of these trends across a wide spectrum of operating conditions – ensuring that the most restrictive conditions are selected for optimization. In some cases, a design compromise is necessary to balance the competing demands of multiple operating conditions.

For the GTGH project, the design point was comparatively assessed between hover performance and forward airspeed requirements. Ultimately, the hover performance requirement, which called for hover out-of-ground effect power at an altitude of 6,000 feet and ISA+20^{o}C atmospheric conditions for a period of 2 hours, proved to be the most restrictive design point for optimization. Not only did it represent an extremely demanding flight condition for a small helicopter, but its lengthy time requirement dictated that the engine operate at or below its maximum continuous power setting.

Engine Cycle Selection

With the prerequisite information determined in terms of performance requirements, engine configuration, and operating conditions, the design of a specific

turboshaft engine that will best perform the mission can now commence. GasTurb 10, a commercially available engine performance simulation software package, provides a one-dimensional, steady-flow analysis tool that simplifies the selection of each propulsion system performance parameter. At this point in the design process, each component functions as a black box – achieving a predicted level of performance based on assumptions that are independent of its internal geometry. However, in the case of the compressor and turbine, an initial configuration selection should be made in order to capture the operating efficiency differences between axial and radial designs.

Component Efficiencies

GasTurb 10 simulates engine performance by evaluating the "real" Brayton Cycle – accounting for the non-ideal component efficiencies and losses. Table 8.1 provides a summary of the polytropic component efficiencies and pressure losses as a function of their appropriate level of technology. Since this table only addresses axial compressors and turbines, a reduction of 4-5% is considered appropriate for the use of radial turbomachinery.

Table 8.1: Component Technology Level Assumptions[1]

			Level of Technology			
Component	Figure of Merit	Type	1 (1945-1965)	2 (1965-1985)	3 (1985-2005)	4 (2005-2025)
Diffuser	$\pi_{d\,(max)}$	Nacelle	0.90	0.95	0.98	0.995
		Internal	0.88	0.93	0.96	0.97
Compressor	η_{pc}		0.80	0.84	0.88	0.90
Burner	π_{b}		0.90	0.92	0.94	0.96
	η_{pb}		0.88	0.94	0.99	1.00
Turbine	η_{pt}	Uncooled	0.80	0.85	0.89	0.91
		Cooled		0.83	0.87	0.89
Maximum T_{04}		(^{o}R)	2000	2500	3200	3600

Parametric Studies

Parametric cycle analysis compares the performance characteristics of engines with different geometries that are defined by a unique set of propulsion system design variables. During this design stage, the size of the engine is completely arbitrary and can be scaled photographically to meet the power demands of the mission. Although every design parameter plays a role in the definition of a specific engine cycle, some are clearly more influential than others. For most turboshaft engine applications, the compressor pressure ratio and turbine inlet temperature represent the most critical design parameters and, thus, serve as the starting point for parametric study. Parametric analysis also utilizes "specific" terms or ratios to define the engine performance metrics – eliminating some of the effects of engine size. For example, specific fuel consumption and specific power use ratios of fuel flow per horsepower and horsepower per mass flow rate, respectively.

Pressure Ratio and Turbine Inlet Temperature Effects

Using the component technology level assumptions listed in Table 8.1, a parametric study can be performed by graphically analyzing the effects of the critical design parameters. Figure 8.2 provides an example carpet plot created using GasTurb10 for the GTGH project – comparing the effects of compressor pressure ratio and turbine inlet temperature on engine SFC and specific power. Varying the compressor pressure ratio from 2:1 to 10:1 and the turbine inlet temperature from 1600^{o}R to 2600^{o}R, the trends clearly show that increasing both factors has a favorable influence on engine performance. However, it is also evident that there are distinct points of diminishing returns for each parameter. Specifically, at pressure ratios above 7:1 and temperatures

above 2300°R, the relative reduction in engine SFC is greatly reduced. In terms of specific power, the higher pressure ratios considered in this analysis also provide minimal benefits, whereas, higher turbine inlet temperatures clearly demonstrate a positive effect in consistently extracting greater work from a given flow.

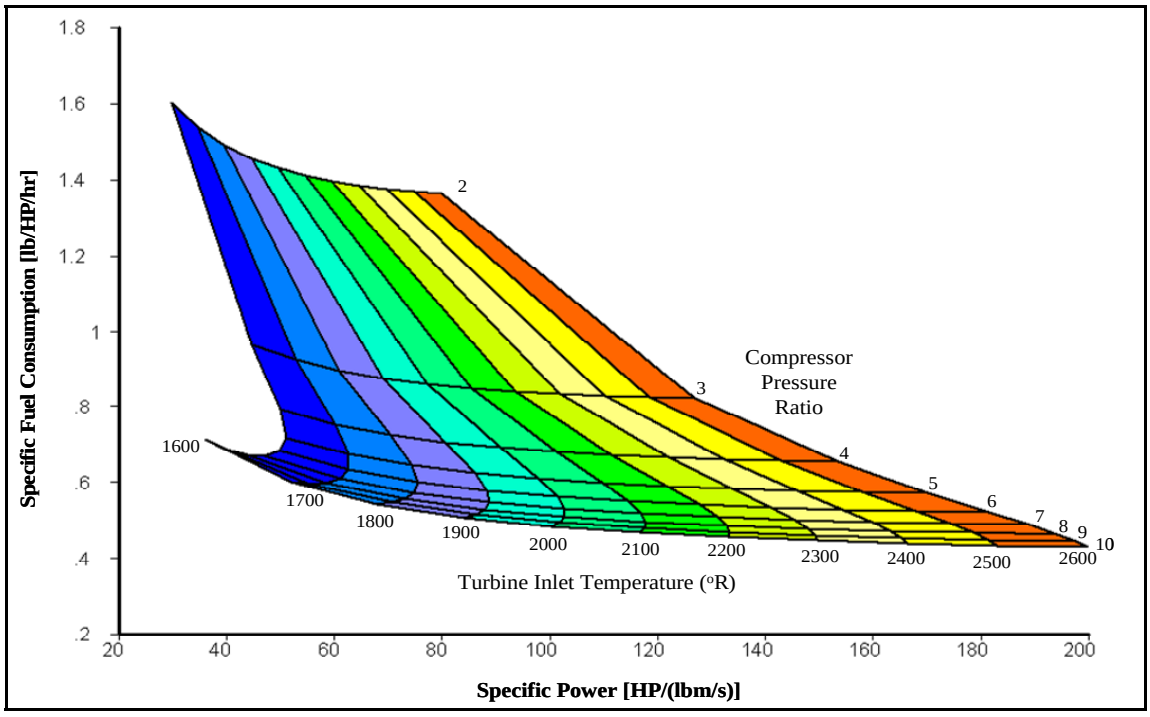

Figure 8.2: Design Point Parametric Analysis (GTGH)

Turbine Cooling Effects

The benefits of increasing turbine inlet temperatures do not come without penalty, however, because at temperatures above approximately 2300°R, or 1278°K, the turbine blades require cooling airflow to maintain their material integrity. In most modern engines, the cooling air is extracted at the exit of the compressor and delivered to the turbine blades through a series of ducts. Three different methods of blade cooling are utilized: convection, film, and transpiration. In convection cooling, the air is pumped into the blade at the root and cools the blade by conduction from its inner surface. Film

cooling forces the cool air out of a series of injection holes on the blade, particularly along its leading edge, to form a protective barrier between the blade and the high-temperature gas from the combustor. Transpiration cooling uses a mesh-type surface on the blade to allow the cooling air to disperse more uniformly – simultaneously cooling the blade and providing a protective barrier.[4] In some cases, a combination of more than one of these cooling techniques is used. Figure 8.3 highlights the relationship between the turbine blade cooling method and the turbine inlet temperature as a function of the level of technology.

A major consideration in the use of turbine blade cooling is the increased design complexity. Turbine cooling is an expensive design alternative due to the manufacturing difficultly associated with blades that contain internal passages and the added challenge of delivering cooling air to the blades from the compressor with minimal losses. Therefore, a parametric study is required to evaluate the engine performance benefits versus the increased cost. In order to estimate the amount of cooling bleed flow required to effectively cool the turbine blades for a given turbine inlet temperature, the turbine cooling algorithm described in NASA Technical Manual 81453 is used (See APPENDIX B).[5] This algorithm is based on the cooling effectiveness factor (E) defined by the following expression:

$$E = \frac{T_g - T_m}{T_g - T_c} \qquad [8.1]$$

Where T_g is the gas temperature, T_m is average metal temperature, and T_c is the cooling air temperature. Figure 8.4 shows the relationship between the cooling effectiveness factor and turbine inlet temperature.

For the GTGH, a trade study was conducted using GasTurb 10 to highlight the performance benefits of increasing the turbine temperatures from 2400-3600^{o}R. Figure 8.5 shows the results of this analysis – identifying a minimum SFC at 3000^{o}R and a consistent increase in specific power with higher temperatures. Since the power output requirements for a small training helicopter were relatively less important than its overall operating efficiency, the specific fuel consumption metric was used as the primary performance indicator. The results showed that the cooled blade achieved an improvement in SFC of less than 2% compared to that of an uncooled blade. This minor improvement in performance did not outweigh the cost of increased design complexity and manufacturing difficulty for the small engine of the GTGH – thus, an uncooled configuration was selected. In applications that require high power availability, however, turbine blade cooling offers a well suited alternative as the higher turbine inlet temperatures translate into significant specific power increases.

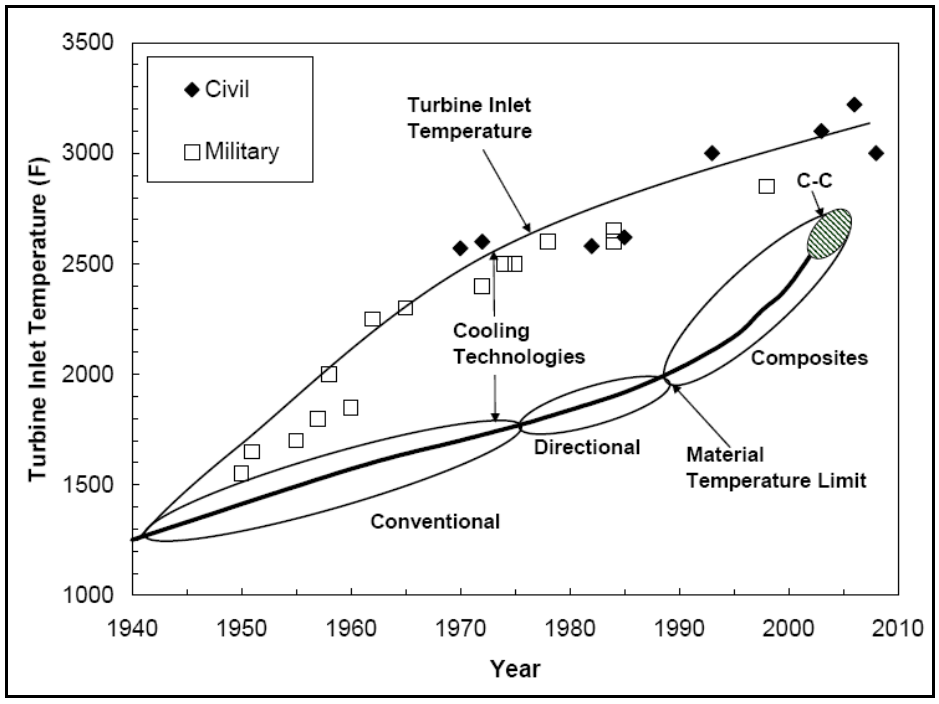

Figure 8.3: Turbine Cooling Technology Assessment[6]

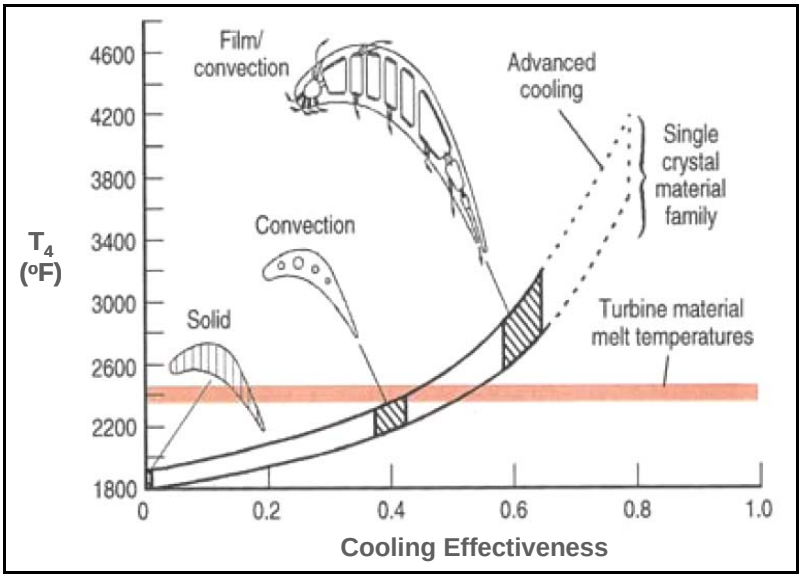

Figure 8.4: Turbine Cooling Effectiveness[7]

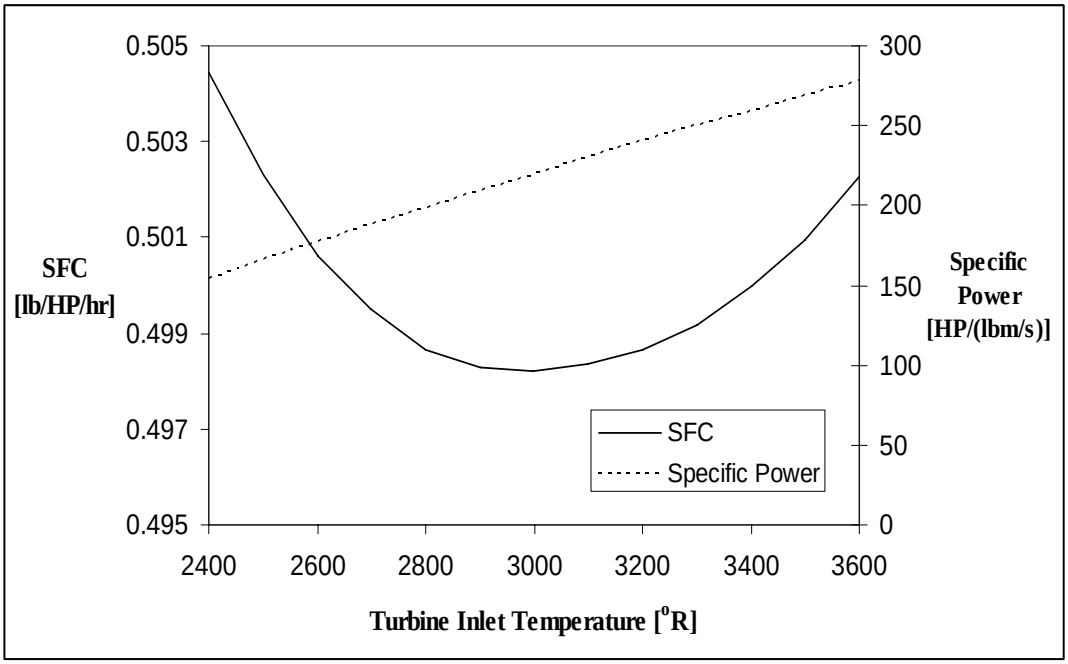

Figure 8.5: Turbine Cooling Trade Study (GTGH)

Integrated Parameter Selection

The final step in parametric engine analysis is to select the design parameters that optimize the engine's performance for a given configuration at the critical design point. This is an iterative process – as each individual design discipline updates the baseline vehicle, the preliminary sizing and performance estimates change – directly influencing the propulsion system requirements. GasTurb 10 provides a valuable tool in automating this iterative process. The component efficiency assumptions and parametric study results are easily integrated into an engine cycle solution for a given power requirement by using the optimization feature. This option in GasTurb 10 allows the user to define ranges for each design variable, establish constraints, and provide a target metric for the optimization function. In completing this step, the key values of airflow, pressure ratio, turbine inlet temperature, and power output are established and, thus, the geometric characteristics of the engine are sufficiently defined.

---

[1] Jack D. Mattingly, William H. Heiser, and David T. Pratt, *Aircraft Engine Design* (Reston, VA: AIAA, 2002).

[2] Headquarters, US Army Materiel Command, *AMC Pamphlet 706-201: Engineering Design Handbook: Helicopter Engineering, Part 1 – Preliminary Design* (Alexandria, VA: GPO, 1974).

[3] Images available from: http://www.gasturb.de/Products/GasTurb/Power_Generation/power_generation.html, Internet; Accessed on 13 September 2006.

[4] Ronald D. Flack, *Fundamentals of Jet Propulsion with Applications* (New York, NY: Cambridge University Press, 2005).

[5] James W. Gauntner, "Algorithm for Calculating Turbine Cooling Flow and the Resulting Decrease in Turbine Efficiency," *NASA Technical Memorandum 81453 (*Cleveland, OH: Lewis Research Center, 1980).

[6] Dilip R. Ballal and Joseph Zelina, "Progress in Aero Engine Technology (1939-2003)," *AIAA Paper 2003-4412* (July 2003).

[7] Bernard L. Koff, "Gas Turbine Technology Evolution – A Designer's Perspective," *AIAA Paper 2003-2722* (July 2003).

CHAPTER 9

PERFORMANCE CYCLE ANALYSIS

With the engine sized for a single reference point, it is necessary to determine its performance characteristics when operating at off-design conditions. In performance cycle analysis, the engine design choices have been selected and the performance of a specific reference point engine must be determined at all possible operating conditions throughout a vehicle's flight envelope.[1] The goal of this analysis is to develop a complete engine deck that describes the power production, fuel burn rate, and SFC as a function of altitude, airspeed, temperature, and throttle setting. These results can then be incorporated into the mission analysis model to provide a more accurate assessment of the overall propulsion system integration.

Engine Operational Envelope

The operational envelope for rotorcraft vehicles is significantly different in comparison to that of fixed-wing aircraft. Helicopter operations are much more limited by the detrimental aerodynamic effects of reduced air density at higher altitudes and the onset of retreating blade stall during high velocity flight. Rotorcraft operating altitudes are also limited by the available level of oxygen supply for pilots. FAA Regulations stipulate that all aircraft crewmembers operating above 14,000 feet altitude, or above 12,500 feet altitude for a period of more than 30 minutes, must have supplemental oxygen available. Maximum level-flight airspeeds for helicopters are limited to

approximately Mach 0.25 (or 165 knots at SLS) due to the aerodynamic limitations of the rotor system. Rotorcraft engines often operate at high power settings without any forward airspeed and must also accommodate sideward and rearward flight regimes. Based on these unique requirements, the engine operational envelope must be tailored to meet the demands of a particular design. For the GTGH, an altitude range from sea-level to 12,000 feet and an airspeed range from hover to Mach 0.2 (132 knots at SLS) was selected as the appropriate engine operating conditions for a small training helicopter.

Off-Design Analysis

While GasTurb 10 was used to complete the parametric cycle analysis, a more detailed engine analysis program known as the NASA Engine Performance Program (NEPP) is used for performance cycle analysis. This program, originally developed and used as the primary aircraft engine analysis tool at the NASA-Lewis Research Center, utilizes a FORTRAN based code to calculate 1-dimensional, steady-state thermodynamic performance for gas turbine engines.

Engine Model

As depicted in Figure 9.1, the NEPP engine model consists of a series of components linked by station properties that describe the flow at the entrance and exit of every component. The individual properties of each physical component are included in the input code – ensuring that the engine is properly arranged to model the desired flowpath. The NEPP input file also includes non-physical components which are used to control, optimize, limit, and schedule engine variables.[2] Finally, the user defines the

appropriate flight conditions to capture the engine's performance characteristics throughout its entire operational envelope (See APPENDIX C for the GTGH NEPP engine model).

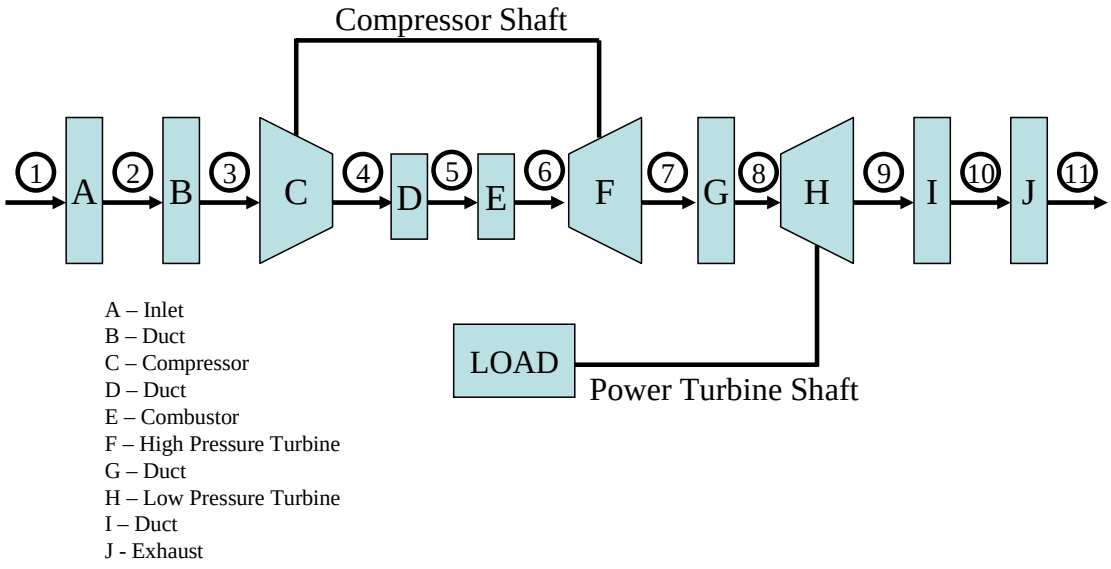

Figure 9.1: NEPP Engine Model (GTGH)

Component Performance

The off-design analysis in NEPP requires the use of "maps" to better describe the thermodynamic performance of each individual component over its actual range of operation.[1] Accurate definitions of these component maps represent the "secret recipes" of the propulsion industry; and, consequently, are highly proprietary in nature and difficult to acquire for any current or future levels of component technology. For preliminary design, however, the tools and methods described in this section provide enough accuracy to generate reasonable performance cycle analysis results.

Dimensional Analysis

Before addressing the individual component performance maps, it is important to understand that dimensionless quantities are typically used for the correlating parameters

to increase the applicability of the data to multiple conditions.[1] Pressure and temperature are made dimensionless at any station *i* by dividing by their SLS values as follows:

$$\delta_i = \frac{p_{0i}}{p_{std}} \quad [9.1]$$

$$\theta_i = \frac{T_{0i}}{T_{std}} \quad [9.2]$$

Where p_{std} = 14.696 psi and T_{std} = 518.69°R. Two "corrected" parameters for mass flow rate and rotational speed are also used to describe engine performance. The corrected mass flow rate and corrected engine speed at any station *i* are defined as:

$$\dot{m}_{ci} = \dot{m}_i \frac{\sqrt{\theta_i}}{\delta_i} \quad [9.3]$$

$$N_{ci} = \frac{N}{\sqrt{\theta_i}} \quad [9.4]$$

Where N is the engine rotational speed.

Compressor Maps

Compressor performance maps typically describe the off-design adiabatic efficiency of the individual component as a function of pressure ratio, corrected mass flow rate, and corrected engine speed. GasTurb 10 produces a scaled axial compressor map based on a given engine cycle. Figure 9.2 shows an example of this output used during the compressor configuration trade study for the GTGH with the operating line highlighted in yellow. The stall, or surge, line indicates the maximum performance measure for the compressor – steady operation above this line is impossible and even momentary excursions beyond it are considered dangerous for the engine and the aircraft.[1] The distance between the stall line and the operating line is known as the surge

margin. GasTurb 10 is a powerful tool in generating compressor performance maps, however, it is somewhat limited in it applicability to turboshaft engines. First, the program is only capable of estimating axial compressor configurations. Second, the resulting component map must be manually converted to the proper input file format for NEPP, an extremely tedious and time consuming process.

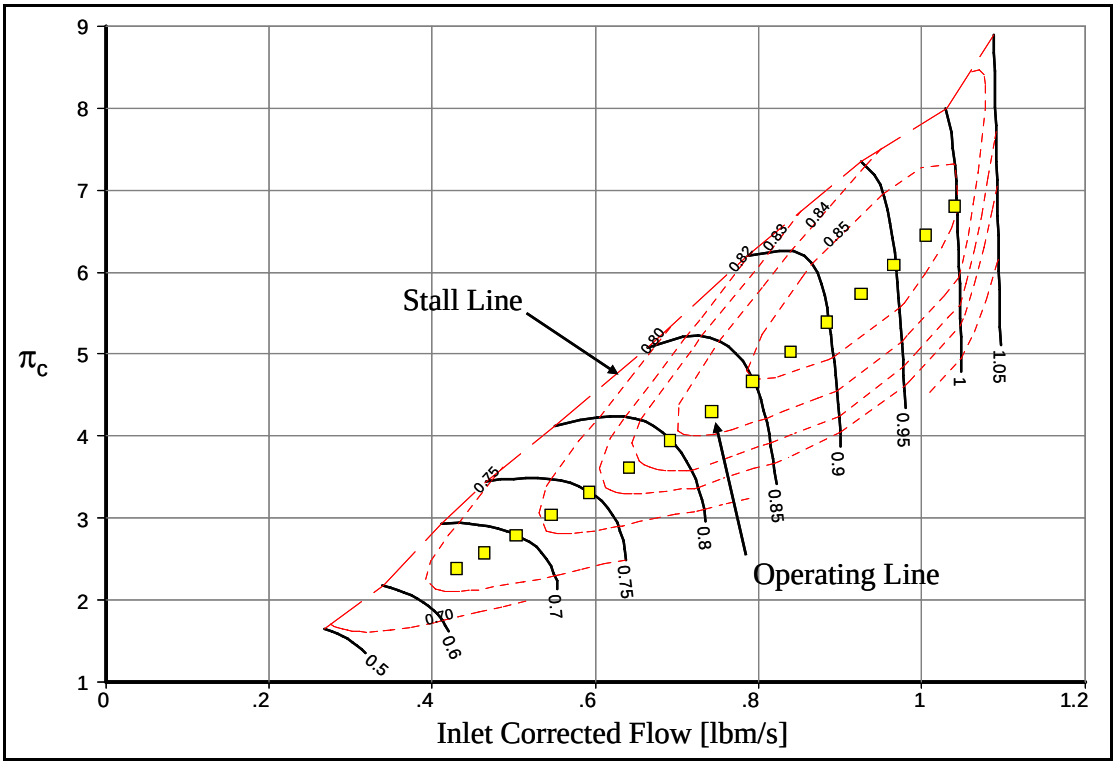

Figure 9.2: Axial Compressor Performance Map (GTGH)

Compressor performance maps can also be presented as a combination of two separate graphs – depicting the efficiency and pressure ratio as a function of corrected speed and corrected flow. Figure 9.3 shows the performance map used for the centrifugal compressor stage on the GTGH – highlighting the tendency for radial compressors to exhibit more consistent performance over a wide range of mass flow rates for a given rotational speed.

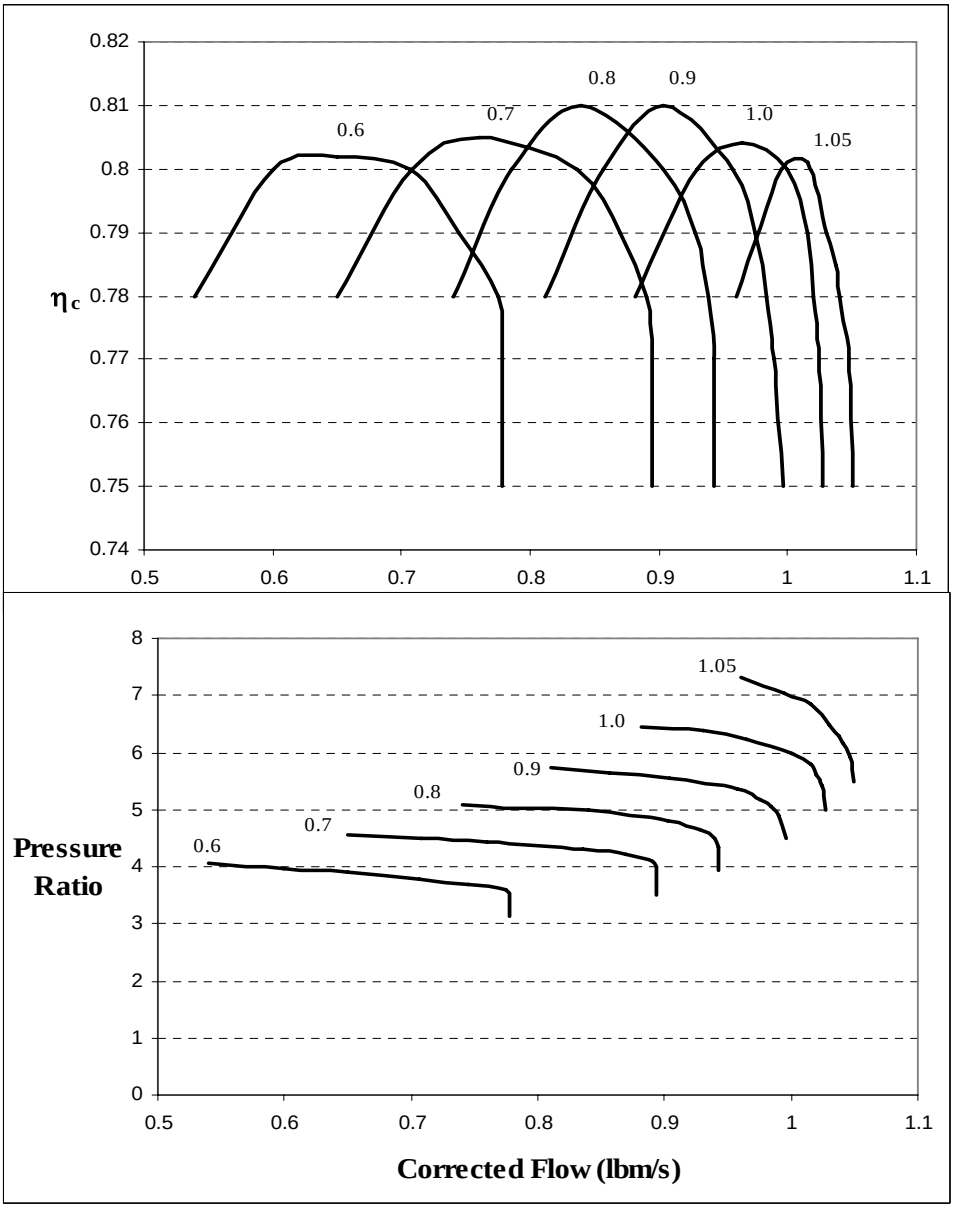

Figure 9.3: Centrifugal Compressor Performance Map (GTGH)

Combustor Maps

Although combustor section performance maps are commonly used to describe off-design performance, the assumption of a constant level of combustion efficiency and pressure loss is considered adequate for the preliminary design stage.

Turbine Maps

Turbine performance maps typically use the same parameters as those used on compressor maps: total pressure ratio, adiabatic efficiency, corrected mass flow, and corrected rotational speed. The performance of a turbine is similar to that of a choked nozzle in terms of pressure ratio versus corrected mass flow – the mass rate is only slightly affected by the rotational speed.[3] Turbine efficiency, while still a function of rotational speed and pressure ratio, remains relatively constant when compared to the performance of a compressor. Additionally, due to the favorable pressure gradient in the turbine, the stall region is not a significant factor.[4]

GasTurb 10 produces scaled turbine maps with the same axial configuration limitation that applied to compressor maps. The requirement to manually convert the maps to the proper format for NEPP, however, is not applicable for the turbine section. A NASA program, the Extended Parametric Representation of Turbines (PART), reproduces the maps in the proper NEPP format using the input data from GasTurb 10.[5] Figures 9.4 and 9.5 show the high pressure turbine (HPT) and low pressure turbine (LPT) performance maps, respectively, that were calculated using GasTurb 10 for the GTGH.

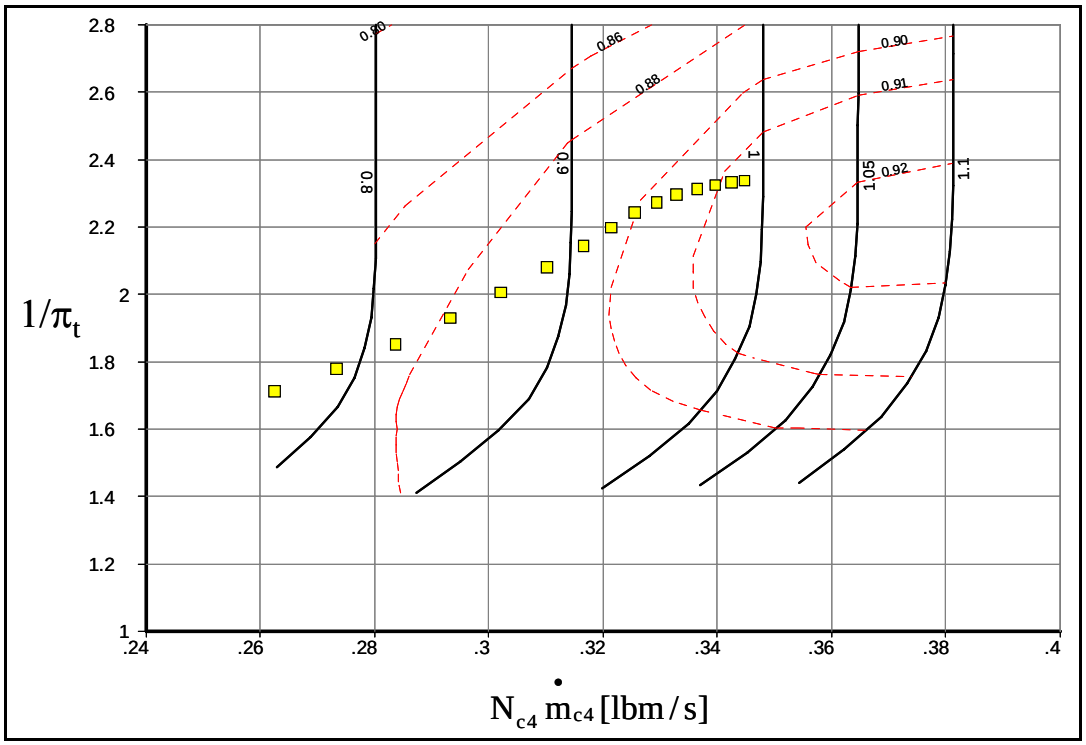

Figure 9.4: High Pressure Turbine Performance Map (GTGH)

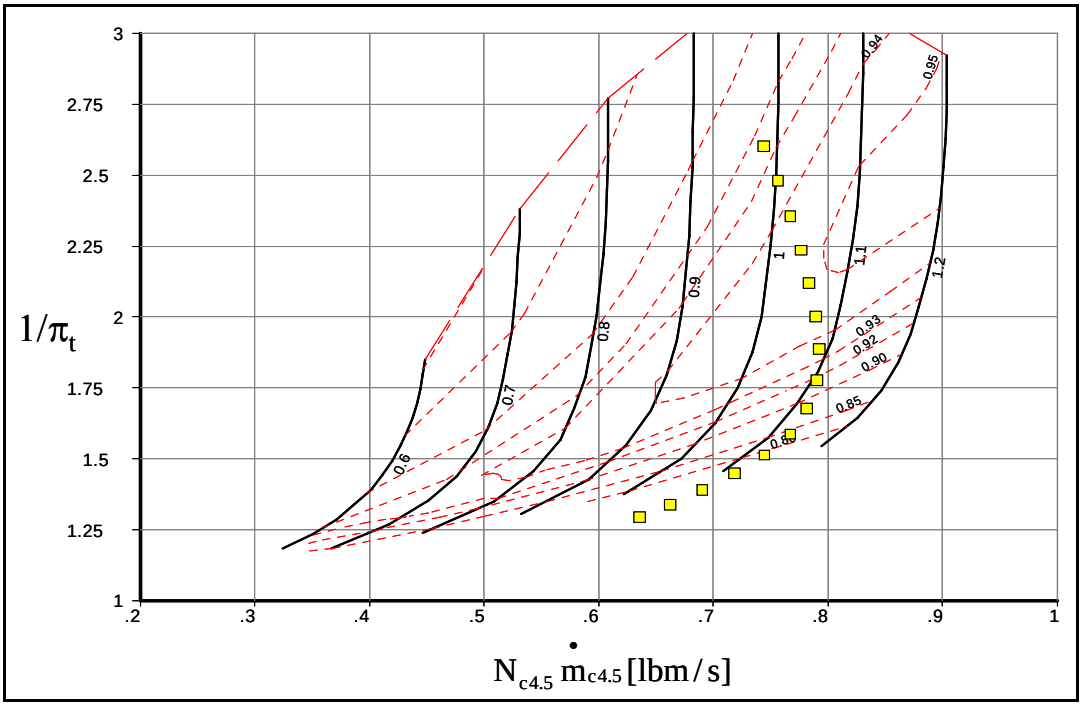

Figure 9.5: Low Pressure Turbine Performance Map (GTGH)

Performance Analysis Results

With the component performance maps defined and integrated into NEPP, the performance cycle analysis is performed by systematically evaluating the engine cycle throughout the entire flight envelope by varying the temperature, altitude, and Mach number. Additionally, the engine's partial power performance is addressed by simulating a complete range of throttle settings by controlling the turbine inlet temperature at a constant rotational speed. As previously mentioned in the parametric cycle analysis section, the process of conducting performance cycle analysis is equally iterative in nature. The vehicle sizing and performance analysis must be continually refined and updated to reflect the changing engine performance characteristics and vice versa until a final optimized solution is achieved. Figure 9.6 and Table 9.1 summarize the engine layout, specifications, and performance for the GTGH. Figures 9.7 – 9.10 provide the engine deck data representative of the final iteration of performance cycle analysis.

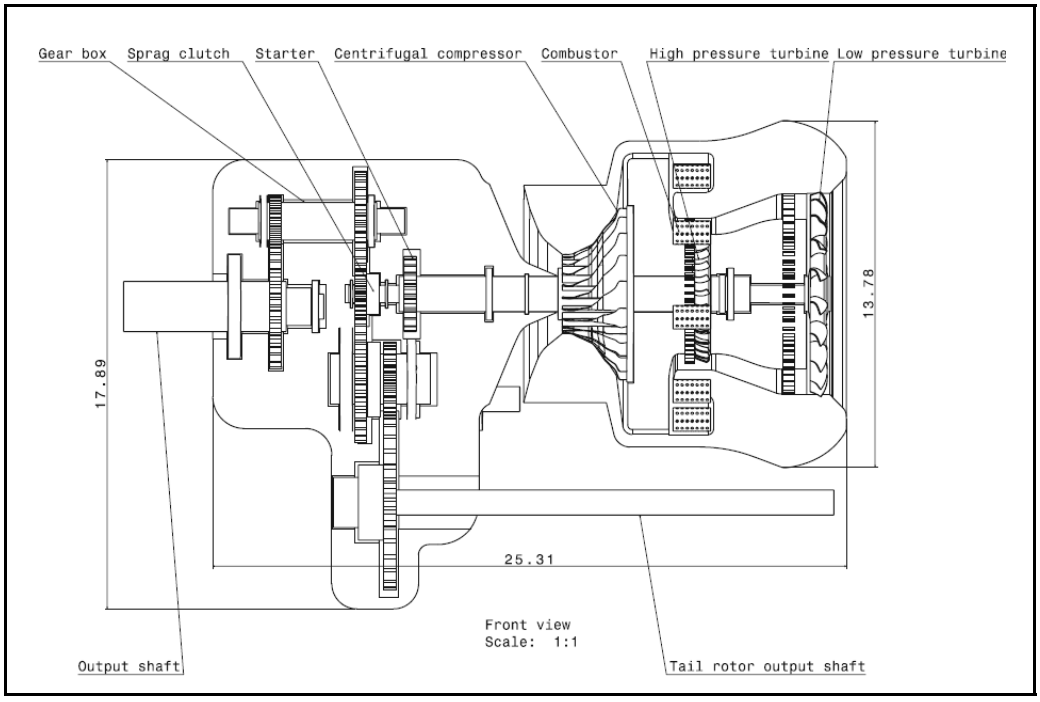

Figure 9.6: Engine Schematic (GTGH)

Table 9.1: Engine Specifications and Performance Summary (GTGH)

Specifications			
Weight	120 lb	**Design Speeds @ 100% RPM:**	
Power-to-Weight Ratio (TO)	1.53 HP/lb	Compressor Shaft	63000 RPM
Airflow Rate (TO)	1.1 lbm/s	Power Turbine Shaft	38000 RPM
Pressure Ratio (TO)	7.1	Main Engine Drive Shaft	6000 RPM

Performance		
Rating	**SHP**	**SFC (lb/HP/hr)**
Take-off Power (5 min)	181 HP	0.49
Maximum Continuous Power	154 HP	0.50
Cruise Power Setting:		
Cruise A (90%)	139 HP	0.52
Cruise B (75%)	116 HP	0.54

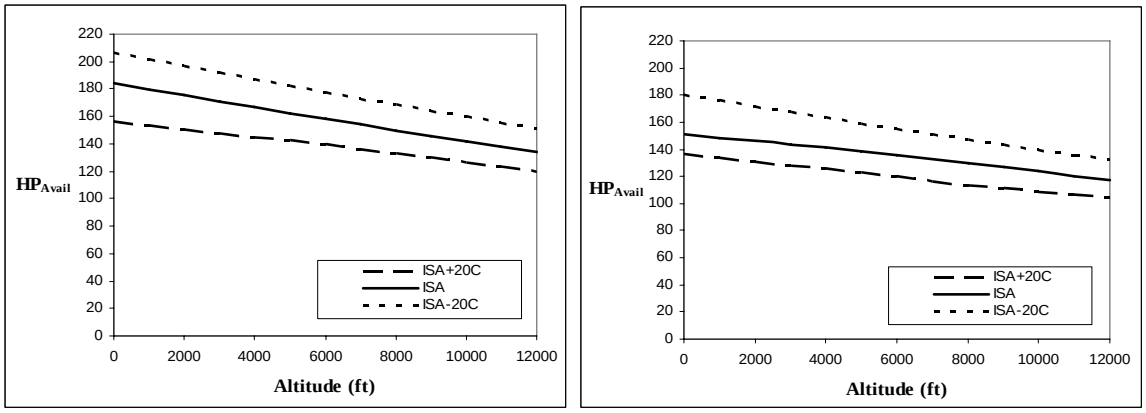

(a) Take-off Power **(b) Maximum Continuous Power**

Figure 9.7: Power Available as a Function of Altitude

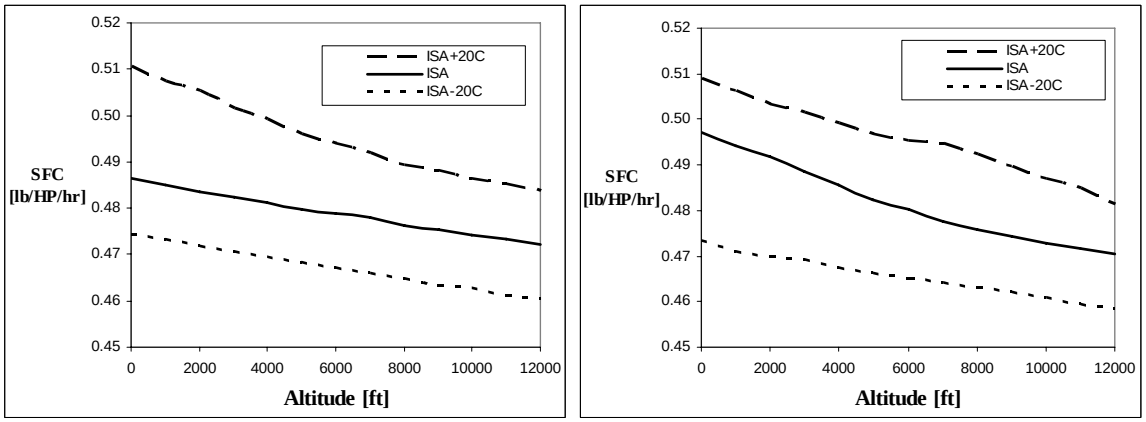

(a) Take-off Power **(b) Maximum Continuous Power**

Figure 9.8: SFC as a Function of Altitude

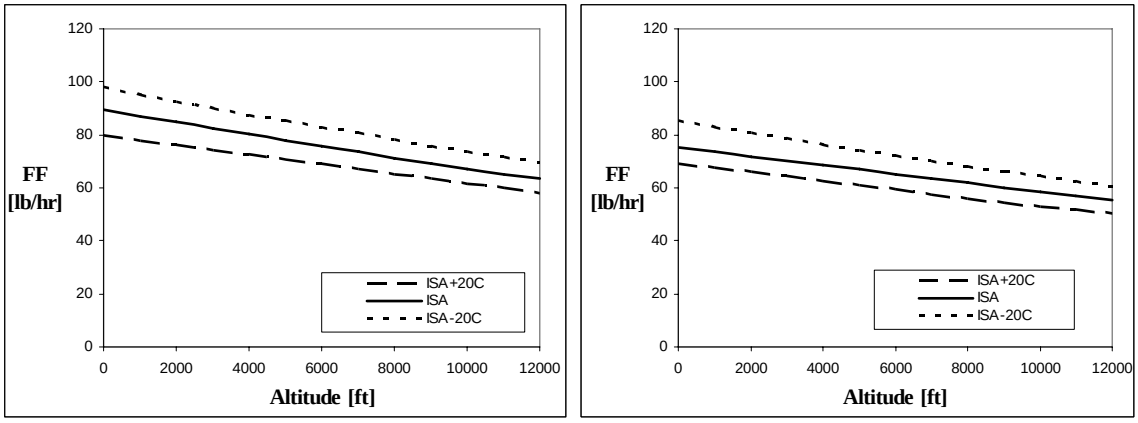

(a) Take-off Power **(b) Maximum Continuous Power**

Figure 9.9: Fuel Flow as a Function of Altitude

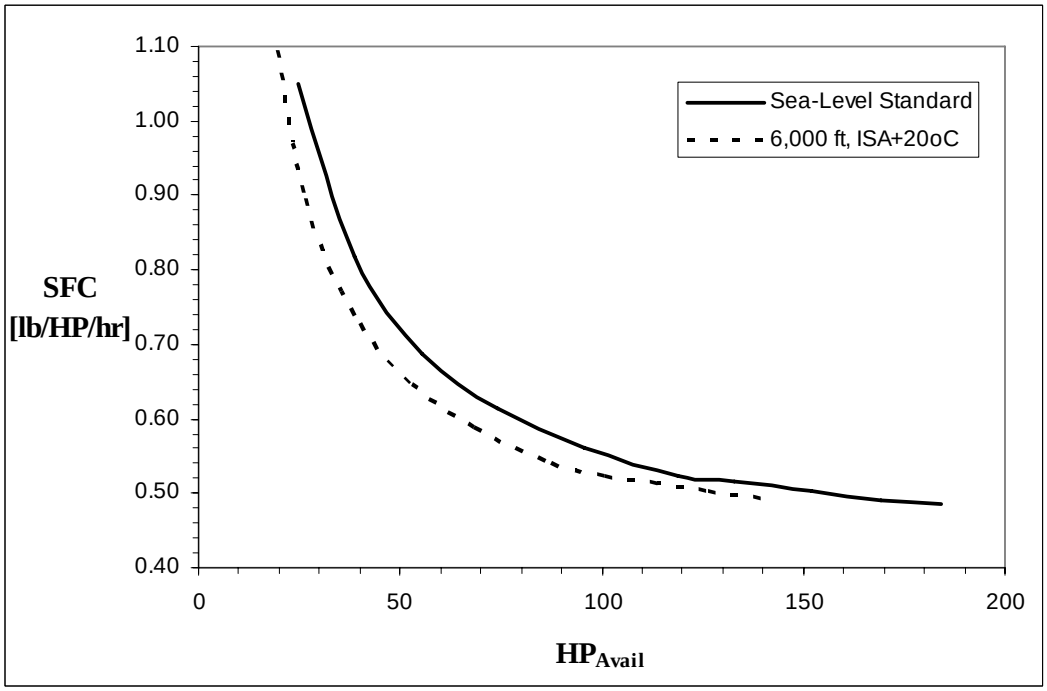

Figure 9.10: Partial Power Engine Performance (GTGH)

---

[1] Jack D. Mattingly, William H. Heiser, and David T. Pratt, *Aircraft Engine Design*, 2nd ed. (Reston, VA: AIAA, 2002).

[2] *NASA Engine Performance Program (NEPP) User's Manual*, 1997.

[3] Nicholas Cumpsty, *Jet Propulsion* (New York, NY: Cambridge University Press, 2003), 142.

[4] Ronald D. Flack, *Fundamentals of Jet Propulsion with Applications* (New York, NY: Cambridge University Press, 2005).

[5] "NASA Extended Parametric Representation of Compressor Fans and Turbines," *NASA CR-174646*, Vol. II, (General Electric: Cincinnati, OH, 1984).

CHAPTER 10

PRELIMINARY COMPONENT DESIGN AND ANALYSIS

The final step in the preliminary turboshaft design methodology is preliminary component design and analysis – aimed at determining the legitimacy of the previous parametric and performance analysis results. The goal of this step is to determine the geometric and material characteristics of the propulsion system's flowpath that will produce the predicted performance and, thus, more accurately establish its weight, manufacturability, and cost parameters. While detailed component design is considered beyond the scope of this initial engine design loop, an examination of the engine's rotating turbomachinery is necessary to produce the level of detail required to validate the assumptions used in previous design steps. Ultimately, the results of this step will serve as a feasibility check for the overall propulsion system design – determining if further iteration is required.

A program known as WATE (Weight Estimation for Turbine Engines) was developed by Boeing Military Aircraft Company in 1979 to automate the process of dimensional and weight analysis for aircraft engines. Over its lifespan, the program has been updated to reflect modern material and manufacturing capabilities. The code uses a database of 29 engines and a combination of empirical and analytical relationships to generate its component sizing and weight estimates. WATE is directly compatible with NEPP and simultaneously produces flowpath analysis for a given engine cycle. However, in the case of the GTGH, WATE was unable to converge on a solution due to the extremely small size parameters of the engine design. So to avoid this limitation and

the tendency to treat all components as “black boxes,” WATE analysis is replaced with more transparent and insightful component design tools.

Axial Compressor

The results for compressor performance previously determined in parametric and performance analysis will now serve as the starting point in turbomachinery design. Additionally, several assumptions and “rules of thumb” will be incorporated to streamline the process without sacrificing applicability or accuracy. This process closely follows the approach used by Mattingly et al. in *Aircraft Engine Design*.

Velocity Diagrams

A mean-line design process is used to evaluate the flowpath, sizing, and stress analysis for axial compressors. The foundation for this approach is the cascade, a constantly repeating array of rotor and stator airfoils designed to increase static pressure without incurring total pressure losses or flow instabilities.[1] Multiple cascades with identical geometries are used in series to model multistage compressors. The analysis of the cascade is based on the trigonometric relationships of the velocity diagrams shown in Figure 10.1. It is important to understand the two reference frames used in this diagram: *absolute*, which is fixed to the machine’s housing, and *relative*, which is fixed to the rotating rotor (indicated by the subscript “R”). The formulae included in Figure 10.1 show how to convert between reference frames as the fluid particles move through a given stage of compression.

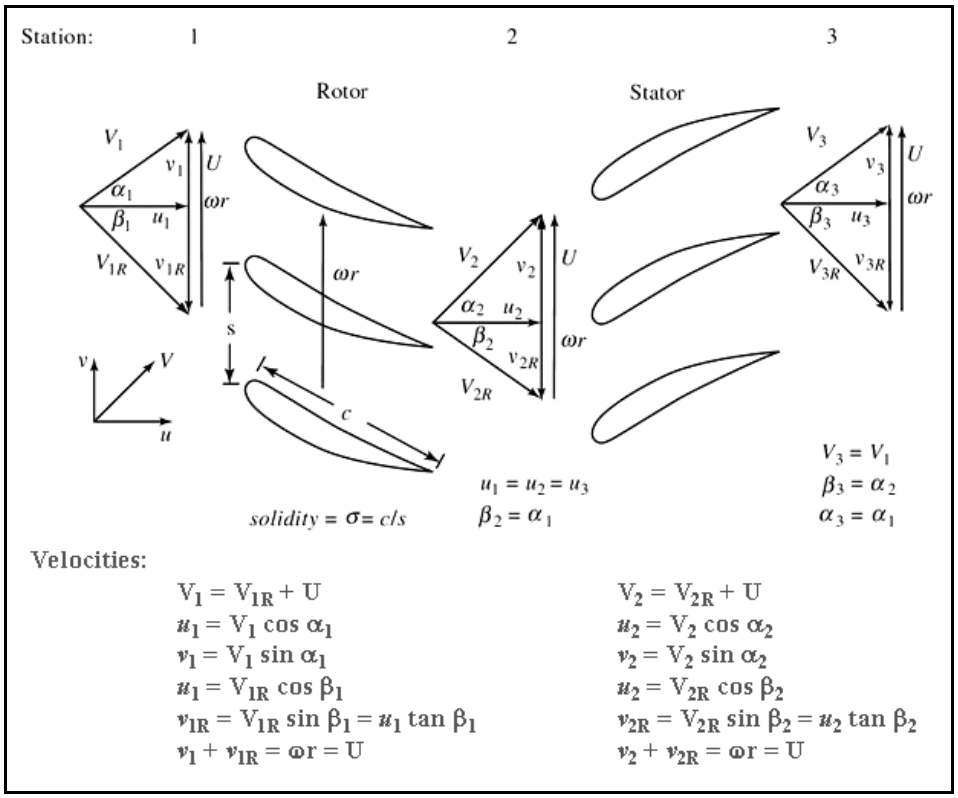

Figure 10.1: Axial Compressor Velocity Diagrams and Nomenclature[1]

Assumptions

The following list of simplifying assumptions plays a critical role in limiting the computational intensity of the design process while still maintaining the accuracy and level of detail required to make effective design choices:[1]

- Repeating row, repeating stage airfoil geometry ($\alpha_1=\beta_2=\alpha_3$ and $\beta_1=\alpha_2=\beta_3$)
- Two-dimensional flow
- Constant axial velocity ($u_1 = u_2 = u_3$)
- Constant mean radius
- Stage polytropic efficiency (η_{pc}) represents stage losses
- Calorically perfect gas with known γ and R

Design Parameters

With the simplifying assumptions established, it is necessary to define some additional design parameters that influence the performance of an axial compressor.

- Diffusion Factor (D) measures the potential for boundary layer separation on the cascade airfoil and, thus, provides a direct indication of the technology level of the design.

$$D \equiv \left(1 - \frac{V_{exit}}{V_{inlet}}\right) + \frac{\upsilon_{inlet} - \upsilon_{exit}}{2\sigma V_{inlet}} \qquad [10.1]$$

Where $\sigma = \frac{c}{s}$ is the solidity, defined as the ratio of blade chord (c) to blade spacing (s). A diffusion factor equal to 0.5 is considered normal; however, state-of-the-art compressors can achieve diffusion factors as high as 0.6 through the use of modern analysis tools and extensive developmental testing.[1]

- Degree of Reaction (Λ_c) is defined as the change in enthalpy of the rotor divided by the change in stagnation enthalpy of the stage – measuring the relative loading of the rotor and stator rows based on the increasing enthalpy of the flow.[2]

$$\Lambda_c = \frac{h_2 - h_1}{h_{03} - h_{01}} \qquad [10.2]$$

Where the subscripts now refer to static and total properties at stations within the stage. Since the velocity triangles for a repeating row, constant axial velocity design are symmetrical, the degree of reaction must equal 0.5. This condition is generally considered good design practice, because it evenly balances the force distributions between the rotor and stator airfoils and maximizes efficiency.

- Stage Total Temperature Ratio (τ_s) is defined using the Euler equation with constant radius for a calorically perfect gas, which establishes the relationship between stage work and rotor velocity as follows:

$$c_p\left(T_{03}-T_{01}\right)=\frac{\omega r}{g_c}\left(\upsilon_2-\upsilon_1\right) \qquad [10.3]$$

Where ω is the angular velocity of the rotor in rad/s. From this relationship, the terms are rearranged and expanded to define the temperature ratio as:[1]

$$\tau_s \equiv \frac{T_{03}}{T_{01}}=\frac{\left(\gamma-1\right)M_1^2}{1+\left(\gamma-1\right)M_1^2/2}\left(\frac{\cos^2\alpha_1}{\cos^2\alpha_2}-1\right)+1 \qquad [10.4]$$

Where M_1 is the Mach number at station 1.

- Stage Pressure Ratio (π_s) is defined in terms of the stage total temperature ratio and polytropic efficiency as follows:

$$\pi_s \equiv \frac{p_{03}}{p_{01}}=\left(\tau_s\right)^{\gamma\eta_{pc}/(\gamma-1)} \qquad [10.5]$$

- Stage Adiabatic Efficiency (η_s) is defined using the following expression:

$$\eta_s=\frac{h_{03s}-h_{01}}{h_{03}-h_{01}} \qquad 0.6]$$

Figure 10.2 shows a temperature-entropy graph of the single-stage compression process – highlighting the losses that occur due to non-isentropic relationships. By assuming constant specific heats, Equation 6.11 can be simplified to the following:[1]

$$\eta_s=\frac{T_{03s}-T_{01}}{T_{03}-T_{01}}=\frac{\pi_s^{(\gamma-1)/\gamma}-1}{\tau_s-1}=\frac{\tau_s^{\eta_{pc}}-1}{\tau_s-1} \qquad [10.7]$$

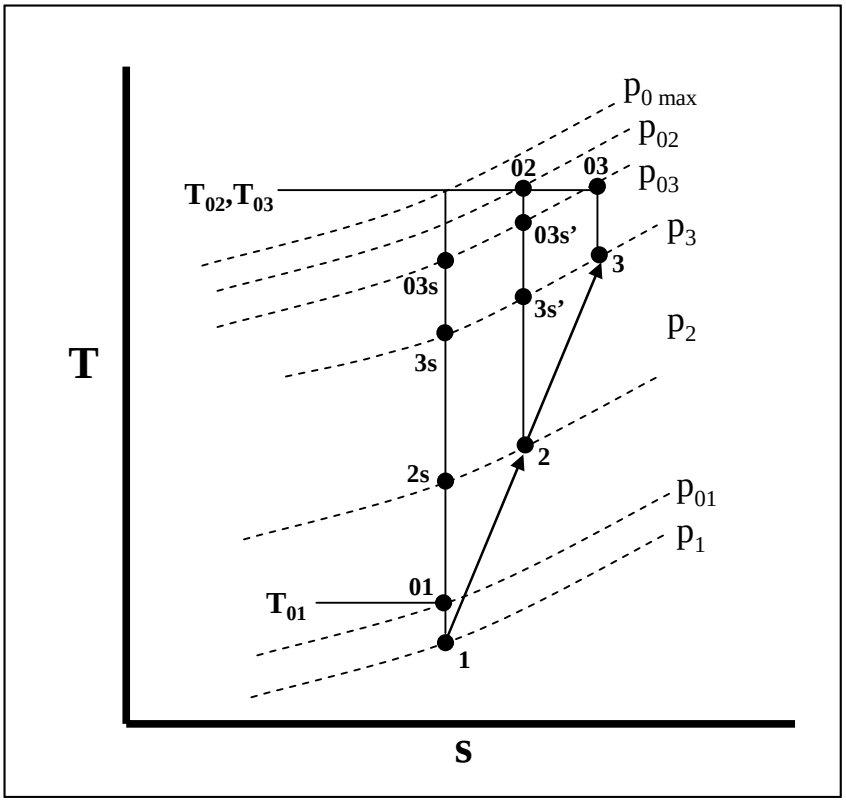

Figure 10.2: Single-Stage Compressor T-s Diagram[2]

- Stage Loading Coefficient (ψ) is defined for a calorically perfect gas as follows:

$$\psi \equiv \frac{g_c c_p \Delta T_t}{(\omega r)^2} \qquad [10.8]$$

- Stage Flow Coefficient (Φ) is the ratio of axial velocity to rotor speed, such that:

$$\Phi = \frac{u_1}{\omega r} \qquad [10.9]$$

- Rotor Loss Coefficient (ϕ_{cr}) describes the pressure losses associated with the rotor section of a given stage as follows:[3]

$$\phi_{cr} \equiv \frac{p_{01R} - p_{02R}}{\rho_1 V_{1R}^2 / (2g_c)} \qquad [10.11]$$

Typical values for this parameter range from 0.05 to 0.12.

- Stator Loss Coefficient (ϕ_{cs}) describes the pressure losses associated with the stator section of a given stage as follows:[3]

$$\phi_{cs} \equiv \frac{p_{02} - p_{03}}{\rho_2 V_2^2/(2g_c)} \qquad [10.12]$$

Typical values for this parameter range from 0.03 to 0.06.

Design Parameter Analysis

Through the combination of assumptions and design parameter definitions previously described, it is possible to develop a series of equations that models the performance of every possible repeating-row compressor configuration in terms of only a few key variables. Based on given values for D, M_1, γ, σ, and η_{pc}, the Mattingly et al. general solution approach starts with an initial value for the inlet flow angle (α_1) and utilizes a series of functional relationships to complete an entire design iteration. The following equations demonstrate the integrated progression of this general solution process:[1]

(1)
$$\alpha_2 = f(D, \sigma, \alpha_1) = \cos^{-1}\left(\frac{2\sigma(1-D)\Gamma + \sqrt{\Gamma^2 + 1 - 4\sigma^2(1-D)^2}}{\Gamma^2 + 1}\right)$$

[10.13]

$$\text{Where } \Gamma = \frac{2\sigma + \sin\alpha_1}{\cos\alpha_1}.$$

(2)
$$\Delta\alpha = \alpha_2 - \alpha_1 \qquad [10.14]$$

(3)
$$\tau_s = f(M_1, \gamma, \alpha_1, \alpha_2) = \text{Equation } 10.4$$

(4)
$$\pi_s = f(\tau_s, \gamma, \eta_{pc}) = \text{Equation } 10.5$$

(5)
$$\eta_s = f(\tau_s, \pi_s, \gamma, \eta_{pc}) = \text{Equation } 10.7$$

(6) $$\frac{\omega r}{V_1} = f(\alpha_1, \alpha_2) = \cos\alpha_1(\tan\alpha_1 + \tan\alpha_2) \quad [10.15]$$

(7) $$\frac{M_{1R}}{M_1} = f(\alpha_1, \alpha_2) = \frac{\cos\alpha_1}{\cos\alpha_2} \quad [10.16]$$

In the application of this general sequence of formulae, sensitivity analysis can be conducted to determine the optimum combination of parameters for a given compressor design. The effects of changing α_1, the diffusion factor, Mach number, and solidity can be explored graphically to isolate favorable design relationships and trends – the following three diagrams illustrate this capability for a repeating mean-line design. Figure 10.3 shows that in order to maximize the stage pressure ratio, higher values for the inlet and exit flow angles (α_1 and α_2), M_1, and wheel speed (ωr) are required. Additionally, in order to maintain subsonic relative flow into the rotor, the value of M_1 should remain below 0.7.[1]

Figure 10.4 depicts the effects of changing the diffusion factor from 0.4 to 0.6 – indicating that increased diffusion results in a higher stage pressure ratio at the expense of increased wheel speed and exit flow angle. Figure 10.5 shows nearly identical trends for increasing the solidity for a given inlet flow angle and velocity. Ultimately, the goal of this sensitivity analysis is to define an initial set of parameters that best captures the operational requirements for the compressor at its critical design point (typically at its highest pressure ratio) and, thus, serves as a reliable framework for evaluating its geometric and performance characteristics. Table 10.1 provides a list of the typical parameter ranges found in modern axial compressor designs.

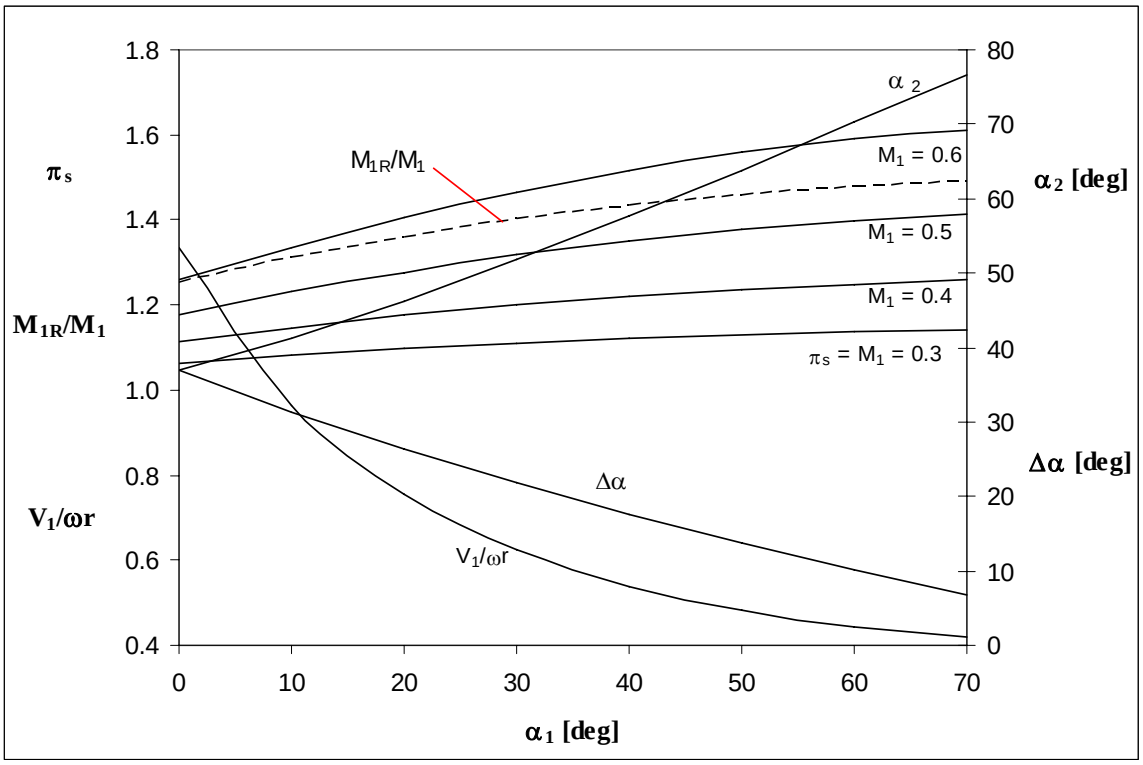

Figure 10.3: Repeating Row Compressor Stage (D=0.5, σ=1, and η_{pc}=0.9)[1]

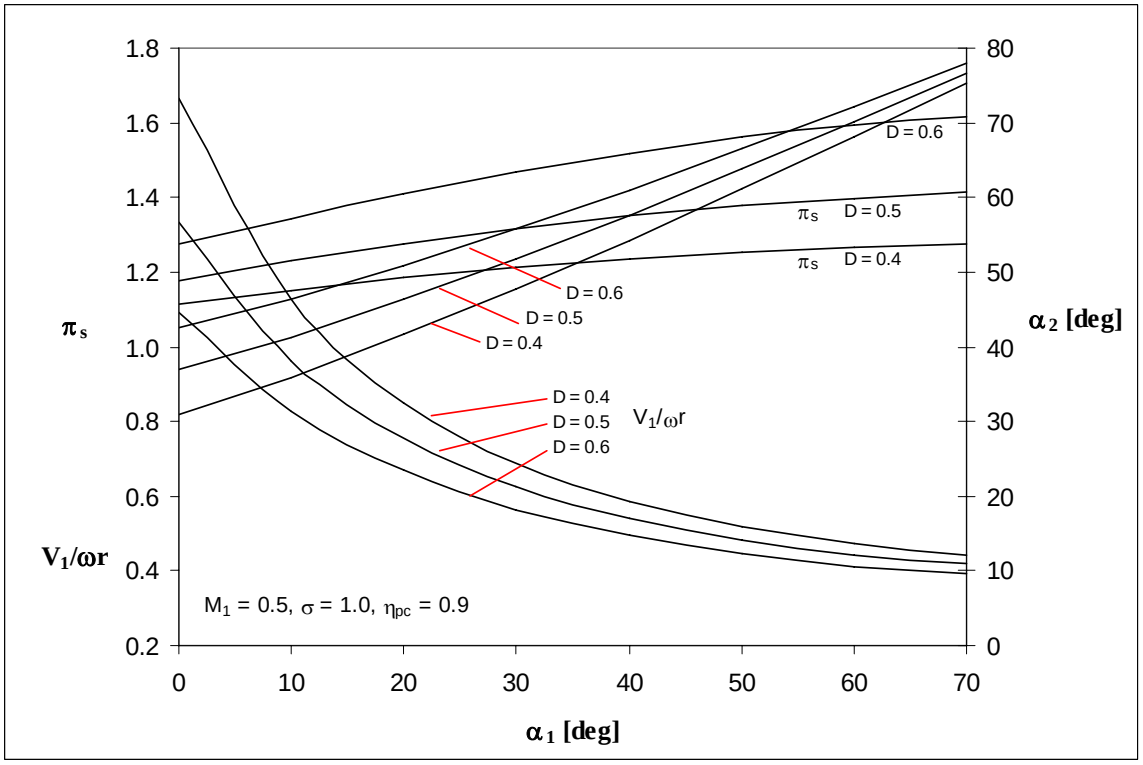

Figure 10.4: Repeating Row Compressor Stage – Variation with D (M_1=0.5, σ=1, and η_{pc}=0.9)[1]

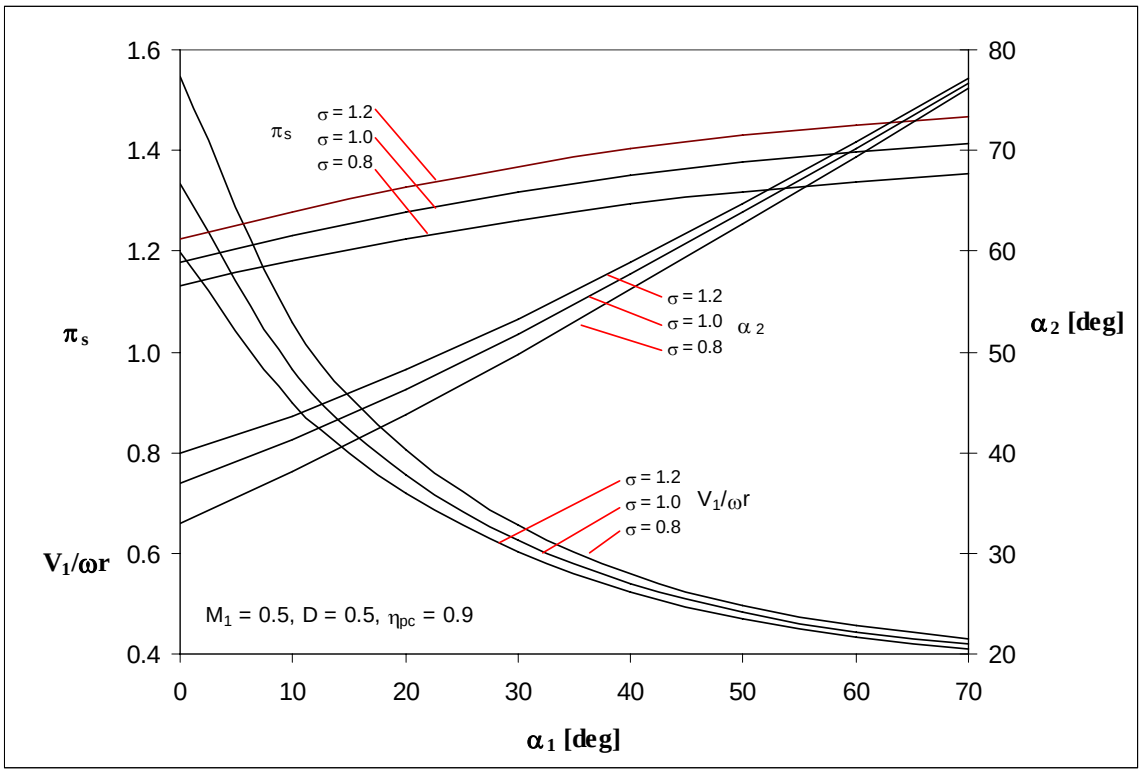

Figure 10.5: Repeating Compressor Stage – Variation with σ (M_1=0.5, D=0.5, and η_{pc}=0.9)[1]

Table 10.1: Axial Compressor Design Parameter Ranges[1]

Parameter		Design Range
ΔT_{stage}		60 - 90 °F
π_{stage}		1.15 - 1.28
Hub/Tip Ratio	Inlet	0.60 - 0.75
	Exit	0.90 - 0.92
Maximum Exit Temperature		1700 - 1800 °R
Maximum Rim Speed	Exit	1300 - 1500 ft/s
Diffusion Factor D		0.50 - 0.55
Stage Loading Coefficient ψ		0.30 - 0.35
Flow Coefficient Φ		0.45 - 0.55

Flowpath Design

With the initial parameters for the compressor design point established, the compressor's flowpath can now be determined in order to validate the previous

parametric and performance engine cycle analysis results and provide an accurate assessment of component size and weight. The Compressor Preliminary Design Program (COMPR) – provided with the *Aircraft Engine Design* textbook and based on the functional relationships previously described – automates much of the design process from this point forward. However, in an effort to avoid treating the design methodology as a "black box" scenario, a simplified Excel code was developed to mirror the basic capabilities of the COMPR program while providing better transparency in implementing the axial compressor preliminary design process (See APPENDIX F).

Number of Stages

The first step defines the estimated number of stages required to achieve the predicted level of performance for the design point used in the parametric engine cycle analysis. Mean-line analysis assumes a constant temperature rise across each stage; therefore, the total temperature rise (ΔT_t) across the compressor is divided by the estimated number of stages such that the temperature rise per stage falls within the acceptable range provided in Table 10.1. The number of stages selected from within this range depends on an assessment of the applicable level of technology for the compressor design.

Single-Stage Analysis

With the number of stages defined, the second step determines the stage characteristics required to achieve the desired temperature rise per stage. Using the repeating row, mean-line analysis relationships and assumptions previously described, the inlet flow angle (α_1) is varied until the desired single-stage temperature rise is

attained. As stated earlier, defining α_1 begins the general solution sequence and, thus, each critical stage design parameter can be determined and compared to typical values listed in Table 10.1. Parameters that fall outside of their respective range may require design compromise or technological justification to ensure the overall feasibility of the compressor's configuration.

The rotor speed (ωr) from the single-stage analysis provides a design starting point for the complicated process of selecting an angular velocity (ω) for the compressor. Because the compressor typically shares a shaft with the turbine, their rotational speeds must be identical. Simultaneous optimization for both components is usually not possible. For a dual-spool design, the high pressure turbine (HPT) typically dictates the rotational shaft speed because the HPT reaches a maximum limit for blade stress more readily than the compressor due to the extreme temperatures at which it operates. Therefore, the selection of the compressor's rotational speed must be sufficiently low to maintain a reasonable turbine stress level. Additionally, the mean radius of the compressor must also meet the engine's geometric requirements previously identified during the requirements analysis.

Multi-Stage Analysis

Once an acceptable array of single-stage parameters is established, these values then serve as the input data for multi-stage analysis. The results of multi-stage analysis provide information concerning the flowpath dimensions for each axial compressor stage. Figure 10.6 provides a diagram of the standard terms used to describe this geometry. Multi-stage analysis estimates the height, chord length, and number of blades required for the rotor and stator vanes as a function of the mean radius (r_m). This information is

important to evaluate in terms of component manufacturability, efficiency, and cost – as the smaller blade heights in the final stages of the compressor may require special design consideration. It is important to note that the multi-stage results for the mean-line design approach represent a "worst case" estimate. By incorporating more detailed design analysis for each stage – such as the radial variation of the degree of reaction and the effects of varying the chord-to-height and taper ratio – the compressor can be optimized in terms of its geometry and performance. For this preliminary design effort, however, the repeating row, repeating stage, mean-line approach is considered adequate.

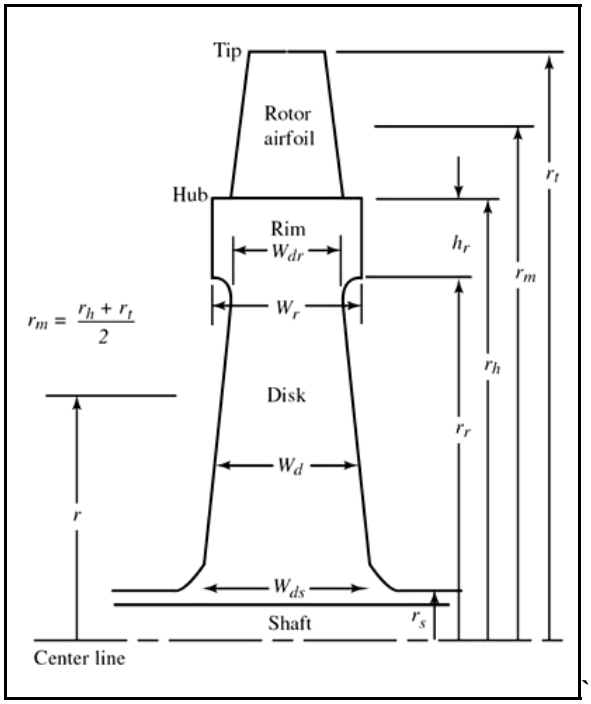

Figure 10.6: Axial Compressor Stage Geometry[1]

Material Selection

The final details of the preliminary axial compressor design involve an evaluation of the critical stress factors per stage – ensuring that the appropriate material is selected to meet the minimum strength requirements and that the geometric dimensions are

properly defined. The axial compressor configuration has three critical areas – the airfoils, rim, and disk – where the stress factors must be considered. Table 10.2 lists the typical materials used for rotating turbomachinery in modern gas turbine engines.

For the airfoils, the allowable blade stress factor (AN^2) is calculated as follows:[1]

$$AN^2 = \frac{3600}{\pi\left(1 + A_t / A_h\right)} \frac{\sigma_c}{\rho} \qquad [10.17]$$

Where A is the flowpath area, N is the rotational speed in RPM, σ_c/ρ is the material strength-to-weight ratio, and (A_t / A_h) is the blade taper ratio (typically between 0.8 and 1.0). Using Figure 10.7, the allowable strength-to-weight ratio is estimated for a given material and used in Equation 10.17 to ensure that the allowable AN^2 is greater than the actual AN^2 required for each compressor stage – otherwise a new material or flowpath redesign is needed. Figure 10.7 is based on 80% of the allowable 0.2% creep stress for aluminum alloys and 50% of the allowable 1% creep stress for 1000 hours for the other alloys listed in Table 10.2.

The geometric characteristics and allowable rotational speed of the rim and disk are determined by estimating the centrifugal stress factors of each component. In order to approximate the stress at the outer radius of the rim, the average stress of the blades at the hub is calculated as follows:[1]

$$\bar{\sigma}_{blades} = \frac{\sigma_c n_b A_h}{2\pi r_h W_r} \qquad [10.18]$$

Where n_b is the number of blades and W_r is the width of the rim approximated as the blade chord. Using an assumption of uniform stress, the geometry of the rim is further defined by the following expression for the ratio of the rim web thickness (W_{dr}) to the rim width (W_r):[1]

$$\frac{W_{dr}}{W_r} = \left[\frac{\bar{\sigma}_{blades}}{\sigma_r} \left(1 + \frac{r_r}{h_r} \right) + \frac{\rho(\omega r_r)^2}{\sigma_r} \left(1 + \frac{h_r}{2r_r} \right)^2 - 1 \right] \frac{h_r}{r_r} \qquad [10.19]$$

Where h_r is the height of the rim approximated by a reasonable design value (close in magnitude to W_r) and σ_r is the tensile strength of the selected material (Note: $\sigma_r = \sigma_d$ because the materials are identical). Assuming uniform stress in the disk, as well, the ratio of the disk width (W_d) to the rim web thickness (W_{dr}) can be established:[1]

$$\frac{W_d}{W_{dr}} = \exp\left\{ \frac{\rho(\omega r_r)^2}{2\sigma_d} \left[1 - \left(\frac{r}{r_r} \right)^2 \right] \right\} \qquad [10.20]$$

Where r is the variable radius of interest and $\frac{\rho(\omega r_r)^2}{2\sigma_d}$ is known as the disk shape factor (DSF). For an approximate width of the disk where it meets the shaft (W_{ds}), select r equal to the estimated radius of the shaft. The final feasibility check for the preliminary axial compressor design is a comparison between the required rim speed and the maximum allowable rim speed, as follows:[1]

$$[\omega r_r]_{max} \approx \sqrt{\frac{4\sigma_d}{\rho}} \qquad [10.21]$$

The relationships and assumptions used for the stress analysis also determine the final geometry of the each compressor stage – allowing an accurate assessment of the component's weight.

Table 10.2: Engine Component Materials[1]

		Density	
Material #	**Type**	slug/ft^3	lb/in^3
1	Aluminum Alloy	5.29	0.099
2	Titanium Alloy	9.08	0.169
3	Wrought Nickel Alloy	16.0	0.298
4	High-Strength Nickel Alloy	17.0	0.317
5	Single-Crystal Nickel Alloy	17.0	0.317

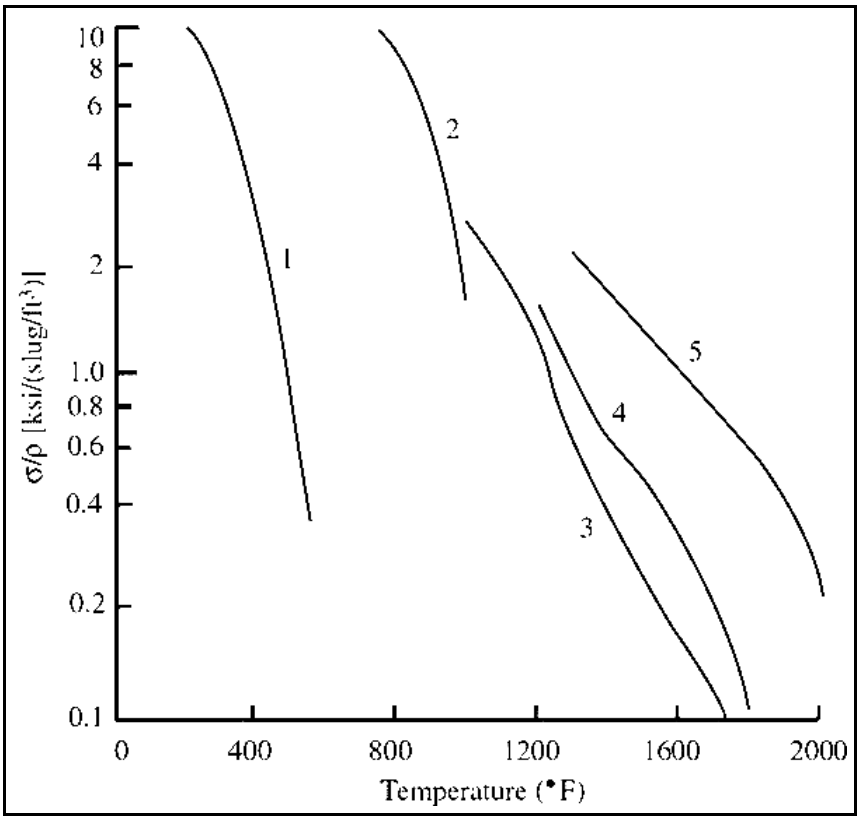

Figure 10.7: Material Selection Diagram[1]

Centrifugal Compressor

The preliminary design process for a radial compressor differs significantly from its axial counterpart because the mechanism of compression is related to displacement in the centrifugal flow field as opposed to deceleration.[2] The one-dimensional, mean-line analysis approach presented in this section is based on a combination of techniques used in multiple turbomachinery textbooks.

Velocity Diagrams

Figure 10.8 shows the configuration and dimensions for a typical radial compressor. Figure 10.9 depicts the velocity diagrams for the rotor inlet with axial-only flow – highlighting the significant increase in relative flow angle from hub to tip that occurs through the inducer, or rotor entrance section. The velocity diagrams for the impeller exit are shown in Figure 10.10 for two separate design conditions: straight radial and backswept impeller blades. When comparing the two designs, straight radial impeller blades are capable of achieving greater pressure rise for a given tip speed, but they also generate higher Mach numbers entering the diffuser. Backward swept blades reduce the exit Mach number, but often exhibit stress related problems in high-speed compressor applications. In both cases, the radial component of velocity (w_2) is approximately equal to the inlet axial velocity (u_1) and the tangential component of velocity (v_2) is about 90% of rotor exit tip speed (U_2) due to the "slip" of the fluid particles. This "slip" condition exists because the Coriolis pressure gradient disappears toward the outlet of the rotor and the flow is unable to continue in a purely radial direction.[2]

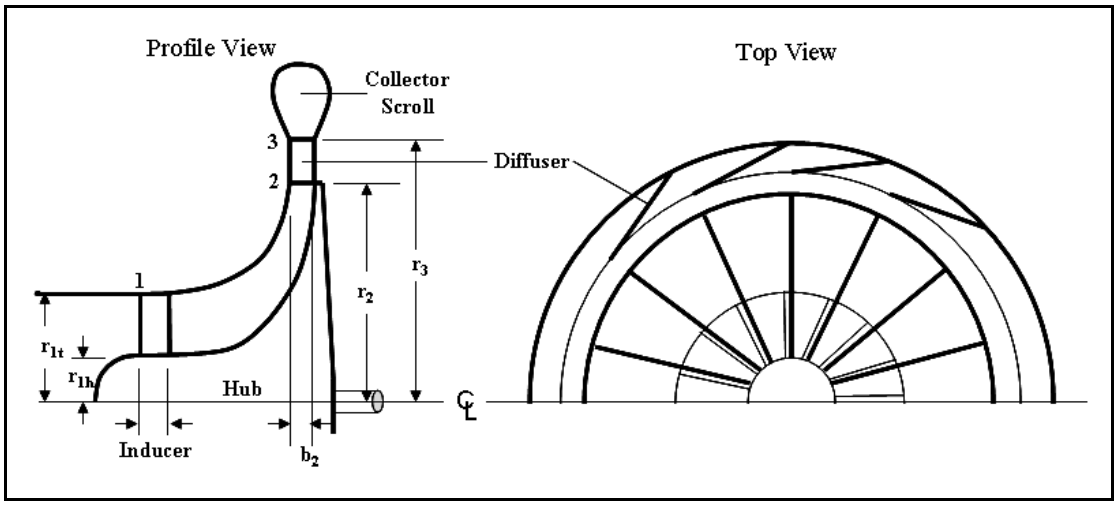

Figure 10.8: Centrifugal Compressor Configuration and Dimensions

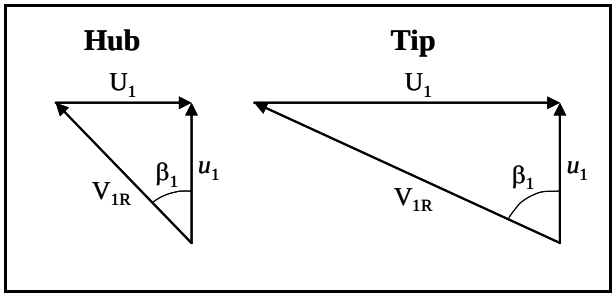

Figure 10.9: Centrifugal Compressor Inlet Velocity Diagrams

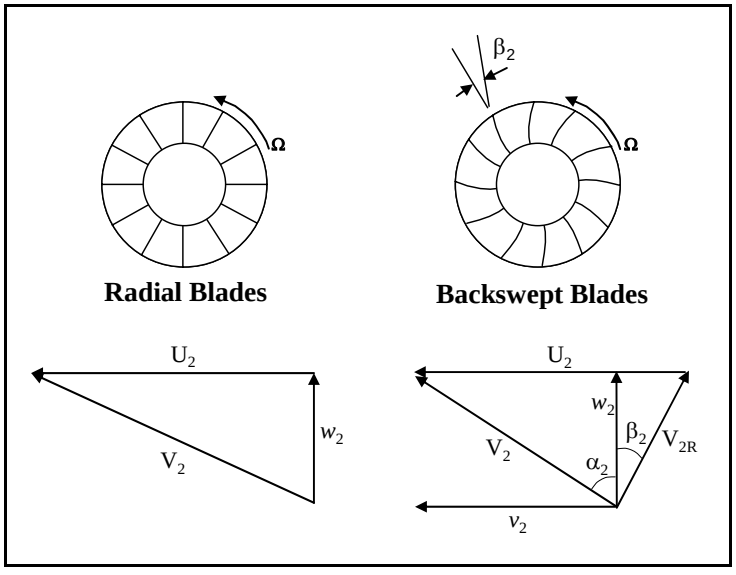

Figure 10.10: Centrifugal Compressor Rotor Exit Velocity Diagrams

Assumptions

In order to simplify the preliminary design process, the following assumptions are incorporated into the analysis:

- Rotor inlet velocity (u_1) is uniform and axial. No prewhirl conditions exist from the use of inlet guide vanes or prior axial compressor stages.
- Adiabatic flow in the diffuser ($T_{03} = T_{02}$).
- Constant width diffuser ($b_2 = b_5$)
- Calorically perfect gas with known γ and R.

Design Parameters

Although many of the design concepts used for radial compressors are identical to those used for axial compressors, there are unique parameters used to describe their applications.

- Stage Total Temperature Ratio (τ_s) is defined using the Euler equation for a calorically perfect gas, which establishes the relationship between stage work and rotor velocity as follows:

$$\left(T_{03} - T_{01}\right) = \frac{\upsilon_2 U_2}{g_c c_p} \qquad [10.22]$$

Where v_2 is the tangential component of velocity and U_2 is the rotational velocity at the rotor exit. Since $T_{03}=T_{02}$ due to adiabatic flow in the diffuser and the inflow is assumed to be purely axial, the terms are rearranged and expanded to define the temperature ratio:

$$\tau_s \equiv \frac{T_{03}}{T_{01}} = \frac{T_{02}}{T_{01}} = 1 + (\gamma - 1)\frac{U_2^2}{a_{01}^2}\left(1 - \frac{w_2}{U_2}\tan\beta_2\right) \qquad [10.23]$$

Where $a_{01} = \sqrt{\gamma R T_{01}}$ is the speed of sound at the inlet stagnation temperature, β_2 is the rotor exit blade angle, and w_2 is the radial component of velocity at the rotor exit.

- Stage Pressure Ratio (π_s) is defined using an assumption for polytropic efficiency as follows:

$$\pi_s = \frac{p_{03}}{p_{01}} = \left[1 + \left(\frac{T_{03} - T_{01}}{T_{01}}\right)\right]^{\gamma \eta_{pc}/(\gamma - 1)} \qquad [10.24]$$

- Slip Factor (ε) is the ratio of tangential velocities at the impeller exit, such that:

$$\varepsilon = \frac{\upsilon_2}{U_2} \qquad [10.25]$$

The slip factor is related to the number of blades on the impeller – as the number of blades increases, the relative "slippage" between the fluid and the rotor reduces and ε approaches unity. However, increasing the number of blades also causes frictional losses in the rotor to increase. The following equation, known as the Wiesner slip factor, provides a useful correlation between the slip factor, number of blades (n_b), and the backsweep angle (β_{2b}):[4]

$$\varepsilon = 1 - \left(\frac{\sqrt{\cos\beta_{2b}}}{n_b^{0.7}}\right) \qquad [10.26]$$

A slip factor of 0.9 usually provides the best balance between maintaining a high slip factor with low frictional losses.

- Flow Coefficient (Φ) is the ratio of axial velocity to rotor speed at the rotor exit, such that:

$$\Phi = \frac{w_2}{U_2} \qquad [10.27]$$

Design Parameter Analysis

The application of these assumptions and design variables leads to the development of general solutions that provide further insight regarding the best choice of parameters to meet a required level of performance. As depicted in Figure 10.11, this generic trend analysis begins with an investigation of the influence of backsweep angle (β_{2b}) on the stage pressure ratio (π_s) and exit Mach number (M_2). The independent axis for Figure 10.11 uses non-dimensional rotor exit tip speed – indirectly providing material strength analysis because the centrifugal stress capability of modern radial compressor materials limits U_2 to approximately 2200 ft/s, or values of (U_t/a_{01}) less than 2. Therefore, Figure 10.11 shows that pressure ratios as high as 20 are possible using this stress limitation, but the extreme value of $M_2 = 1.6$ would likely cause significant shock-related losses in the diffuser. Generally, keeping the value of M_2 below approximately 1.3 will ensure that an efficient diffuser design is feasible.

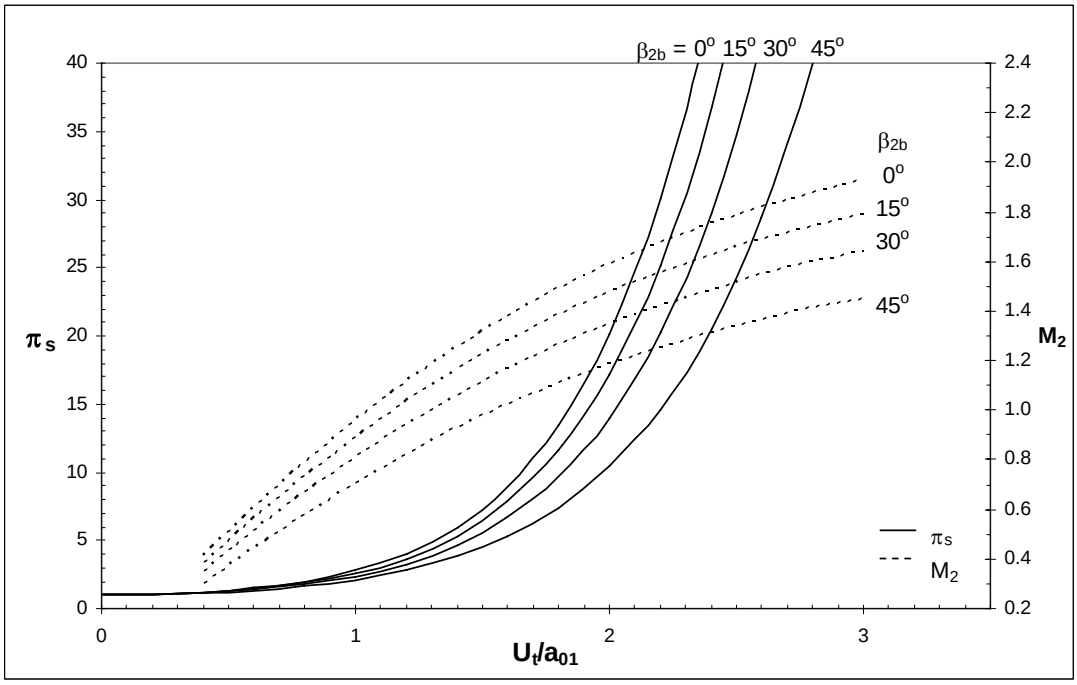

Figure 10.11: Centrifugal Compressor Stage Analysis (η_c=0.85, ϕ=0.3)[2]

The aerodynamic limitations of the inducer provide guidance concerning the maximum turning angle (β_1) and inlet relative Mach number. In order to avoid flow separation along the inducer surface, the maximum turning angle is approximately 50^o. The allowable Mach number relative to the inducer blade tip at the inlet is also important to address because it plays a critical role in determining the size of the compressor.[1] High Mach numbers at the inlet increase the potential for shocks which can dramatically reduce component performance. Modern advances in flow analysis allow for efficient compressor designs that have inlet relative Mach numbers as high as 1.4. Table 10.3 lists the typical design parameter ranges found in modern centrifugal compressors.

Table 10.3: Centrifugal Compressor Design Parameter Ranges

Parameter	Design Range
Maximum Rotor Tip Speed U_2	2200 ft/s
Inlet Relative Mach Number M_{1R}	< 1.4
Rotor Exit Mach Number M_2	< 1.3
Turning Angle β_1	< 55 deg
Rotor Exit Blade Backsweep β_{2b}	0 - 40 deg
Absolute Exit Flow Angle α_2	50 - 80 deg
Slip Factor ε	0.9

Flowpath Design

The flowpath design process for a centrifugal compressor uses the predicted pressure and temperature conditions from the engine cycle analysis to determine the performance and geometry of the actual component. It should be noted that the process presented in this section only addresses single-stage centrifugal compressor configurations (See APPENDIX E for a detailed design example from the GTGH).

Shaft Speed and Inlet Geometry

Using the required pressure ratio from engine cycle analysis, the rotor exit tip speed (U_2) is determined using the following expression:

$$U_2 = \sqrt{\left(\frac{g_c c_p T_{01}}{\varepsilon}\right)\left(\pi_c^{(\gamma-1)/(\gamma\eta_{pc})} - 1\right)} \qquad [10.28]$$

Figure 10.12 shows a plot of this relationship between pressure ratio and tip speed for three different polytropic efficiencies. The calculated value of U_2 should be less than the stress-limited maximum tip speed presented in Table 10.4 or else an advanced material assumption or new compressor configuration is in order.

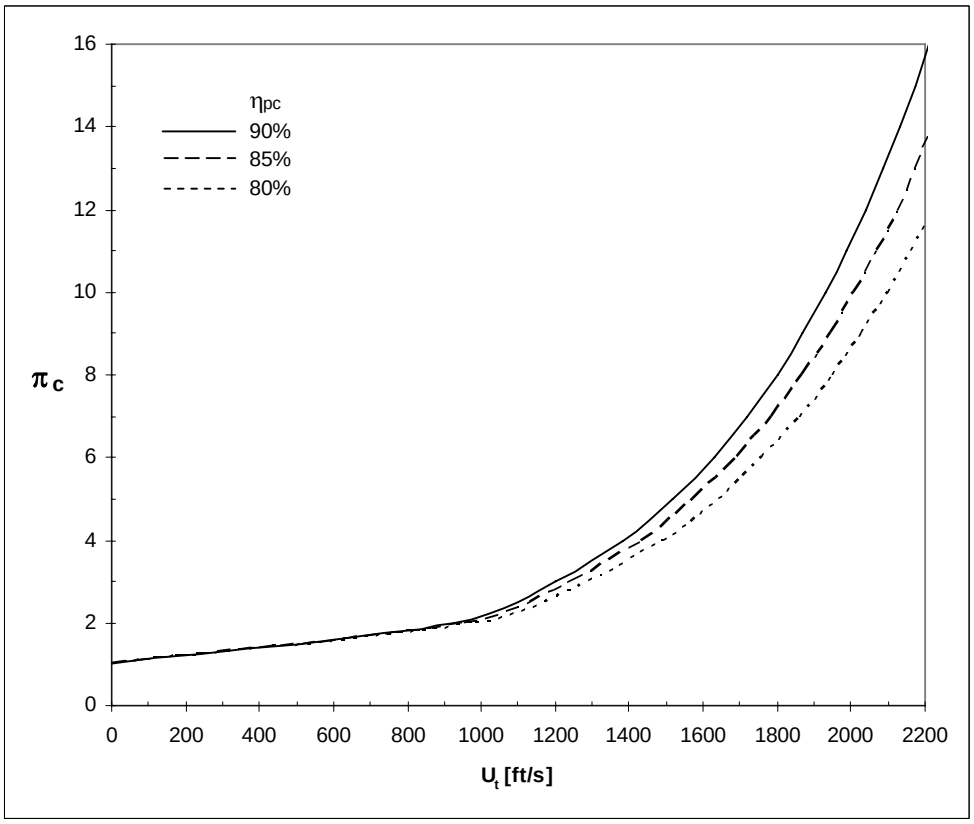

Figure 10.12: Centrifugal Compressor Pressure Ratio vs. Tip Speed[3]

With the necessary tip speed established, the size of the compressor inlet is determined by the aerodynamic limitations of the design which dictate the maximum allowable rotational speed (N). Consideration must also be given to the maximum rotational speed of the high pressure turbine, as each component shares a common shaft. Inevitably, geometric and performance related design compromises are required to optimize the RPM of the gas generator shaft. The following sequence of equations – used to describe the inlet conditions and geometry for a given flow – quantify the effects of changing M_1, M_{1R}, hub-to-tip ratio (ζ), and the inducer blade angle at the tip (β_{1t}) on the maximum allowable shaft speed (N).[2]

(1)
$$M_{1R} = \frac{M_1}{\cos\beta_{1t}} \qquad [10.29]$$

(2)
$$T_1 = \frac{T_{01}}{\left(1+\frac{\gamma-1}{2}M_1^2\right)} \qquad [10.30]$$

(3)
$$\rho_1 = \frac{\rho_{01}}{\left(1+\frac{\gamma-1}{2}M_1^2\right)^{1/(\gamma-1)}} \qquad [10.31]$$

(4)
$$u_1 = M_1\sqrt{\gamma R g_c T_1} \qquad [10.32]$$

(5)
$$U_{1t} = u_1 \tan\beta_{1t} \qquad [10.33]$$

(6)
$$D_{1t} = \sqrt{\frac{4}{\pi}\frac{\dot{m}}{\rho_1 u_1}\left(1-\zeta^2\right)} \qquad [10.34]$$

(7)
$$N = \frac{60}{\pi}\frac{U_{1t}}{D_{1t}} \qquad [10.35]$$

Figure 10.13 provides a graphical representation of this sensitivity analysis at sea-level standard (SLS) conditions. Using this trade study method, the best combination of design parameters for a specific compressor application can be identified. Selecting the appropriate values for β_{1t}, M_1, and ζ plays a critical role in determining the performance and geometry of the entire component. If the maximum allowable shaft speed (N) is dictated by the high pressure turbine design, then values for M_{1R} and β_{1t} are selected within the appropriate design limitations. And by assuming a value for ζ, the rotor inlet geometry is fully established.

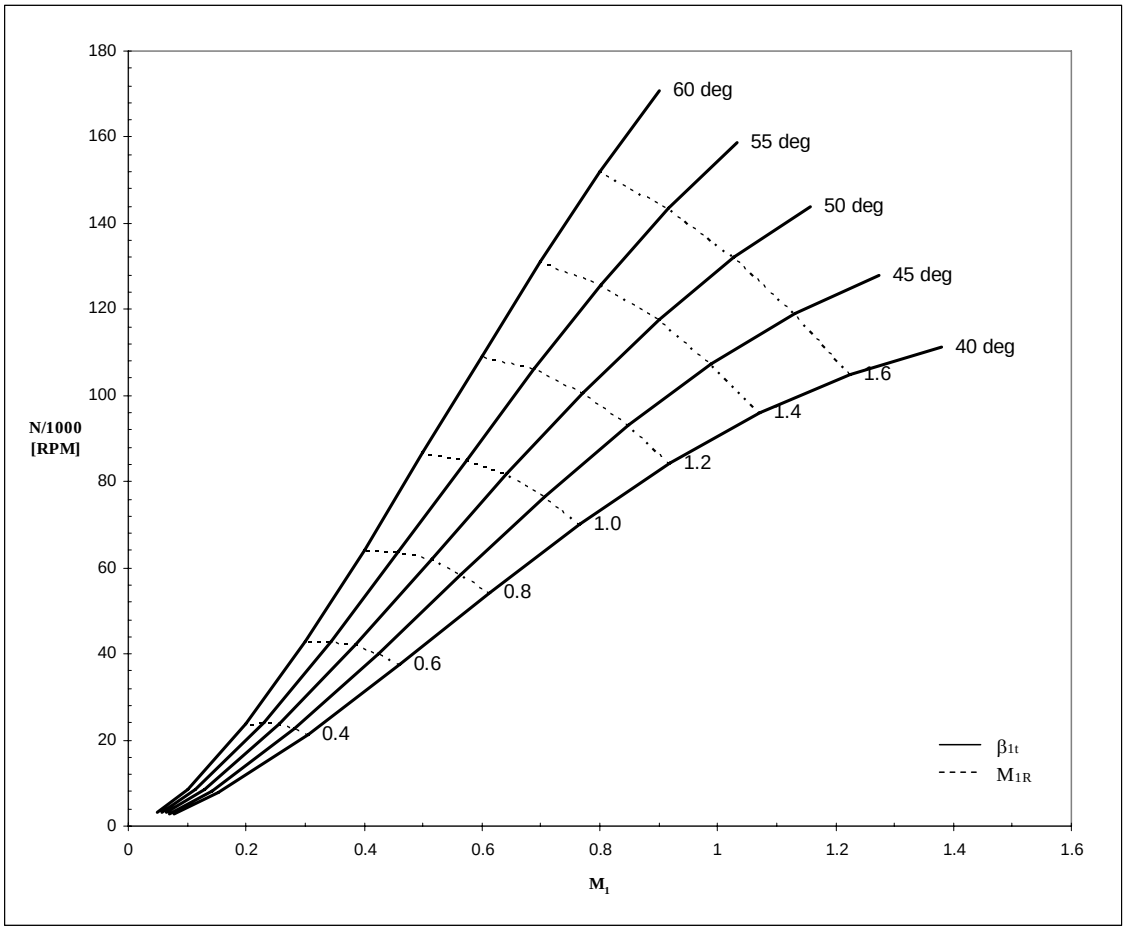

Figure 10.13: Rotor Inlet Design Parameter Trade Study (SLS)

Rotor Geometry

With the inlet geometry defined, it is now possible to determine the outlet diameter of the rotor based on a ratio of the required tip speed to the rotational speed, such that:

$$D_2 = \frac{2U_2}{\Omega} \qquad [10.36]$$

Where Ω replaces N, measured in rad/s. The second parameter used to describe the shape of the impeller design is the axial width of the rotor blades at the rotor exit (b_2). The following expression provides an approximate relationship for estimating this value:

$$b_2 = D_2 \left\{ \frac{\left(\frac{\gamma+1}{2}\right)^{1/(\gamma-1)} \left(1-\xi^2\right) \left(\frac{D_{1t}}{D_2}\right)^2}{4\left[1+\left(\frac{1+\eta_c}{2}\right)\left(\frac{\gamma-1}{2}\right)\left(\frac{U_2}{\sqrt{Rg_c T_{01}}}\right)^2 \varepsilon\right]^{1/(\gamma-1)}} \right\} \qquad [10.37]$$

One important design note is that for a given tip speed, higher values of M_{1R} are beneficial in reducing the relative size of D_2 and increasing the relative size of b_2 – ultimately allowing for smaller, more efficient clearance ratios for the impeller.[2]

Diffuser Geometry

For simplicity, only the vaneless diffuser configuration is addressed in this design section to provide a conservative estimate of the overall diameter required for the compressor. While vaned diffusers allow for a reduced frontal area by increasing the pressure more rapidly, the details of their layout are beyond the scope of this preliminary design effort. The vaneless diffuser design approach uses the conservation of angular momentum and an isentropic flow assumption to develop the following relationships for

calculating the angle between the velocity and the radial direction (α) and the radius (r), respectively:[2]

$$\frac{\tan\alpha^*}{\tan\alpha} = \left[\frac{2}{\gamma+1}\left(1+\frac{\gamma-1}{2}M^2\right)\right]^{1/(\gamma-1)} \qquad [10.38]$$

$$\frac{r^*\sin\alpha^*}{r\sin\alpha} = M\left[\frac{(\gamma+1)/2}{1+[(\gamma-1)/2]M^2}\right]^{1/2} \qquad [10.39]$$

Where * denotes the value attained in reversible, adiabatic flow from the local condition to sonic velocity.[2] Figure 10.14 shows a graphical representation of Equations 10.38 and 10.39 for a given value of $\gamma = 1.4$. Using this plot, the initial radius ratio $(r/r^*)_2$ and α^* is determined from the known diffuser inlet conditions M_2 and α_2. With α^* remaining constant, the final radius ratio $(r/r^*)_5$ corresponds to the desired diffuser outlet Mach number, M_5. Thus, the actual diffuser radius ratio is calculated as follows:

$$\frac{r_5}{r_2} = \frac{(r/r^*)_5}{(r/r^*)_2} \qquad [10.40]$$

In order to study the effects of reducing this ratio through the use of a vaned diffuser, the Excel design code described in APPENDIX E uses a simple linear reduction schedule to model the potential geometric and performance benefits.

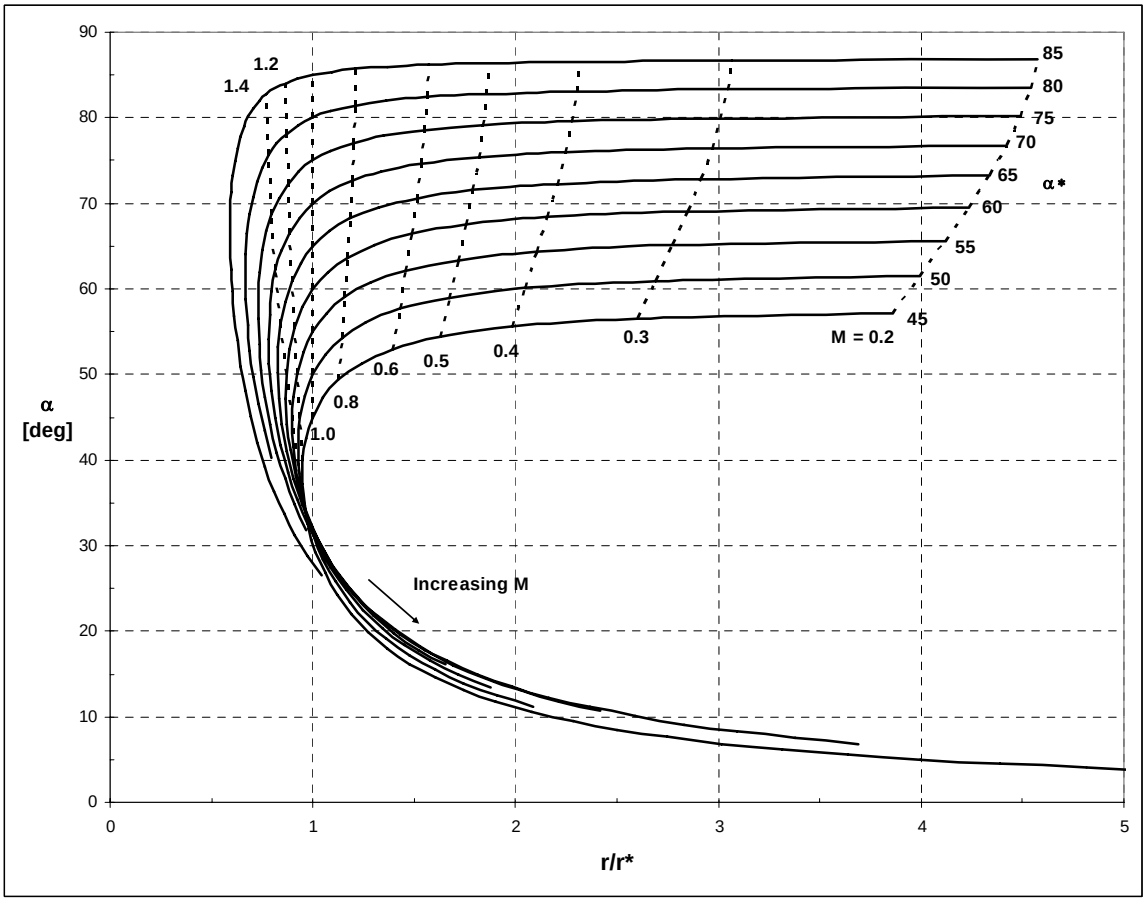

Figure 10.14: Compressible Flow in a Vaneless Diffuser (γ=1.4)[2]

Performance Analysis

With the initial geometry set during the previous steps, a mean-line velocity analysis of the flowpath is completed to verify that the selected design parameters provide the required level of performance. The solution process follows the sample problem calculations and techniques described in Chapter 4 of the *Introduction to Turbomachinery* textbook.[4] Based on assumptions for the slip factor and rotor efficiency, the rotor exit velocity triangle is calculated using an iterative process of guessing the rotor exit Mach number (M_2) and then continuously calculating a new value for M_2 until the two converge. The converged solution provides an accurate assessment of the overall

stage pressure ratio achieved. If the geometry and pressure ratio meet the requirements set during the engine cycle analysis, then the preliminary centrifugal compressor design is sufficiently complete.

Material Selection

The complex geometry of radial compressors makes the application of material strength relationships equally complex. Therefore, explicit calculations that determine the centrifugal stress of each blade are considered beyond the scope of preliminary design. However, Table 10.4 presents a list of the typical materials used in modern centrifugal compressors – highlighting their specific temperature and tip speed limitations. This level of detail sufficiently addresses the feasibility of the overall design and identifies an accurate material density for component weight estimation.

Table 10.4: Centrifugal Compressor Material Comparison[4]

Material	Nomenclature	Temperature Limit [^{o}R]	Tip Speed Limit [ft/s]	Density [lbm/in^{3}]	Yield Stress [ksi]*	Ultimate Strength [ksi]*
Aluminum Alloy	Al C355 T-6		1550	0.098	25.0	35.0
Advanced Aluminum Alloy	Al 2618 T-61	760-810	1700	0.0998	50.5	58.0
Titanium Alloy	Ti 6A1-4V	1260	2150	0.160	150.0	160.0

* At room temperature

Axial Turbine

Similar to the axial compressor design methodology in many ways, the preliminary design process for an axial turbine generates the geometric and performance characteristics required to justify the previous engine cycle analysis. This process closely

follows the approach presented by Mattingly et al. in *Aircraft Engine Design* and is applicable to the design of both high pressure and low pressure turbine components.

Velocity Diagrams

The trigonometric relationships and terminology used to describe the mean-line design for the turbine section is identical to that used in the compressor section. However, as Figure 10.15 demonstrates, there are significant differences in the magnitude of the angles in the velocity diagrams. Due to the acceleration of the flow, a favorable pressure gradient occurs – allowing the turbine stator and rotor to achieve more turning.

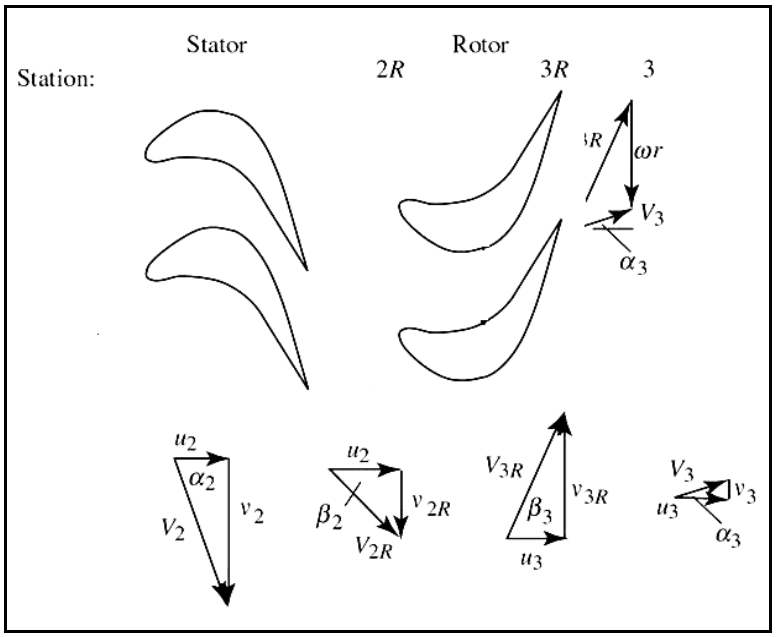

Figure 10.15: Turbine Velocity Diagrams[1]

Assumptions

The following list of simplifying assumptions, only slightly different from that of the axial compressor, plays a critical role in limiting the computational intensity of the

design process while still maintaining the accuracy and level of detail required to make effective design choices:[1]

- Two-dimensional flow
- Constant axial velocity ($u_1 = u_2 = u_3$)
- Constant mean radius
- Adiabatic flow in the stator and rotor
- Calorically perfect gas with known γ_t and R_t

Design Parameters

With the simplifying assumptions established, it is also necessary to highlight the design parameters that influence the performance of an axial turbine.

- Degree of Reaction (Λ_t) is defined as the change in static enthalpy of the rotor divided by the change in stagnation enthalpy of the stage:[2]

$$\Lambda_t = \frac{h_2 - h_3}{h_{01} - h_{03}} \qquad [10.41]$$

Unlike the repeating-row, mean-line compressor design, the degree of reaction for an individual turbine stage does not necessarily equal 0.5. At $\Lambda_t = 0.5$ (50% reaction), the enthalpy decrease across the rotor and stator is equal and the velocity diagrams are symmetric. If the Λ_t differs significantly from 0.5, then a large enthalpy decrease occurs in either the stator ($\Lambda_t < 0.5$) or the rotor ($\Lambda_t > 0.5$). Two special cases result at the extreme conditions of $\Lambda_t = 1$ and $\Lambda_t = 0$ – referred to as "reaction" and "impulse" turbines, respectively. In a "reaction" turbine, all of the decrease in pressure occurs in the rotor; whereas, for an "impulse" turbine, all of the pressure decrease occurs across the stator.[5]

- Stage Total Temperature Ratio (τ_s) is defined by the following expression:[3]

$$\tau_s \equiv \frac{T_{03}}{T_{01}} = 1 - \psi \frac{(\omega r)^2}{g_c c_p T_{01}} \qquad [10.41]$$

- Stage Pressure Ratio (π_s) is defined by the following relationship:

$$\pi_s \equiv \frac{p_{03}}{p_{01}} = \left(\tau_s\right)^{\gamma/[(\gamma-1)\eta_{pc}]} \qquad [10.42$$

- Stage Adiabatic Efficiency (η_s) is defined as:

$$\eta_s = \frac{h_{01} - h_{03}}{h_{01} - h_{03s}} \qquad [10.43]$$

Figure 10.16 shows an h-s diagram for a single-stage turbine – highlighting the losses that occur due to non-isentropic relationships. By assuming constant specific heats, Equation 10.43 can be simplified to the following:[3]

$$\eta_s = \frac{c_p\left(T_{01} - T_{03}\right)}{c_p\left(T_{01} - T_{03s}\right)} = \frac{1 - \tau_s}{1 - \pi_s^{(\gamma-1)/\gamma}} \qquad [10.44]$$

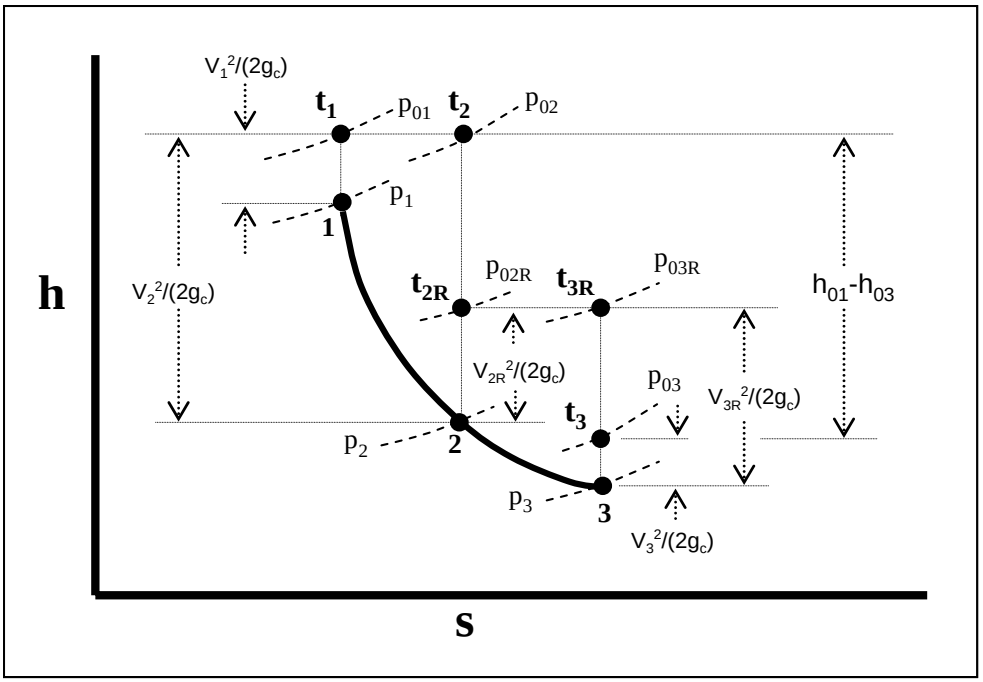

Figure 10.16: Single-Stage Turbine h-s Diagram[3]

- Stage Loading Coefficient (ψ) – Same as axial compressor design.

- Stage Flow Coefficient (Φ) is the ratio of axial velocity entering the rotor to rotor speed, such that:

$$\Phi = \frac{u_2}{\omega r} \qquad [10.45]$$

- Rotor and Stator Loss Coefficients (ϕ_{tr} and ϕ_{ts}) describe the pressure losses associated with each turbine section as follows:[3]

$$\phi_t \equiv \frac{p_{0i} - p_{0e}}{p_{0e} - p_e} \qquad [10.46]$$

Where the subscripts *i* and *e* refer to the inlet and exit states, respectively. Typical values for these parameters range from 0.08 to 0.15 for the rotor and 0.02 to 0.06 for the stator.

- Zweifel Coefficient (Z) is a ratio of tangential forces used as an initial estimate in determining the minimum solidity and number of blades required for the turbine. For preliminary turbine design, the coefficient can be expressed as follows for the stator and rotor, respectively:[3]

$$Z_s = \frac{2s}{c_x}\left(\cos^2 \alpha_2\right)\left(\tan \alpha_1 + \frac{u_2}{u_1}\tan \alpha_2\right)\left(\frac{u_1}{u_2}\right)^2 \qquad [10.47]$$

$$Z_r = \frac{2s}{c_x}\left(\cos^2 \beta_3\right)\left(\tan \beta_2 + \frac{u_3}{u_2}\tan \beta_3\right)\left(\frac{u_2}{u_3}\right)^2 \qquad [10.48]$$

Where c_x is the axial chord of the blade.

Design Parameter Analysis

Similar to the axial compressor design, the aforementioned assumptions and definitions can be combined to generate a generic solution process that effectively describes the behavior and required geometry for turbine flow. The difference, however,

is that the turbine's general solution approach is limited to an individual stage because the effects of supersonic flow would otherwise contradict the design constraints. Based on known values for M_2, α_2, M_{3R}, and rotational speed, the following sequence of formulae represents the general solution process described by Mattingly et al. in *Aircraft Engine Design*:[1] (Note: Dimensionless quantities are used throughout this section by dividing by the maximum velocity, $V' = \sqrt{g_c c_{pt} T_{01}}$)

(1) $$\frac{V_2}{V'} = \sqrt{\frac{(\gamma_t - 1)M_2^2}{1 + (\gamma_t - 1)M_2^2/2}} \qquad [10.49]$$

(2) $$\frac{u}{V'} = \frac{V_2}{V'}\cos\alpha_2 \qquad [10.49]$$

(3) $$\frac{\upsilon_2}{V'} = \frac{V_2}{V'}\sin\alpha_2 \qquad [10.50]$$

(4) $$\frac{\upsilon_{2R}}{V'} = \frac{\upsilon_2}{V'} - \Omega \qquad (\text{where } \Omega = \frac{\omega r}{V'}) \qquad [10.51]$$

(5) $$\tan\beta_2 = \frac{\upsilon_{2R}/V'}{u/V'} \qquad [10.52]$$

(6) $$\frac{T_{02R}}{T_{01}} = 1 + \Omega^2\left(\frac{1}{2} - \frac{\upsilon_2/V'}{\Omega}\right) \qquad [10.53]$$

(7) $$\tan\beta_3 = \sqrt{\frac{T_{02R}/T_{01}}{u^2/V'^2}\frac{(\gamma_t - 1)M_{3R}^2}{1 + (\gamma_t - 1)M_{3R}^2/2} - 1} \qquad [10.54]$$

(8) $$\text{Turning angle} = \beta_2 + \beta_3 \qquad [10.55]$$

(9) $$\frac{\upsilon_3}{V'} = \frac{u}{V'}\tan\beta_3 - \Omega \qquad [10.56]$$

(10) $$\tan\alpha_3 = \frac{\upsilon_3/V'}{u/V'} \qquad [10.57]$$

(11)
$$\frac{T_3}{T_{01}} = \frac{T_{02R}/T_{01}}{1+(\gamma_t - 1)M_{3R}^2/2} \qquad [10.58]$$

(12)
$$\tau_s = \frac{T_{03}}{T_{01}} = \frac{T_3}{T_{01}} + \frac{u^2}{V'^2}\frac{1+\tan^2\alpha_3}{2} \qquad [10.59]$$

(13)
$$\Lambda_t = \frac{\upsilon_{3R}^2 - \upsilon_{2R}^2}{2(1-\tau_s)V'^2} \qquad [10.60]$$

(14)
$$\text{Rotor solidity}(\sigma) = \frac{s}{c} = \frac{2\cos^2\beta_3(\tan\beta_2 + \tan\beta_3)}{Z} \qquad [10.61]$$

Sensitivity analysis is conducted – using the general solution formulae and reasonable values for M_{3R}, α_2, and the dimensionless rotor speed (Ω) – to identify favorable trends that assist in the selection of the initial turbine design parameters. Specifically, using values such as $M_{3R} = 0.9$, $60^o < \alpha_2 < 75^o$, and $0.2 < \Omega < 0.3$ has historically marked the limits for optimum turbine performance.[1] Additionally, the performance differences between choked and unchoked stages are addressed by assuming supersonic and subsonic values for M_1, respectively. Figures 10.17 – 10.22 show the results of this analysis.[1]

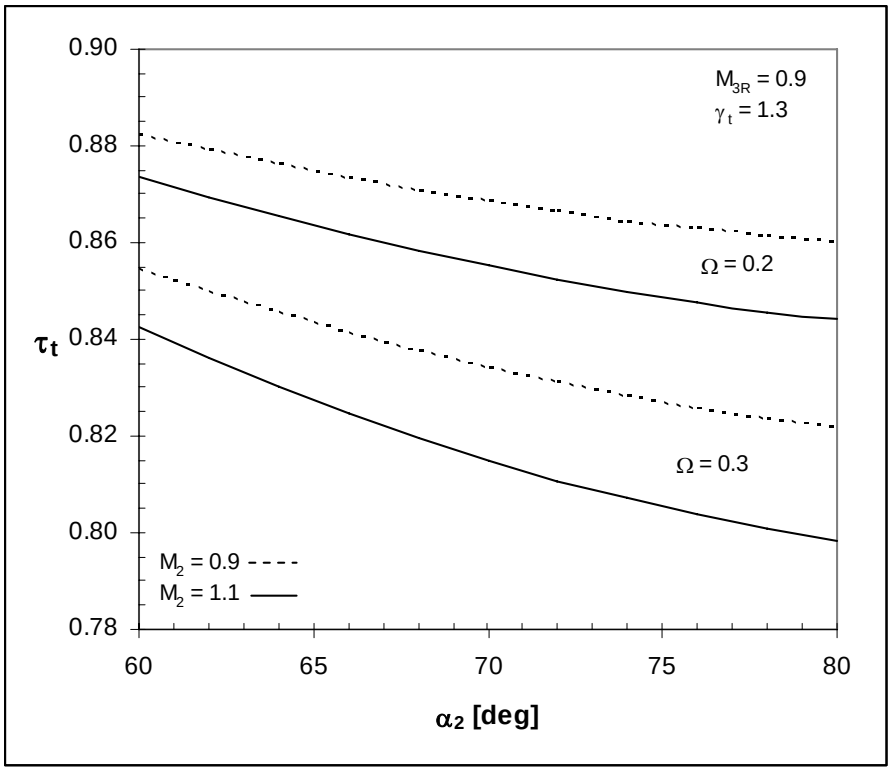

Figure 10.17: Turbine Stage Total Temperature Ratio

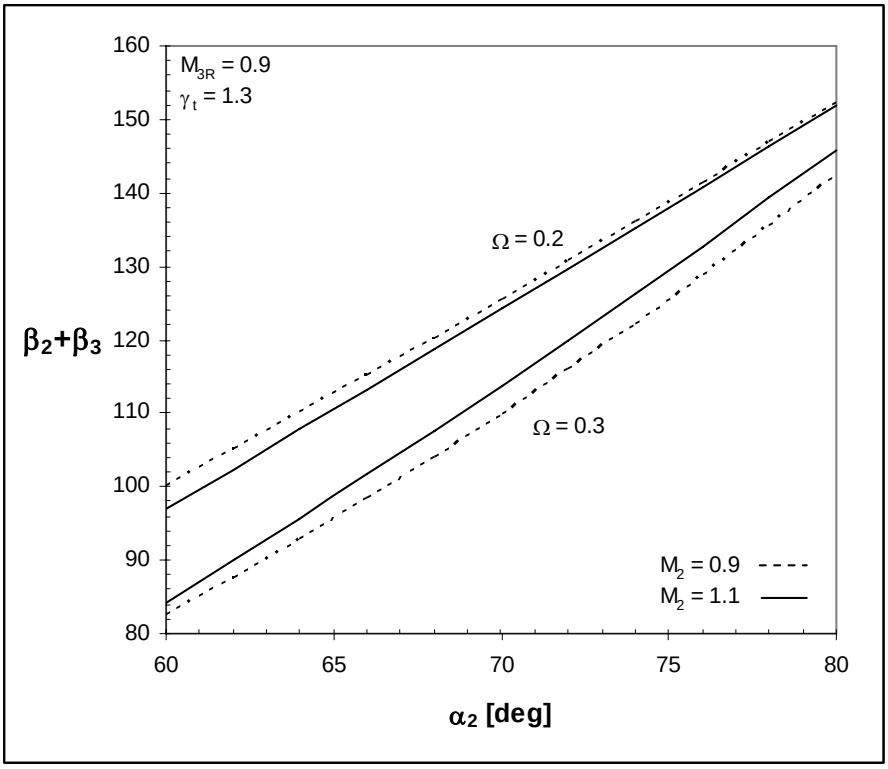

Figure 10.18: Turbine Rotor Flow Turning Angle

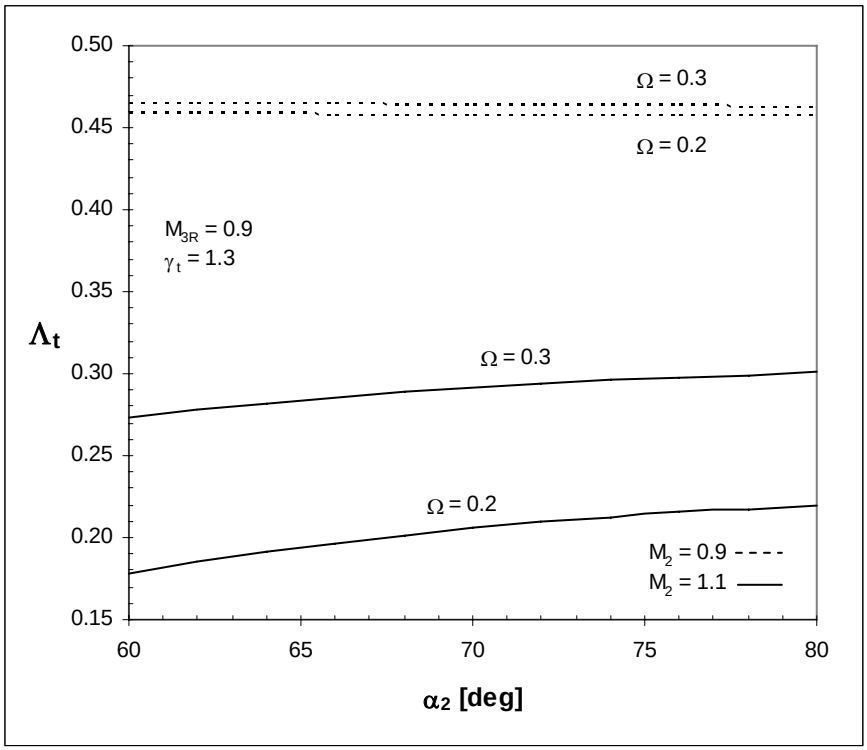

Figure 10.19: Turbine Rotor Degree of Reaction

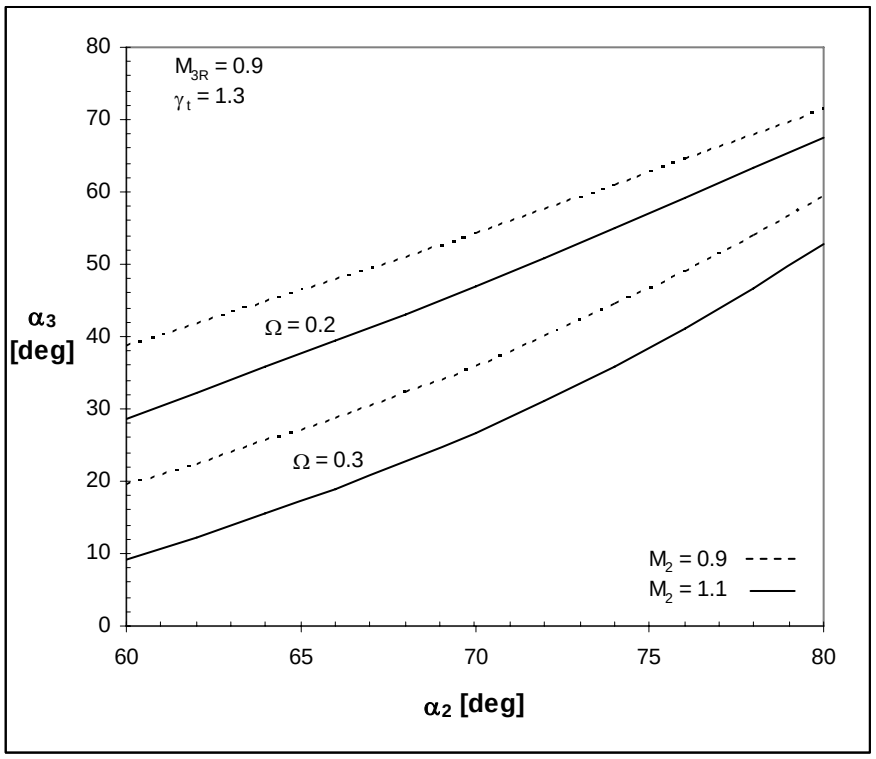

Figure 10.20: Turbine Stage Exit Flow Angle

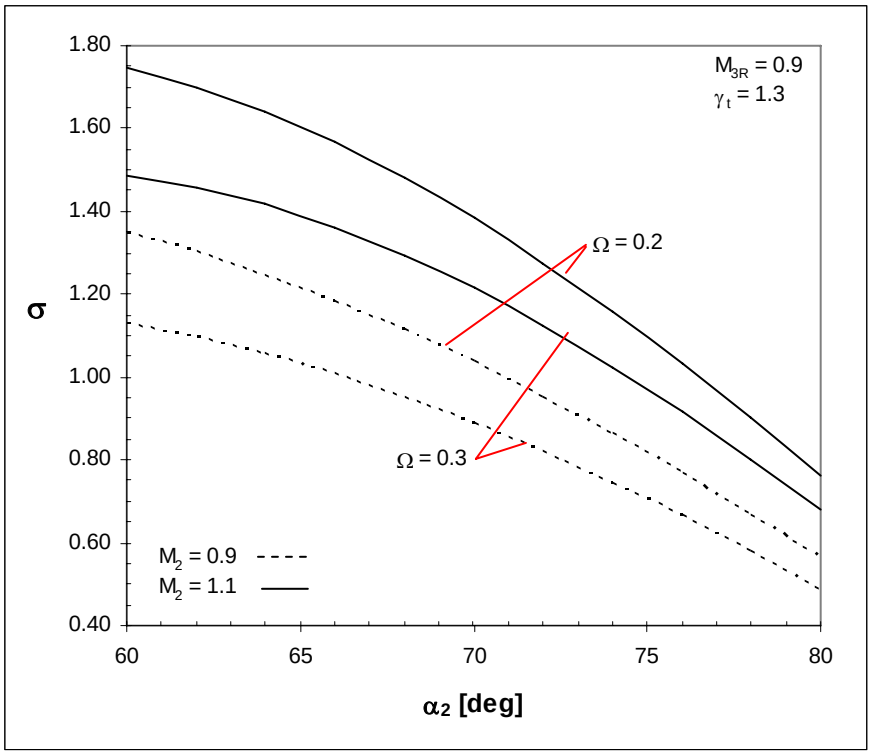

Figure 10.21: Turbine Rotor Solidity (Z=1)

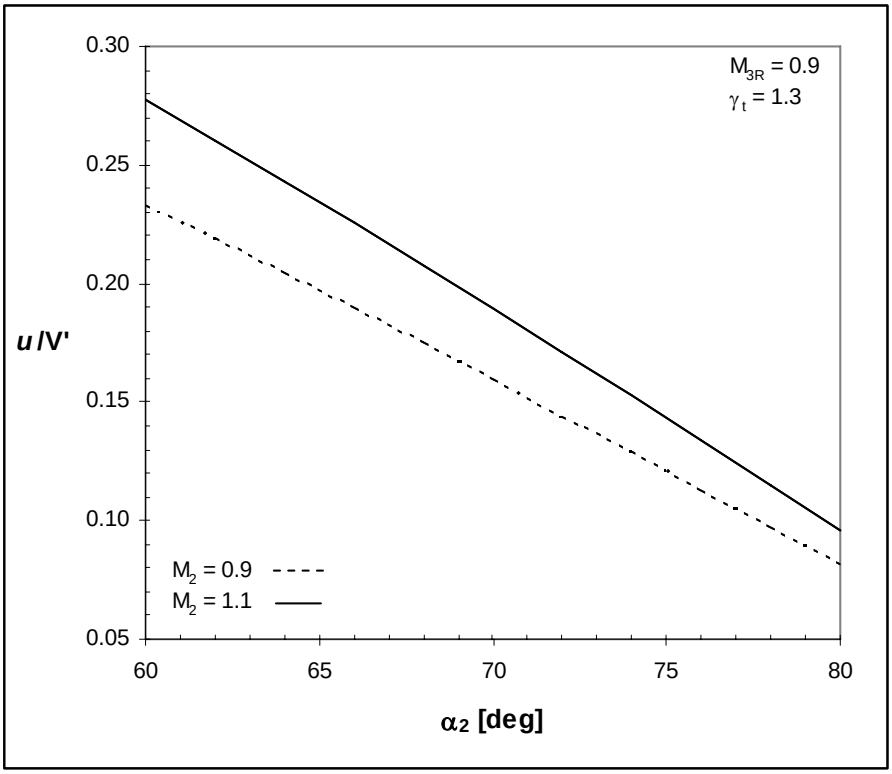

Figure 10.22: Turbine Stage Axial Velocity

The generalized turbine design guidance demonstrated by industry practice and these plots is summarized, as follows:

- Increasing Ω always has a beneficial effect on turbine performance; however, the rotational speed is limited by material and structural properties.
- Increasing α_2 within its normal range will reduce the total temperature ratio (τ_s) for both choked and unchoked stages – minimizing the required number of stages.
- Increasing α_2 causes a significant rise in the rotor flow turning angle – an indicator of increased potential for boundary layer separation. Current industry practice indicates that flow turning angles of 120-130^o are possible as long as Λ_t exceeds 0.2. Therefore, α_2 should be limited to 70^o when $0.2 < \Omega < 0.3$.[1]
- General industry practice dictates that α_3 should not exceed 40^o; however, many acceptable combinations of α_2, Ω, and M_1 can cause α_3 to extend as high as 70^o.
- Increasing α_2 reduces the rotor solidity for a given value of Z – minimizing the number of airfoils and reducing manufacturing cost.
- Reducing α_2 has a beneficial effect in terms of increasing the axial velocity – which minimizes the flowpath area and, thus, minimizes the airfoil height, weight, and centrifugal stress.

These trends indicate that certain levels of design compromise are required in selecting the value of α_2, whereas, maximizing the value of Ω proves to be beneficial in all circumstances. As a guide for design parameter selection, Table 10.5 provides a summary of the typical ranges used on modern axial turbines.

Table 10.5: Axial Turbine Design Parameter Ranges[1]

Parameter		Design Range
High Pressure Turbine:		
Maximum AN^2		4 - 5 x 10^{10} in^2-RPM^2
Stage Loading Coefficient ψ		1.4 - 2.0
Exit Mach Number M_3		0.4 - 0.5
Exit Swirl Angle α_3		0 - 40 deg
Turning Angle $\beta_2+\beta_3$		< 120-130 deg
Low Pressure Turbine:		
Hub/Tip Ratio	Inlet	0.35 - 0.50
Maximum Stage Loading ψ	Hub	2.4
Exit Mach Number M_3		0.4 - 0.5
Exit Swirl Angle α_3		0 - 40 deg

Flowpath Design

Understanding the trends associated with each turbine design parameter, the process of turbine flowpath design can begin. Once again, the Turbine Preliminary Design Program (TURBN) – provided as part of the *Aircraft Engine Design* software package – automates most of this design process. But, in the same manner used for the axial compressor design, a simplified Excel program was developed to provide more transparency in applying the preliminary turbine design general solution equations (See APPENDIX D).

Number of Stages

The first step in turbine design is to determine the number of stages required to generate the predicted turbine output from engine cycle analysis at the design point. Typically, the turbine design point is evaluated as the maximum turbine inlet temperature (T_4) at sea-level conditions. Due to the manufacturing complexity, weight, and high cost

of turbine components, the number of stages must be minimized. An initial material selection is made for the turbine disk in order to estimate its maximum allowable rim speed using Equation 10.62. Increasing the rim speed by 10% gives an initial approximation for mean wheel speed. This value is then used to determine Ω such that:

$$\Omega = \frac{\omega r_m}{\sqrt{g_c c_{pt} T_{01}}} \qquad [10.62]$$

The turbine temperature ratio (τ_t) determined during engine cycle analysis and Ω are now evaluated using Figure 10.17 to identify if more than one turbine stage is required. If a single-stage is considered adequate, then initial estimates for α_2, M_2, and M_{3R} can be established.

However, if multiple stages are necessary to maintain M_2 and α_2 within the ranges specified in Table 10.5, then the following design parameter guidance applies:[1]

- Inlet flow angle (α_2) and exit relative Mach number (M_{3R}) should be the same for each stage.
- Mach number leaving the turbine stators of the first stage needs to be supersonic ($M_2 > 1$); whereas, for each subsequent stage, the same Mach number should be subsonic ($M_2 < 1$).

Initial estimates for α_2, M_2, and M_{3R} for multi-stage applications are established based on the combined effects of each individual stage temperature ratio (τ_{ts}) and Ω_s. The relationship between subsequent stages is expressed as follows:

$$\Omega_{\text{stage i}} = \frac{\Omega_{\text{stage (i-1)}}}{\sqrt{(\tau_{ts})_{\text{stage (i-1)}}}} \qquad [10.63]$$

The value of $\Omega_{\text{stage i}}$ determines the value of $(\tau_t)_{\text{stage i}}$ and, thus, the overall turbine temperature ratio can be evaluated against its predicted performance requirements:

$$\tau_t = (\tau_{ts})_{\text{stage1}} (\tau_{ts})_{\text{stage2}} \ldots (\tau_{ts})_{\text{stage n}} \quad [10.64]$$

Performance Analysis

The estimated values of ωr_m, α_2, M_2, and M_{3R} are used as the input data in determining the overall performance of the turbine design. As demonstrated in Equations 10.49 – 10.61, the general solution of the mean-line design process defines the aerodynamic and thermodynamic attributes of each stage. The results are then compared with the ranges presented in Table 10.5 to justify the feasibility of the design and determine if further iteration is necessary.

Material Selection

Similar to the axial compressor, the final step in turbine design involves stress analysis based on material selection – the goal of which is to finalize the rotational speed and geometry of the component. Assuming a strength-to-weight ratio for the turbine blade material based on Figure 10.7, the following expression is used to determine the angular velocity (ω):[1]

$$\omega = \sqrt{\frac{4\pi}{A(1 + A_t / A_h)} \frac{\sigma_c}{\rho}} \quad [10.65]$$

Where A is the average annulus area of the first stage. It is important to highlight, once again, that this value of ω for the high pressure turbine usually represents the limiting factor involved in component matching with the compressor. The mean radius is calculated by dividing the estimated mean wheel speed (ωr_m) by ω – thus defining the

geometric and stress properties of the blades. The stress analysis for the rim and the disk follows the same process outlined for the axial compressor. Ultimately, if all of the resultant values for the stress analysis and geometry of the blades, rim, and disk are considered acceptable in terms of performance, manufacturability, and cost – the preliminary turbine design is sufficiently complete.

Component Weight Estimation

Once the dimensions and material properties are set for the compressor and turbine sections, a weight estimate is determined using the material density characteristics of each component. The technique of weight estimation is fundamentally simple – component volume multiplied by material density produces component weight. The challenge lies in accurately estimating the volume of components whose geometry is inherently complex. As mentioned at the outset of preliminary component design, WATE provides an automated tool for estimating the geometry and weight of engine components, but it demonstrates limited capability in handling extremely small airflows common in rotorcraft turboshaft engines.

The Excel code used to design the compressor and turbine sections incorporates a simplified approximation of volume based on the dimensions of the major rotating components to generate an initial weight estimate. However, the accuracy of this estimate is greatly improved by incorporating a detailed engine model using CAD (Computer Aided Design) software which can calculate the exact volume of 3-dimensional components. Thus, as the details of the CAD model are updated to reflect the dimensions of each component, the accuracy of the volume measurements also

improves. APPENDICES D and E show examples of the GTGH compressor and turbine section models that were created using CATIA™ modeling software and Table 10.6 shows the CAD volume measurements and corresponding component weights for the GTGH engine.

Table 10.6: Engine Weight Assessment (GTGH)

Component	Volume (in^3)	Density (lb/in^3)	Weight (lb)
Compressor	35.20	0.170	6.0
Combustor	18.60	0.283	5.3
High Pressure Turbine	12.97	0.298	3.9
Low Pressure Turbine	24.06	0.298	7.2
Compressor Shaft	11.88	0.298	3.5
Power Turbine Shaft	7.58	0.276	2.1
Gearbox	220.96	0.283 / 0.098	51.9
Housing	141.99	0.283	40.2
		Total Weight	**120.0**

[1] Jack D. Mattingly, William H. Heiser, and David T. Pratt, *Aircraft Engine Design*, 2nd ed. (Virginia: AIAA, 2002).

[2] Phillip G. Hill and Carl R. Peterson, *Mechanics and Thermodynamics of Propulsion* (Reading, MA: Addison-Wesley Publishing, 1992).

[3] Jack D. Mattingly, *Elements of Gas Turbine Propulsion* (Reston, VA: AIAA, 2005).

[4] David Japikse and Nicholas C. Baines, *Introduction to Turbomachinery* (White River Junction, VT: Concepts ETI, 1997).

[5] Ronald D. Flack, *Fundamentals of Jet Propulsion with Applications* (New York, NY: Cambridge University Press, 2005).

CHAPTER 11

PROPULSION SYSTEM INTEGRATION

With the core engine design completed, it is now appropriate to consider some additional design factors that influence the integration of the propulsion system into the total vehicle concept. Up to this point, very little attention has been given to the relationship between the engine and its external environment. Although a basic set of geometric requirements was incorporated early-on in the design process, there are many other interactive details yet to address. The pilot controls, transmission, main rotor, anti-torque system, and airframe structural design are all directly influenced by the configuration and performance of the propulsion system. The purpose of this chapter is to highlight the key engine integration concepts that will ultimately drive an effective overall vehicle design solution.

Engine Control Systems

The engine control system provides the link between pilot control inputs and engine response. This link usually consists of physical and electrical connections that equate the power demand from the cockpit to the power output of the engine. For rotorcraft, the engine control system response time is particularly important due to the increased frequency of transient power requirements compared with fixed-wing applications. Due to advances in computer processing capability, engine control systems have significantly increased in sophistication over time – providing the ability to monitor, limit, and detect faults in engine performance.

Full-Authority Digital Electronic Control (FADEC)

Over the past decade, FADEC has emerged as the standard control system used on modern rotorcraft vehicles with turboshaft engines. The system has evolved to represent one of the key elements enabling improvements in engine performance, lifetime, reliability, testability, and maintainability.[1] The FADEC system consists of a digital electronic control unit (ECU), a hydro-mechanical metering assembly (HMA), which includes a fuel pump and flow control section, and wiring harnesses that connect the ECU and the HMA to sensors on the engine and airframe. The operation of the engine control system is best described in Figure 11.1, which shows a typical functional schematic diagram. In its simplified form, input data is used to determine the desired engine state and then compares this information with the actual engine state to generate an error vector. A micro-processing unit then produces an output vector that will drive the error vector to zero. In physical terms, the computational outputs control a series of motors and actuators that carry out the requested commands. Typical inputs include the inlet pressure, inlet temperature, and collective position; whereas, gas generator fuel flow is the standard output.

As FADEC systems continue to evolve, their functionality offers ever increasing benefits. The system constrains its potential solution space by incorporating thermodynamic (compressor stall margin), chemical (minimum combustor fuel-air ratio to avoid flameout), and mechanical (rotational speed and temperature) limits.[2] Specific capabilities such as overspeed protection, temperature limiting, surge detection and avoidance, flameout detection and relight, fault monitoring, and automatic engine starting are commonplace. Modern FADEC can simultaneously monitor and interpret hundreds

of parameters from aircraft subsystems and sensors – providing a fully redundant and fault tolerant control system. The improved responsiveness of FADEC systems allows pilots to move the collective as fast as physically possible without risking a stall, surge, or damage to the transmission.[3] This precise level of control also translates into better fuel efficiency for the entire propulsion system. Figure 11.2 shows the FADEC system used on the Bell 430 helicopter.

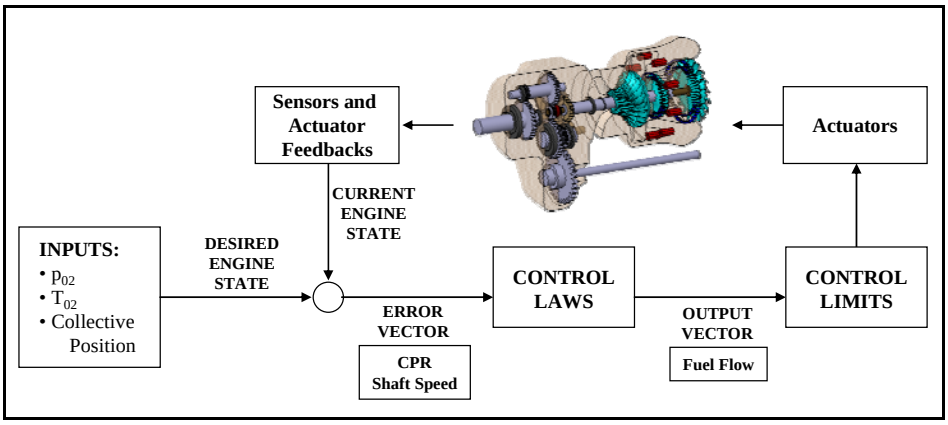

Figure 11.1: Typical FADEC Functional Architecture

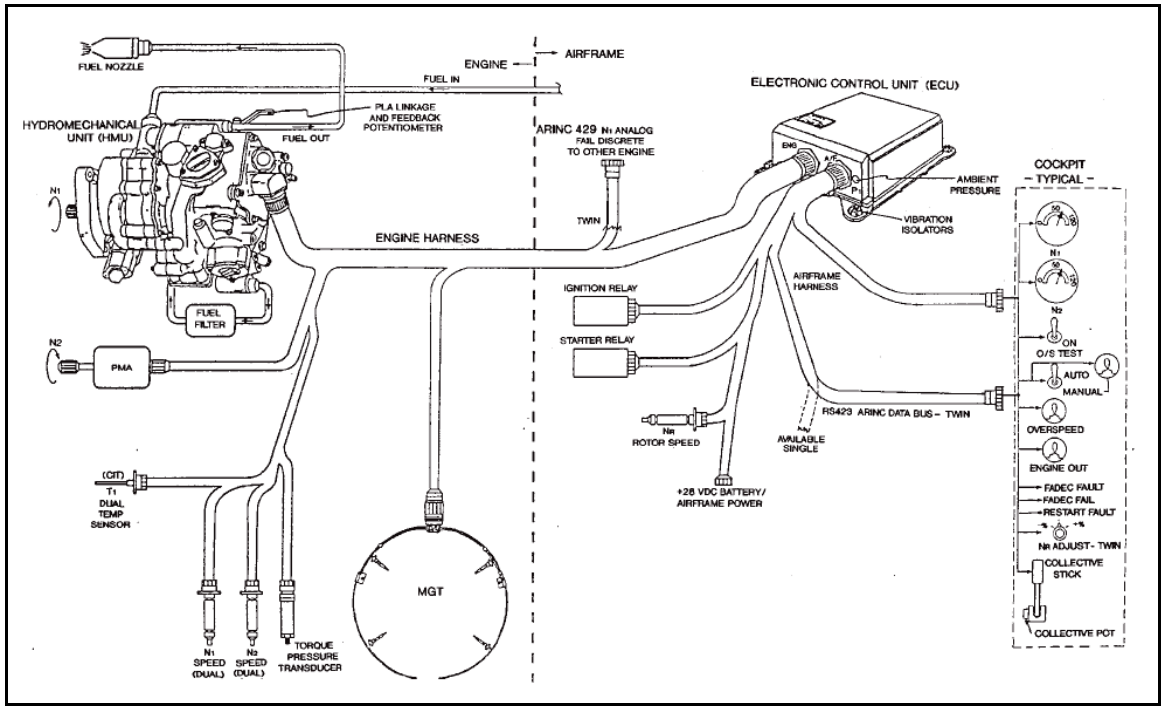

Figure 11.2: Bell 430 Helicopter FADEC System (*with permission*) [4]

Health and Usage Monitoring System (HUMS)

Many rotorcraft engine control systems also incorporate health and usage monitoring systems (HUMS) to provide a non-intrusive means for accurately assessing the remaining service life for critical engine components – reducing maintenance costs while increasing reliability and safety. HUMS use accelerometers and oscillatory sensors to evaluate a vehicle's flight-by-flight usage spectrum and calculate the loading conditions experienced by each life-limited part. This data is then used to diagnose and predict engine maintenance actions based on specific vehicle usage. As Figure 11.3 demonstrates, the ability to assess a component's remaining service life based on usage offers significant safety and financial benefits. HUMS data is used to predict rotor, transmission, and airframe fatigue life estimates, as well.

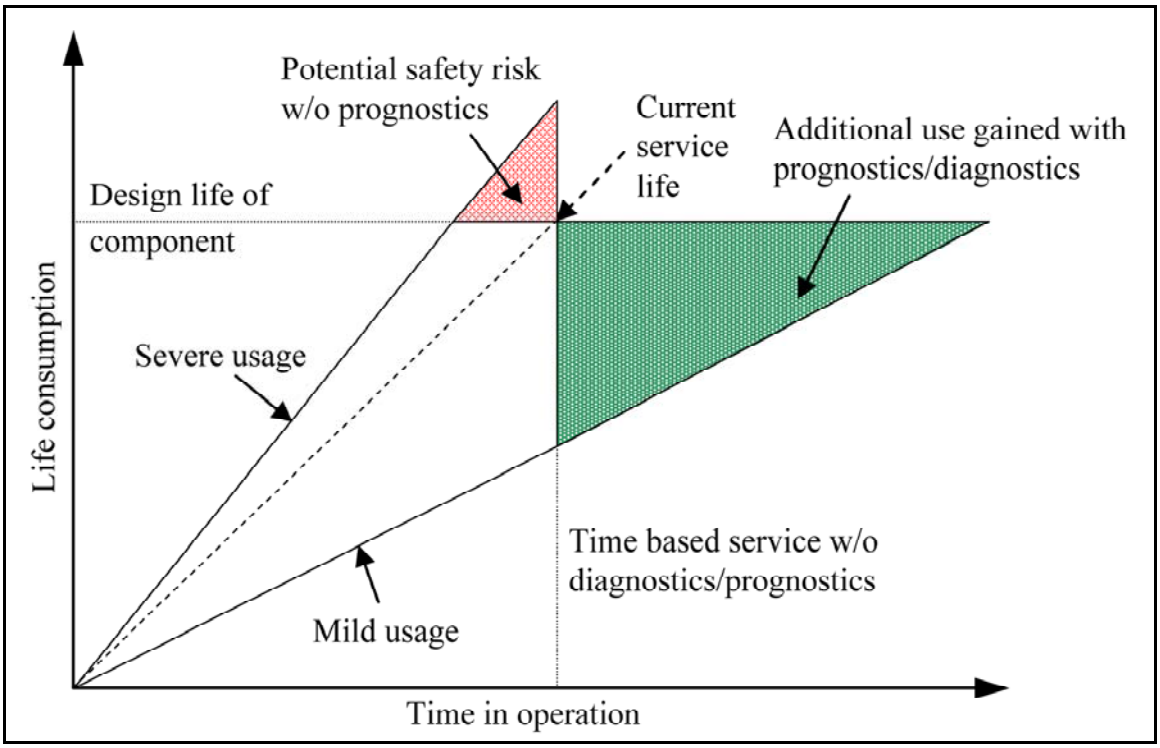

Figure 11.3: Economic and Safety Benefits of HUMS[5]

Control System Redundancy

The use of digital electronic engine controls has not eliminated the need for backup systems in the case of partial or complete failure. Federal Aviation Regulations (FAR) require that all electrical engine control systems be designed and constructed such that no probable combination of electrical or electrical component failures will lead to an unsafe flight condition.[6] Some FADEC systems use an independent, dual-channel concept to increase redundancy and reduce the probability and severity of failures. Engine control units also incorporate partial failure modes that operate with varying levels of functionality based on the severity of the failure. In the case of a complete failure, the engine control will typically operate in a manual mode in which the pilot directly controls the flow of fuel to the engine with the throttle and hydro-mechanical unit linkage. This emergency operating mode greatly increases pilot workload and is intended to only provide the essential functionality required for safe landing and recovery of the aircraft.

Air Induction System

The air induction system is a key ingredient in the functional relationship between engine installation and performance. The inlet must provide the required quantity of airflow to the engine with a maximum level of energy and minimal distortion, while also protecting engine components from foreign object damage. Inefficiencies in engine inlet design are magnified throughout the subsequent stages of the engine, resulting in significant performance penalties. Non-uniform, unsteady flow can also induce

compressor stall, which can cause damaging internal engine temperatures.[7] For rotorcraft, in particular, the air induction system has many unique challenges resulting from the speed, attitude, and directional change capability of such vehicles. The following sections highlight some quantitative and qualitative design considerations for engine inlets that should be included during the preliminary design sequence.

Inlet Design

During preliminary design, three concepts drive the aerodynamic design of the engine inlet: high total pressure recovery, low compressor distortion, and low external vehicle drag. Design success is measured in the ability to minimize losses from wall friction, contraction, diffusion, bends, and distorted flow resulting from obstructions in the duct. Smooth internal duct surfaces that avoid protrusions (i.e. bolts, rivets, sheet metal connections, etc.) ensure friction and contraction losses are small. Maintaining low internal flow speeds also helps reduce frictional losses. Plenum chambers combined with bell mouth inlets are recommended when sharp bends are required. As a rule of thumb, each percentage point of inlet pressure loss equates to a loss of 1.5-2.0% of engine rated power at MCP and, thus, the importance of minimizing such losses cannot be overstated.[7]

Inlet Types

The basic types of air intake systems can be classified as either static or dynamic. For static air intakes, the plane of the inlet is parallel with the general airflow direction. The advantages of this configuration are design simplicity and reductions in system weight, ingestion of foreign debris, and fuselage drag. The disadvantages are increased flow distortion in the compressor plane and greater potential for hot gas intake. By

incorporating a large radius curvature on their upstream edge, fully optimized static inlets can prevent flow separation and recover up to 50% of the ram pressure in forward flight.[8] Dynamic, or "ram" intakes, are generally perpendicular to the airflow direction in order to maximize their pressure recovery in forward flight and minimize flow distortion at the face of the compressor. Fuselage integration of dynamic inlets usually requires longer ducts which can result in greater inherent pressure losses, but this condition is offset by the reduction of exhaust gas re-ingestion (EGR) during hovering flight and the increased dynamic pressure recovery in forward flight.[8] Figure 11.4 shows a schematic view of both static and dynamic inlets for hover and forward flight conditions, respectively.

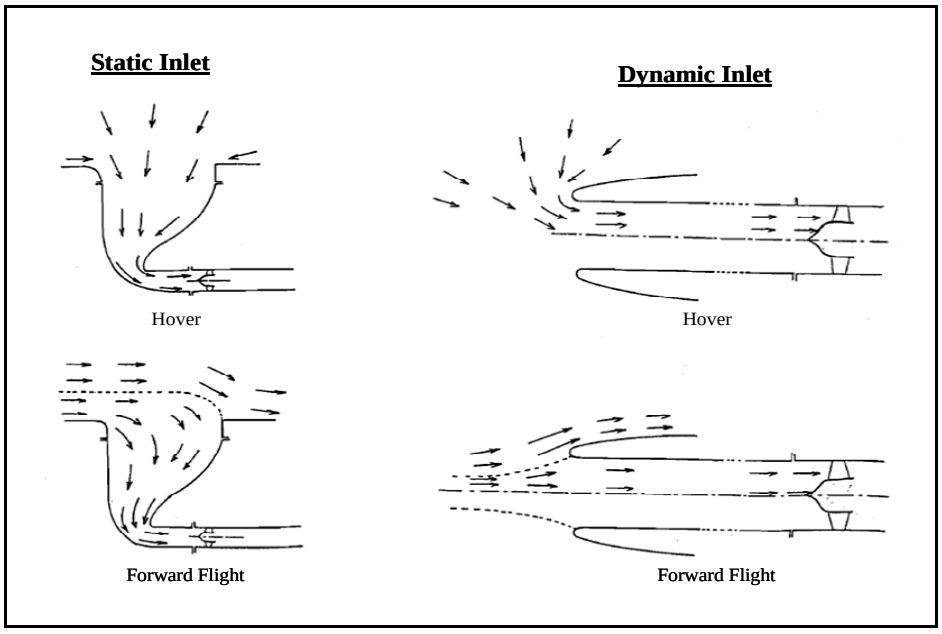

Figure 11.4: Static and Dynamic Inlet Schematic Diagrams[8]

Inlet Location

Several factors influence the selection of the engine air induction system location. It is necessary to consider the overall fuselage pressure distribution to help avoid placing the inlet in locations prone to high velocities, decelerating flows, or in the wake of

aircraft components that disturb the flow. Changes in aircraft attitude as a result of flight maneuvering should not significantly effect the pressure distribution at the inlet. Submerged inlets or inlet scoops should avoid areas of boundary layer buildup.[7] The height of the inlet on the fuselage should also be maximized to reduce the potential ingestion of foreign objects that could damage the engine's rotating components.

Inlet Area

The inlet capture area for maximum efficiency, where local velocity gradients and flow separation are minimized, can be defined in terms of the ratio between inlet and freestream velocity as $0.40 \leq V_i/V_o \leq 0.65$. Selection of the specific ratio within this range depends on the vehicle's mission and – when combined with engine power, airflow, and cruise speed – defines the inlet area.[9]

Duct Pressure Losses

While airflow testing provides the final performance assessment for a given air induction system, a simplified one-dimensional flow analysis provides an initial indication of overall duct performance sufficient for preliminary design. The total pressure loss due to duct friction (Δp_f) is approximated using the following expression:[7]

$$\Delta p_f = \frac{4 f \, Lq}{D_h} \qquad [11.1]$$

Where f is the friction factor[10] determined as a function of Reynolds number and surface roughness (typically varies between 0.003 and 0.007), L is the duct length, $q = \frac{\rho V^2}{2}$ is the dynamic pressure, and $D_h = \frac{4(\text{duct cross} - \text{sectional area})}{\text{wetted perimeter}}$ is the hydraulic diameter.

The pressure loss due to turns, diffusion, acceleration, or flow obstructions is estimated using a loss factor (k) as follows:[7]

$$\Delta p_k = kq \qquad [11.2]$$

Where k is determined as a function of the geometry (see Reference 10) and q is the dynamic pressure immediately prior to the geometric feature. The total pressure loss is then calculated as the sum of the frictional and geometric losses for a given design. In order to simplify the calculations, duct pressure losses at sea-level air density are assumed to remain constant throughout the flight envelope such that an evaluation of the engine for maximum power at SLS conditions will satisfy every other condition.

Engine Air Particle Separator (EAPS)

The unique operational characteristics of rotorcraft often require prolonged flight in and around unimproved sites where the potential to ingest foreign debris is greatly increased. Foreign object damage (FOD) can significantly influence engine performance – large objects can destroy an engine, small particles (> 1000 micron diameter) can damage compressor blades, and even smaller particles (< 1000 micron diameter) can cause airfoil erosion and flowpath restrictions due to accumulation over extended time periods.[7] Engine air particle separators (EAPS) are used to filter the air prior to the engine compressor to eliminate or reduce FOD. The design goals for such systems can be summarized as follows: high separation rate, low pressure drop, low weight, and low cost. While each EAPS application presents unique design challenges, general guidelines dictate that the total pressure at the face of the engine should be at least 99% of ambient static pressure for all flight modes in which the system is operational.[7] Modern

helicopter engine installations primarily use two particle filtration methods: inertial separators and barrier filters.

Inertial Separators

Based on simple momentum principles, inertial separators work by quickly changing the direction of motion of the clean airflow while the flow of entrained particles continues on its original trajectory. Three primary methods are used in the design of inertial separators: scavenged bend, vortex tube, and integrated particle separators.

Scavenged Bend Separator

The separation efficiency for this system, with typical geometry depicted in Figure 11.5, is approximately 60-85% for course test sand particles. Large scavenge bypass flows (about 20-30%) are required to achieve efficiencies above 70% at acceptable pressure losses (< 1%). A scavenger pump is often required, resulting in significant power loss at high separation efficiencies. The advantages of the scavenged bend configuration are low installation weight, small frontal area, and no flow bypass requirement.[7]

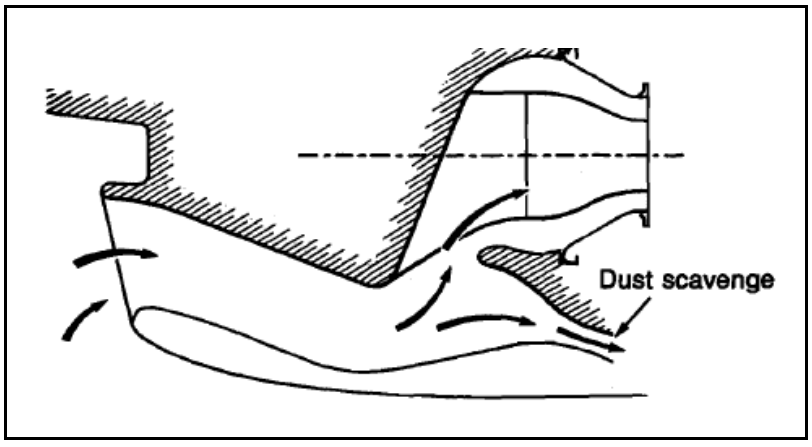

Figure 11.5: Scavenged Bend Separator Schematic[11]

Vortex Tube Separator

As depicted in Figure 11.6, vortex tube separators consist of a cylindrical tube with helical inlet swirl vanes that rotate the incoming flow such that higher momentum particles are centrifuged to the outer wall of the tube for disposal and clean airflow exits through a diffuser. The scavenged airflow and particles must be ejected overboard using a fan or engine bleed air. A matrix of individual tubes is arranged on panels suitable for aircraft installation. Vortex tubes demonstrate low pressure losses and separation efficiency as high as 93% for course test sand with maximum scavenge flow of 5-10%. The disadvantages, however, are large panel area requirements (only 1-2 lbm/s of airflow per square foot) and poor compatibility with snow, ice, and larger particles that can clog the individual tubes.[7] The panels are normally mounted perpendicular to the airflow to help minimize the ingestion of large particles. Figure 11.7 shows the effect of cross flow (or increasing forward speed) on vortex tube panel efficiency.

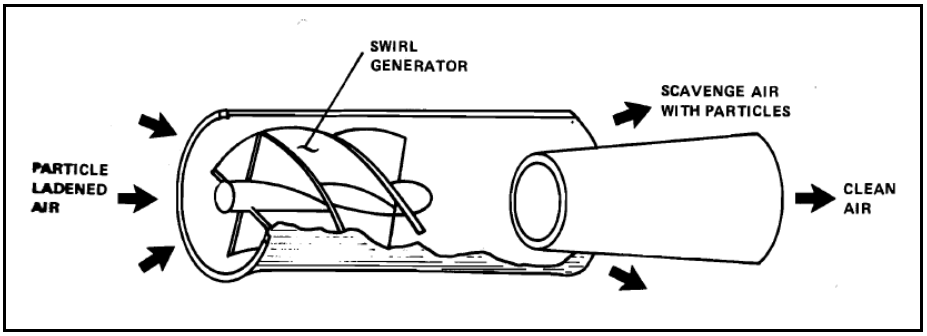

Figure 11.6: Vortex Tube Separator Schematic[7]

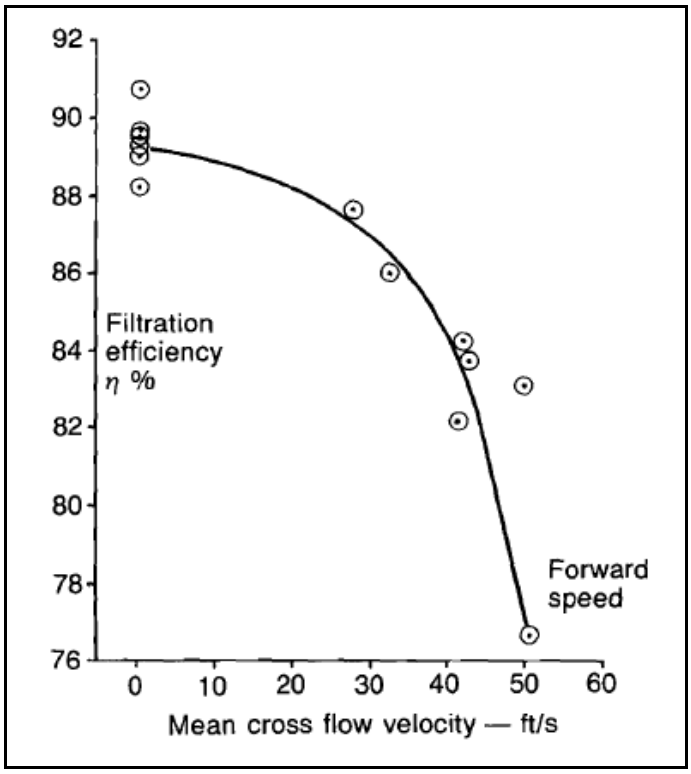

Figure 11.7: Cross Flow Effect on Vortex Tube Panel Efficiency[11]

Integrated Particle Separator (IPS)

An integrated particle separator (IPS), shown in Figure 11.8, uses the same separation mechanism as that of the vortex tube – with the key differences being its size and location. IPS consist of only one large cyclone integrally attached to the engine and have performed with separation efficiencies as high as 85% for course test sand. The advantages of this approach are higher airflows per square foot of inlet area (> 10 lbm/s) and improved engine integration which provides better optimization potential and reduced installation difficulties. The disadvantages of an integral design, however, are reduced separation efficiency for smaller particles and no bypass capability which increases the engine's operational penalties outside of the sand and dust environment.[12]

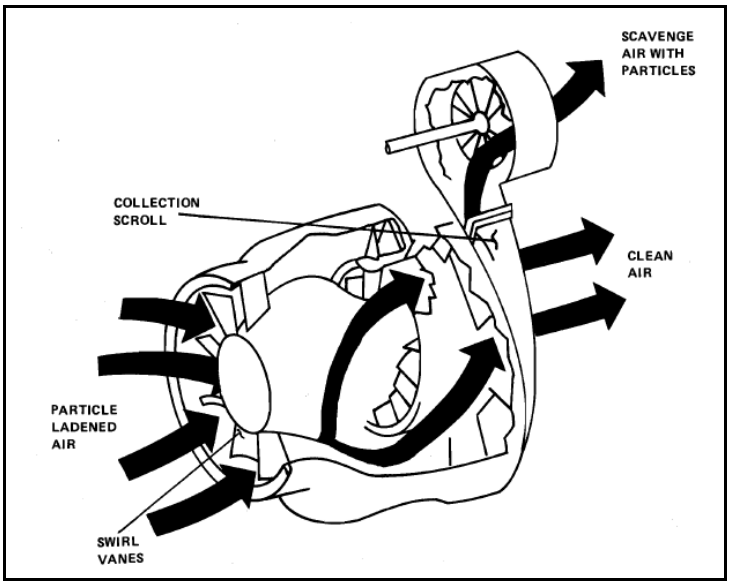

Figure 11.8: Integrated Particle Separator Schematic

Inlet Barrier Filters (IBF)

Historically, barrier filters were not utilized due to poor particle separation performance and frequent replacement requirements. However, recent technological advances have made inlet barrier filters (IBF) a promising alternative to inertial separators. Over the past 5 years, IBF systems have been employed on military helicopters operating in the harsh environments of Iraq and Afghanistan with tremendous success. The system uses a washable fabric air filter with oil resin that achieves a particle separation efficiency of over 99% for course sand and dust. This superior performance virtually eliminates engine damage due to FOD – significantly reducing maintenance requirements and increasing engine life. Each filter is designed for 15 cleaning cycles that are completed on a conditional basis – typically ranging from 100 to 300 flight hours depending on the severity of the operating environment.[13]

In the event that a filter becomes completely clogged, an electronically operated bypass door allows unfiltered air to reach the engine. By measuring the pressure differential across the filter, an impending bypass condition can be identified with sufficient prior notice to safely alert the pilot for corrective action. It should be noted that the US Army's OH-58D helicopter, with over 500,000 hours of service using IBF filters in desert environments, does not have a single documented case in which the bypass system was activated. Figure 11.9 shows the retrofitted IBF installation used for the OH-58D helicopter. IBF systems also eliminate the need for bleed air and typically reduce inlet pressure losses by 50% in comparison to inertial systems – allowing the engine to operate at a lower temperature for a given power demand.[14] This added margin in measured gas temperature (MGT) translates to longer life for the engine's hot section components.

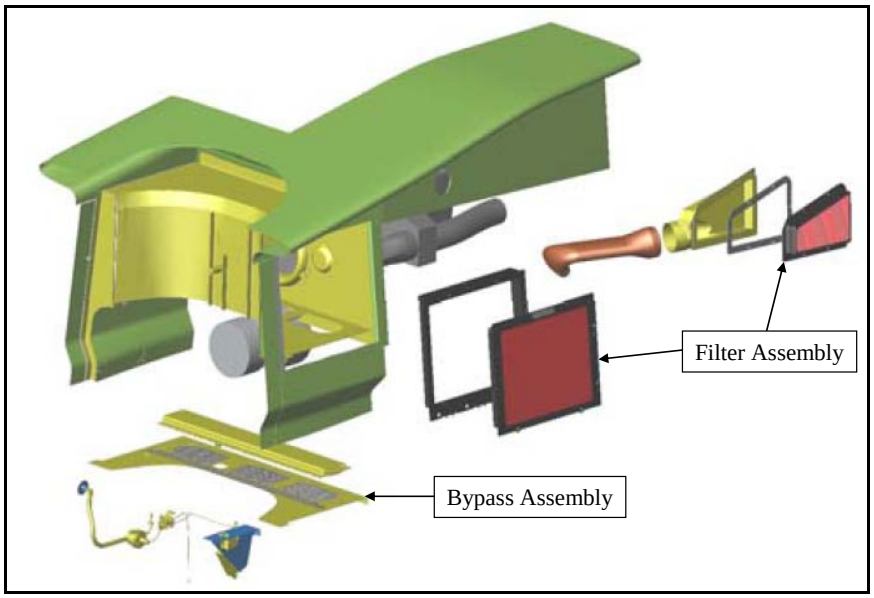

Figure 11.9: IBF System Retrofit on OH-58D Kiowa Warrior *(with permission)*[13]

Engine Anti-Ice System

Regardless of the environmental and mission requirements for a given rotorcraft vehicle, the engine air induction system must include protection from icing based on the potential for inadvertent flight into such conditions. The two most common methods of anti-ice will be discussed in this section: electrical heating mats and compressor bleed air. The goal of both anti-ice techniques is to maintain inlet duct temperatures at approximately 40^{o} F and Reference 12 provides an iterative procedure for approximating the thermal energy requirements of each approach. For general design guidelines, however, the following considerations are applicable for preliminary design:[12]

- Electrical systems impact aircraft generator sizing and gearbox design.
- Bleed air system flow requirements must be less than engine bleed air capability or an alternate source of air provided. This requirement is particularly restrictive at low power settings.
- Bleed air systems usually have a larger negative impact on aircraft power because the energy conversion efficiency of a gearbox is much higher than that of the compressor bleed air.
- Electrical systems tend to be heavier due to increased generator weight.
- System reliability generally favors bleed air systems in which the main engine(s) directly provide the heating energy.
- Bleed air systems only penalize vehicle performance when the anti-ice system is operating; whereas, electrical systems require added vehicle weight for all conditions.

Engine Exhaust System

As previously described, the engine exhaust system for rotorcraft vehicles is considerably simplified compared to other gas turbine configurations where the exhaust contributes propulsive energy. The following preliminary design considerations are tailored specifically for rotorcraft exhaust applications.

Exhaust Location

The location and directional flow of the exhaust wake should meet the following general guidelines:[12]

- Avoid exhaust airflow through the aircraft tail rotor to maximize efficiency.
- Prevent impingement of exhaust gases on aircraft surfaces to minimize structural effects and avoid personnel injury during ground maintenance operations.
- Minimize engine-mounted exhaust duct length to prevent vibration-induced fatigue failures.
- Locate the exhaust outside of the rotor inner wake to minimize exhaust gas re-ingestion (EGR) during hovering flight. Figure 11.10 shows a graphical representation of the inner wake as a function of aircraft hover height and Figure 11.11 provides a plot of the inner wake boundary versus the ratio of the rotor height to rotor radius (Z/R).

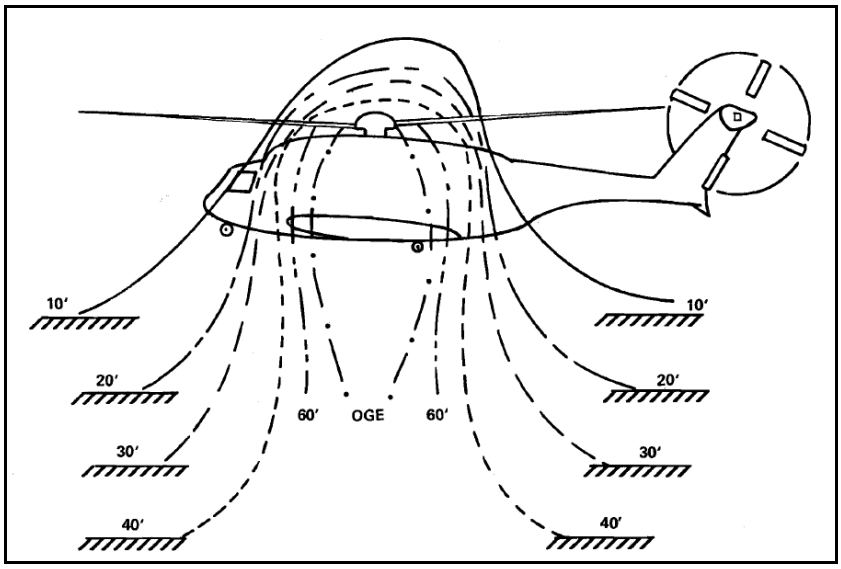

Figure 11.10: Rotor Inner Wake as a Function of Aircraft Hover Height[12]

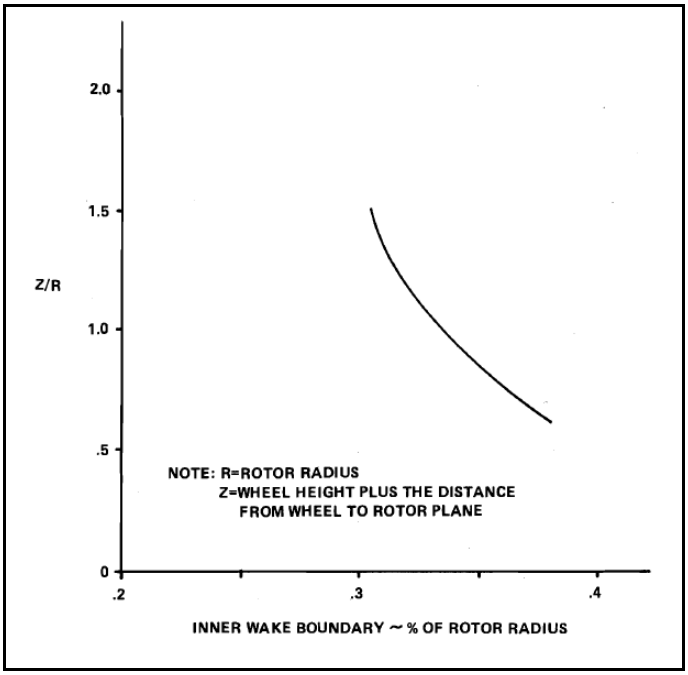

Figure11.11: Rotor Inner Wake Boundary Location[12]

Exhaust Performance

Similar to the inlet design, smooth ducts free of sharp bends and obstructions are essential in maximizing the performance of engine exhaust systems. Estimation of

pressure losses follows the same methods used for the inlet. As a rule of thumb, exhaust pressure losses should be held to 1% or less because each percentage point equates to a loss of 0.5-1.0% of rated engine power at MCP.[7]

Additional Design Considerations

Depending on the specific mission requirements of the vehicle, additional design considerations may be required during the preliminary design process. The following discussion provides a qualitative introduction to some of these potential requirements.

Noise Reduction

Whether for military stealth or neighborly flight requirements, engine exhaust noise reduction may be an important design consideration. For ground operations, a slight noise reduction is gained by directing the exhaust duct upward. More sizeable reductions over a wide range of sound frequencies can be achieved by lining the exhaust duct with absorptive materials; however, a significant weight and pressure loss penalty also results. For specific low frequencies, resonance mufflers may be more effective than absorptive mufflers.[7]

Infrared Radiation (IR) Suppression

For military rotorcraft intended for combat use, IR suppression is an important design characteristic which reduces the effectiveness of enemy thermal sensors and weapons. The amount of IR energy radiated from the surface of a given source is a function of the area, surface temperature, and surface emissivity. Although many techniques are used to reduce the IR signature, the most common methods use shielding and/or cooling airflows. The intent of shielding is to hide the hot surface – this is

typically done by enclosing the hot surface with insulating material or surrounding it with a secondary duct that creates a gap where cooling air can flow. Cooling airflows can also be used to reduce surface temperatures through transpiration or film cooling along the exposed exhaust duct – this approach also reduces the exhaust gas temperature through mixing, but can require more than 10% of the total engine airflow. Ultimately, detailed design trade studies are required to accurately assess the performance benefits and penalties of a given IR suppression system.[7]

Engine Drive Train

A detailed analysis of the engine drive train is beyond the scope of preliminary design, however, consideration of some basic configuration and layout requirements are applicable during this stage.

Engine Gearbox

An initial assessment of the location and gear reduction ratio of the engine accessories gearbox is necessary to provide an accurate component weight estimate. The key design challenge is the highly-integrated nature of this component – the following list describes the basic details that should be addressed:

- Gearbox location supports engine architecture and functionality.
- Gearbox-transmission interface should minimize length of the main drive shaft and ensure compatibility of gear reduction ratios (typical engine gearbox output speeds range from 5000-7000 RPM).

- Efficient integration of the vehicle's anti-torque system shaft power requirements into the drive train design.
- Material selection meets strength requirements and minimizes engine weight.
- Gearbox layout supports the space requirements for accessories such as electrical generators, fuel and oil pumps, and potential future growth add-ons, as applicable.

Direct Drive Configuration

Another approach used in drive train design completely eliminates the traditional engine-mounted accessory gearbox and provides a high speed output shaft driven directly by the power turbine. This technique simplifies the overall engine configuration and increases the versatility of a given engine design for multiple vehicle applications. By removing the engine accessory gearbox, design responsibility for specific accessory power requirements shifts to the vehicle designer – providing the potential for better integration and optimization. Direct drive engine configurations offer several advantages:

- Reduced engine weight and cross-section requirements.
- Reduced severity of temperature and vibratory effects for remotely mounted units.
- Improved engine and accessory installation, removal, and maintenance capability due to better component accessibility.

The main disadvantage of direct drive configurations is that the gear reduction requirements significantly increase for the vehicle's transmission.

Engine Freewheeling Unit

In order to meet the autorotation requirements inherent with all rotorcraft vehicles, a clutch mechanism is incorporated into the drive train design to allow the main

rotor and tail rotor to continue to rotate in the event of an engine failure or seizure. The sprag clutch is the most common freewheeling unit design – utilizing a series of sprags (figure-eight shaped bearings) within an inner and outer race. As depicted in Figure 11.12, the engine drives the outer race which jams the sprags between the inner and outer races and, thus, drives the transmission driveshaft.[15] However, if the transmission driveshaft attempts to drive the engine, the pressure fit of the sprags is relieved and the driveshaft rotates without the engine. The freewheeling unit is usually incorporated into the transmission, but can also be integrated into the engine gearbox assembly. Ultimately, the clutch location along the drive train must support emergency operation of the main rotor, tail rotor, and gear-driven accessories required for safe recovery during autorotation.

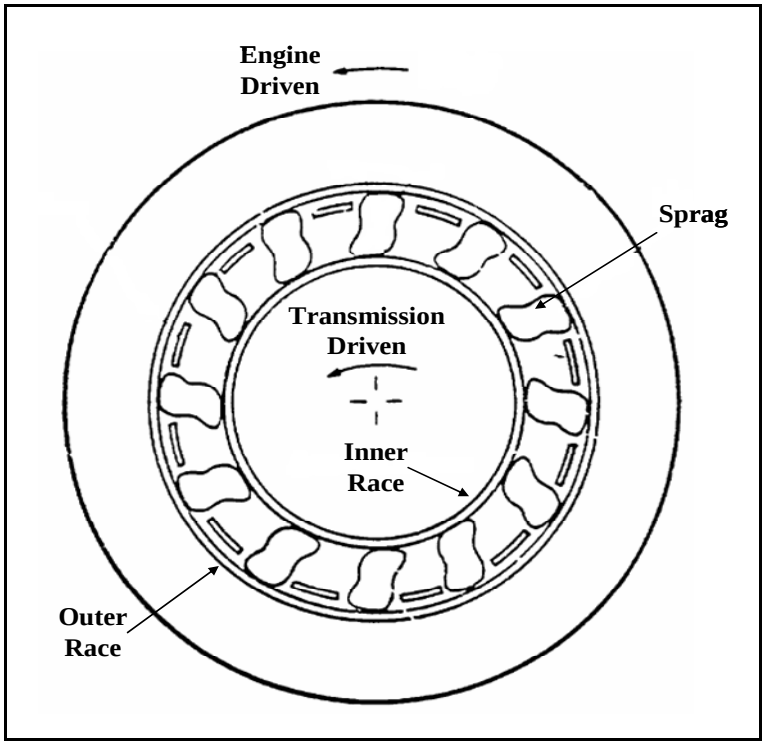

Figure 11.12: Sprag Clutch Schematic[16]

[1] Franco Tortarolo, Guido Crosetti, and Carmine Difilippo, "Safety Critical Software Development for Advanced Full Authority Control Systems," *AGARD CP-572 Advanced Aero-Engine Concepts and Controls* (Quebec, Canada: Canada Communication Group, 1996).

[2] T. J. Lewis, "Distributed Architectures for Advanced Engine Control Systems," *AGARD CP-572 Advanced Aero-Engine Concepts and Controls* (Quebec, Canada: Canada Communication Group, 1996).

[3] Peter Donaldson, "Power is Control," *Helicopter World* (February 1998).

[4] *Bell 430 Product Data Book* (Fort Worth, TX: Bell Helicopter Textron, 2003).

[5] R. Romero, H. Summers, and J. Cronkhite, "Feasibility Study of a Rotorcraft Health Usage Monitoring System (HUMS): Results of Operator's Evaluation," *NASA Report CR-198446* (February 1996).

[6] Federal Aviation Regulation (FAR) Part 33.28c, available online at: http://ecfr.gpoaccess.gov.

[7] Headquarters, US Army Materiel Command, *AMC Pamphlet 706-201: Engineering Design Handbook: Helicopter Engineering, Part 1 – Preliminary Design* (Alexandria, VA: GPO, 1974).

[8] X. De la Servette and P. Cabrit, "Helicopter Air Intake Protection Systems," *AGARD LS-148 Engine-Airframe Integration for Rotorcraft* (Essex, England: Specialised Printing Services, 1986).

[9] Headquarters, US Army Materiel Command, *AMC Pamphlet 706-202: Engineering Design Handbook: Helicopter Engineering, Part 2 – Detail Design* (Alexandria, VA: GPO, 1976).

[10] "Thermodynamics of Incompressible and Compressible Fluid Flow," *SAE Aerospace Applied Thermodynamics Manual AIR1168/1* (Warrendale, PA: Society of Automotive Engineers, 1989).

[11] J. R. Ballard, "Impact of IPS and IRS Configurations on Engine Installation Design," *AGARD LS-148 Engine-Airframe Integration for Rotorcraft* (Essex, England: Specialised Printing Services, 1986).

[12] R. C. Frawley and H. N. Shohet, "Engine-Airframe Integration Considerations for Preliminary Air Vehicle Performance Analysis," *AGARD LS-148 Engine-Airframe Integration for Rotorcraft* (Essex, England: Specialised Printing Services, 1986).

[13] Information available from: http://www.afsfilters.com, Internet; Accessed on 27 October 2006.

[14] Telephonic interview with Tom Newman, Project Engineering Manager, *Aerospace Filtration Systems, Inc*., 26 October 2006.

[15] Joe Schafer, *Helicopter Maintenance* (Frankfurt, Germany: Jeppesen and Company, 1992).

[16] Robert L. Mullen, Ronald J. Zab, and Antonius S. Kurniawan, "Thermal Mechanical Analysis of Sprag Clutches," *NASA Technical Report CA-190686* (Cleveland, OH: Case Western Reserve University, 1992).

CHAPTER 12

MANUFACTURING REQUIREMENTS

The focus of this report is the product development of a turboshaft engine for rotorcraft applications; however, successful product development must also address the concurrent development of the processes by which it is manufactured. As depicted in Figure 1.1, product and process development requires an integrated design environment.

Design for Manufacture / Design for Assembly (DFM/DFA)

The principles of DFM/DFA can be summarized as reducing the cost and manufacturing cycle times for a given product while simultaneously improving its overall quality and value.[1]

Design Complexity

While a detailed analysis of specific fabrication techniques for each engine component is beyond the scope of this report, minimizing design complexity ensures that manufacturing requirements are sufficiently addressed during preliminary design. The direct correlation between design complexity and manufacturing difficulty, or cost, is a critical factor that must be integrated into the selection process for each specific design choice. Performance versus cost trade studies drive preliminary product development and determine the optimum (or minimum) level of design complexity required to meet the customer's demands. For example, the engine configuration, turbine cooling

requirements, and number of compressor stages are all design choices that significantly impact the overall complexity and, thus, manufacturability of a given engine.

Computer Aided Manufacturing (CAM)

Computer aided manufacturing (CAM) software, when used in conjunction with computer aided design (CAD) software, provides a powerful tool in achieving product and process design synthesis. Utilization of software technology allows the creation of virtual settings in which the time, resources, and capital typically needed to develop a new product can be greatly reduced. Integration between state-of-the-art CAD and CAM software provides the digital environment necessary to balance the product, process, and resource requirements for a given design. Figure 12.1 shows an example of the engine gearbox assembly process used on the GTGH.

Manufacturing engineers can plan the processes and resources needed to build the design in accordance with the overall production rate and cost requirements. This manufacturing plan, based only on theory and static analysis, can then be exported to a simulation tool for validation in a dynamic environment. The design engineer can optimize the product assembly process by conducting trade studies using a virtual workbench to identify component integration problems in terms of contact, collision, or clearance between parts. The resource requirements identified in the manufacturing plan provide the input for 3D factory analysis and layout optimization aimed at maintaining production line balance. Critical product assembly steps that cause bottle-necks in the manufacturing flow can be identified and avoided. This factory analysis is used to update the original manufacturing plan and, thus, creates an integrated product and process design loop.

The benefits of incorporating this optimized design approach are many. An independent study in 2003 indicated that, on average, it reduces the time to market for a given product by 30% and the number of design changes by 65%.[2] This can be attributed to the early detection of assembly problems through simulation and the reduced need for physical prototypes. Additionally, time and financial savings are realized in the reduction of tool design cost, optimized factory layout, and better utilization of labor. Communication and collaboration, both internally and externally, are improved as product and process engineers can immediately visualize the effects of their design decisions across multiple disciplines and suppliers can better understand product requirements. Digital manufacturing also allows "proven" processes to be categorized and re-used in future applications, reducing process planning time.

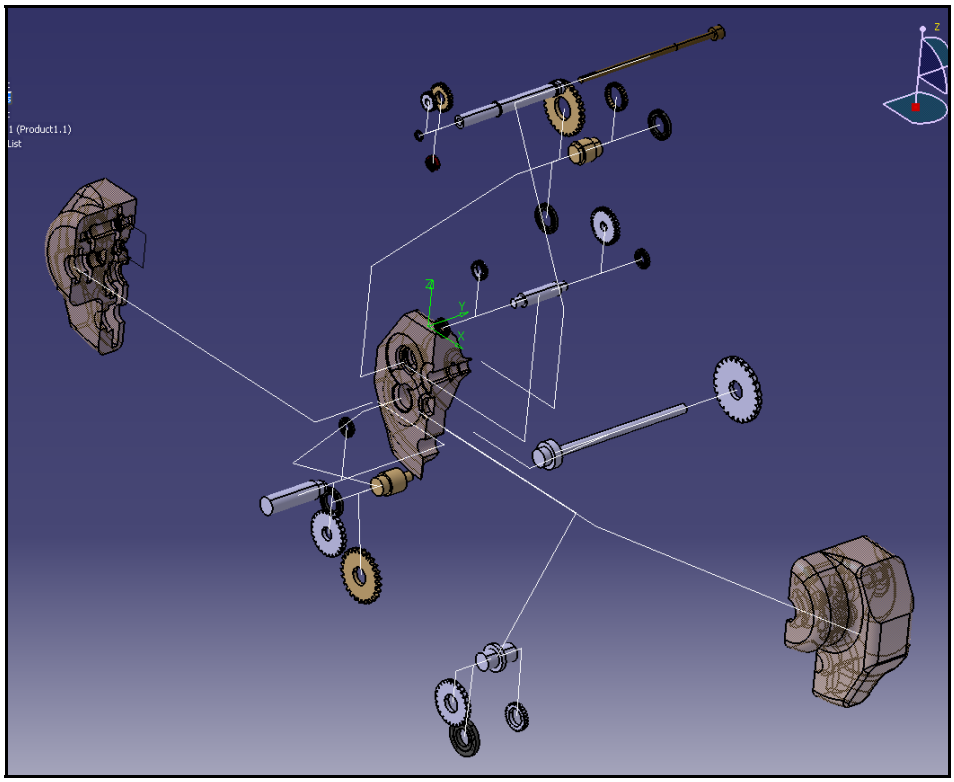

Figure 12.1: Engine Gearbox Assembly Plan (GTGH)

[1] A. K. Kundu, S. Crosby, R. Curran, and S. Raghunathan, "Aircraft Component Manufacture Case Studies and Operating Cost Reduction Benefit," *AIAA Paper 2003-6829* (November 2003).

[2] "The Benefits of Digital Engineering," *CIMData Report* (2003).

CHAPTER 13

REGULATORY REQUIREMENTS

This chapter identifies some of the fundamental engine design measures that are required by the Federal Aviation Administration (FAA) for vehicle and engine certification – highlighting only those salient design considerations that are applicable during preliminary propulsion system design. The specific Federal Aviation Regulations (FAR) exist under Title 14 – Aeronautics and Space, Chapter 1 – Federal Aviation Administration, Subchapter C – Aircraft. A complete reference for the Code of Federal Regulations is available online at: http://ecfr.gpoaccess.gov.

Part 27 – Airworthiness Standards: Normal Category Rotorcraft

Table 13.1 summarizes the most important engine requirements that apply to rotorcraft with gross weight less than 7000 lbs and seating capacity less than 10 passengers.

Table 13.1: Summary of FAR Part 27 Engine Requirements

Para.	Title	Summary
27.907	Engine Vibration	-- Engine and rotor drive system must be free from excessive vibrations
27.917	Rotor Drive System Design	-- Engine must automatically disengage from rotor drive system for autorotational capability
27.1091	Air Induction	-- Inlets must supply the engine with the required air during all operating conditions and minimize the ingestion
27.1093	Induction System Icing Prevention	-- Engine must be capable of operating at all power settings without accumulating ice on the inlet detrimental to engine operation
27.1141	Powerplant Controls: General	-- No single point failure in any powerplant control system can cause the loss of a powerplant function necessary for safety
27.1191	Firewalls	-- Engine must be isolated from personnel compartments, structures, controls, and rotor mechanisms by a firewall or shroud

Part 29 – Airworthiness Requirements: Transport Category Rotorcraft

This regulation applies different levels of requirements based on vehicle category classification. Table 13.2 defines the vehicle category as a function of gross weight and passenger seating capacity. The key engine requirements outlined in Table 13.1 also apply to FAR Part 29 – with the most notable difference being the application of one engine inoperative (OEI) standards for multi-engine takeoff and climb performance.

Table 13.2: Rotorcraft Category Definitions

GW	Number of Passenger Seats: < 10	Number of Passenger Seats: ≥ 10
> 20,000 lb	**B** (Note: Must meet Cat A requirements for Subparts C, D, E, and F)	**A**
≤ 20,000 lb	**B**	**B** (Note: Must meet Cat A requirements for para. 29.67(a)(2), 29.87, 29.1517, and Subparts C, D, E, and F)

Part 33 – Airworthiness Standards: Aircraft Engines

Part 33 is focused on the specific testing and evaluation requirements used during the certification process of new aircraft engines. Table 13.3 summarizes the requirements that should be considered during preliminary design.

Table 13.3: Summary of FAR Part 33 Requirements

Para.	Title	Summary
33.7	Engine Ratings and Operating Limits	-- Established relating to horsepower, RPM, gas temperature, and time for MCP, TOP, and OEI (if applicable)
33.15	Materials	-- Suitability and durability must be based on experience or testing
33.67	Induction System Icing	-- No accumulation of ice on engine components that adversely effects engine operation throughout its flight power range (including idling) during maximum icing conditions
33.75	Safety Analysis	-- No probable engine malfunction or improper operation can result in a fire, engine burst, loads greater than ultimate loads, or loss of engine shut down capability
33.76	Bird Ingestion	-- Large birds must not cause engine fire, hazardous fracture, excessive loads, or loss of shutdown capability -- Small and medium birds must not cause a loss of more than 25% power in addition to the large bird
33.77	Foreign Object Ingestion (Ice)	-- Ice ingestion must not cause sustained loss of engine power or shutdown -- Protective devices remove this requirement, but must demostrate their effectiveness
33.78	Rain and Hail Ingestion	-- No mechanical issues or power loss from ingestion of hailstones at MCP up to 15,000 ft -- Rain simulated by 4% water-to-airflow ratio at inlet must not cause unacceptable engine performance

CHAPTER 14

EMERGING CONCEPTS

The following concept descriptions are intended to provide a summary of the current state-of-the-art for gas turbine engines. An understanding of these topics is important in accurately evaluating the technological risk and cost factors of a preliminary engine design.

Wave Rotor Topping

Steady improvements in gas turbine performance have traditionally been achieved through aerodynamic and thermodynamic advances such as increased component efficiencies and improved thermal capabilities for materials. The current maturity level of gas turbine engines indicates that significant performance improvement resulting from traditional aerodynamic and material analysis is unlikely. Therefore, research efforts involving advanced thermodynamic processes offer more upside performance potential. Wave rotor topping represents one such research effort aimed at improving the overall efficiency and specific power of traditional gas turbine cycles. Wave rotor technology has been investigated since early in the twentieth century and Reference 4 provides a detailed synopsis of its historical development – highlighting that recent advances have stimulated new interest in its modern engine applicability.

Wave rotors use shock waves to pressurize fluids by transferring energy from a high-pressure flow to a low-pressure flow. As depicted in Figure 14.1, the wave rotor consists of series of straight or curved channels around the axis of a rotating drum with stationary ports at either end that allow entry and exit of the working fluid. While the exact architecture varies based on the application, the most promising arrangement uses

four ports: low-pressure air (LPA) from the compressor becomes high-pressure air (HPA) delivered to the combustor and high-pressure gas (HPG) from the combustor expands to become low-pressure gas (LPG) sent to the turbine. The opening and closing of the ports creates shock and expansion waves from pressure differentials. The channels along the drum are self-cooled as a result of their exposure to both hot and cold gases.[1] Wave rotors can achieve significant improvements in efficiency by increasing the pressure and temperature of the gas prior to combustion while simultaneously maintaining, or even reducing, the temperature of the gas in the high pressure turbine.

Figure 14.2 shows a T-s diagram comparing a wave rotor topped cycle to a traditional gas turbine cycle – highlighting the higher relative pressure at the turbine inlet for the wave rotor topped cycle. Untopped cycles experience a decrease in the pressure between the compressor and turbine sections due to losses during combustion; whereas, wave rotors can generate a total pressure increase of 15-20%.[2] This advantage translates to increased work extraction across the turbine and, thus, higher specific power and thermal efficiency for wave rotor topped cycles. Experimentation with four-port wave rotors conducted at the NASA Lewis Research Laboratory indicates that increases in specific power of ~20% and corresponding reductions in specific fuel consumption of ~15% are possible.[3] Figure 14.3 demonstrates that smaller engines will benefit the most from wave rotor topping because as the compression ratio increases, the relative improvement in both specific power and SFC diminishes.

Despite these appealing advantages, mainstream implementation of wave rotor technology is limited by several factors. The inherent complexities of modeling unsteady flow aerodynamics and the challenges of matching an optimized wave rotor design with a

specific engine application require further research. Improved mechanical seals and advanced materials that can handle higher temperatures for combustion and thermal expansion within the wave rotor are required.[4] Finally, limited research funding has historically constrained wave rotor development; but recent increases in fuel prices and diminishing advances in older technology have stimulated new research efforts in this area.

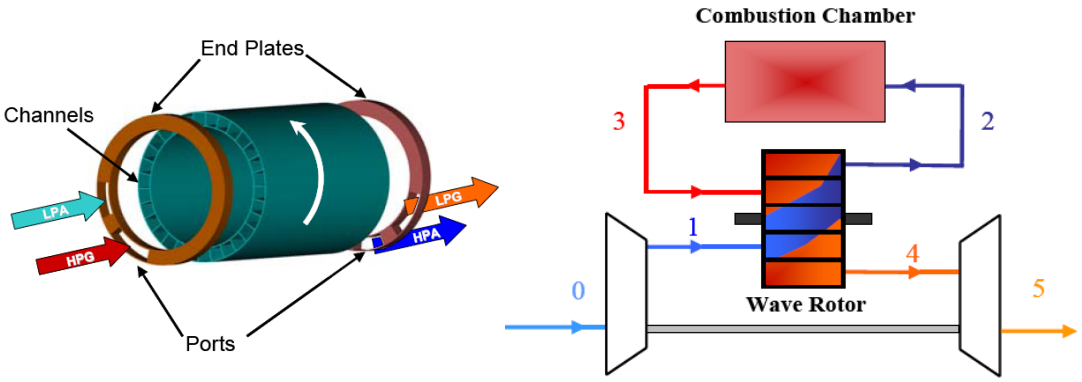

Figure 14:1: Wave Rotor Schematic and Implementation Diagram[1]

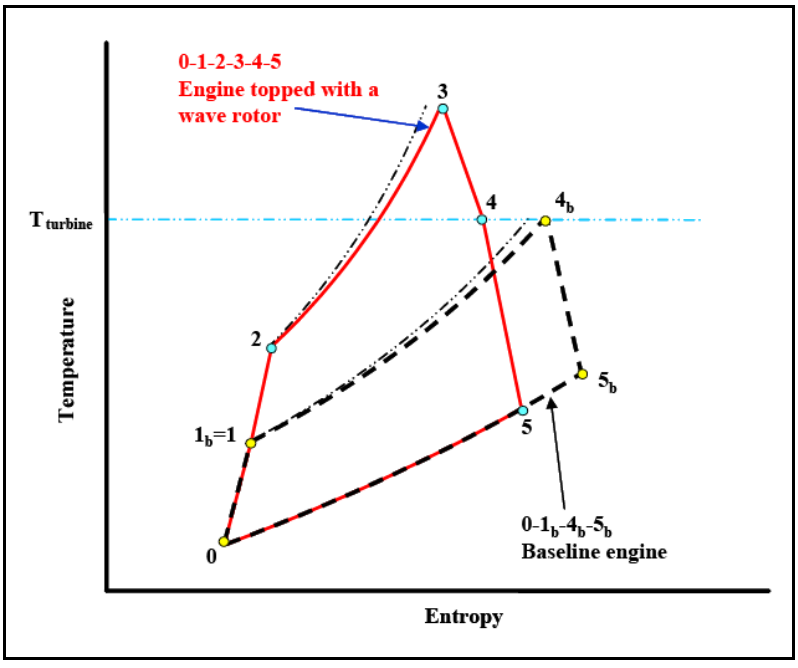

Figure 14.2: Comparison T-s Diagram for Wave Rotor Applications[5]

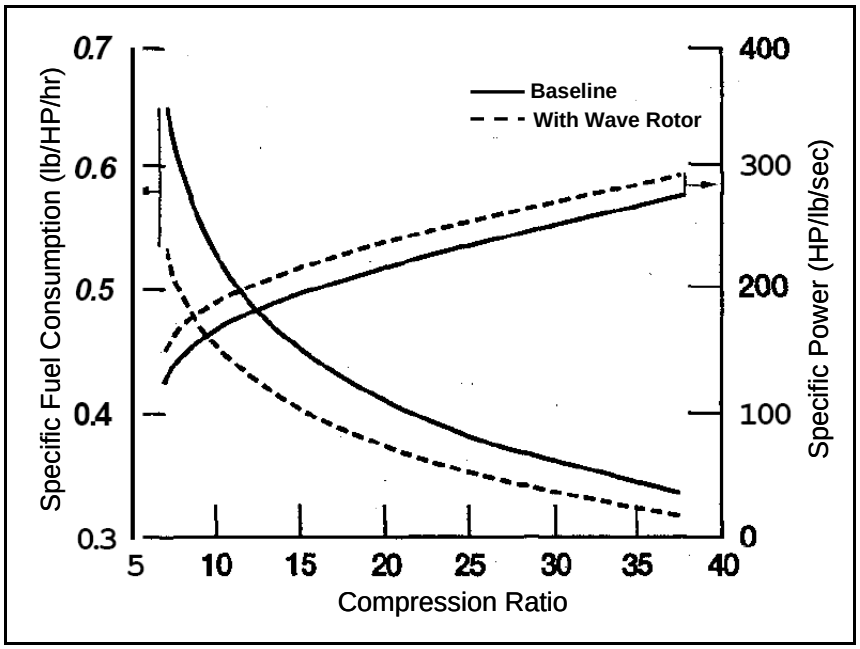

Figure 14.3: Specific Power and SFC Analysis for Wave Rotor Topped Engines[6]

Advanced Ceramic Materials

As modern nickel-based superalloys approach their technological maturity, advanced ceramic materials have emerged as a promising alternative – offering unmatched potential for improving the hot-section performance of gas turbine engines. The higher temperature capability of advanced ceramics translates to significant gains in engine efficiency by allowing increased combustion and turbine inlet temperatures with reduced bleed-air cooling requirements. When compared to metal superalloys, ceramic materials have lower density (approximately 30-50%) and exhibit reduced thermal expansion. These properties should result in many important engine benefits such as reduced engine design complexity, reduced component weight, higher blade frequencies, reduced blade clearances, higher thrust, and reduced emissions.[7] However, despite such attractive capabilities, the use of advanced ceramics in real-world gas turbine applications

has been extremely limited due to several key factors: low fracture toughness, vulnerability to impact resistance, limited environmental resistance, high manufacturing costs, and insufficient design and test experience.[8]

Research efforts aimed at minimizing these limitations involve two ceramic material design approaches – ceramic matrix composites (CMC) and environmental barrier coatings (EBC). CMC mixes ceramic particles, whiskers, or fibers during fabrication to provide a reinforced material that exhibits greater fracture toughness than monolithic ceramic materials. Overcoming the technological challenges associated with CMC requires better understanding of composite material interactions and failure modes, higher temperature stability and durability, reduced manufacturing costs, and increased material consistency.[9] Current research efforts have advanced the state-of-the-art for CMC materials – achieving acceptable strength characteristics at temperatures well above the capability of metal alloys (1315^{o}C vs. 1100^{o}C).[8] As depicted in Figure 14.4, silicon carbide fiber-reinforced silicon carbide matrix (SiC/SiC) composite was coated with an advanced EBC and successfully tested as a turbine vane subelement. Future goals include increasing the temperature capability in excess of 1450^{o}C and increasing strength properties to support turbine blade applications.

In order to achieve long life for ceramic gas turbine components, environmental barrier coatings (EBC) are used to protect non-oxide monolithic ceramics and CMCs against oxidation and corrosion damage.[9] Unprotected ceramic materials suffer from accelerated oxidation and volatilization when exposed to water-vapor and alkali salts in the gas turbine environment. Barium-Strontium-Alumino-Silicate (BSAS) is the most widely used EBC system because its coefficient of thermal expansion (CTE) is

compatible with silicon-based ceramics and it also offers thermal barrier protection.[10] Technological challenges that limit the use of EBCs result from adhesion problems and mismatched thermal expansion properties between the coating and substrate material. State-of-the-art EBCs have demonstrated high temperature water vapor stability and cyclic durability for stationary turbine and combustor component applications at temperatures greater than 1450^{o}C for time periods of 300 hours.[11] Such promising results underscore the importance of EBC technology in facilitating the future development of ceramic hot-section gas turbine engine components.

Figure 14.4: CMC Turbine Vane with Protective EBC[12]

---

[1] E. Dempsey, N. Mueller, P.Akbari, and M. R. Nalim, "Performance Optimization of Gas Turbines Utilizing Four-Port Wave Rotors," *AIAA Paper 2006-4152* (June 2006).

[2] Gerald E. Welch, "Overview of Wave-Rotor Technology for Gas Turbine Engine Topping Cycles," *Novel Aero Propulsion Systems International Symposium* (London: The Institution of Mechanical Engineers, 2000).

[3] Jack Wilson, "Design of the NASA Lewis 4-Port Wave Rotor Experiment," *NASA Report CR – 202351* (June 1997).

[4] Pezhman Akbari, Razi Nalim, and Norbert Mueller, "A Review of Wave Rotor Technology and Its Applications," *Journal of Engineering for Gas Turbines and Power* (January 2006).

[5] Pezhman Akbari and Norbert Mueller, "Wave Rotor Research Program at Michigan State University," *AIAA Paper 2005-3844* (July 2005).

[6] Jack Wilson and Daniel E. Paxson, "Wave Rotor Optimization for Gas Turbine Engine Topping Cycles," *Journal of Propulsion and Power* (July 1996).

[7] James A. DiCarlo, Hee Man Yun, Gregory N. Morscher, and Ramakrishna T. Bhatt, "High-Performance SiC/SiC Ceramic Composite Systems Developed for 1315°C (2400°F) Engine Components," *NASA Research Report* (2005).

[8] US Department of Energy – Distributed Energy website:http://www.ornl.gov/sci/de_materials/projects-monolithic.shtml, Internet; Accessed on 25 October 2006.

[9] "Advanced Ceramics Technology Roadmap – Charting Our Course," *US Advanced Ceramics Association* and *US Department of Energy* (December 2000).

[10] K. Sharma, P. S. Shankar, and J. P. Singh, "Mechanical Behavior of Si_3N_4 Substrates with Environmental Barrier Coatings," Presented at the *Symposium on Innovative Processing and Synthesis of Ceramics, Glasses, and Composites* at the *105th American Ceramic Society Annual Meeting and Exposition* (27-30 April 2003).

[11] Dongming Zhu, Sung R. Choi, and Raymond C. Robinson, "Advanced Testing and Performance Evaluation of Environmental Barrier Coatings," Presented at the *Environmental Barrier Coatings Workshop* (15-16 November 2005).

[12] Michael J. Verrilli, Craig Robinson, and Anthony Calomino, "Ceramic Matrix Composite Vane Subelements Tested in a Gas Turbine Environment," *NASA Research Report* (2005).

CHAPTER 15

CONCLUSIONS

A comprehensive engine design methodology – representing a subelement of the Georgia Tech Integrated Product and Process Development (IPPD) approach – is presented. The work is focused on turboshaft engine design considerations, while utilizing existing analysis techniques and processes, to provide a preliminary propulsion system design approach that is fully-integrated with current rotorcraft design practices. The overall procedure is generic in nature, thus, maintaining its applicability to a wide range of potential rotorcraft propulsion system design problems. The methodology addresses the complex relationship between propulsion system design and preliminary vehicle sizing and performance analysis – highlighting the iterative steps needed to achieve a solution that is optimized for a specific set of requirements. As such, the importance of accurate and detailed requirements analysis is emphasized as the single-most critical step in ensuring that the vehicle and engine design specifications are fully-integrated and compatible. These requirements represent the foundation for engine cycle analysis and preliminary component design which ultimately define the geometry and performance of the engine.

On a larger scale, this work serves as a propulsion system design reference in the study of rotorcraft vehicles. Design parameter guidelines for system and component level performance help limit the available design space and validate results based on a desired level of technology. A discussion of fundamental thermodynamic concepts and the basic principles of air-breathing gas turbine engines is included to provide a more

thorough context for describing the propulsion system design methodology. Understanding these foundational concepts ensures the effective implementation of analytical engine design tools and simplifying assumptions. Finally, the Georgia Tech Generic Helicopter (GTGH) engine design case study serves as a unifying working example – highlighting the integration and level of detail required for each step of the preliminary design process.

CHAPTER 16

FUTURE WORK

As is the case in most academic research efforts, there are areas of the presented design methodology where more detailed analysis is recommended. Particularly in dealing with non-traditional engine cycle modifications, the level of detail of this report fails to address the use of reheat, regeneration, and reaction drive systems as potential design alternatives. While the wave rotor is presented as an emerging concept in this area, additional engine cycle adjustments may lead to a propulsion system that is better optimized for a given application and, therefore, deserve further investigation.

Combustor design should be incorporated into future versions of this design methodology. While it was not considered a critical element of preliminary design for this report, including the basic sizing and performance calculations for the combustor section would increase the accuracy of the engine's weight estimate and overall architectural layout.

Micro-turbine technology is another area where further research and documentation would be highly beneficial. As the need for unmanned rotorcraft vehicles continues to increase, micro-turbine technology has entered the forefront of a new generation of propulsion systems. The use of radial turbines better suited for small airflows will undoubtedly play a significant role in advancing micro-turbine technology. Future work concerning turboshaft engine design should include analysis of the design challenges and configurations that dominate micro-turbine engine development.

APPENDIX A

STANDARD REFERENCE TERMINOLOGY

Table A.1: Standard Thermodynamic Terminology and Conversion Factors

	British Engineering Units (BE)				International System of Units (SI)			
Standard Terminology								
Mass	slug	=	32.174	lbm				
Force	lbf	=	32.174	$(lbm\text{-}ft)/s^2$	Newton (N)	=	1	$(kg\text{-}m)/s^2$
Energy	BTU	=	778.16	ft-lbf	Joule (J)	=	1	N-m
Power	HP	=	550	(ft-lbf)/s	Watt (W)	=	1	J/s
Pressure	atm	=	14.696	lbf/in^2	Pascal (Pa)	=	1	N/m^2
Gravitational Acceleration	g_0	=	32.174	ft/s^2	g_0	=	9.807	m/s^2
Newton Constant	g_c	=	32.174	$(lbm\text{-}ft)/(lbf\text{-}s^2)$	g_c	=	1	
Sea-Level Standard (SLS) Conditions								
Temperature	T_{std}	=	518.69	^oR	T_{std}	=	288.15	K
Pressure	p_{std}	=	2116.2	lbf/ft^2	p_{std}	=	101,325	N/m^2
Density	ρ_{std}	=	0.07647	lbm/ft^3	ρ_{std}	=	1.225	kg/m^3
Speed of Sound	a_{std}	=	1116	ft/s	a_{std}	=	340.3	m/s
Temperature Conversion								
	$T(^oF)$	=	$1.8\ T(^oC) + 32$					
	$T(^oR)$	=	$T(^oF) + 459.69$					
	$T(^oR)$	=	$1.8\ T(K)$					

APPENDIX B

TURBINE COOLING CALCULATIONS

The following sample calculation based on the GTGH design estimates the amount of bleed air required to cool the high pressure turbine in accordance with the procedures outlined in NASA Technical Memorandum 81453.[1]

Given Information:

Cooling air properties (compressor discharge):

$T_{03} = 965.6\ ^{o}R$

$h_{03} = 232.2$ BTU/lbm

$\dot{m}_{03} = 1.060$ lbm/s

Turbine inlet conditions:

$T_{04} = 2540.7\ ^{o}R$

$h_{04} = 657.1$ BTU/lbm

$\dot{m}_{g4} = 1.086$ lbm/s

Combustor:

$\dot{m}_{fuel} = 0.026$ lbm/s

Assumptions:

Temperature safety factor (SF) = $150\ ^{o}R$

Pattern factor (PF) = 0.3 (first row of airfoils) and 0.13 (all subsequent rows)

Calculations:

1) Maximum allowable metal temperature

$$T_{m(vane)} = [10(year) - 17640] - [100\log(life) - 400] \quad [B.1]$$

$$T_{m(blade)} = [10(year) - 17740] - [100\log(life) - 400] \quad [B.2]$$

Where *year* is the first year of service for the respective material and *life* is the desired life of the component in hours. Based on an assumed material service life beginning in 1995 for both the turbine vanes and blades and a service life of 15,000 hours, the following maximum allowable metal temperatures were calculated:

$$T_{mv} = [10(1995) - 17640] - [100\log(15000) - 400] = 2292^{o}R$$

$$T_{mb} = [10(1995) - 17740] - [100\log(15000) - 400] = 2192^{o}R$$

2) Stator vane cooling air requirements

- Gas temperature at the vane adjusted for the safety factor:

$$T_{gv} = T_{04} + SF = 2540.7 + 150 = 2690.7^{o}R$$

- Cooling effectiveness (E'):

$$E' = \frac{T_{gv} - T_{mv}}{T_{gv} - T_{cool}} = \frac{2690.7 - 2292}{2690.7 - 965.6} = 0.231$$

- Cooling effectiveness adjusted for pattern factor (E):

$$E = \frac{PF + E}{PF + 1} = \frac{0.3 + 0.231}{0.3 + 1} = 0.408 \quad [B.3]$$

- Vane cooling flow ($\dot{m}_{cv}$):

The dimensionless vane cooling flow is calculated using the following relationship derived from the heat balance across the surface of the turbine airfoil for turbulent flow:

$$\dot{m}_{cv}/\dot{m}_{g4} = 0.222\,F\left(\frac{E}{1-E}\right)^{1.25} \qquad [B.4]$$

Where F is the factor of relative cooling flow based on the airfoil cooling configuration (See Table B.1). Based on an assumption of full cover film cooling, the following dimensionless vane cooling calculation results:

$$\dot{m}_{cv}/\dot{m}_{g4} = 0.022\,(1.0)\left(\frac{0.408}{1-0.408}\right)^{1.25} = 0.0138$$

To account for end wall, shroud, and disk cooling and leakage, this result is increased by a factor of 4/3 before calculating the total vane cooling flow:

$$\dot{m}_{cv} = \frac{4}{3}\left(\dot{m}_{cv}/\dot{m}_{g4}\right)\dot{m}_{g4} = \frac{4}{3}(0.0138)(1.086) = 0.020\,\text{lbm/s}$$

3) Rotor blade cooling requirements

Calculate the rotor inlet temperature by mixing in the vane cooling air previously determined. Begin by calculating the mass flow rate including vane cooling flow as follows:

$$\dot{m}_{g4.1} = \dot{m}_{g4} + \dot{m}_{cv} = 1.086 + 0.020 = 1.106\,\text{lbm/s}$$

Using energy conservation, the enthalpy after vane cooling equals:

$$h_{4.1} = \frac{h_4\,\dot{m}_{g4} + h_{cv}\,\dot{m}_{cv}}{\dot{m}_{g4.1}} = \frac{(657.1)(1.086) + (232.2)(0.02)}{1.106} = 649.4\,\text{BTU/lbm}$$

The fuel-air ratio (*f*) is determined using the following expression:

$$f = \frac{\dot{m}_{fuel}}{\dot{m}_{g4.1} - \dot{m}_{fuel}} = \frac{0.026}{1.106 - 0.026} = 0.024$$

After determining the enthalpy and fuel-air ratio, use the gas tables to look up the value for gas temperature at the rotor blades. In this case, $T_{g4.1}$ = 2443.6 ^{o}R. From this point forward, the calculations used to determine the blade cooling flow follow the same format as those completed for the stator. Using a pattern factor (PF) of 0.13 for the rotor blade and relative cooling factor (F) of 1.2 for the blade cooling configuration, the following results were found:

- Gas temperature at rotor blade adjusted for safety factor:

$$T_{gb} = T_{g4.1} + SF = 2443.6 + 150 = 2593.6^{o}R$$

- Cooling effectiveness (E'):

$$E' = \frac{T_{gb} - T_{mb}}{T_{gb} - T_{cool}} = \frac{2593.6 - 2192}{2593.6 - 965.6} = 0.247$$

- Cooling effectiveness adjusted for pattern factor (E):

$$E = \frac{PF + E'}{PF + 1} = \frac{0.13 + 0.247}{0.13 + 1} = 0.333$$

- Rotor blade cooling flow ($\dot{m}_{cb}$):

$$\dot{m}_{cb} / \dot{m}_{g4.1} = 0.022(1.2)\left(\frac{0.333}{1 - 0.333}\right)^{1.25} = 0.011$$

$$\dot{m}_{cb} = \frac{4}{3}(0.011)(1.106) = 0.016\,\text{lbm/s}$$

4) Total cooling flow requirement ($\dot{m}_{cool}$)

$$\dot{m}_{cool} = \dot{m}_{cv} + \dot{m}_{cb} = 0.020 + 0.016 = 0.036\,\text{lbm/s}$$

$$\%\,\text{bleed} = \frac{\dot{m}_{cool}}{\dot{m}_{03}} = \frac{0.036}{1.060} = 3.4\%$$

This result allows the engine designer to perform trade studies concerning the relationship between added performance and turbine cooling bleed air requirements.

Table B.1: Turbine Airfoil Relative Cooling Factors[1]

Airfoil Cooling Configuration	% Trailing Edge Ejection	Relative Cooling Factor (F)
Uncooled	0	0
Convection	100	2.0
Convection with coat	100	1.5
Advanced convection	100	1.4
Film with convection	75	1.3
Film with convection	50	1.2
Film with convection	25	1.1
Transpiration with convection	25	0.9
Full cover film	0	1.0
Transpiration	0	0.8

[1] James W. Gauntner, "Algorithm for Calculating Turbine Cooling Flow and the Resulting Decrease in Turbine Efficiency," *NASA Technical Memorandum 81453 (*Cleveland, OH: Lewis Research Center, 1980).

APPENDIX C

NEPP ENGINE MODEL (GTGH)

GEORGIA TECH GENERIC HELICOPTER (GTGH) ENGINE MODEL

```
/* GLOBAL INPUTS */
&D
CALBLD=F,                /* Calibrate Bleed Call */
AMAC=T,                  /* Aircraft Mission Analysis Code Created */
MAPLOT=F,                /* Plots Component Maps */
MAXNIT=100,              /* Maximum Number of Iterations */
ITERM=2,                 /* Screen Printout During Run */
DRAW=T,                  /* Schematic Block Diagrams */
DOUTHD=T,                /* Output Headers */
TLOAD=T,
LONG=F,                  /* Output Length */
&END

/* First Mode */

&D
MODE=1,
IWT=1,                   /* Data for WATE */
INST=0,                  /* Calls INSTAL */
ELIFE=10000,             /* Engine Life (hours) */

/* INLET */
KONFIG(1,1)=1,
KONFIG(2,1)=1,
KONFIG(3,1)=0,
KONFIG(4,1)=2,
KONFIG(5,1)=0,
SPEC(1,1)=0,
SPEC(2,1)=0,
SPEC(3,1)=0,
SPEC(4,1)=0,
SPEC(5,1)=0,
SPEC(6,1)=0,             /* Inlet Pressure Recovery */
SPEC(7,1)=0,
SPEC(8,1)=0,
SPEC(9,1)=6000,          /* Geometric Altitude (ft) */
SPEC(10,1)=0,
SPEC(11,1)=0,
SPEC(12,1)=36,           /* Temperature Difference from Std (deg R) */
SPEC(13,1)=0,
SPEC(14,1)=1.06,         /* Corrected Mass Flow at Exit (lbm/s) */
```

```
/* DUCT */
KONFIG(1,2)=2,
KONFIG(2,2)=2,
KONFIG(3,2)=0,
KONFIG(4,2)=3,
KONFIG(5,2)=0,
SPEC(1,2)=0,
SPEC(2,2)=0.3,              /* Design Point Entrance Mach Number */
SPEC(3,2)=0,
SPEC(4,2)=0,
SPEC(5,2)=0,
SPEC(6,2)=0,
SPEC(7,2)=0,
SPEC(8,2)=0,

/* CENTRIFUGAL COMPRESSOR */
KONFIG(1,3)=4,
KONFIG(2,3)=3,
KONFIG(3,3)=0,
KONFIG(4,3)=4,
KONFIG(5,3)=0,
SPEC(1,3)=2,                /* "R" Value */
SPEC(2,3)=0,                /* Ratio Bleed to Total Flow */
SPEC(3,3)=1,                /* Scale Factor (Speed) */
SPEC(4,3)=1201,             /* Corrected Weight Flow Rate Table */
SPEC(5,3)=1,                /* Scale Factor (Flow) */
SPEC(6,3)=1202,             /* Off-design Adiabatic Efficiency */
SPEC(7,3)=1,                /* Scale Factor (Efficiency) */
SPEC(8,3)=1203,             /* Off-design Pressure Ratio Table */
SPEC(9,3)=1,                /* Scale Factor (PR) */
SPEC(10,3)=0,
SPEC(11,3)=0,
SPEC(12,3)=0.8,             /* Design Point Adiabatic Efficiency */
SPEC(13,3)=6.5,             /* Design Point Total Pressure Ratio */
SPEC(14,3)=1,

/* DUCT */
KONFIG(1,5)=2,
KONFIG(2,5)=4,
KONFIG(3,5)=0,
KONFIG(4,5)=5,
KONFIG(5,5)=0,
SPEC(1,5)=0.01,             /* Relative Total Pressure Drop */
SPEC(2,5)=0,
SPEC(3,5)=0,
SPEC(4,5)=0,
SPEC(5,5)=0,
SPEC(6,5)=0,
SPEC(7,5)=0,
SPEC(8,5)=0,
```

```
/* BURNER */
KONFIG(1,6)=2,
KONFIG(2,6)=5,
KONFIG(3,6)=0,
KONFIG(4,6)=6,
KONFIG(5,6)=0,
SPEC(1,6)=0.05,          /* Friction Relative Pressure Drop */
SPEC(2,6)=0,
SPEC(3,6)=0,
SPEC(4,6)=2300,          /* Desired Exit Temp (deg R) */
SPEC(5,6)=0.99,          /* Combustion Efficiency */
SPEC(6,6)=18550,         /* Fuel Heating Value */
SPEC(7,6)=0,
SPEC(8,6)=0,
SPEC(9,6)=0,
SPEC(10,6)=0,
SPEC(11,6)=0,

/* HIGH PRESSURE TURBINE */
KONFIG(1,7)=5,
KONFIG(2,7)=6,
KONFIG(3,7)=0,
KONFIG(4,7)=7,
KONFIG(5,7)=0,
SPEC(1,7)=2.22,          /* Total Pressure Ratio */
SPEC(2,7)=0,
SPEC(3,7)=1,             /* Scale Factor (Speed) */
SPEC(4,7)=2124,          /* Corrected Flow Table */
SPEC(5,7)=1,             /* Scale Factor (Flow) */
SPEC(6,7)= 2125,         /* Adiabatic Efficiency Table */
SPEC(7,7)=1,             /* Scale Factor (Efficiency) */
SPEC(8,7)=1,             /* Scale Factor (PR) */
SPEC(9,7)=0,
SPEC(10,7)=1,            /* Variable Geometry Setting */
SPEC(11,7)=.91,          /* Design Point Adiabatic Efficiency */
SPEC(12,7)=63000,        /* Design Point RPM */
SPEC(13,7)=1,

/* DUCT */
KONFIG(1,8)=2,
KONFIG(2,8)=7,
KONFIG(3,8)=0,
KONFIG(4,8)=8,
KONFIG(5,8)=0,
SPEC(1,8)=0.01,          /* Relative Total Pressure Drop */
SPEC(2,8)=0,
SPEC(3,8)=0,
SPEC(4,8)=0,
SPEC(5,8)=0,
SPEC(6,8)=0,
SPEC(7,8)=0,
```

```
SPEC(8,8)=0,

/* POWER TURBINE */
KONFIG(1,9)=5,
KONFIG(2,9)=8,
KONFIG(3,9)=0,
KONFIG(4,9)=9,
KONFIG(5,9)=0,
SPEC(1,9)=2.88,          /* Total Pressure Ratio */
SPEC(2,9)=0,
SPEC(3,9)=1,             /* Scale Factor (Speed) */
SPEC(4,9)=2126,          /* Corrected Flow Table */
SPEC(5,9)=1,             /* Scale Factor (Flow) */
SPEC(6,9)=2127,          /* Adiabatic Efficiency Table */
SPEC(7,9)=1,             /* Scale Factor (Efficiency) */
SPEC(8,9)=1,             /* Scale Factor (PR) */
SPEC(9,9)=0,
SPEC(10,9)=1,            /* Variable Geometry Setting */
SPEC(11,9)=0.91,         /* Design Point Adiabatic Efficiency */
SPEC(12,9)=38000.        /* Design Point RPM */
SPEC(13,9)=0,
SPEC(14,9)=0,

/* DUCT */
KONFIG(1,10)=2,
KONFIG(2,10)=9,
KONFIG(3,10)=0,
KONFIG(4,10)=10,
KONFIG(5,10)=0,
SPEC(1,10)=.01,          /* Relative Total Pressure Drop */
SPEC(2,10)=0,
SPEC(3,10)=0,
SPEC(4,10)=0,
SPEC(5,10)=0,
SPEC(6,10)=0,
SPEC(7,10)=0,
SPEC(8,10)=0,

/* EXHAUST */
KONFIG(1,11)=9,
KONFIG(2,11)=10,
KONFIG(3,11)=0,
KONFIG(4,11)=11,
KONFIG(5,11)=0,
SPEC(1,11)=0,
SPEC(2,11)=1,            /* Discharge Coefficient */
SPEC(3,11)=0,
SPEC(4,11)=0,
SPEC(5,11)=0.99,         /* Velocity Coefficient */
SPEC(6,11)=0,
SPEC(7,11)=0,
```

```
SPEC(8,11)=0,
SPEC(9,11)=1,

/* SHAFT LOAD */
KONFIG(1,12)=10,
KONFIG(2,12)=0,
KONFIG(3,12)=0,
KONFIG(4,12)=0,
KONFIG(5,12)=0,
SPEC(1,12)=-120,          /* Desired Load (HP) */

/* GAS GENERATOR SHAFT */
KONFIG(1,13)=11,
KONFIG(2,13)=3,
KONFIG(3,13)=7,
KONFIG(4,13)=0,
KONFIG(5,13)=0,
SPEC(1,13)=63000,         /* Shaft Speed (RPM) */
SPEC(2,13)=1,
SPEC(3,13)=1,
SPEC(4,13)=1,
SPEC(5,13)=1,
SPEC(6,13)=1,             /* Mech Efficiency of 1st Component */
SPEC(7,13)=1,             /* 2d component */
SPEC(8,13)=1,             /* 3d component */

/* POWER SHAFT */
KONFIG(1,14)=11,
KONFIG(2,14)=12,
KONFIG(3,14)=9,
KONFIG(4,14)=0,
KONFIG(5,14)=0,
SPEC(1,14)=38000,         /* Shaft Speed (RPM) */
SPEC(2,14)=1,
SPEC(3,14)=1,
SPEC(4,14)=1,
SPEC(5,14)=1,
SPEC(6,14)=1,             /* Mech Efficiency of 1st Component */
SPEC(7,14)=1,             /* 2d component */
SPEC(8,14)=1,             /* 3d component */

/* SPECIAL CONTROLS */

KONFIG(1,15)=12,
SPCNTL(1,15)=14,          /* Vary mass flow rate */
SPCNTL(2,15)=1,           /* at the inlet */
SPCNTL(3,15)=100,
SPCNTL(4,15)=8,           /* So that flow rate error */
SPCNTL(5,15)=3,           /* prior to the compressor */
SPCNTL(6,15)=0,           /* equals 0 */
SPCNTL(7,15)=0,
```

```
SPCNTL(8,15)=0,
SPCNTL(9,15)=0,

KONFIG(1,18)=12,
SPCNTL(1,18)=1,          /* Vary "R" value */
SPCNTL(2,18)=3,          /* of the compressor */
SPCNTL(3,18)=100,
SPCNTL(4,18)=8,          /* So that flow rate error */
SPCNTL(5,18)=6,          /* prior to the HPT */
SPCNTL(6,18)=0,          /* equals 0 */
SPCNTL(7,18)=0,
SPCNTL(8,18)=0,

KONFIG(1,19)=12,
SPCNTL(1,19)=1,          /* Vary the PR */
SPCNTL(2,19)=7,          /* of the HPT */
SPCNTL(3,19)=100,
SPCNTL(4,19)=8,          /* So that flow rate error */
SPCNTL(5,19)=8,          /* prior to the LPT */
SPCNTL(6,19)=0,          /* equals 0 */
SPCNTL(7,19)=0,
SPCNTL(8,19)=0,

KONFIG(1,20)=12,
SPCNTL(1,20)=1,          /* Vary the PR */
SPCNTL(2,20)=9,          /* of the LPT */
SPCNTL(3,20)=100,
SPCNTL(4,20)=8,          /* So that flow rate error */
SPCNTL(5,20)=10,         /* prior to the exhaust */
SPCNTL(6,20)=0,          /* equals 0 */
SPCNTL(7,20)=0,
SPCNTL(8,20)=1,
SPCNTL(9,20)=0,

KONFIG(1,21)=12,
SPCNTL(1,21)=1,          /* Vary RPM */
SPCNTL(2,21)=13,         /* of the compressor shaft */
SPCNTL(3,21)=200,
SPCNTL(4,21)=8,          /* So that net shaft HP */
SPCNTL(5,21)=13,         /* of the compressor shaft */
SPCNTL(6,21)=0,          /* equals 0 */
SPCNTL(7,21)=0,
SPCNTL(8,21)=0,
SPCNTL(9,21)=0,

KONFIG(1,22)=12,
SPCNTL(1,22)=1,          /* Vary the shaft load */
SPCNTL(2,22)=12,         /* of the shaft load */
SPCNTL(3,22)=200,
SPCNTL(4,22)=8,          /* So that the error in net shaft HP */
SPCNTL(5,22)=14,         /* of the load shaft */
```

```
SPCNTL(6,22)=0,          /* equals 0 */
SPCNTL(7,22)=0,
SPCNTL(8,22)=0,
SPCNTL(9,22)=0,

KONFIG(1,23)=12,
SPCNTL(1,23)=1,          /* Vary "R" value */
SPCNTL(2,23)=3,          /* of the compressor */
SPCNTL(3,23)=100,
SPCNTL(4,23)=8,          /* So that flow rate error */
SPCNTL(5,23)=6,          /* prior to the HPT */
SPCNTL(6,23)=0,          /* equals 0 */
SPCNTL(7,23)=0,
SPCNTL(8,23)=0,

KONFIG(1,24)=12,
SPCNTL(1,24)=14,         /* Vary mass flow rate */
SPCNTL(2,24)=1,          /* at the inlet */
SPCNTL(3,24)=200,
SPCNTL(4,24)=9,          /* So that the PR */
SPCNTL(5,24)=11,         /* of the exhaust */
SPCNTL(6,24)=1.03,       /* equals 1.01 */
SPCNTL(7,24)=0,
SPCNTL(8,24)=0,

KONFIG(1,31)=12,
SPCNTL(1,31)=4,          /* Vary CET */
SPCNTL(2,31)=6,          /* of the burner */
SPCNTL(3,31)=400,
SPCNTL(4,31)=4,          /* So that the net jet thrust */
SPCNTL(5,31)=0,
SPCNTL(6.31)=0,          /* equals 0 */
SPCNTL(7,31)=0,
SPCNTL(8,31)=0,
&END
```

Sample Code for Performance Cycle Analysis (SLS, Hover)

```
/*  Power Hook    VEL: 0 knots    TEMP: ISA */
 &D SPEC(9,15)=1,SPEC(9,17)=0,SPEC(9,18)=0,
      SPEC(9,19)=1,SPEC(9,20)=1,SPEC(9,21)=1,SPEC(9,22)=1,
      SPEC(9,23)=1,SPEC(5,1)=0.0,SPEC(9,1)=0.0,
      SPEC(12,1)=0,SPEC(4,6)=2450,IWT=1,&END
 &D SPEC(4,6)=2375.,&END
 &D SPEC(4,6)=2300.,&END
 &D SPEC(4,6)=2200.,&END
 &D SPEC(4,6)=2100.,&END
 &D SPEC(4,6)=2000.,&END
 &D SPEC(4,6)=1900.,&END
 &D SPEC(4,6)=1800.,&END
 &D SPEC(4,6)=1700.,&END
```

Component Performance Maps

Centrifugal Compressor

```
1201    AIRFLOW (PR=4,CENTRIFUGAL)
ANGL  1       0.00
SPED  6      0.600    0.700    0.800    0.900    1.000    1.050
R    8      1.000    1.100    1.200    1.300    1.400    1.500    1.600
          1.700
FLOW  8      0.5400   0.6000   0.6500   0.7070   0.7450   0.7750   0.7780
          0.7780
FLOW  8      0.6500   0.7080   0.7600   0.8360   0.8700   0.8900   0.8940
          0.8940
FLOW  8      0.7400   0.7850   0.8400   0.9030   0.9280   0.9390   0.9430
          0.9430
FLOW  8      0.8110   0.8570   0.9040   0.9580   0.9750   0.9840   0.9900
          0.9960
FLOW  8      0.8820   0.9300   0.9650   1.0000   1.0150   1.0200   1.0250
          1.0270
FLOW  8      0.9600   0.9950   1.0150   1.0300   1.0370   1.0400   1.0470
          1.0500
EOT

 1202    EFFICIENCY (PR=4,CENTRIFUGAL)
ANGL  1       0.00
SPED  6      0.600    0.700    0.800    0.900    1.000    1.050
R    8      1.000    1.100    1.200    1.300    1.400    1.500    1.600
          1.700
EFF   8      0.7800   0.8000   0.8020   0.8000   0.7900   0.7800   0.7700
          0.7500
EFF   8      0.7800   0.8000   0.8050   0.8000   0.7900   0.7800   0.7700
```

```
          0.7500
EFF  8     0.7800    0.8000    0.8100    0.8000    0.7900    0.7800    0.7700
          0.7500
EFF  8     0.7800    0.8000    0.8100    0.8000    0.7900    0.7800    0.7700
          0.7500
EFF  8     0.7800    0.8000    0.8040    0.8000    0.7900    0.7800    0.7700
          0.7500
EFF  8     0.7800    0.8000    0.8010    0.7900    0.7850    0.7800    0.7700
          0.7500
EOT

 1203     PRESSURE RATIO (PR=6.5,CENTRIFUGAL)
ANGL  1        0.00
SPED  6       0.600     0.700     0.800     0.900     1.000     1.050
R     8       1.000     1.100     1.200     1.300     1.400     1.500     1.600
           1.700
PR    8       4.0500    3.9750    3.9000    3.7950    3.7050    3.6000    3.4650
          3.1275
PR    8       4.5450    4.4850    4.4400    4.3200    4.2150    4.0800    3.8850
          3.5100
PR    8       5.0700    5.0250    4.9800    4.8120    4.6650    4.5000    4.3500
          3.9300
PR    8       5.7300    5.6400    5.5500    5.3700    5.1750    5.0400    4.8900
          4.5000
PR    8       6.4500    6.3750    6.2250    6.0000    5.8050    5.6250    5.4300
          4.9950
PR    8       7.3050    7.0500    6.8400    6.4800    6.3000    6.1800    5.9250
          5.4750
EOT
```

High Pressure Turbine

```
2124       TURBINE FLOW FUNCTION VS. PR, RPM, AND AREA
AREA  1        1.00
RPM   5        80.       90.      100.      105.      110.
PR    9       1.400     1.600     1.800     2.000     2.200     2.400     2.600
PR    9       2.800     3.000
FLOW  9       0.146     0.163     0.174     0.180     0.183     0.186     0.187
FLOW  9       0.188     0.189
FLOW  9       0.145     0.161     0.171     0.177     0.181     0.184     0.185
FLOW  9       0.187     0.187
FLOW  9       0.144     0.159     0.169     0.175     0.179     0.181     0.183
FLOW  9       0.184     0.185
FLOW  9       0.144     0.159     0.168     0.174     0.178     0.180     0.182
FLOW  9       0.183     0.184
FLOW  9       0.144     0.158     0.167     0.173     0.177     0.179     0.181
FLOW  9       0.183     0.184
EOT
```

```
 2125      TURBINE EFFICIENCY VS. PR, RPM, AND AREA
AREA  1       1.00
RPM   5       80.     90.     100.    105.    110.
PR    9       1.400   1.600   1.800   2.000   2.200   2.400   2.600
PR    9       2.800   3.000
EFF   9       0.8603  0.8804  0.8760  0.8643  0.8528  0.8411  0.8283
EFF   9       0.8173  0.8077
EFF   9       0.8452  0.8878  0.8940  0.8893  0.8820  0.8714  0.8606
EFF   9       0.8511  0.8426
EFF   9       0.8151  0.8818  0.9001  0.9027  0.9003  0.8915  0.8829
EFF   9       0.8750  0.8678
EFF   9       0.7948  0.8744  0.8992  0.9055  0.9057  0.8981  0.8907
EFF   9       0.8837  0.8772
EFF   9       0.7724  0.8642  0.8958  0.9060  0.9088  0.9027  0.8964
EFF   9       0.8904  0.8846
EOT
```

Power Turbine

```
2126      TURBINE FLOW FUNCTION VS. PR, RPM, AND AREA
AREA  1       1.00
RPM   7       60.     70.     80.     90.     100.    110.    120.
PR    11      1.200   1.400   1.600   2.000   2.200   2.400   2.600
PR    11      2.800   3.000   3.200   3.400
FLOW  11      0.466   0.611   0.688   0.757   0.771   0.779   0.783
FLOW  11      0.784   0.784   0.784   0.784
FLOW  11      0.469   0.603   0.676   0.746   0.762   0.772   0.777
FLOW  11      0.781   0.782   0.782   0.782
FLOW  11      0.476   0.598   0.666   0.735   0.751   0.762   0.769
FLOW  11      0.774   0.777   0.779   0.779
FLOW  11      0.489   0.597   0.661   0.726   0.743   0.754   0.762
FLOW  11      0.767   0.771   0.773   0.775
FLOW  11      0.503   0.599   0.657   0.718   0.734   0.745   0.753
FLOW  11      0.758   0.762   0.765   0.767
FLOW  11      0.522   0.604   0.657   0.713   0.728   0.739   0.746
FLOW  11      0.752   0.756   0.759   0.761
FLOW  11      0.542   0.612   0.659   0.710   0.724   0.734   0.741
FLOW  11      0.747   0.750   0.753   0.756
EOT
 2127      TURBINE EFFICIENCY VS. PR, RPM, AND AREA
AREA  1       1.00
RPM   7       60.     70.     80.     90.     100.    110.    120.
PR    11      1.200   1.400   1.600   2.000   2.200   2.400   2.600
PR    11      2.800   3.000   3.200   3.400
EFF   11      0.7363  0.8339  0.8357  0.8110  0.7986  0.7855  0.7739
EFF   11      0.7638  0.7549  0.7470  0.7399
EFF   11      0.6772  0.8376  0.8605  0.8543  0.8452  0.8349  0.8257
EFF   11      0.8174  0.8099  0.8032  0.7966
EFF   11      0.5971  0.8213  0.8674  0.8814  0.8762  0.8695  0.8630
```

```
EFF  11     0.8568   0.8510   0.8444   0.8375
EFF  11     0.5053   0.7884   0.8592   0.8946   0.8941   0.8913   0.8877
EFF  11     0.8839   0.8793   0.8728   0.8669
EFF  11     0.4067   0.7420   0.8384   0.8960   0.9009   0.9023   0.9018
EFF  11     0.9005   0.8965   0.8914   0.8866
EFF  11     0.3058   0.6843   0.8067   0.8869   0.8982   0.9039   0.9067
EFF  11     0.9081   0.9053   0.9016   0.8979
EFF  11     0.2056   0.6175   0.7658   0.8690   0.8872   0.8974   0.9036
EFF  11     0.9077   0.9068   0.9046   0.9023
EOT
```

APPENDIX D

AXIAL TURBINE PRELIMIARY DESIGN (GTGH)

The following preliminary axial turbine component design example provides a detailed example of the procedures outlined in Chapter 10. The goal of this analysis is to determine the feasibility of the predicted engine cycle performance and to define the initial geometry and weight estimates for the high pressure and power turbine shown in Figure D.1.

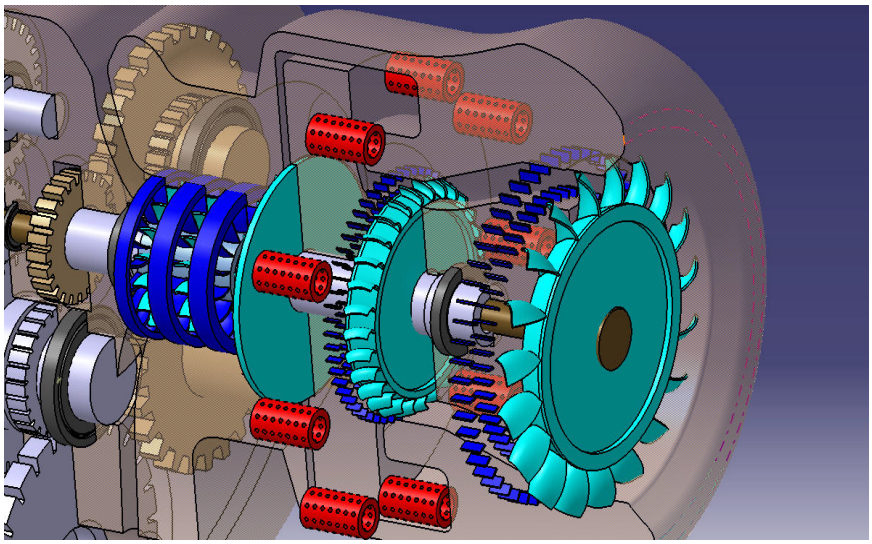

Figure D.1: GTGH Turbine Section CAD Model

High Pressure Turbine (HPT)

Preliminary turbomachinery design begins with the high pressure turbine (HPT) section where the extreme operating environment typically determines the maximum allowable rotational speed. The following initial data was determined during engine cycle analysis for the turbine design point – take-off power at SLS conditions.

Input Data:

$T_{04.1} = 2450^{o}R$ $p_{04.1} = 98.08$ psia $\dot{m}_{04.1} = 1.125$ lbm/s

$\tau_{HPT} = 0.8408$ $\pi_{HPT} = 0.4348$ $\eta_{pt} = 0.89$

Assumptions:

- Two-dimensional flow
- Constant axial velocity ($u_1 = u_2 = u_3$)
- Constant mean radius
- Adiabatic flow in the stator and rotor
- Calorically perfect gas with known γ_t and R_t

  $\gamma_t = 1.3$

  $R_t = 53.4$ (ft-lbf)/(lbm-^{o}R)
- Zweifel coefficient (Z) = 1.0
- Chord-to-height ratio $(c/h)_{rotor} = (c/h)_{stator} = 1.0$
- Solidity (σ) = 1.0
- Shaft radius (r_{shaft}) = 0.5 in
- Taper ratio (A_t/A_h) = 0.8

Design Process:

1) Number of stages

- Select turbine disk material properties

  Single-Crystal Nickel Alloy $\rho = 17.0$ slugs/ft^3 $\sigma_d = 30$ ksi
- Determine maximum allowable rim speed using Equation 10.21:

$$\left[\omega r_r\right]_{max} = \sqrt{\frac{4\sigma_d}{\rho}} = 1008 \text{ ft/s}$$

- Estimate initial mean wheel speed by increasing the maximum rim speed by 10%

$$\left[\omega r_m\right] \approx 1109 \text{ ft/s}$$

- Calculate the dimensionless rotor speed (Ω) using Equation 10.62:

$$\Omega = \frac{\omega r_m}{\sqrt{g_c c_{pt} T_{04.1}}} = \frac{1109}{\sqrt{(7445)(2450)}} = 0.26$$

- Determine the feasibility of a single stage design

Evaluate τ_{HPT} = 0.8408 and Ω = 0.26 using Figure 10.17 The results depicted on Figure D.2 indicate that the combination of temperature ratio and dimensionless wheel speed supports a reasonable single-stage design because M_2 and α_2 fall within a normal range.

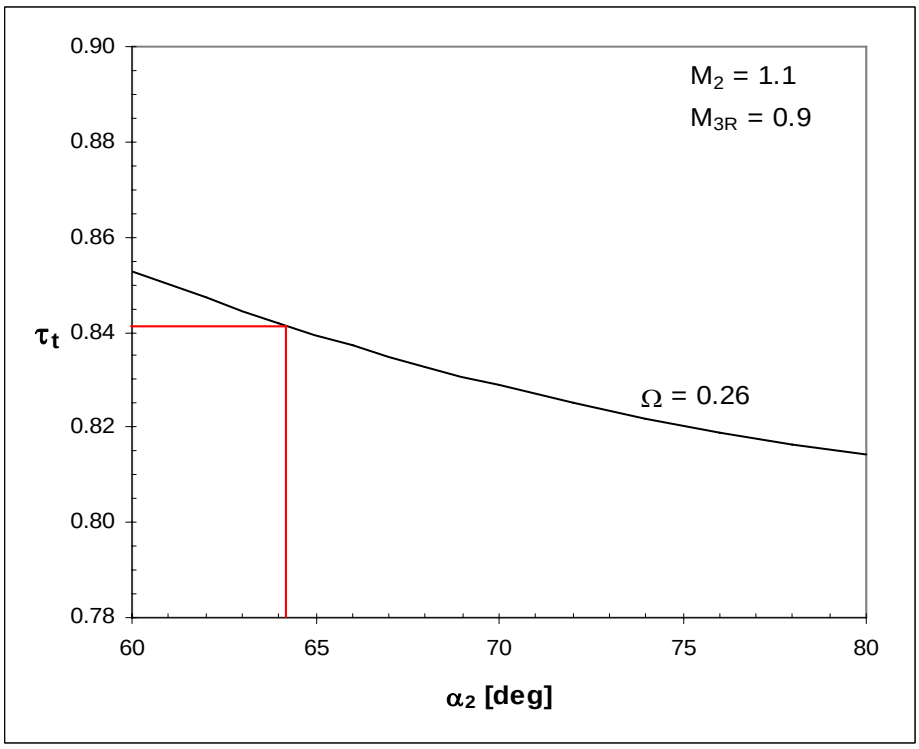

Figure D.2: High Pressure Turbine Single Stage Analysis (GTGH)

2) Stage performance

- Analyze the aerodynamic performance

Evaluate Equations 10.49 – 10.61 using the estimated values for ωr_m, M_2, α_2, and M_{3R} and the Excel HPT design spreadsheet (results shown in Table D.1) to ensure the feasibility of the design in terms of the parameter ranges listed in Table 10.5.

- Select the turbine blade material properties

  Single-Crystal Nickel Alloy $\rho = 17.0$ slugs/ft^3 $\sigma_c = 14.75$ ksi

- Estimate the angular velocity using Equation 10.65:

$$\omega = \sqrt{\frac{4\pi\sigma_c}{\rho A\left(1 + A_t / A_h\right)}} \approx 6600 \text{ rad/s} \approx 63000 \text{ RPM}$$

Where A is the average annulus area of the first HPT stage and A_t/A_h is the taper ratio assumed to be 0.8. The annulus area (A) for any station *i* can be determined as a direct function of the total temperature, total pressure, Mach number, α, and mass flow rate:[1]

$$A_i = \frac{\dot{m}\sqrt{T_{0i}}}{MFP\left(M_i\right) p_{0i} \cos\alpha_i} \qquad [D.1]$$

- Determine the mean radius (r_m) as a function of the estimated rotational velocity

$$r_m = \frac{\left(\omega r_m\right)}{\omega} = \frac{1109}{6600} = 0.168\,\text{ft} \approx 2.0\,\text{in}$$

- Calculate the blade height (h) at each station *i* using the following relationship:

$$h_i = \frac{A_i}{2\pi r_m} \qquad [D.2]$$

- Determine the airfoil geometry, axial spacing, and number of blades

Assume values for solidity (σ) and chord-to-height ratio (c/h) for both the stator vanes and rotor blades. Calculate the airfoil chord by multiplying the appropriate (c/h) and h_i – it should be noted that 0.25 inches is the minimum chord permitted on the Excel spreadsheet in accordance with the TURBN program configuration. Axial spacing (s_{axial}) is calculated as (chord/4) with a minimum acceptable value of 0.13 inches. The number of stator vanes (n_v) or rotor blades (n_b) is determined as the mean circumference divided by the blade spacing ($s = c/\sigma$). An example of these calculations is shown below.

$$c_{stator} = h_1\left(c/h\right)_{stator} = 0.18 < 0.25 \quad \therefore c_{stator} = 0.25\,\text{in}$$

$$s_{axial} = \frac{c_{stator}}{4} = \frac{0.18}{4} = 0.045 < 0.13 \quad \therefore s_{axial} = 0.13\,\text{in}$$

$$n_v = \frac{2\pi r_{m1}}{\left(c/\sigma\right)} = \frac{2\pi\left(2.09\right)}{\left(0.25/1.0\right)} = 50.3 \approx 51\,\text{vanes}$$

- Evaluate the stress characteristics of the rotor blades

Blade stress analysis considers the blade stress factor (AN^2) and its relationship to the material specific strength (σ_c/ρ). Figure D.3 shows the stress analysis for the GTGH HPT based on the relative total temperature of the blades (T_{02R}). These results indicate that the HPT rotational speed is near its maximum value for the selected advanced material.

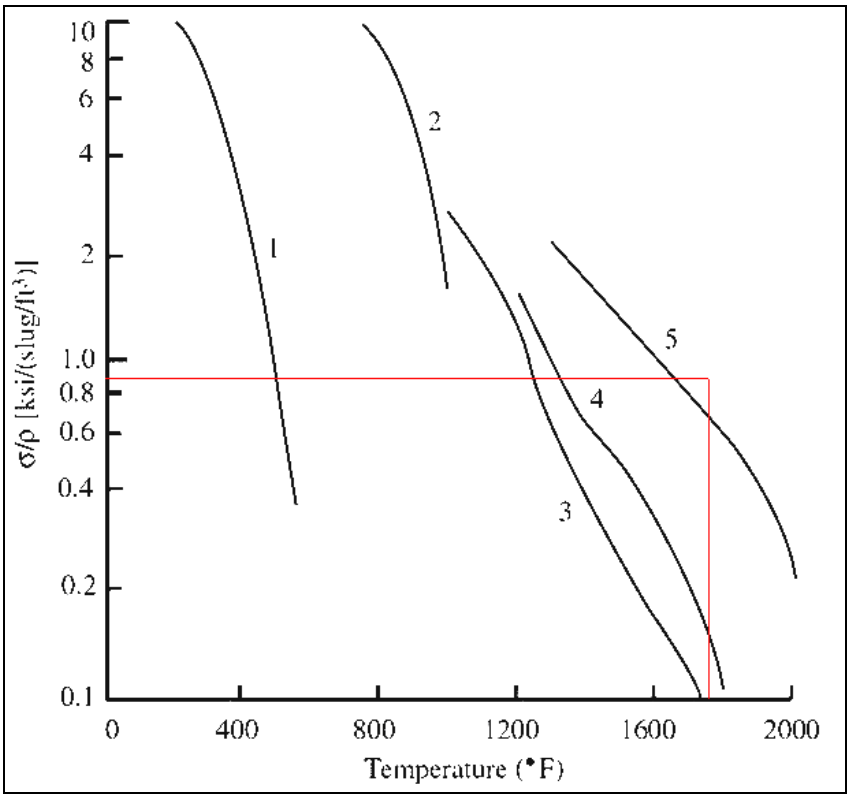

Figure D.3: High Pressure Turbine Blade Stress Analysis (GTGH)

- Determine the geometry and stress characteristics of the turbine rim and disk

The following assumptions were used in calculating the geometric properties of the rim and disk:

$$\text{Rim Width}\left(W_r\right) = 1.1\left(c_{rotor}\right) = 1.1(0.25) = 0.28\,\text{in}$$

$$\text{Rim Height}\left(h_r\right) = \frac{W_r}{2} = \frac{0.28}{2} = 0.14\,\text{in}$$

Material selection for the rim and the disk assumed the same properties throughout:

Single-Crystal Nickel Alloy $\quad \rho = 17.0$ slugs/ft^3 $\quad \sigma_d = \sigma_r = 30$ ksi

The value of $\left(\overline{\sigma}_{blades} / \sigma_r\right)$ is assumed to equal 0.2 for turbines.[2] Applying Equation 10.19, the stress analysis and remaining geometry for the rim and disk were calculated.

$$(\omega r_r)_{actual} = 961\,\text{ft/s} \;\le\; (\omega r_r)_{max} = 1008\,\text{ft/s}$$

$$\frac{W_{dr}}{W_r} = \left[\frac{\bar{\sigma}_{blades}}{\sigma_r}\left(1+\frac{r_r}{h_r}\right)+\frac{\rho(\omega r_r)^2}{\sigma_r}\left(1+\frac{h_r}{2r_r}\right)^2-1\right]\frac{h_r}{r_r} = 0.446 \;\therefore\; W_{dr} = 0.12\,\text{in}$$

$$W_{ds} = W_r\left(\exp\left\{\frac{\rho(\omega r_r)^2}{2\sigma_d}\left[1-\left(\frac{r_{shaft}}{r_r}\right)^2\right]\right\}\right) = 0.65\,\text{in}$$

The results in Table D.1 indicate that results are acceptable because the rim wheel speed is lower than the initial estimate of 1008 ft/s, the disk shape factor (DSF) is less than 2.0, and the rim web thickness ratio (W_{dr}/W_r) is less than 1.0.

3) Weight Estimation

The material density was multiplied by a simple cylindrical volume measurement using the rim width and rotor tip radius (r_t) to approximate the weight. This approach provides a rough estimate sufficient for preliminary design; however, CAD based volume calculations are recommended when a high fidelity component model is available.

Table D.1: High Pressure Turbine Design Results (GTGH)

Assumptions:

γ_t	1.3	
$g_c\ c_{pt}$	7445	$ft^2/(s^2\text{-}^oR)$
R_t	53.4	(ft-lbf)/(lbm-^{o}R)
g_c	32.17	(lbm-ft)/(lbf-s^2)

Input Data:

m_dot	1.125	lbm/s
$T_{04.1}$	2450	^{o}R
$T_{04.4}$	2060	^{o}R
$p_{04.1}$	98.08	psia
M_1	0.3	
η_{pt}	0.89	
z	1	

Stage Input:

# of Stages		1	
Shaft Radius	r_{shaft}	0.5	in
Turbine Inlet Angle	α_1	0	deg
Hub-to-tip Ratio	A_t/A_h	0.8	
Solidity	σ	1.0	

Airfoil Material Selection:

Airfoil Strength	σ_c	14750	psi
Density	ρ	17	$slug/ft^3$

Overall Results:

Temp Ratio	τ_t	0.8420	
Weight Estimate	W_t	2.5	lb
Mean Radius	r_m	2.02	in
Angular Velocity	ω	6598	rad/s
Rotational Speed	N	63006	RPM

Stage 1

Stage Input Data:

M_2	1.1	
M_{3R}	0.9	
α_2	64	deg

Output Data:

	1	2	2R	3R	3	
T_t	2450	2450	2216	2216	2063	^{o}R
p_t	98.08	98.08	--	--	42.5	psia
V	697	2367	1454	1891	1140	ft/s
u	697	1038	1038	1038	1038	ft/s
v	0	2128	1019	1580	471	ft/s
α	0	64	--	--	24.42	deg
β	--	--	44.47	56.71	--	deg
M	0.3	1.1	--	0.9	0.54	
MFP	0.2522	0.5136			0.4069	
A	2.25	2.52			3.25	in^2
h	0.18	0.20			0.26	in
r_t	2.11	2.12			2.15	in
r_h	1.93	1.92			1.89	in

Stator:	n_{vanes}	51		τ_{ts}	0.8420	
	Chord	0.25	in	Ω	0.260	
	Spacing	0.13	in	$\beta_2+\beta_3$	101.2	deg
	(c/h)	1.00		Λ_t	0.2532	
				ψ	2.343	
Rotor:	n_{blades}	51		π_{ts}	0.4328	
	Chord	0.25	in	AN^2	1.00E+10	$in^2\ RPM^2$
	Spacing	0.13	in			
	(c/h)	1.00				

Stress Analysis

Blades:	(σ_c/ρ)	0.87	$ksi/(slug/ft^3)$
Rim & Disk:	σ_r, σ_d	30000	ksi
	σ_r/ρ	1.76	$ksi/(slug/ft^3)$
	σ_{blades}/σ_r	0.20	
	h_r	0.14	in
	r_r	1.77	in
	$[\omega r_r]_{actual}$	971	ft/s
	$[\omega r_r]_{max}$	1008	ft/s
	$\rho(\omega r_r)^2/2\sigma_r$	1.854	DSF
	W_{dr}/W_r	0.449	
	W_{ds}	0.68	in
	W_{dr}	0.12	in
	W_r	0.28	in
Weight Estimate		2.5	lb

Power Turbine (PT)

The procedures used to design the GTGH power turbine (PT) design are identical to those described for the HPT. Only the key differences are highlighted in this section, beginning with changes to the input data and assumptions reflected below.

Input Data:

$T_{04.5} = 2060^{o}R$ $p_{04.5} = 42.2$ psia $\dot{m}_{04.5} = 1.125$ lbm/s

$\tau_{PT} = 0.8037$ $\pi_{PT} = 0.3622$ $\eta_{pt} = 0.89$

$M_1 = 0.54$

Assumptions:

- Taper ratio (A_t/A_h) = 1.0

Design Process:

1) Number of stages

The power turbine for a turboshaft engine is particularly unique in terms of it rotational speed design flexibility. In most dual-shaft gas turbine engines, the low pressure turbine shares its shaft with a fan or low pressure compressor which typically determines the maximum rotational speed. Additionally, the lower temperatures and slower speeds of the power turbine usually alleviate most of the material related design restrictions. Turboshaft engine designers generally have more design space available to optimize the power turbine shaft speed for sizing, performance, and gear reductions.

- Select turbine disk material properties

Nickel Alloy $\rho = 17.0$ slugs/ft^3 $\sigma_d = 32$ ksi

- Determine maximum allowable rim speed using Equation 10.21:

$$[\omega r_r]_{max} = \sqrt{\frac{4\sigma_d}{\rho}} = 1041 \text{ ft/s}$$

- Estimate initial mean wheel speed by increasing the maximum rim speed by 10%

$$[\omega r_m] \approx 1145 \text{ ft/s}$$

- Calculate the dimensionless rotor speed (Ω) using Equation 10.62:

$$\Omega = \frac{\omega r_m}{\sqrt{g_c c_{pt} T_{04.5}}} = \frac{1145}{\sqrt{(7445)(2060)}} = 0.29$$

- Determine the feasibility of a single stage design

Evaluate τ_{PT} = 0.8037 and Ω = 0.29 using Figure 10.17. The results depicted on Figure D.4 indicate that the combination of τ and Ω falls at the upper design limit for a single stage turbine because it requires higher values for M_2 and α_2. In this case, the added design risk for the single stage option was considered acceptable in avoiding the large weight penalty associated with multiple stages.

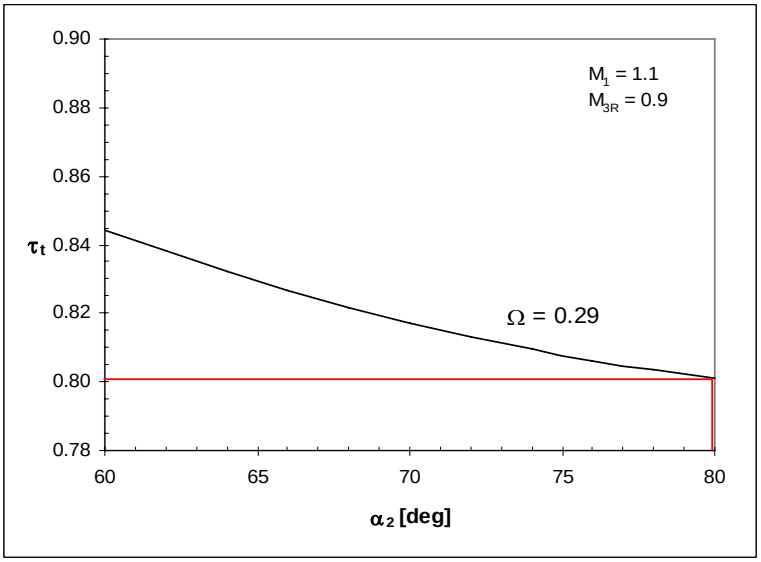

Figure D.4: Power Turbine Single Stage Analysis (GTGH)

2) Stage performance and weight estimation

Table D.2 shows the results of increasing M_2 to 1.2 and α_2 to 73°. It is also important to consider the increased size of the power turbine radius to ensure that a smooth transition duct from the high pressure turbine is feasible.

Table D.2: Power Turbine Design Results (GTGH)

Assumptions:		
γ_t	1.3	
$g_c\ c_{pt}$	7445	$ft^2/(s^2\text{-}^oR)$
R_t	53.4	(ft-lbf)/(lbm-°R)
g_c	32.17	(lbm-ft)/(lbf-s^2)

Input Data:		
m_dot	1.125	lbm/s
$T_{04.1}$	2060	°R
$T_{04.4}$	1652	°R
$p_{04.1}$	42.2	psia
M_1	0.54	
η_{pt}	0.89	
Z	1	

Stage Input:			
# of Stages		1	
Shaft Radius	r_{shaft}	0.5	in
Turbine Inlet Angle	α_1	0	deg
Hub-to-tip Ratio	A_t/A_h	1.0	
Solidity	σ	1.0	
Airfoil Material Selection:			
Airfoil Strength	σ_c	20000	psi
Density	ρ	17	$slug/ft^3$

Overall Results:			
Temp Ratio	τ_t	0.8020	
Weight Estimate	W_t	16.1	lb
Mean Radius	r_m	3.45	in
Angular Velocity	ω	3989	rad/s
Rotational Speed	N	38094	RPM

	Stage 1					
Stage Input Data:	M_2	1.2				
	M_{3R}	0.9				
	α_2	73	deg			

Output Data:

	1	**2**	**2R**	**3R**	**3**	
T_t	2060	2060	1805	1805	1652	°R
p_t	42.2	42.2	--	--	14.4	psia
V	1134	2334	1283	1706	801	ft/s
u	1134	682	682	682	682	ft/s
v	0	2232	1087	1564	418	ft/s
α	0	73	--	--	31.51	deg
β	--	--	57.87	66.42	--	deg
M	0.54	1.2	--	0.9	0.42	
MFP	0.4056	0.5018			0.3377	
A	2.98	8.25			11.02	in^2
h	0.14	0.38			0.51	in
r_t	3.51	3.64			3.70	in
r_h	3.38	3.25			3.19	in

Stator:	n_{vanes}	84		τ_{ts}	0.8020	
	Chord	0.26	in	**Ω**	0.292	
	Spacing	0.13	in	$\beta_2+\beta_3$	124.3	deg
	(c/h)	1.00		Λ_t	0.2082	
				ψ	2.314	
Rotor:	n_{blades}	49		π_{ts}	0.3416	
	Chord	0.44	in	AN^2	1.20E+10	$in^2\ RPM^2$
	Spacing	0.13	in			
	(c/h)	1.00				

Stress Analysis			
Blades:	(σ_c/ρ)	1.18	$ksi/(slug/ft^3)$
Rim & Disk:	σ_r, σ_d	30000	ksi
	σ_r/ρ	1.76	$ksi/(slug/ft^3)$
	σ_{blades}/σ_r	0.20	
	h_r	0.24	in
	r_r	2.98	in
	$[\omega r_r]_{actual}$	990	ft/s
	$[\omega r_r]_{max}$	1008	ft/s
	$\rho(\omega r_r)^2/2\sigma_r$	1.929	DSF
	W_{dr}/W_r	0.478	
	W_{ds}	1.52	in
	W_{dr}	0.23	in
	W_r	0.49	in
Weight Estimate		16.1	lb

[1] Jack D. Mattingly, William H. Heiser, and David T. Pratt, *Aircraft Engine Design* (Reston, VA: AIAA, 2002).

[2] Jack D. Mattingly, *Elements of Gas Turbine Propulsion* (Reston, VA: AIAA, 2005).

APPENDIX E

RADIAL COMPRESSOR PRELIMINARY DESIGN (GTGH)

The following preliminary centrifugal compressor design provides a detailed example of the procedures outlined in Chapter 10. The goal of this analysis was to determine the feasibility of the predicted engine cycle performance and to define the initial geometry and weight estimates for the GTGH compressor shown in Figure E.1. Similar to the turbine, the design point for this compressor was selected to address the maximum pressure ratio at SLS conditions. An Excel design code was used to automate this analysis.

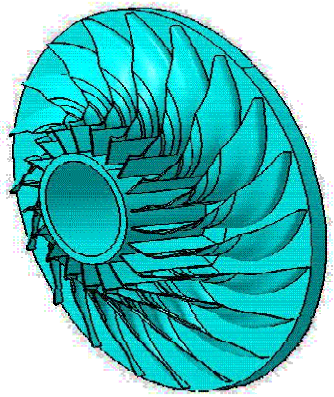

Figure E.1: GTGH Centrifugal Compressor CAD Model

Input Data:

$T_{02} = 518.67^{o}R$	$p_{02} = 14.696$ psia	$\dot{m}_{02} = 1.10$ lbm/s
$\rho_{02} = 0.0766$ lbm/ft^3	$\pi_c = 7.1$	$\eta_{pc} = 0.85$

Assumptions:

- Rotor inlet velocity (u_1) is uniform and axial (No prewhirl conditions exist from the use of inlet guide vanes)
- Adiabatic flow in the diffuser ($T_{03} = T_{02}$)
- Constant width diffuser ($b_2 = b_5$)
- Calorically perfect gas with known γ and R

  $\gamma_c = 1.4$

  $R_c = 53.3$ (ft-lbf)/(lbm-^oR)
- Slip factor (ε) = 0.9
- Rotational velocity (N) = 63000 RPM [determined during HPT analysis]
- Hub-to-tip ratio (ζ) = 0.30
- Straight radial blades at impeller exit ($\beta_{2b} = 0^o$)

Design Process:

1) Rotor geometry

- Calculate rotor tip speed (U_2) using Equation 10.28 and Figure 10.12:

$$U_2 = \sqrt{\left(\frac{g_c c_p T_{01}}{\varepsilon}\right)\left(\pi_c^{(\gamma-1)/(\gamma\eta_{pc})} - 1\right)} = 1797\,\text{ft/s}$$

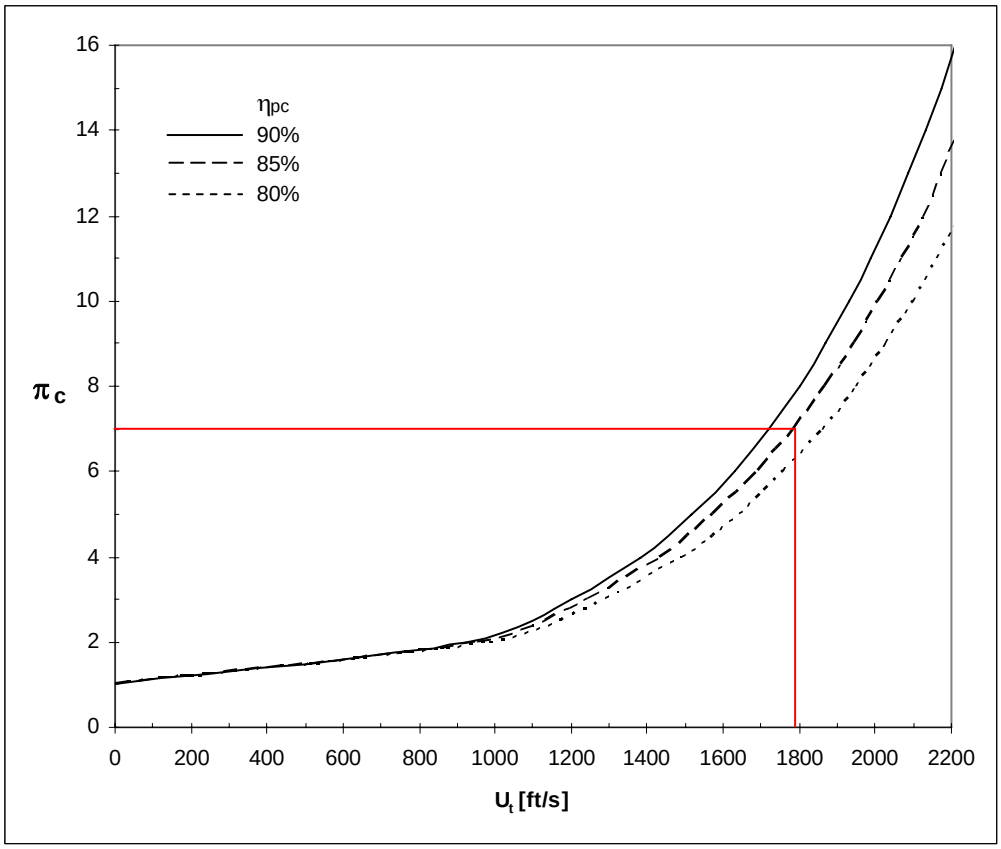

Figure E.2: Compressor Pressure Ratio vs. Tip Speed (GTGH)

- Determine the inlet conditions

Using the compressor input data and parameter assumptions in conjunction with the general sequence of Equations 10.29 – 10.35, Figure E.3 is generated – providing a valuable tool in selecting the appropriate design parameters for the compressor inlet based on the rotational speed (N) of the HPT. In this case, $\beta_{1t} = 50^{o}$, $M_{1R} = 0.8$, and $M_1 = 0.51$ were selected as reasonable design parameters.

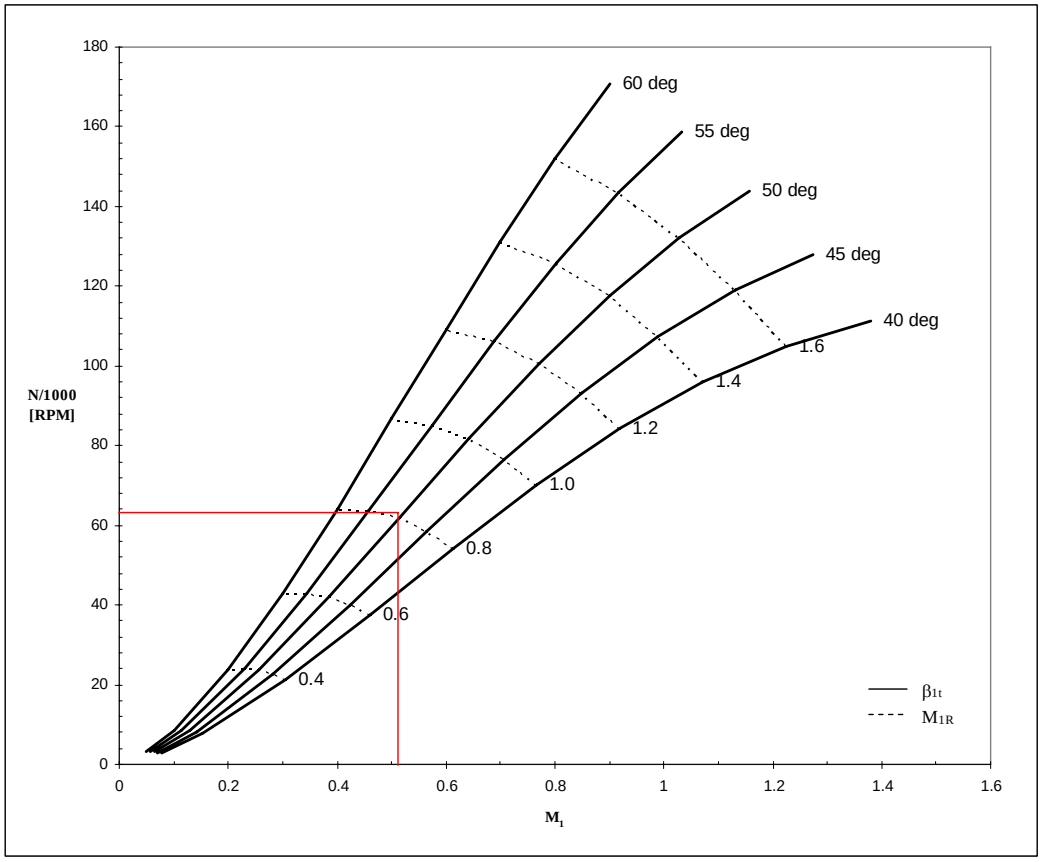

Figure E.3: Compressor Inlet Conditions Trade Study (GTGH)

Using these parameters, the inlet conditions were established as follows:

$$T_1 = \frac{T_{01}}{\left(1+\frac{\gamma-1}{2}M_1^2\right)} = \frac{518.67}{\left(1+\frac{1.4-1}{2}(0.51)^2\right)} = 492.6^{o}\,R$$

$$\rho_1 = \frac{\rho_{01}}{\left(1+\frac{\gamma-1}{2}M_1^2\right)^{1/(\gamma-1)}} = \frac{0.07655}{\left(1+\frac{1.4-1}{2}(0.51)^2\right)^{1/(1.4-1)}} = 0.067\,lbm/ft^3$$

$$u_1 = M_1\sqrt{\gamma R g_c T_1} = (0.51)\sqrt{(1.4)(53.3)(32.17)(492.6)} = 559\,ft/s$$

$$U_{1t} = u_1 \tan\beta_{1t} = (559)\tan(50) = 667\,ft/s$$

- Calculate the specific geometric parameters

$$D_{1t} = \sqrt{\frac{4}{\pi}\frac{\dot{m}}{\rho_1 u_1}\left(1-\zeta^2\right)} = \sqrt{\frac{4}{\pi}\frac{1.1}{(0.067)(559)}\left(1-0.3^2\right)} = 0.20\,\text{ft} = 2.43\,\text{in}$$

$$D_h = D_{1t}\xi = (2.43)(0.3) = 0.73\,\text{in}$$

Since N = 63000 RPM, Ω = 6597 rad/s.

$$D_2 = \frac{2U_2}{\Omega} = \frac{2(1797)}{6597} = 6.54\,\text{in}$$

$$b_2 = D_2\left\{\frac{\left(\frac{\gamma+1}{2}\right)^{1/(\gamma-1)}\left(1-\xi^2\right)\left(\frac{D_{1t}}{D_2}\right)^2}{4\left[1+\left(\frac{1+\eta_c}{2}\right)\left(\frac{\gamma-1}{2}\right)\left(\frac{U_2}{\sqrt{Rg_c T_{01}}}\right)^2\varepsilon\right]^{1/(\gamma-1)}}\right\} = 0.10\,\text{in}$$

- Determine the number of impeller blades (n_b) by rearranging Equation 10.26:

$$n_b = \left[\frac{\sqrt{\cos\beta_{2b}}}{(1-\varepsilon)}\right]^{1/0.7} = \left[\frac{\sqrt{\cos(0)}}{(1-0.9)}\right]^{1/0.7} = 27\,\text{blades}$$

2) Rotor exit performance

Note: This analysis follows the sequence of steps outlined in Chapter 4 of *Introduction to Turbomachinery* textbook.[1]

- Apply slip factor (ε) correction

$$v_2 = \varepsilon U_2 = (0.9)(1797) = 1617\,\text{ft/s}$$

- Determine rotor exit conditions

$$\Delta h_o = U_2 v_2 = (1797)(1617) = 2905107\,\text{BTU/lbm}$$

$$T_{02} = T_{01} + \frac{\gamma - 1}{\gamma R g_c} \Delta h_0 = 518.67 + \frac{1.4 - 1}{(1.4)(53.3)(32.17)}(2906307) = 1002.5^{o}\,R$$

$$p_{02} = p_{01}\left(1 + \frac{\eta_{rotor}(\gamma - 1)\Delta h_o}{\gamma R g_c T_{01}}\right)^{\gamma/(\gamma-1)} = p_{01}\left(1 + \frac{(0.85)(1.4 - 1)\Delta h_o}{(1.4)(53.3)(32.17)(518.67)}\right)^{\gamma/(\gamma-1)} = 113.4\,psia$$

The following sequence of equations was solved iteratively by guessing an initial value for M_2 and continuing until the solution converged. The solver function in Excel was useful in expediting this iterative process. The final results are reflected in Table E.1.

$$T_2 = \frac{T_{02}}{\left(1 + \frac{\gamma - 1}{2} M_2^2\right)} \qquad [E.1]$$

$$p_2 = \frac{p_{02}}{\left(\frac{T_{02}}{T_2}\right)^{\gamma/(\gamma-1)}} \qquad [E.2]$$

$$w_2 = \frac{\dot{m} R T_2}{p_2 (2\pi r_2 b_2)} \qquad [E.3]$$

$$V_2 = \sqrt{w_2^2 + v_2^2} \qquad [E.4]$$

$$M_2 = \frac{V_2}{\sqrt{\gamma R g_c T_2}} \qquad [E.5]$$

Once the iterations have converged, the exit velocity triangle was determined as follows:

$$V_{2R} = \sqrt{(U_2 - v_2)^2 + w_2^2} = \sqrt{(1797 - 1617)^2 + (489)^2} = 521 ft/s$$

$$\beta_2 = \cos^{-1}\left(\frac{w_2}{V_{2R}}\right) = \cos^{-1}\left(\frac{489}{521}\right) = 20^{o}$$

$$\alpha_2 = \tan^{-1}\left(\frac{v_2}{w_2}\right) = \tan^{-1}\left(\frac{1617}{489}\right) = 73^{o}$$

3) Diffuser geometry

- Determine diffuser inlet conditions

A vaneless diffuser is assumed for simplification. Using the rotor exit conditions for α_2 and M_2, Equations 10.38 and 10.39 were rearranged and evaluated to determine the value of α^* and $(r/r^*)_2$, respectively.

$$\alpha^* = \tan^{-1}\left[\tan\alpha_2\left[\frac{2}{\gamma+1}\left(1+\frac{\gamma-1}{2}M_2^2\right)\right]^{1/(\gamma-1)}\right] = 76^o$$

$$\left(\frac{r}{r^*}\right)_2 = \frac{\dfrac{\sin\alpha^*}{\sin\alpha_2}}{M_2\left[\dfrac{(\gamma+1)/2}{1+[(\gamma-1)/2]M_2^2}\right]^{1/2}} = 0.85$$

Since α^* remains constant, the final radius ratio $(r/r^*)_5$ corresponds to the desired diffuser outlet Mach number (M_5) and the diffuser exit angle (α_5). In this case, $M_5 = 0.4$ and $\alpha_5 = \alpha_2$ because the diffuser width is constant.

$$\left(\frac{r}{r^*}\right)_5 = \frac{\dfrac{\sin\alpha^*}{\sin\alpha_5}}{M_5\left[\dfrac{(\gamma+1)/2}{1+[(\gamma-1)/2]M_5^2}\right]^{1/2}} = 2.35$$

$$\frac{r_5}{r_2} = \frac{(r/r^*)_5}{(r/r^*)_2} = \frac{2.36}{0.85} = 2.76$$

$$r_5 = \left(\frac{r_5}{r_2}\right)r_2 = (2.77)(3.27) = 9.05\,\text{in}$$

Because the vaneless diffuser provides a worse case radius, a 30% reduction was assumed based on the use of a vaned section immediately following the impeller exit. Although the calculations for the vaned section were beyond the scope of this report, a

diffuser radius (r_5) of 6.33 inches was considered a sufficient approximation for this preliminary design.

4) Overall compressor performance

- Determine the pressure loss coefficient (K) assuming $c_{p(2\text{-}5)} = 0.6$

$$c_{p(ideal)} = 1 - \left(\frac{r_2 b_2}{r_5 b_5}\right)^2 \frac{\cos^2 \alpha_2}{\cos^2 \alpha_5} = 0.73$$

$$K = c_{p(ideal)} - c_{p(2-5)} = 0.73 - 0.6 = 0.13$$

- Calculate the static pressure (p_5) and total pressure (p_{05}) at the diffuser exit

$$p_5 = p_2 - c_{p(2-5)}(p_{02} - p_2) = 85.59\,\text{psia}$$

$$p_{05} = p_{02} - K(p_{02} - p_2) = 104.11\,\text{psia}$$

- Determine the total pressure ratio (π_c)

$$\pi_c = \frac{p_{05}}{p_{01}} = \frac{104.10}{14.696} = 7.1$$

5) Weight estimation

A titanium alloy was selected as the compressor material because it is better suited to handle high tip speeds as demonstrated in Table 10.4. The weight is calculated by estimating the volume of the compressor section and multiplying by the material density. For the GTGH compressor, a weight of 5.85 lbs was determined using this method.

Table E.1: Radial Compressor Design Results (GTGH)

Assumptions		
γ	1.4	
R	53.3	(ft-lbf)/(lbm-^{o}R)
R g_c	1716	ft^2/(s^2-^{o}R)
g_c	32.17	(lbm-ft)/(lbf-s^2)
g_c c_p	6006	ft^2/(s^2-^{o}R)
π_c	7.1	
η_{pc}	0.85	

Given Data		
m_dot	1.10	lbm/s
T_{01}	518.67	^{o}R
p_{01}	14.70	psia

Design Choices		
β_{1t}	50	deg
M_{1R}	0.8	
ζ	0.3	
ε	0.9	
Mat'l Density	0.16	lbm/in^3

Impeller Inlet		
M_1	0.51	
T_1	492.62	^{o}R
p_{1t}	12.27	psia
ρ_{01}	0.0765	lb/ft^3
ρ_1	0.0673	lb/ft^3
u_1	559.4	ft/s
U_{1t}	666.7	ft/s
D_{1t}	2.43	in
r_{1t}	1.21	in
D_h	0.73	in
r_h	0.36	in

Calculated Values		
N	62973	RPM
Ω	6595	rad/s
η_c	0.805	
D_{1t}/D_2	0.371	

Impeller Exit		
Guess M_2	**1.25**	
β_{2b}	0	deg
n_{blades}	27	
U_2	1796.6	ft/s
D_2	6.54	in
r_2	3.27	in
b_2	0.10	in
v_2	1617.0	ft/s
Δh_o	2905107	BTU/lbm
T_{02}	1002.3	^{o}R
π_{tt1-2}	7.7	
p_{02}	113.34	psia
T_2	764.8	^{o}R
p_2	43.975	psia
w_2	489.1	ft/s
V_2	1689.3	ft/s
V_{2R}	521.0	ft/s
β_2	20.2	deg
α_2	73.2	deg
M_2	**1.25**	

Diffuser Exit		
α^*	76.4	deg
$(r/r^*)_2$	0.85	
M_5	0.40	
$(r/r^*)_5$	2.35	
r_5/r_2	2.76	
Vaned Reduction	30	%
r_5	6.33	in
b_5	0.10	in
$C_{p\,(2-5)}$	0.6	
p_5	85.59	psia
π_{ts}	5.8	
α_5	73.2	deg
$C_{p\,(ideal)}$	0.73	
K	0.133	
p_{05}	104.11	psia
π_{tt}	**7.1**	**stage**
Estimated Weight	**5.85**	**lb**

[1] David Japikse and Nicholas C. Baines, *Introduction to Turbomachinery* (White River Junction, VT: Concepts ETI, 1997).

APPENDIX F

AXIAL COMPRESSOR PRELIMINARY DESIGN (GTGH)

Although the GTGH design does not include an axial compressor, the following preliminary design example is provided for reference. The design point conditions are identical to those used for the centrifugal compressor – take-off power at SLS – however, higher polytropic efficiency (η_{pc}) was used for the axial configuration. An Excel design code was written to reproduce the capabilities of the COMPR program and to provide more computational transparency.

Input Data from Engine Cycle Analysis:

$T_{02} = 518.67^{o}R$ $p_{02} = 14.696$ psia $\dot{m}_{02} = 1.1$ lbm/s

$\rho_{02} = 0.0766$ lbm/ft^3 $\pi_c = 7.1$ $\eta_{pc} = 0.90$

$\Delta T_t = 447.7^{o}R$

Assumptions:

- Repeating row, repeating stage airfoil geometry ($\alpha_1=\beta_2=\alpha_3$ and $\beta_1=\alpha_2=\beta_3$)
- Two-dimensional flow
- Constant axial velocity ($u_1 = u_2 = u_3$)
- Constant mean radius
- Stage polytropic efficiency (η_{pc}) represents stage losses
- Calorically perfect gas with known γ and R

  $\gamma_c = 1.4$

  $R_c = 53.3$ (ft-lbf)/(lbm-^{o}R)

- Rotational velocity (N) = 63000 RPM [determined during HPT analysis]
- Diffusion factor (D) = 0.5
- Solidity (σ) = 1.0
- Inlet Mach number (M_1) = 0.6
- Chord-to-height ratio $(c/h)_{rotor} = (c/h)_{stator} = 0.6$
- Rotor loss coefficient $(\phi)_{rotor} = 0.09$
- Stator loss coefficient $(\phi)_{stator} = 0.03$
- Shaft radius (r_{shaft}) = 0.5 in

Design Process:

1) Number of stages

The estimated temperature rise per stage (ΔT_{ts}) was evaluated using the design guidelines presented in Table 10.1 which indicate that the typical ΔT_{ts} ranges from 60-90^oR. A conservative initial selection of 6 stages was used because it only requires $\Delta T_{ts} = 74.6^oR$. Although 5 stages would offer weight savings, this configuration requires $\Delta T_{ts} = 89.5^oR$ which is close to the upper design limit. Considering the extremely small airflow rate for this compressor, the aerodynamic design of the airfoils would be significantly more demanding for a 5 stage compressor – resulting in a higher degree of inherent developmental risk.

2) Single-stage analysis

The single-stage geometric and performance characteristics were defined based on the desired ΔT_{ts} and the assumptions and input data previously described. In applying the

general solution sequence presented in Equations 10.13 – 10.16, the inlet angle (α_1) was varied until $\Delta T_{ts} = 74.6^oR$. Table F.1 summarizes the results determined with the Excel axial compressor design code.

Table F.1: Single-Stage Axial Compressor Analysis Results (GTGH)

Assumptions			**Design Choices**			**Solution Sequence**		
γ	1.4		D	0.5		α_1	42.4	deg
R	53.34	(ft-lbf)/(lbm-^{o}R)	M_1	0.6		Γ	3.62	
η_{pc}	0.9		σ	1.0		α_2	59.1	deg
$g_c\ c_p$	6006	ft^2/(s^2-^{o}R)	# Stages	6		$\Delta\alpha$	16.7	deg
g_c	32.17	(lbm-ft)/(lbf-s^2)				τ_s	1.14	
						π_s	1.53	
Given Data			**Calculated Values**			η_s	0.89	
π_c	7.1		T_1	483.8	^{o}R	$\omega r/V_1$	1.91	
m_dot	1.10	lbm/s	a_1	1078.1	ft/s	$V_1/\omega r$	0.52	
T_{01}	518.67	^{o}R	V_1	646.9	ft/s	M_{1R}/M_1	1.44	
p_{01}	14.70	psia	ΔT_t	447.7	^{o}R	M_{1R}	0.86	
			$\Delta T_{t\ stage}$	74.6	^{o}R	M_3/M_1	0.93	
						ωr	1234.5	ft/s
						u_1	478.0	ft/s
						ΔT	74.6	^{o}R
						V_2	930.8	ft/s
						ψ	0.294	
						Φ	0.387	

3) Multi-stage analysis

- Determine the mean radius (r_m)

$$N = 63000\,\text{RPM} \;\therefore\; \omega = 6597\,\text{rad/s}$$

$$r_m = \frac{(\omega r_m)}{\omega} = \frac{1234.5}{6597} = 0.19\,\text{ft} = 2.25\,\text{in}$$

The remaining analysis is identical to that presented for the axial turbine design example. Table F.2 provides an overall summary of the results for each compressor stage. Note that the last 4 stages all require blade heights less than 0.25 inches. Such extremely small

blades would have a severe negative impact on the compressor's manufacturability, cost, and overall performance – clearly underscoring the need for a radial compressor for this propulsion system design.

Table F.2: Multi-Stage Axial Compressor Analysis Results (GTGH)

Stage 1

	1	1R	2R	2	3	
T_t	518.69	555.98	555.98	593.29	593.29	^oR
T	483.85	483.85	521.15	521.15	558.45	^oR
a	1078.15	--	--	1118.92	1158.26	ft/s
P_t	14.70	18.74	18.20	22.84	22.63	psia
P	11.52	11.52	14.51	14.51	18.31	psia
M	0.60	0.86	0.58	0.83	0.56	
V	646.89	930.83	646.86	930.86	646.89	ft/s
u	478.05	478.05	478.05	478.05	478.05	ft/s
v	435.82	798.69	435.77	798.73	435.82	ft/s
α	42.35	--	--	59.10	42.35	deg
β	--	59.10	42.35	--	--	deg
MFP	0.448			0.518	0.428	
A	5.2			4.4	3.7	in^2
r_h	2.06			2.09	2.11	in
r_t	2.43			2.40	2.38	in
h	0.37			0.31	0.27	in

Rotor:	n_{blades}	57		η_s	0.894
	Chord	0.25	in	ψ	0.2940
	Spacing	0.13	in	Φ	0.3872
Stator:	n_{blades}	57		π_s	1.5269
	Chord	0.25	in	τ_s	1.1438
	Spacing	0.13	in		

Stress Analysis:

Blades:	At/Ah	1	
	AN^2	1.76E+10	in^2 RPM^2
	σ_c/ρ	1.48	ksi/(slug/ft^3)
	T_{t1R}	96.29	^oF
	h	0.37	in
	σ_c	13.45	ksi
Rim & Disk:	σ_r	25	ksi
	σ_r/ρ	2.75	ksi/(slug/ft^3)
	σ_{blades}/σ_r	0.10	
	ωr_h	1134.1	ft/s
	h_r	0.14	in
	r_r	1.93	in
	ωr_r	1058.5	ft/s
	$[\omega r_r]_{max}$	1259.3	ft/s
	$\rho(\omega r_r)^2/2\sigma_r$	1.413	DSF
	W_{dr}/W_r	0.252	
	W_{ds}	0.26	in
	W_{dr}	0.07	in
	W_r	0.28	in
	Weight:	0.8	lb

Stage 2

	1	1R	2R	2	3	
T_t	593.29	630.58	630.58	667.88	667.88	^oR
T	558.45	558.45	595.74	595.74	633.04	^oR
a	1158.28	--	--	1196.32	1233.20	ft/s
P_t	22.63	28.01	27.27	33.34	33.06	psia
P	18.31	18.31	22.35	22.35	27.41	psia
M	0.56	0.80	0.54	0.78	0.52	
V	646.90	930.82	646.86	930.87	646.90	ft/s
u	478.06	478.06	478.06	478.06	478.06	ft/s
v	435.82	798.68	435.77	794.74	435.82	ft/s
α	42.35	--	--	59.10	42.35	deg
β	--	59.10	42.35	--	--	deg
MFP	0.428			0.507	0.410	
A	3.7			3.3	2.8	in^2
r_h	2.11			2.13	2.15	in
r_t	2.38			2.36	2.35	in
r_h/r_t	0.27			0.23	0.20	in

Rotor:	n_{blades}	57		η_s	0.895
	Chord	0.25	in	ψ	0.2940
	Spacing	0.13	in	Φ	0.3872
Stator:	n_{blades}	57		π_s	1.4522
	Chord	0.25	in	τ_s	1.1257
	Spacing	0.13	in		

Stress Analysis:

Blades:	At/Ah	1	
	AN^2	1.30E+10	in^2 RPM^2
	σ_c/ρ	1.10	ksi/(slug/ft^3)
	T_{t1R}	170.89	^oF
	h	0.27	in
	σ_c	9.96	ksi
Rim & Disk:	σ_r	25	ksi
	σ_r/ρ	2.75	ksi/(slug/ft^3)
	σ_{blades}/σ_r	0.10	
	ωr_h	1161.6	ft/s
	h_r	0.14	in
	r_r	1.98	in
	ωr_r	1086.0	ft/s
	$[\omega r_r]_{max}$	1259.3	ft/s
	$\rho(\omega r_r)^2/2\sigma_r$	1.487	DSF
	W_{dr}/W_r	0.259	
	W_{ds}	0.29	in
	W_{dr}	0.07	in
	W_r	0.28	in
	Weight:	0.8	lb

Stage 3

	1	1R	2R	2	3	
T_t	667.88	705.17	705.17	742.48	742.48	°R
T	633.04	633.04	670.34	670.34	707.64	°R
a	1233.22			1269.00	1303.83	ft/s
P_t	33.06	39.98	39.00	46.71	46.34	psia
P	27.41	27.41	32.66	32.66	39.17	psia
M	0.52	0.75	0.51	0.73	0.50	
V	646.91	930.82	646.86	930.88	646.91	ft/s
u	478.06	478.06	478.06	478.06	478.06	ft/s
v	435.83	798.68	435.76	798.74	435.83	ft/s
α	42.35			59.10	42.35	deg
β		59.10	42.35			deg
MFP	0.410			0.496	0.395	
A	2.8			2.5	2.2	in^2
r_h	2.15			2.16	2.17	in
r_t	2.35			2.33	2.32	in
r_h/r_t	0.20			0.18	0.16	in

Rotor:	n_{blades}	57		η_s	0.895	
	Chord	0.25	in	ψ	0.2940	
	Spacing	0.13	in	Φ	0.3873	
Stator:	n_{blades}	57		π_s	1.3959	
	Chord	0.25	in	τ_s	1.1117	
	Spacing	0.13	in			

Stress Analysis:

Blades:	**At/Ah**	1	
	AN^2	1.00E+10	in^2 RPM^2
	σ_c/ρ	0.84	ksi/(slug/ft^3)
	T_{t1R}	245.48	°F
	h	0.20	in
	σ_c	7.65	ksi
Rim & Disk:	σ_r	25	ksi
	σ_r/ρ	2.75	ksi/(slug/ft^3)
	σ_{blades}/σ_r	0.10	
	ωr_h	1179.3	ft/s
	h_r	0.14	in
	r_r	2.01	in
	ωr_r	1103.7	ft/s
	$[\omega r_r]_{max}$	1259.3	ft/s
	$\rho(\omega r_r)^2/2\sigma_r$	1.536	DSF
	W_{dr}/W_r	0.263	
	W_{ds}	0.31	in
	W_{dr}	0.07	in
	W_r	0.28	in
	Weight:	0.8	lb

Stage 4

	1	1R	2R	2	3	
T_t	742.48	779.77	779.77	817.07	817.07	°R
T	707.64	707.64	744.93	744.93	782.23	°R
a	1303.85			1337.75	1370.83	ft/s
P_t	46.34	55.01	53.75	63.31	62.84	psia
P	39.17	39.17	45.81	45.81	53.95	psia
M	0.50	0.71	0.48	0.70	0.47	
V	646.92	930.82	646.86	930.89	646.92	ft/s
u	478.07	478.07	478.07	478.07	478.07	ft/s
v	435.83	798.67	435.76	798.75	435.83	ft/s
α	42.35			59.10	42.35	deg
β		59.10	42.35			deg
MFP	0.395			0.485	0.380	
A	2.2			2.0	1.8	in^2
r_h	2.17			2.17	2.18	in
r_t	2.32			2.32	2.31	in
r_h/r_t	0.16			0.14	0.13	in

Rotor:	n_{blades}	57		η_s	0.896	
	Chord	0.25	in	ψ	0.2940	
	Spacing	0.13	in	Φ	0.3873	
Stator:	n_{blades}	57		π_s	1.3520	
	Chord	0.25	in	τ_s	1.1005	
	Spacing	0.13	in			

Stress Analysis:

Blades:	**At/Ah**	1	
	AN^2	7.93E+09	in^2 RPM^2
	σ_c/ρ	0.67	ksi/(slug/ft^3)
	T_{t1R}	320.08	°F
	h	0.16	in
	σ_c	6.06	ksi
Rim & Disk:	σ_r	25	ksi
	σ_r/ρ	2.75	ksi/(slug/ft^3)
	σ_{blades}/σ_r	0.10	
	ωr_h	1191.3	ft/s
	h_r	0.14	in
	r_r	2.03	in
	ωr_r	1115.7	ft/s
	$[\omega r_r]_{max}$	1259.3	ft/s
	$\rho(\omega r_r)^2/2\sigma_r$	1.570	DSF
	W_{dr}/W_r	0.266	
	W_{ds}	0.32	in
	W_{dr}	0.07	in
	W_r	0.28	in
	Weight:	0.8	lb

Stage 5

	1	1R	2R	2	3	
T_t	817.07	854.36	854.36	891.67	891.67	^oR
T	782.23	782.23	819.53	819.53	856.83	^oR
a	1370.85			1403.13	1434.71	ft/s
P_t	62.84	73.46	71.90	83.50	82.92	psia
P	53.95	53.95	62.15	62.15	72.13	psia
M	0.47	0.68	0.46	0.66	0.45	
V	646.93	930.82	646.87	930.90	646.93	ft/s
u	478.08	478.08	478.08	478.08	478.08	ft/s
v	435.84	798.67	435.75	798.76	435.84	ft/s
α	42.35			59.10	42.35	deg
β		59.10	42.35			deg
MFP	0.380			0.473	0.368	
A	1.8			1.6	1.5	in^2
r_h	2.18			2.19	2.19	in
r_t	2.31			2.30	2.30	in
r_h/r_t	0.13			0.11	0.10	in

Rotor:	n_{blades}	57		η_s	0.896	
	Chord	0.25	in	ψ	0.2940	
	Spacing	0.13	in	Φ	0.3873	
Stator:	n_{blades}	57		π_s	1.3168	
	Chord	0.25	in	τ_s	1.0913	
	Spacing	0.13	in			

Stress Analysis:

Blades:	**At/Ah**	1	
	AN^2	6.42E+09	in^2 RPM^2
	σ_c/ρ	0.54	ksi/(slug/ft^3)
	T_{t1R}	394.67	^oF
	h	0.13	in
	σ_c	4.91	ksi
Rim & Disk:	σ_r	25	ksi
	σ_r/ρ	2.75	ksi/(slug/ft^3)
	σ_{blades}/σ_r	0.10	
	ωr_h	1199.8	ft/s
	h_r	0.14	in
	r_r	2.05	in
	ωr_r	1124.2	ft/s
	$[\omega r_r]_{max}$	1259.3	ft/s
	$\rho(\omega r_r)^2/2\sigma_r$	1.594	DSF
	W_{dr}/W_r	0.268	
	W_{ds}	0.33	in
	W_{dr}	0.07	in
	W_r	0.28	in
	Weight:	0.8	lb

Stage 6

	1	1R	2R	2	3	
T_t	891.67	928.96	928.96	966.26	966.26	^oR
T	856.83	856.83	894.12	894.12	931.42	^oR
a	1434.73			1465.60	1495.85	ft/s
P_t	82.92	95.71	93.80	107.66	106.96	psia
P	72.13	72.13	82.05	82.05	94.06	psia
M	0.45	0.65	0.44	0.64	0.43	
V	646.94	930.82	646.87	930.91	646.94	ft/s
u	478.08	478.08	478.08	478.08	478.08	ft/s
v	435.85	798.66	435.74	798.76	435.85	ft/s
α	42.35			59.10	42.35	deg
β		59.09	42.35			deg
MFP	0.368			0.462	0.356	
A	1.5			1.3	1.2	in^2
r_h	2.19			2.20	2.20	in
r_t	2.30			2.29	2.29	in
r_h/r_t	0.10			0.09	0.09	in

Rotor:	n_{blades}	57		η_s	0.896	
	Chord	0.25	in	ψ	0.2940	
	Spacing	0.13	in	Φ	0.3873	
Stator:	n_{blades}	57		π_s	1.2880	
	Chord	0.25	in	τ_s	1.0837	
	Spacing	0.13	in			

Stress Analysis:

Blades:	**At/Ah**	1	
	AN^2	5.31E+09	in^2 RPM^2
	σ_c/ρ	0.45	ksi/(slug/ft^3)
	T_{t1R}	469.27	^oF
	h	0.10	in
	σ_c	4.05	ksi
Rim & Disk:	σ_r	25	ksi
	σ_r/ρ	2.75	ksi/(slug/ft^3)
	σ_{blades}/σ_r	0.10	
	ωr_h	1206.1	ft/s
	h_r	0.14	in
	r_r	2.06	in
	ωr_r	1130.5	ft/s
	$[\omega r_r]_{max}$	1259.3	ft/s
	$\rho(\omega r_r)^2/2\sigma_r$	1.612	DSF
	W_{dr}/W_r	0.270	
	W_{ds}	0.34	in
	W_{dr}	0.07	in
	W_r	0.28	in
	Weight:	0.8	lb

REFERENCES

"Advanced Ceramics Technology Roadmap – Charting Our Course." *US Advanced Ceramics Association* and *US Department of Energy*, December 2000.

Aerospace Filtration Systems, Inc. website: http://www.afsfilters.com, Internet; Accessed on 27 October 2006.

Akbari, Pezhman, and Norbert Mueller. "Wave Rotor Research Program at Michigan State University." *AIAA Paper 2005-3844*, July 2005.

Akbari, Pezhman, Razi Nalim, and Norbert Mueller. "A Review of Wave Rotor Technology and Its Applications." *Journal of Engineering for Gas Turbines and Power*, January 2006.

Alcock, Joseph F., and J. Walter Smith. *Introduction to Gas Turbine Performance Analysis.* West Palm Beach, FL: Pratt and Whitney Aircraft Group, 1979.

Anderson, John D. Jr. *Fundamentals of Aerodynamics.* Boston, MA: McGraw-Hill, 2001.

Aviation Week and Space Technology, January 17, 2005: 122-134.

Ballal, Dilip R., and Joseph Zelina. "Progress in Aero Engine Technology (1939-2003)." *AIAA Paper 2003-4412*, July 2003.

Ballard, J. R. "Impact of IPS and IRS Configurations on Engine Installation Design." *AGARD LS-148 Engine-Airframe Integration for Rotorcraft.* Essex, England: Specialised Printing Services, 1986.

Bell 430 Product Data Book. Fort Worth, TX: Bell Helicopter Textron, 2003.

Cumpsty, Nicholas. *Jet Propulsion.* New York, NY: Cambridge University Press, 2003.

De la Servette, X., and P. Cabrit. "Helicopter Air Intake Protection Systems." *AGARD LS-148 Engine-Airframe Integration for Rotorcraft.* Essex, England: Specialised Printing Services, 1986.

Dempsey, E., N. Mueller, P.Akbari, and M. R. Nalim. "Performance Optimization of Gas Turbines Utilizing Four-Port Wave Rotors." *AIAA Paper 2006-4152*. June 2006.

DiCarlo, James A., Hee Man Yun, Gregory N. Morscher, and Ramakrishna T. Bhatt. "High-Performance SiC/SiC Ceramic Composite Systems Developed for 1315°C (2400°F) Engine Components." *NASA Research Report,* 2005.

Dieter, George E. *Engineering Design: A Materials and Processing Approach.* Boston, MA: McGraw-Hill, 2000.

Donaldson, Peter. "Power is Control." *Helicopter World,* February 1998.

Eames, David J. H. "Turboshaft Engine Overview." *Rolls-Royce Presentation to University of Maryland Graduate Students*. 23 March 2006.

Federal Aviation Regulation (FAR) Part 33.28c, available online at: http://ecfr.gpoaccess.gov, Internet; Accessed on 01 November 2006.

Flack, Ronald D. *Fundamentals of Jet Propulsion with Applications.* New York, NY: Cambridge University Press, 2005.

Frawley, R. C., and H. N. Shohet. "Engine-Airframe Integration Considerations for Preliminary Air Vehicle Performance Analysis." *AGARD LS-148 Engine-Airframe Integration for Rotorcraft.* Essex, England: Specialised Printing Services, 1986.

GasTurb website: http://www.gasturb.de/Products/GasTurb/Power_Generation/power_generation.html, Internet; Accessed on 13 September 2006.

Gauntner, James W. "Algorithm for Calculating Turbine Cooling Flow and the Resulting Decrease in Turbine Efficiency." *NASA Technical Memorandum 81453.* Cleveland, OH: Lewis Research Center, 1980.

Headquarters, US Army Materiel Command. *AMC Pamphlet 706-201: Engineering Design Handbook: Helicopter Engineering, Part 1 – Preliminary Design.* Alexandria, VA: GPO, 1974.

Headquarters, US Army Materiel Command. *AMC Pamphlet 706-202: Engineering Design Handbook: Helicopter Engineering, Part 2 – Detail Design.* Alexandria, VA: GPO, 1976.

Hill, Phillip G., and Carl R. Peterson. *Mechanics and Thermodynamics of Propulsion.* Reading, MA: Addison-Wesley Publishing, 1992.

Hourmouziadis, Jean, and Horst B. Kreiner. "Advanced Component Development Design Basis for Next Generation Medium Power Helicopter Engines." *Helicopter Propulsion Systems: AGARD Conference Proceedings No. 302.* London, UK: Technical Editing and Reproduction, 1981.

Japikse, David, and Nicholas C. Baines. *Introduction to Turbomachinery*. White River Junction, VT: Concepts ETI, 1997.

Koff, Bernard L. "Gas Turbine Technology Evolution – A Designer's Perspective." *AIAA Paper 2003-2722,* July 2003.

Kundu, A. K., S. Crosby, R. Curran, and S. Raghunathan. "Aircraft Component Manufacture Case Studies and Operating Cost Reduction Benefit." *AIAA Paper 2003-6829*, November 2003.

Lewis, T. J. "Distributed Architectures for Advanced Engine Control Systems" *AGARD CP-572 Advanced Aero-Engine Concepts and Controls.* Quebec, Canada: Canada Communication Group, 1996.

Leyes, Richard A., and William A. Fleming. *The History of North American Small Gas Turbine Aircraft Engine.* Reston, VA: AIAA, 1999.

Mattingly, Jack D. *Elements of Gas Turbine Propulsion.* Reston, VA: AIAA, 2005.

Mattingly, Jack D., William H. Heiser, and David T. Pratt. *Aircraft Engine Design.* 2nd ed. Reston, VA: AIAA, 2002.

Mullen, Robert L., Ronald J. Zab, and Antonius S. Kurniawan. "Thermal Mechanical Analysis of Sprag Clutches." *NASA Technical Report CA-190686.* Cleveland, OH: Case Western Reserve University, 1992.

NASA Engine Performance Program (NEPP) User's Manual, 1997.

"NASA Extended Parametric Representation of Compressor Fans and Turbines." *NASA CR-174646*. Vol. II. General Electric: Cincinnati, OH, 1984.

Newman, Tom. Telephonic interview with a Project Engineering Manager, *Aerospace Filtration Systems, Inc*., 26 October 2006.

Pilot Friend website: http://www.pilotfriend.com/training/flight_training/tech/jet_engine_components.htm, Internet; Accessed on 28 August 2006.

Romero, R., H. Summers, and J. Cronkhite. "Feasibility Study of a Rotorcraft Health Usage Monitoring System (HUMS): Results of Operator's Evaluation." *NASA Report CR-198446*, February 1996.

Schafer, Joe. *Helicopter Maintenance.* Frankfurt, Germany: Jeppesen and Company, 1992.

Schrage, Daniel P. *AE6333 Rotorcraft Design I: Individual and Team Projects.* Atlanta, GA: Georgia Institute of Technology, 2005.

Schrage, Daniel P. "Extension of R_f Method To VTOL Aircraft Conceptual and Preliminary Design." *AE6333 Rotorcraft Design I Course Notes.* Atlanta, GA: Georgia Institute of Technology, 2005.

Sharma, K., P. S. Shankar, and J. P. Singh. "Mechanical Behavior of Si_3N_4 Substrates with Environmental Barrier Coatings." Presented at the *Symposium on Innovative Processing and Synthesis of Ceramics, Glasses, and Composites* at the *105th American Ceramic Society Annual Meeting and Exposition*, 27-30 April 2003.

Sonntag, Richard E., and Gordon J. Van Wylen. *Introduction to Thermodynamics: Classical and Statistical.* New York, NY: John Wiley and Sons, 1991.

"The Benefits of Digital Engineering," *CIMData Report,* 2003.

"Thermodynamics of Incompressible and Compressible Fluid Flow." *SAE Aerospace Applied Thermodynamics Manual AIR1168/1*. Warrendale, PA: Society of Automotive Engineers, 1989.

Thai Technics website: http://www.thaitechnics.com/engine/engine_type.html, Internet; accessed on 21 August 2006.

Tortarolo, Franco, Guido Crosetti, and Carmine Difilippo. "Safety Critical Software Development for Advanced Full Authority Control Systems." *AGARD CP-572 Advanced Aero-Engine Concepts and Controls.* Quebec, Canada: Canada Communication Group, 1996.

US Department of Energy – Distributed Energy website: http://www.ornl.gov/sci/de_materials/projects -monolithic.shtml, Internet; Accessed on 25 October 2006.

Verrilli, Michael J., Craig Robinson, and Anthony Calomino. "Ceramic Matrix Composite Vane Subelements Tested in a Gas Turbine Environment." *NASA Research Report,* 2005.

Welch, Gerald E. "Overview of Wave-Rotor Technology for Gas Turbine Engine Topping Cycles." *Novel Aero Propulsion Systems International Symposium.* London: The Institution of Mechanical Engineers, 2000.

Wikimedia Commons website: http://commons.wikimedia.org/wiki/Image:Turboshaft_operation.png; Internet; accessed on 18 August 2006.

Wikipedia website: http://en.wikipedia.org/wiki/Image:Axial-flow-compressor.png, Internet; Accessed on 28 August 2006.

Wilson, Jack. "Design of the NASA Lewis 4-Port Wave Rotor Experiment." *NASA Report CR – 202351*, June 1997.

Wilson, Jack, and Daniel E. Paxson. "Wave Rotor Optimization for Gas Turbine Engine Topping Cycles." *Journal of Propulsion and Power*, July 1996.

Zhu, Dongming, Sung R. Choi, and Raymond C. Robinson. "Advanced Testing and Performance Evaluation of Environmental Barrier Coatings." Presented at the *Environmental Barrier Coatings Workshop*, 15-16 November 2005.